Laboratory Medicine

January 2022 Vol 53 No 1 Pgs 1–106

labmedicine.com

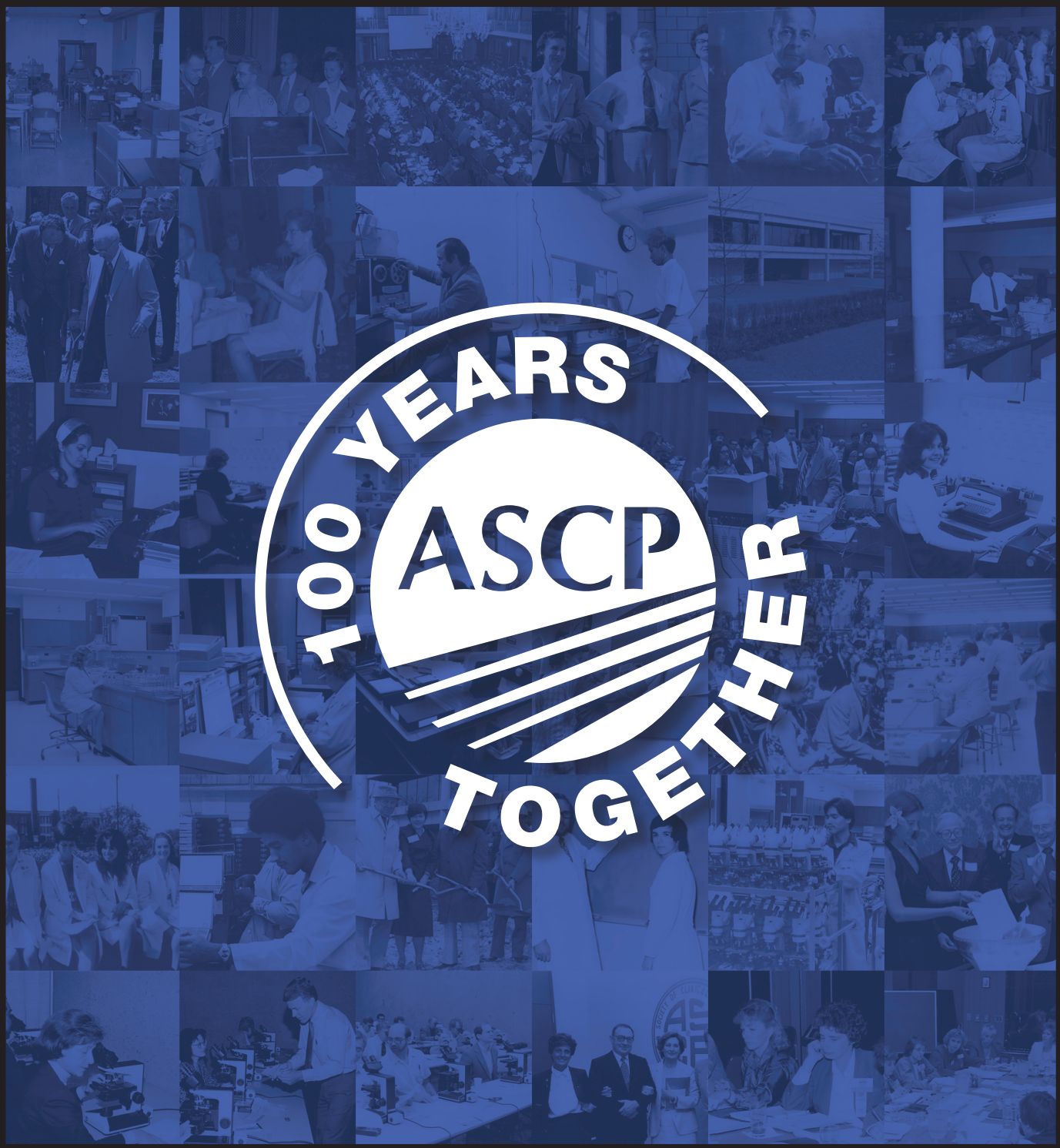

LaboratoryMedicine

January 2022
Vol 53, No 1
p. 1–106

EDITORIAL

SCIENCE

CASE STUDY

The following are online-only papers that are available as part of Issue 53(1) online.

ON THE COVER: The American Society of Clinical Pathologists was founded in May, 1922, by Dr. Ward Burdick and 39 other physicians at the 1922 meeting of the American Medical Society in St. Louis, Missouri. Dr. Philip Hillkowitz was elected the first ASCP President, and the society was based in Dr. Burdick's Denver laboratory. The ASCP offices eventually moved to Chicago, where they remain today. In 2001, the name of the organization was changed to the American Society for Clinical Pathology, to recognize the inclusion of non-pathologist laboratory professionals. On the cover of this first issue of *Laboratory Medicine* in 2022, we display the official logo to commemorate the 100th anniversary of the ASCP, and we congratulate the society for its rich history of service and education in the interest of quality patient care.

Lab Medicine (ISSN 0007-5027), is published 6 times per year (bimonthly). Periodicals Postage paid at Chicago, IL and additional mailing offices. POSTMASTER: Send address changes to *Lab Medicine*, Journals Customer Service Department, Oxford University Press, 2001 Evans Road, Cary, NC 27513-2009.

SUBSCRIPTION INFORMATION: Annually for North America, $173 (electronic) or $225 (electronic and print); single issues for individuals are $29 and for institutions $64. Annually for Rest of World, £112/€159 (electronic) or £144/€206 (electronic and print); single issues for individuals are £19/€27 and for institutions £40/€57. All inquiries about subscriptions should be sent to Journals Customer Service Department, Oxford Journals, Great Clarendon Street, Oxford OX2 6DP, UK, Tel: +44 (0) 1865-35-3907, e-mail: jnls.cust.serv@oup.com. In the Americas, please contact Journals Customer Service Department, Oxford Journals, 2001 Evans Road, Cary, NC 27513. Tel: 800-852-7323 (toll-free in USA/Canada) or 919-677-0977, e-mail: jnlorders@oup.com.

MEMBERSHIP INFORMATION: The ASCP membership fees for pathologists are as follows: fellow membership is $349; fellow membership plus 1-year unlimited online CE is $519; 2-year fellow membership is $675; and 2-year fellow membership plus 2-year unlimited online CE is $1,015. The ASCP membership fees for laboratory professionals are as follows: newly certified membership is $49; annual membership is $99; annual membership plus 1-year unlimited online CE is $129; 3-year membership is $349. All inquiries about membership should be sent to American Society for Clinical Pathology, 33 West Monroe Street, Suite 1600, Chicago, IL 60603, Tel: 312-541-4999, e-mail: ascp@ascp.org.

CLAIMS: Publisher must be notified of claims within four months of dispatch/ order date (whichever is later). Subscriptions in the EEC may be subject to European VAT. Claims should be made to Lab Medicine, Journals Customer Service Department, Oxford University Press, 2001 Evans Road, Cary, NC 27513, Tel: 800-852-7323 (toll-free in USA/Canada) or 919-677-0977, e-mail: jnlorders@oup.com.

Lab Medicine is published bimonthly by Oxford University Press (OUP), on behalf of the ASCP, a not-for-profit corporation organized exclusively for educational, scientific, and charitable purposes. Devoted to the continuing education of laboratory professionals, *Lab Medicine* features articles on the scientific, technical, managerial, and educational aspects ofthe clinical laboratory. Publication of an article, column, or other item does not constitute an endorsement by the ASCP of the thoughts expressed or the techniques, organizations, or products described therein. *Lab Medicine* is indexed in the following: MEDLINE/PubMed, Science Citation Index, Current Contents—Clinical Medicine, and the Cumulative Index to Nursing and Allied Health Literature.

Printed in the USA

ASCP
Lab Medicine
33 West Monroe Street, Suite 1600
Chicago, IL 60603

T: 312-541-4999
F: 312-541-4750

LaboratoryMedicine

January 2022
Vol 53, No 1
p. 1–106

EDITORIAL

SCIENCE

CASE STUDY

The following are online-only papers that are available as part of Issue 53(1) online.

ON THE COVER: The American Society of Clinical Pathologists was founded in May, 1922, by Dr. Ward Burdick and 39 other physicians at the 1922 meeting of the American Medical Society in St. Louis, Missouri. Dr. Philip Hillkowitz was elected the first ASCP President, and the society was based in Dr. Burdick's Denver laboratory. The ASCP offices eventually moved to Chicago, where they remain today. In 2001, the name of the organization was changed to the American Society for Clinical Pathology, to recognize the inclusion of non-pathologist laboratory professionals. On the cover of this first issue of *Laboratory Medicine* in 2022, we display the official logo to commemorate the 100th anniversary of the ASCP, and we congratulate the society for its rich history of service and education in the interest of quality patient care.

EDITORIAL

Evolution and Reflection

Laboratory Medicine 2022;53:5; https://doi.org/10.1093/labmed/lmab112

Something Old, Something New

This issue of *Laboratory Medicine* introduces changes that include the ninth cover design for the journal since its inception in 1970, and the first redesign since 2012. At 10 years, the previous "*Lab Medicine*" cover was the longest running cover design in the journal's history, eclipsing the original and "*LABMEDICINE*" covers, both of which lasted 8 years.

This new cover design incorporates certain features of past designs yet represents an entirely new look for the journal. Perhaps the biggest change is that the title has reverted to its original "*Laboratory Medicine*," the name under which the journal has always been registered with the National Library of Medicine. The title on the cover was changed to *LABMEDICINE* in 2004, but now returns to its original, more stately and complete form. The basic color scheme remains the same as the previous design, with the formality of a black background, along with the dark blue-highlighted "Medicine" in the title, which also has returned to the top of the cover. The cover image now extends to the left and right borders. Subtle changes have been made to the formatting of papers published in the journal, to improve readability and aesthetics. The text has been slightly compressed to accommodate more articles, as the number of submitted manuscripts continues to climb commensurate with the steadily improving Impact Factor for the journal.

I sincerely hope you like the new look and share my pride in *Laboratory Medicine*.

A Momentous Milestone

The year 2022 marks the 100th anniversary of the American Society for Clinical Pathology (until 2001, the organization was called the American Society of Clinical Pathologists). The centennial will be celebrated in several ways throughout this year, reaching a climax at the ASCP Annual Meeting Chicago, IL, September 6-8, 2022. The Society has much to celebrate in its 100-year history. Dr Fred Rodriguez, a former ASCP President, and Dr John Ball, former ASCP Executive Vice President, compiled an impressive list (*Lab Med* 2007;38:596-601) of ASCP "firsts," including:

- The first certifying agency for laboratory personnel, the Board of Registry, created in 1928
- Creation of the American Board of Pathology in 1934
- Creation of the College of American Pathologists in 1946
- Election of Dr Emma Moss as president of the ASCP, the first female president of any national medical organization
- Creation of the National Accrediting Agency for Clinical Laboratory Sciences (NAACLS), formerly the ASCP Board of Schools, in 1973
- Creation of the Resident In-Service Exam (RISE) in 1983
- Accreditation of the Board of Registry by the American National Standards Institute (ANSI) in 2007

Throughout its history, the ASCP has been the premier professional organization for pathology and laboratory medicine, true to their founding goal to "achieve greater scientific proficiency in clinical pathology, and to maintain the status of clinical pathologists on an equal plane with other specialties." On behalf of the Editorial Board, editorial office, and Oxford University Press, our publisher, I extend my sincerest and heartiest congratulations to the leadership and members of the ASCP for reaching this momentous milestone.

Roger L. Bertholf, PhD
Editor in Chief

SCIENCE

A Fluorescence-Based Quantitative Analysis for Total Bilirubin in Blood and Urine

Tran Tien Tai, MD, PhD,[1,2] Yasushi Adachi, MD, PhD,[3,4] and Shigeru Taketani, PhD[1,5]*

[1]Department of Biotechnology, Kyoto Institute of Technology, Kyoto 606-8585, Japan; [2]Department of Physiology-Pathophysiology-Immunology, Pham Ngoc Thach University of Medicine, Ho Chi Minh, Vietnam; [3]Division of Diagnostic Pathology, Toyooka Hospital, Hyogo 668-8501, Japan; [4]Department of Pediatrics, Kansai Medical University, Hirakata, Osaka, 573-1010, Japan; [5]Research Complex, Kansai Medical University, Hirakata, Osaka, 573-1010, Japan; *To whom correspondence should be addressed. Corresponding author. atakechan.man9@gmail.com

Keywords: conjugated bilirubin, unconjugated bilirubin, β-glucuronidase, UnaG, serum, urine

Abbreviations: RBC, red blood cell; Cr, creatinine; BOD, bilirubin oxidase; LOD, limit of detection

Laboratory Medicine 2022;53:6–11; DOI: 10.1093/labmed/lmab043

ABSTRACT

Background: Bilirubin is a catabolic product of heme metabolism that circulates in the bloodstream in its unconjugated or glucuronide-conjugated form. Because the accumulation of bilirubin in the blood is a common symptom of liver diseases, its measurement in plasma (serum) is important for the diagnosis of these diseases.

Method: We developed a method to assess total bilirubin levels in serum and urine, using the fluorescent protein UnaG and β-glucuronidase.

Results: Our results indicate good correlation in serum total bilirubin levels between UnaG and the conventional bilirubin oxidase (BOD) methods. We found low levels of conjugated and unconjugated bilirubin in the urine of healthy subject individuals. Urinary bilirubin levels were elevated in patients with liver or bile duct diseases. A simple spot test of bilirubin using serum and urine showed a strong signal in patients with liver diseases.

Conclusion: The proposed method to assess bilirubin levels in serum and urine will contribute to the accurate diagnosis of health conditions such as jaundice, anemia, and liver disease.

Bilirubin is a yellow pigment and the catabolic product of heme metabolism, which is formed by the breakdown of heme in hemoglobin, myoglobin, cytochromes, catalase, peroxidase, and tryptophan pyrrolase.[1] Bilirubin circulates in the bloodstream in its unconjugated insoluble form (*indirect bilirubin*) or glucuronide-conjugated soluble form (*direct bilirubin*).[2,3] Serum bilirubin is mostly unconjugated and is tightly bound to serum albumin. It is taken up by hepatocytes and is conjugated with glucuronic acid by the enzyme β-glucuronyltransferase, producing conjugated bilirubin. This process is clinically important because bilirubin accumulates in body tissues and is elevated in the blood of most patients with jaundice. The accumulation of this substance in the blood is a common symptom of liver diseases.[3,4] Thus, bilirubin in plasma (serum) has potential as a marker of these diseases. The accurate measurement of blood bilirubin levels is also important, particularly in the treatment of neonatal jaundice, because the decision to initiate or discontinue treatment is often based on bilirubin levels.[3–5]

Most bilirubin is secreted into bile and delivered into the small intestine. After several modifications, the metabolite, urobilinogen (or urobilin) is excreted by the kidneys into urine.[5,6] Normal urine contains as much as 4 mg urobilinogen per day; excessive amounts of urobilinogen in urine indicate hepatic damage and increased red blood cell (RBC) destruction. Accompanied by an increase in excreted urobilinogen, bilirubin levels in urine may be elevated by several diseases, including hemolysis, as well as hepatic and renal dysfunctions.[7] However, because individual laboratories establish their own normal reference values and the data obtained are dependent on the method performed, this is not a reliable index of diseases.[8–10] Thus, a suitable method for measuring urinary bilirubin has not yet been established.

The eel fluorescent protein UnaG binds with high affinity to bilirubin[11,12]; thus, the quantification of bilirubin in tissues and serum by the reaction of UnaG with heme oxygenase has been suggested as a useful application. We previously reported a simple and sensitive assay of heme oxygenase activity.[13] Other investigators[14,15] also demonstrated the use of UnaG to measure unconjugated bilirubin in serum. We have continued our research on the availability of UnaG for bilirubin assays and herein describe a simple method to measure total bilirubin levels in serum using only a small amount of serum (<1 μL) and UnaG. Urinary bilirubin levels markedly differed between patients with liver diseases and healthy subjects.

Materials and Methods

Control urine specimens were obtained from healthy volunteers (age, 12–70 years). Also, urine specimens were obtained from patients with liver diseases or bile-duct neoplasms, and all serum specimens were obtained from Toyooka Hospital (Hyogo, Japan). All subjects enrolled in the present study provided informed consent; the study protocol was approved by the Ethics Committee on Human Research of Toyooka Hospital.

Serum (1 μL) or urine (1–25 μL) was placed in the wells of a 96-plate analyzer, and was diluted with 50 mM Tris-HCl, pH 8.0, at the final volume of 100 μL. The mixture was incubated without or with 1 unit of *E. coli* β-glucuronidase (Wako Pure Chemicals Co., Tokyo, Japan) at 37°C for 30 minutes, followed by incubation with UnaG (100 μg of protein).[12,13] The fluorescence of the unconjugated bilirubin-UnaG complex was directly measured using an Enspire Multilabel Reader (PerkinElmer, Inc). The fluorescence was examined at 530 nm, with an excitation at 480 nm.

For spot testing of bilirubin, 1 μL of serum or urine treated without or with β-glucuronidase was incubated with UnaG (10 μg of protein) in 50 mM Tris-HCl (pH 8.0). An aliquot of the mixture was drawn and spotted onto filter paper, which was then exposed to a Fluoro blue/green LED lamp (Nippon Genetics Co.). Total and conjugated bilirubin levels in serum specimens were also examined using the bilirubin oxidase (BOD) method (Kanto Chemicals Co.).[16,17] The difference in absorbance at 450 nm plus/minus BOD was examined with a ND100 spectrophotometer (Thermo-Fisher Scientific Inc.).

In case of the examination of urinary bilirubin, a urinalysis dipstick test for urobilinogen (Uropaper α III, Eiken Chemicals Co., Ltd.) was performed as a reference. Creatinine (Cr) corrections were performed for the aforementioned values using urinary Cr with a colorimetric method (Cayman Co.).

A statistical analysis (*t* testing) was conducted with GraphPad Prism software, version 5.02 (GraphPad Software, Inc). Correlation of total bilirubin level between the UnaG method and BOD method was assessed by Spearman rank correlation coefficient. $P < .05$ was considered statistically significant.

Results

Deconjugation of Conjugated Bilirubin

UnaG was incubated with some forms of bilirubin, followed by measurements of the UnaG-bilirubin complexes by a fluorometer, and was shown to bind to unconjugated bilirubin but not conjugated bilirubin or the artificial-conjugated bilirubin, known as ditaurobilirubin (Supplemental Figure 1). Therefore, the deconjugation of conjugated bilirubin is required to assess total bilirubin levels in serum with UnaG. A previous study report[18] stated that *Escherichia coli* β-glucuronidase effectively hydrolyzed conjugated bilirubin into bilirubin and glucuronic acid at an alkaline pH.

Serum was incubated with *E. coli* β-glucuronidase at 37°C to hydrolyze conjugated bilirubin. The formation of UnaG-bilirubin in β-glucuronidase-treated serum increased in a time-dependent manner and reached a plateau at the 15-minute incubation (Supplemental Figure 2A). To confirm the loss of conjugated bilirubin by β-glucuronidase, we examined the BOD-dependent oxidation of conjugated bilirubin because BOD oxidizes conjugated bilirubin to biliverdin at acidic pH but not unconjugated bilirubin.[16,17] β-Glucuronidase-treated serum was mixed with 0.1 M sodium citrate buffer (pH 4.0), and the mixture was then incubated with BOD.

As shown in Supplemental Figure 2B, biliverdin was not produced after the treatment of serum with β-glucuronidase. Thus, increases in unconjugated bilirubin with UnaG were consistent with decreases in conjugated bilirubin with BOD. The treatment of serum from patients with alcoholic liver disease with β-glucuronidase also increased the level of the bilirubin-UnaG complex, in parallel with a decrease in conjugated bilirubin (unpublished observations). Thus, the treatment of serum with β-glucuronidase, followed by the UnaG method, enabled the quantitative analysis of total bilirubin levels.

To assess the intraday and interday precision of the UnaG method, 3 serum specimens with different concentrations of total bilirubin were used. The reference method used was the BOD method at neutral pH for the measurement of total bilirubin. All coefficient variation values were less than 10% (Supplemental Table 1).

The present method showed that the level of total serum bilirubin increased linearly with that of standard bilirubin up to 2 mg per dL, using 1 μL of serum. In the case of higher concentrations of bilirubin, the dilution of the specimen was required for the estimation.

Level of Bilirubin in Serum

Unconjugated bilirubin and total bilirubin levels in serum were assessed using UnaG. Serum (1 μL) treated without or with β-glucuronidase was incubated with UnaG, and the bilirubin-UnaG complexes formed were measured using the fluorospectrometer. **FIGURE 1A** shows the level of bilirubin treated without or with β-glucuronidase in healthy subjects. In total, 15% to 28% of total bilirubin consisted of conjugated bilirubin in all specimens from healthy controls. In the control experiment, serum total bilirubin was measured with BOD under neutral conditions (pH 7.2).

The results obtained by analyzing 1 μL of serum via the UnaG method were consistent with those by the conventional method (**FIGURE 1B**). Total bilirubin levels in healthy control serum specimens were less than 0.3 mg per dL (**FIGURE 1A**), which was consistent with the data obtained with the standard for the healthy controls.[3]

We then examined total bilirubin levels in serum specimens (0.05–1 μL) from patients with liver diseases who had obstructive jaundice. These diseases included bile duct disease, alcoholic liver disease, hepatic cancer, choledocholithiasis liver failure, and gallbladder disease. Total bilirubin levels of those patients were markedly higher than those of the controls (**FIGURE 1A**) and correlated with the levels obtained using the enzyme method ($R = 0.984828842$; $P < .001$) (**FIGURE 1B**). Thus, less than 1 μL of serum was sufficient to measure serum bilirubin levels via the UnaG method. By using β-glucuronidase, the UnaG method allowed for simultaneous data to be obtained on total and unconjugated bilirubin. Due to the high specificity of UnaG for bilirubin, precise data on total bilirubin levels were obtained from patients with liver diseases. These results indicated that we simultaneously obtained accurate data on conjugated and unconjugated serum bilirubin using a small blood specimen (<1 μL).

Level of Bilirubin in Urine

Examination of urinary urobilinogen was the general method as a marker of the excretion of the bilirubin metabolite. Bilirubin is gen-

FIGURE 1. Comparison of unconjugated and total bilirubin levels in serum by UnaG and bilirubin oxidase (BOD) methods. A, Serum specimens from healthy control individuals and patients with liver diseases treated without or with β-glucuronidase (1 unit) were incubated with UnaG (50 μg of protein) at 37°C for 5 minutes. Fluorescence was directly measured. Total and conjugated bilirubin levels in sera were also examined via the BOD method. Values for unconjugated bilirubin, as meansured by the BOD method, were obtained based on the difference between total and conjugated bilirubin. Data are shown as the mean (SD) of triplicate experiments. Column 1–5, sera from healthy controls; 6, serum from a patient with bile duct disease; 7, serum from a patient with alcoholic liver disease; 8, serum from a patient with hepatic cancer; 9, serum from a patient with choledocholithiasis liver failure; 10, serum a patient with gallbladder disease. B, Correlation of total bilirubin in serum via the UnaG and BOD methods (*n* = 52).

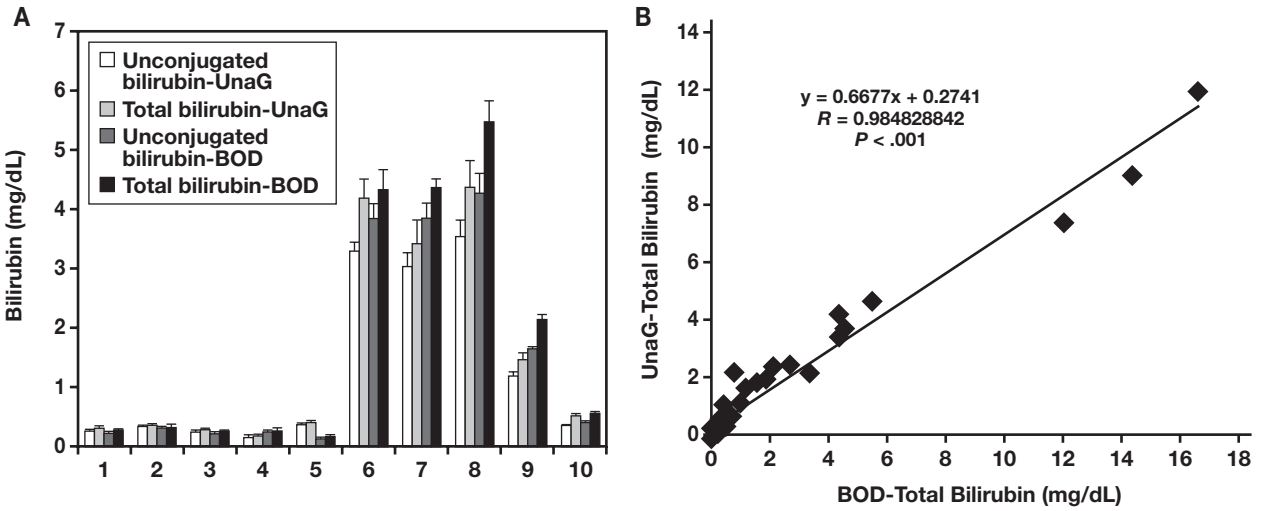

erally not detectable in the urine of healthy individuals, whereas urine from patients with liver diseases contains conjugated bilirubin.[10,19] We examined the level of urinary bilirubin from healthy subjects using BOD, but bilirubin was actually undetectable, due to low sensitivity. Because UnaG exhibits extremely high affinity for bilirubin, and the fluorescence of UnaG associated with bilirubin is highly sensitive (limit of detection, ~10 ng), the UnaG method described herein may be applicable to the measurement of urinary bilirubin using a small volume of urine. The incubation of urine from healthy subjects with UnaG showed a fluorescence profile similar to that observed in serum (Supplementary Figure 1A), indicating that urine from healthy subjects contained a small amount of unconjugated bilirubin.

When urine from healthy controls was treated with β-glucuronidase, bilirubin levels were several-fold higher than those in untreated urine, indicating that a major proportion of bilirubin in normal specimens is conjugated. When urine was separated into a supernatant and pellet by centrifugation at 12,000*g* for 10 minutes, and both fractions were incubated with UnaG, 80% to 90% of bilirubin was detected in the supernatant. Because unconjugated bilirubin is not water-soluble, most bilirubin may associate with excreted compounds, including peptides, lipids, and organic materials, in urine.

In our experimental results, we demonstrated that 0.009 to 0.028 mg/dL of total bilirubin was detected in normal urine, and the average was estimated to be 0.037 mg/g * Cr of total bilirubin, via the UnaG method (**FIGURE 2**, part A and part B). The ratio of conjugated bilirubin to unconjugated bilirubin varied by 1.2- to 10-fold.

Next, we examined urinary bilirubin from patients with liver diseases (**FIGURE 2**, parts A and B), including bile-duct disease, alcoholic liver disease, chronic hepatitis, choledocholithiasis liver failure, and gallbladder disease. In urine from these patients, the urobilinogen test result was positive, and conjugated bilirubin and unconjugated bilirubin levels were 50- to 200-fold higher than those in healthy controls, reaching as much as 2.8 to 19 mg/g * Cr of total bilirubin (**FIGURE 2B**). The ratio of total to unconjugated bilirubin was 1.1- to 1.6-fold.

Other study reports[19,20] revealed that urinary bilirubin was excreted as the conjugated form. The present data from this study show that conjugated bilirubin levels in urine specimens from healthy subjects were much higher than those of unconjugated bilirubin. In contrast, 70% to 85% of total bilirubin was detected as the unconjugated form in the urine of patients with liver diseases.

The ratio of urinary conjugated to unconjugated bilirubin was similar to that in serum. Excess bilirubin in blood did not change to other metabolites, with liver damage and remaining unmetabolized bilirubin leaked (excreted) into urine (**FIGURE 1A** and **FIGURE 2B**), thereby decreasing the ratio of conjugated to unconjugated bilirubin. Although urinary bilirubin from healthy subjects was not detected via the BOD method, the UnaG method enabled us to examine small amounts of unconjugated and total bilirubin. Further, comparisons of total bilirubin levels in the urine of patients with liver damage between the UnaG and enzyme methods revealed good agreement (**FIGURE 2C**). Thus, the examination of bilirubin with UnaG contributes to the sensitive detection of bilirubin.

Spot Test of Bilirubin in Serum and Urine

We performed a spot test of bilirubin in serum and urine as a simple examination to estimate bilirubin levels. After the incubation of bilirubin with UnaG for 5 minutes, the mixtures were spotted onto filter paper. Supplemental Figure 3A shows the fluorescence of the bilirubin-

FIGURE 2. Unconjugated and total bilirubin levels in urine. A, Urine (10–25 µL) from healthy controls (n = 51) and urine (1 µL) from patients with liver diseases (n = 21) were treated with or without β-glucuronidase and then incubated with UnaG at 37°C for 5 minutes. The fluorescence of the bilirubin-UnaG complex was measured. B, Creatinine corrections were performed; urinary bilirubin is expressed as bilirubin (mg) by Cr (g). C, Comparison of total bilirubin in urine by the UnaG and bilirubin oxidase (BOD) methods. Urine specimens from patients with liver diseases were analyzed, as described herein. Data are shown as the mean (SD) of triplicate experiments. Serum specimens (listed by column number) are from the following individuals: 1, urine from a patient with bile duct disease; 2 and 3, urine from patients with alcoholic liver disease; 4, urine from a patient with choledocholithiasis liver failure; and 5, urine from a patient with gallbladder disease.

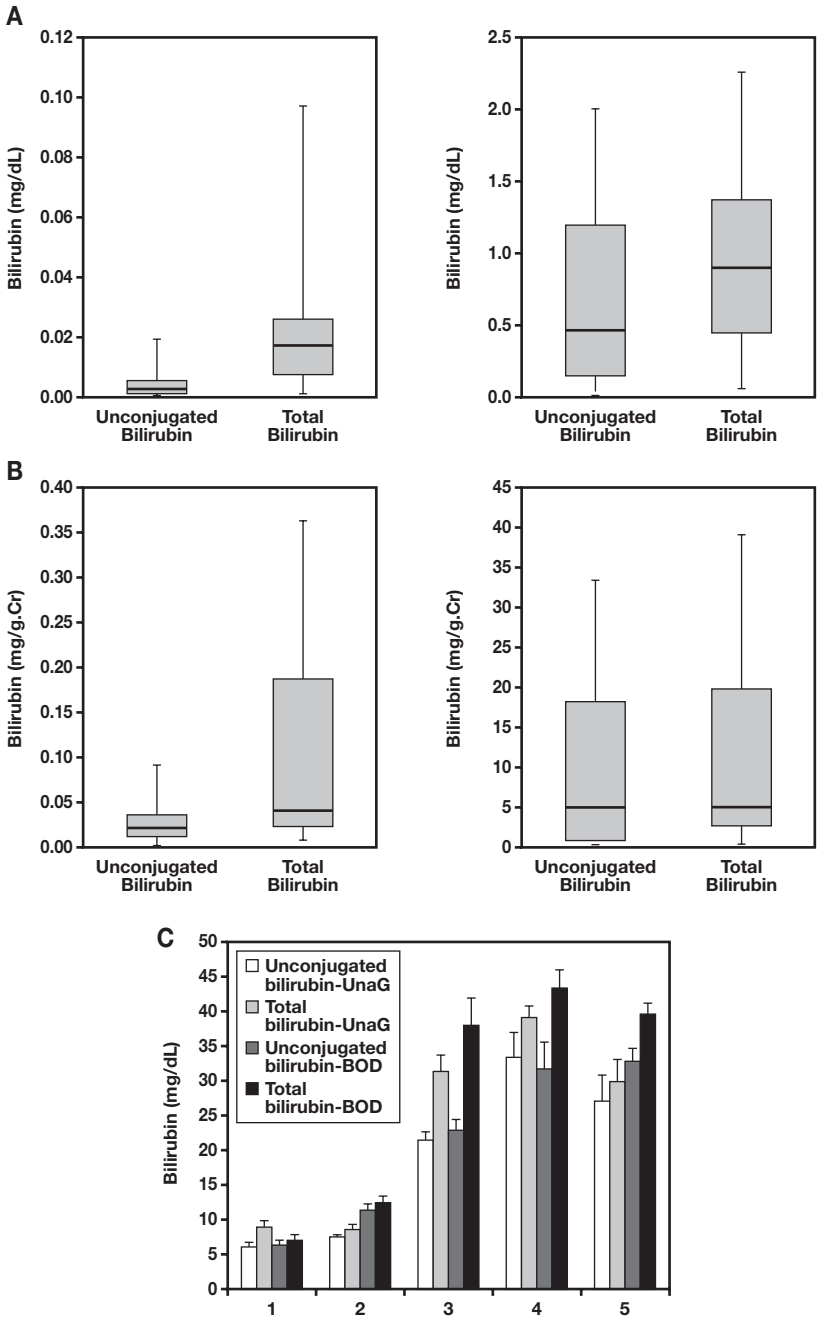

UnaG complex exposed to the Fluoro blue/green LED lamp. The fluorescence intensity increased with the increase in the amount of bilirubin. We confirmed that the fluorescence intensity was higher in the sera of the patients with liver diseases than in those of control subjects (**FIGURE 3A**). The treatment of serum from patients with liver diseases with β-glucuronidase lead to a small difference in the intensity of the fluorescence (Supplemental Figure 3B).

Regarding urine from the patients, the high background of the broad fluorescence due to the presence of unknown metabolites was observed without UnaG, but the treatment with UnaG led to an

FIGURE 3. Spot test of serum and urinary bilirubin with UnaG. Sera and urine specimens were treated without or with UnaG (10 μg). The mixture was drawn and spotted onto filter paper, which was then exposed to the Fluoro blue/green LED lamp. A, Effect of the serum volume. Serum specimens (listed by column number) are from the following individuals: 1–3, healthy controls; 4, a patient with alcoholic liver disease; 5, a patient with chronic hepatitis; and 6, a patient with gallbladder disease. B, Effect of the urine volume. Urine specimens (listed by column number) are from the following individuals: 1, 2, healthy controls; 3, a patient with alcoholic liver disease; 4, a patient with gallbladder disease.

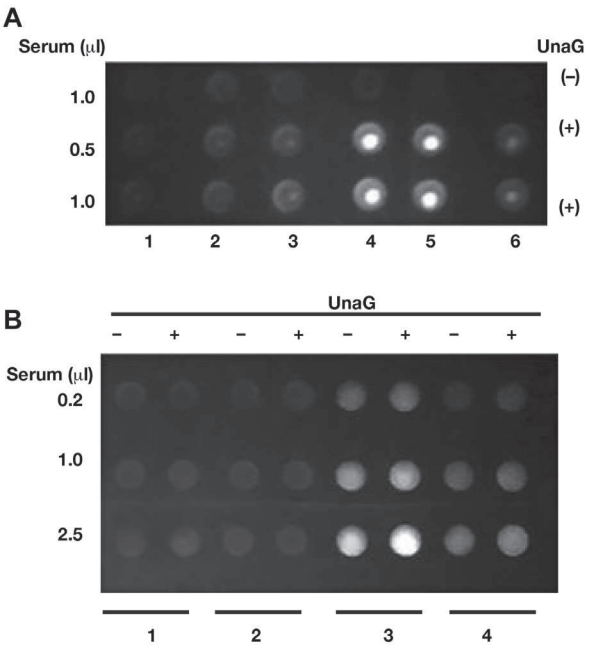

increase in the green fluorescence derived from bilirubin (**FIGURE 3B** and Supplemental Figure 3C). Therefore, fluorescent images obtained using this simple method provide useful information for estimating bilirubin levels in blood and urine.

Discussion

Several methods to measure bilirubin have been widely used; however, the findings obtained varied in a method-dependent manner.[9,10] We developed the UnaG fluorescene-based method for the determination of bilirubin in serum and urine, and found that the treatment of with β-glucuronidase led to the simultaneous measurement of unconjugated and conjugated bilirubin. The advantage of this method is that it enables simple, rapid, and accurate measurement with a small volume of specimens.

There is a limitation in the proposed method. The total bilirubin in serum by the UnaG method did not include δ-bilirubin, covalently bound to albumin. δ-Bilirubin increases in the sera of patients with severe jaundice.[21] Because only unconjugated bilirubin is associated with UnaG, values of total bilirubin, as determined by the UnaG method, were lowered, compared with those by the enzyme method (**FIGURE 1B**).

The conventional methods using chemical reagents or enzymes often led to false negatives and positives by various ingredients in urine.[9,20] During the present study, the urinary bilirubin from healthy controls was undetectable by the BOD method due to low sensitivity, or false values for bilirubin were observed due to the broad substrate specificity of the enzyme. Because UnaG has extremely high specificity for bilirubin with high affinity, its use is advantageous for this measurement.

We found that urine from healthy subjects contained low levels of conjugated and unconjugated bilirubin, and obtained 0.037 mg/g * Cr of total bilirubin as the normal value in control urine. Urinary bilirubin levels in urobilinogen-positive urine markedly increased with liver damage (50- to 200-fold that of the controls). Although conjugated bilirubin is easily excreted into urine, the results of this study showed that unconjugated bilirubin was the major form in urine specimens from patients with liver diseases. Due to the appearance of urinary bilirubin in several disorders,[7] such highly sensitive measurement of urinary bilirubin can be useful to identify the microdamage in biliary, glomerular, or other extrahepatic tissues.

Previous study reports[19,20] mentioned that the presence of urinary bilirubin strongly correlated with elevations in serum bilirubin levels. In our study findings, we demonstrated that liver dysfunction (including alcoholic liver disease, chronic hepatitis, choledocholithiasis liver failure, gallbladder disease, and biliary obstruction) increased urinary bilirubin levels in a manner that was dependent on changes in urobilinogen levels. However, the urinary bilirubin level was not predictive of an abnormal liver function test result because the serum bilirubin was also elevated by hemolysis.

The presence of urinary bilirubin was shown to be highly specific for elevated serum bilirubin levels due to hepatocellular or biliary tree injury rather than intravascular hemolysis. However, an increase in urobilinogen is attributed to hemolysis.[20] Otherwise, findings obtained from urinary bilirubin via urinalysis dipstick testing are ambiguous. We did not have any opportunities to examine urinary bilirubin in patients with hemolysis.

Because the UnaG method is highly sensitive, it will be interesting to examine the relation of variations of urinary bilirubin to those of urobilinogen of patients with hemolysis. The simple spot test of urinary bilirubin with UnaG showed that urinary total bilirubin levels may facilitate the differentiation between RBC hemolysis, liver diseases, and biliary obstruction. The accurate diagnosis of internal diseases, such as jaundice and other disorders, may be achieved by extending the UnaG method to urine and serum.

In conclusion, we have established procedures that combine the UnaG method with the deconjugation enzyme method for the examination of total bilirubin in urine and serum. This highly sensitive technique has application in the estimation and/or detection of a trace amount of urinary and serum bilirubin in patients with various diseases, for which usual methods give ambiguous results.

Acknowledgments

We thank A. Miyawaki, PhD, for the gift of the UnaG expression vector. This work was supported in part by grants from the Ministry of Health, Labor and Welfare of Japan (H30-Nanchi-R-021).

Personal and Professional Conflicts of Interest

None declared.

Supplementary Data

Supplemental figures and tables can be found in the online version of this article at www.labmedicine.com.

REFERENCES

1. Gollan JL, Schmid R. Bilirubin update: formation, transport, and metabolism. *Prog Liver Dis.* 1982;7:261–283.
2. Sticova E, Jirsa M. New insights in bilirubin metabolism and their clinical implications. *World J Gastroenterol.* 2013;19(38):6398–6407.
3. Vítek L, Ostrow JD. Bilirubin chemistry and metabolism; harmful and protective aspects. *Curr Pharm Des.* 2009;15(25):2869–2883.
4. Levitt DG, Levitt MD. Quantitative assessment of the multiple processes responsible for bilirubin homeostasis in health and disease. *Clin Exp Gastroenterol.* 2014;7:307–328.
5. McDonagh AF, Vreman HJ, Wong RJ, Stevenson DK. Photoisomers: obfuscating factors in clinical peroxidase measurements of unbound bilirubin? *Pediatrics.* 2009;123(1):67–76.
6. Chowdhury JR, Chowdhury NR. Conjugation and excretion of bilirubin. *Semin Liver Dis.* 1983;3(1):11–23.
7. Bräsen JH, Mederacke Y-S, Schmitz J, et al. Cholemic nephropathy causes acute kidney injury and is accompanied by loss of aquaporin 2 in collecting ducts. *Hepatology.* 2019;69(5):2107–2119.
8. Nakayama K. Differences between enzymatic and diazo methods for measuring direct bilirubin. *Eur J Clin Chem Clin Biochem.* 1995;33(8):513–517.
9. Echeverry G, Hortin GL, Rai AJ. Introduction to urinalysis: historical perspectives and clinical application. *Methods Mol Biol.* 2010;641:1–12.
10. Foley KF, Wasserman J. Are unexpected positive dipstick urine bilirubin results clinically significant? A retrospective review. *Lab Med.* 2014;45(1):59–61.
11. Kumagai A, Ando R, Miyatake H, et al. A bilirubin-inducible fluorescent protein from eel muscle. *Cell.* 2013;153(7):1602–1611.
12. Takeda T-A, Mu A, Tai TT, Kitajima S, Taketani S. Continuous *de novo* biosynthesis of haem and its rapid turnover to bilirubin are necessary for cytoprotection against cell damage. *Sci Rep.* 2015;5:10488.
13. Liem PH, Mu A, Kikuta S, Ohta K, Kitajima S, Taketani S. A simple and highly sensitive method of measuring heme oxygenase activity. *Biol Chem.* 2015;396(11):1265–1268.
14. Iwatani S, Nakamura H, Kurokawa D, et al. Fluorescent protein-based detection of unconjugated bilirubin in newborn serum. *Sci Rep.* 2016;6:28489.
15. Adeosun SO, Moore KH, Lang DM, Nwaneri AC, Hinds TD Jr, Stec DE. A novel fluorescence-based assay for the measurement of biliverdin reductase activity. *React Oxyg Species (Apex).* 2018;5(13):35–45.
16. Otsuji S, Mizuno K, Ito S, Kawahara S, Kai M. A new enzymatic approach for estimating total and direct bilirubin. *Clin Biochem.* 1988;21(1):33–38.
17. Sulistyaningdyah WT, Ogawa J, Tanaka H, Maeda C, Shimizu S. Characterization of alkaliphilic laccase activity in the culture supernatant of Myrothecium verrucaria 24G-4 in comparison with bilirubin oxidase. *FEMS Microbiol Lett.* 2004;230(2):209–214.
18. Shinya F, Toshima T, Takahashi W, Suzuki N. Effects of pH on the deconjugation of conjugated bilirubin in human bile. *Tohoku J Exp Med.* 1985;147(3):281–293.
19. Tiribelli C, Ostrow JD. Intestinal flora and bilirubin. *J Hepatol.* 2005;42(2):170–172.
20. Urinalysis. In: *Clinical Methods: The History, Physical, and Laboratory Examinations*. Butterworths; 1990. ISBN 9780409900774.
21. Kozaki N, Shimizu S, Higashijima H, et al. Significance of serum delta-bilirubin in patients with obstructive jaundice. *J Surg Res.* 1998;79(1):61–65.

Application of QuantiFERON ELISA for Detection of Interferon-Gamma Autoantibodies in Adult-Onset Immunodeficiency Syndrome

Rommanee Khositnithikul, PhD,[1,2]✉ Wannada Laisuan, MD,[3] Chavachol Setthaudom, MSc,[2] Kanchana Sriwanichrak, MSc,[2] Mongkol Kunakorn, MD,[2] Toemsak Srikhirin, PhD,[4] Putthapoom Lumjiaktase, PhD,[2] Apirom Vongsakulyanon, MD, PhD[2,]✉*

[1]Clinical Pathology Programme, Faculty of Medicine, Ramathibodi Hospital, Mahidol University, Bangkok, Thailand; [2]Department of Pathology, Faculty of Medicine, Ramathibodi Hospital, Mahidol University, Bangkok, Thailand; [3]Division of Allergy, Immunology and Rheumatology, Department of Medicine, Faculty of Medicine, Ramathibodi Hospital, Mahidol University, Bangkok, Thailand; [4]Department of Physics, Faculty of Science, Mahidol University, Bangkok, Thailand; *To whom correspondence should be addressed. apirom_odd@yahoo.com

Keywords: interferon-gamma autoantibodies, adult-onset immunodeficiency syndrome, QuantiFERON, enzyme-linked immunosorbent assay, neutralization assay

Abbreviations: IFN-ɣ autoAbs, interferon-gamma autoantibodies; AOID, adult-onset immunodeficiency; ELISA, enzyme-linked immunosorbent assay; dNTM, disseminated nontuberculous mycobacteria; nAIGA, neutralizing anti-IFN-ɣ autoAbs; TB, tuberculosis; OD, optical density; SD, standard deviation.

Laboratory Medicine 2022;53:12–17; DOI: 10.1093/labmed/lmab039

ABSTRACT

Objective: Patients who develop interferon-gamma autoantibodies (IFN-ɣ autoAbs) in adult-onset immunodeficiency (AOID) syndrome are more likely to develop opportunistic and recurrent intracellular infections. The assay to detect IFN-ɣ autoAbs is essential for the diagnosis and therapeutic monitoring of AOID syndrome. Therefore, this study applied the QuantiFERON assay for the detection of IFN-ɣ autoAbs.

Methods: Serum from patients with AOID syndrome (n = 19) and serum from healthy patients (n = 20) was collected and applied using 2 neutralizing platforms of enzyme-linked immunosorbent assay (ELISA) kits (the BD ELISA and the QuantiFERON ELISA) for IFN-ɣ autoAbs detection.

Results: The pooled serum from patients with AOID syndrome showed >50% inhibition at 1:5000 dilution (positive), whereas the pooled serum from healthy patients showed <50% inhibition at 1:5000 dilution (negative) according to the neutralizing QuantiFERON ELISA. Each specimen showed the same result according to both the neutralizing BD ELISA and the neutralizing QuantiFERON ELISA. Moreover, the patient serum showed a variation in titer ranging from 1:5000 to >1:5,000,000 according to the neutralizing QuantiFERON ELISA.

Conclusion: The QuantiFERON ELISA kit could be applied for the detection of IFN-ɣ autoAbs for the diagnosis and therapeutic monitoring of AOID syndrome.

Interferon-gamma (IFN-ɣ) plays a crucial role in host defense against intracellular organisms, especially mycobacterial infections.[1-3] Patients who develop IFN-ɣ autoantibodies (IFN-ɣ autoAbs), especially among Asian populations, gain the risk of recurrent disseminated nontuberculous mycobacteria (dNTM) infection.[4-8] Research has shown that IFN-ɣ autoAbs have the ability to neutralize and disturb the activity of IFN-ɣ function.[5,9-11] The first reports of neutralizing anti-IFN-ɣ autoAbs (nAIGA) associated with the dNTM infection were published in 2004.[12,13] More recently, nearly 200 patients with high levels of the IgG antibody against IFN-ɣ were reported.[8] The amount of IFN-ɣ autoAbs influences clinicians' decision regarding treatment.[11] The high titers of IFN-ɣ autoAbs (>1:100,000 dilution) indicate a high chance for recurrent dNTM infection.[11] Therefore, the amount of IFN-ɣ autoAbs is necessary to determine for monitoring the disease. Moreover, recent studies have shown that the presence of nAIGA capacity is more important than the antibody concentration itself for determining the predisposition for a disease.[5,7] Those patients with negative HIV status who develop IFN-ɣ autoAbs associated with the dNTM infection are diagnosed with what is called adult-onset immunodeficiency (AOID) syndrome.[14-16]

The diagnosis and treatment for AOID syndrome is challenging because of the variation in the analytical assays.[17-19] Several methods that have been developed, such as the in-house assays, eg, the particle-based assay, the enzyme-linked immunosorbent assay (ELISA), the Dot-ELISA, and flow cytometry, are limited only to a few laboratories.[7,16,17,20,21] Most previous studies applied the neutralizing ELISA for the detection of IFN-ɣ autoAbs.[16,22] However, there has been no standard method, and the variation between each method makes the result difficult to compare.

QuantiFERON-tuberculosis (TB) is one of the IFN-ɣ release assays based on the ELISA part of the assay to measure IFN-ɣ in response to the specific TB antigen[20] and has been used as the worldwide commercial test

for the diagnosis of latent TB.[23,24] According to Suárez and colleagues,[19] the mitogen component of the whole blood QuantiFERON-TB in-tube assay can be used for the detection of clinically relevant IFN-ɤ autoAbs. By using QuantiFERON-TB, the IFN-ɤ autoAbs levels are readily measured and there is less variation in the test results. This study focused on the utilization of QuantiFERON-TB for the detection of nAIGA in patients with dNTM infection by using only the ELISA part of the QuantiFERON-TB assay.

Methods

Study Population

Nineteen specimens of serum from patients with AOID syndrome and 20 specimens of serum from healthy patients were included in this study. All patients had an average age of 54 years (ranging from 40 to 65 years). Seven patients with AOID syndrome were female (37%) and 12 were male (63%). All patients had HIV-negative status with a history of recurrent intracellular pathogen infection (dNTM, *Mycobacterium* spp., *Salmonella* spp., *Cryptococcus* spp., herpes simplex virus, and herpes zoster virus) as shown in Supplemental Data Table 1.

The bacterial pathogens were detected from blood or tissue culture and the virus by was detected using real-time polymerase chain reaction. The bacterial species (spp.) were identified using a standard biochemical technique except for *Mycobacterium* spp., which was identified using a sequencing technique. Serum from healthy patients was obtained from participants ages 20 to 50 years without underlying disease, no current drugs taken, and testing negative for anti-HIV antibodies, hepatitis B antigen, and anti-hepatitis C antibodies (Architect i2000 analyzer). This study was conducted through the approval of the Ethics Clearance Committee on Human Right related to research involving human patients at the Faculty of Medicine, Ramathibodi Hospital, Mahidol University (Bangkok, Thailand).

Specimen Collection and Preparation

The specimens from the patients with AOID syndrome and the healthy patients were centrifuged at 1000 g for 10 minutes. The specimens were separated, aliquoted, and stored at –70°C before use. The pooled patient serum was the pool of equal volume (10 µL) from each patient's specimen (n = 19). The pooled healthy serum was the pool of equal volume (10 µL) from each healthy patient specimen (n = 20). Both of the pooled serum specimens were used to determine the optimal dilution for IFN-ɤ autoAbs detection and served as the positive and negative control in each experiment.

Standard Curve of BD and QuantiFERON ELISA

For the BD ELISA standard curve, 100 mL of each standard IFN-ɤ antigen at 0, 9.4, 18.8, 37.5, 75, 150, and 300 pg/mL were added into each well. For the QuantiFERON standard curve, 50 mL of standard IFN-ɤ at 0, 0.25, 1 and 4 international units (IU/mL) were added into each well. Each concentration of standard was done in duplicate. The following steps were carried out as described per the instruction manual of each company. The instruction manual of the BD ELISA (catalog number 555142) can be found at https://www.bdbiosciences.com/ds/pm/tds/555142.pdf, and the instruction manual of the QuantiFERON ELISA (catalog number 622130) can be found at https://www.quantiferon.com/us. The 4-parameter logistic curve fit was used to create a standard curve. The graph was plotted between the concentrations of the standard IFN-ɤ antigen on the *x* axis and the optical density (OD) was plotted at 450 nm on the *y* axis. In addition, the QuantiFERON ELISA kit had its own acceptable quality control criteria (**TABLE 1**).

Neutralizing BD ELISA

The OptEIA human IFN-ɤ ELISA kit II is a sandwich ELISA used to detect the IFN-ɤ antigen in human serum (BD Biosciences, San Diego, CA). The procedure was adapted from the original manual protocol by adding a neutralization step for IFN-ɤ autoAbs detection. The patient serum at dilution 1:5000 was incubated with 100 pg/mL of the standard IFN-ɤ at a final volume of 100 µ L at 37°C for 1 hour. The following steps were performed as described in the instruction manual. The results were reported as the percentage of inhibition. The formula for percentage of inhibition is 100 – {[OD of neutralizing specimen (pg/mL)/OD of standard IFN-ɤ 100 pg/mL] × 100} as used for these calculations.[25] Any patient serum with a percentage of inhibition of >50% was defined as positive.

Neutralizing QuantiFERON ELISA

The QuantiFERON-TB gold plus (QFT-Plus) was applied, and only the ELISA part was used for the detection of IFN-ɤ autoAbs by adding the neutralization step (the diluted serum was incubated with standard IFN-ɤ) (Qiagen, Hilden, Germany). The optimal dilution for IFN-ɤ autoAbs detection was attained using 10-fold serial dilution of the pooled patient serum and the pooled healthy serum from 1:50 to 1:500,000,000. Each dilution was incubated with 2 IU/mL of standard IFN-ɤ antigen at 37°C for 1 hour. The following steps were performed as described in the instruction manual. The optimal dilution at 1:5000 was further used in each serum specimen to detect IFN-ɤ autoAbs. The results were reported as the percentage of inhibition. The formula of percentage of inhibition is 100 – {[OD of neutralized serum (IU/mL)/OD of standard IFN-ɤ 2 IU/

TABLE 1. Passing Criteria of QuantiFERON ELISA Standard Curve and Results of Quality Control

IFN-ɤ Concentration	Passing Criteria	Results (Mean ± SD)[c]
0 IU/mL	OD ≤0.15	0.008 ± 0.005
	Variation of duplicate OD[a] ≤ 0.04	0.008 ± 0.013
0.25 IU/mL	Variation of duplicate OD[a] ≤ 0.04	0.01 ± 0.006
1 IU/mL	%CV[b] of duplicate OD ≤15	4.65 ± 3.44
4 IU/mL	OD ≥0.6	0.76 ± 0.09
	%CV of duplicate OD ≤15	4.02 ± 3.48
Correlation coefficient	*r* ≥0.98	0.999 ± 0.001

ELISA, enzyme-linked immunosorbent assay; IFN-ɤ, interferon-gamma; OD, optical density; SD, standard deviation.
[a]*Variation of duplicate OD was the absolute different value between the duplicates.*
[b]*Percentage of coefficient of variation (%CV) was calculated from SD/mean × 100 of the duplicates.*
[c]*Mean ± SD of the 10 standard curves (each standard curve passing all criteria)*

mL] × 100} used for calculation.[25] Any patient serum with a percentage of inhibition of >50% at a dilution of 1:5000 was defined as positive.

Statistical Analysis

The correlations between the percentage of inhibition from the BD ELISA and the QuantiFERON ELISA were analyzed by STATA 15 using the Pearson correlation coefficient.

Results

Different concentrations of standard IFN-ɣ were used to create the standard curves: 0 to 300 pg/mL with the BD ELISA, and 0 to 4 IU/mL with the QuantiFERON ELISA. The graphs were plotted between the concentrations of the standard IFN-ɣ antigen on the *x* axis and the OD was plotted at 450 nm on the *y* axis. The correlation coefficient (*r*) of the standard curves by 4-parameter logistic curve fit with the BD ELISA and the QuantiFERON ELISA were nearly equal to 1 (**FIGURE 1**). Ten standard curves with the QuantiFERON ELISA passed all quality control criteria, and the results are represented by mean ± standard deviation (SD; **TABLE 1**).

To evaluate the optimal dilution for the detection of IFN-ɣ autoAbs using the neutralizing QuantiFERON, the percentage of inhibition of the pooled patient serum and the pooled healthy serum at dilutions of 1:50 to 1:500,000,000 were performed. The pooled patient serum (as positive)

FIGURE 1. The standard curve of the BD ELISA (A) and the QuantiFERON ELISA (B). The standard concentration of human IFN-ɣ antigen at a concentration of 0 to 300 pg/mL using the BD ELISA and 0 to 4 IU/mL using the QuantiFERON ELISA were plotted on the *x* axis against the OD at 450 nm on the *y* axis. ELISA, enzyme-linked immunosorbent assay; IFN-ɣ, interferon-gamma.

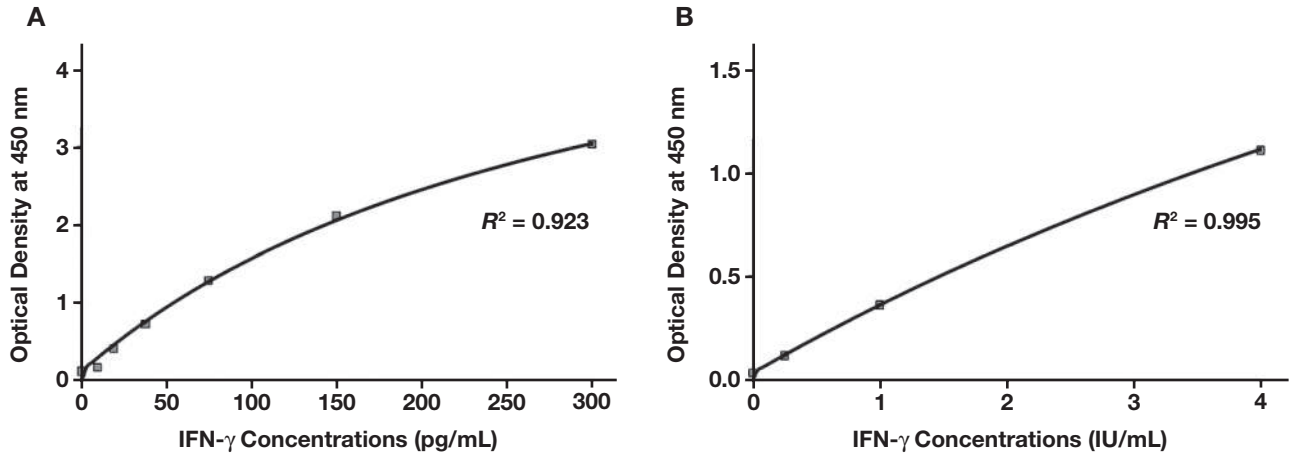

FIGURE 2. The optimal dilution of the neutralizing QuantiFERON ELISA. The pooled patient serum (positive) and the pooled healthy serum (negative) at the dilution of 1:5000 showed clear discrimination, whereas the dilution of > 1:50,000 showed an equivocal result with no discrimination. ELISA, enzyme-linked immunosorbent assay.

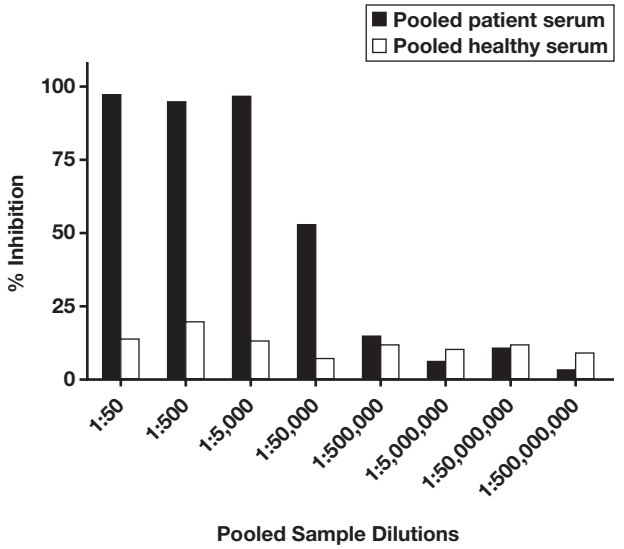

FIGURE 3. The comparison of percentage of inhibition using the neutralizing BD and the neutralizing QuantiFERON ELISA. The result shows the percentage of inhibition of each patient serum specimen (n = 19) and each healthy patient serum specimen (n = 20) at the titer of 1:5000 using the neutralizing BD ELISA (triangles) and the neutralizing QuantiFERON ELISA (squares). Each pair of triangle and square marks on the same vertical axis was derived from the same specimen. ELISA, enzyme-linked immunosorbent assay.

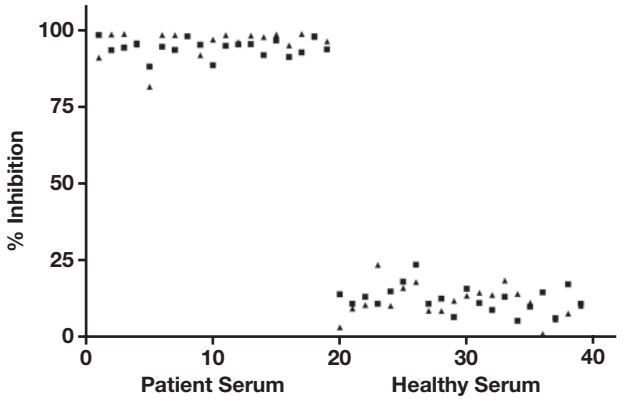

and the pooled healthy serum (as negative) at a dilution of 1:50 to 1:5000 clearly showed discrimination, whereas the dilution at 1:50,000 showed an equivocal result with no discrimination (**FIGURE 2**).

Both the neutralizing BD and neutralizing QuantiFERON ELISA discriminated between the patient serum (>50% inhibition) and the healthy serum (<50% inhibition) at a dilution of 1:5000 in all specimens (**FIGURE 3**). The percentage of inhibition of the 19 specimens from patients with AOID syndrome using the neutralizing BD ELISA was 96.1% ± 4.2% (mean ± SD) and using the neutralizing QuantiFERON ELISA was 94.1% ± 2.8%. The percentage of inhibition of the 20 specimens from healthy patients using the neutralizing BD ELISA was 11.9% ± 5.3% (mean ± SD) and using the neutralizing QuantiFERON ELISA was 12.8% ± 4.3% (mean ± SD). The percentage of inhibition using these 2 assays had a strong correlation (r = .992, P >.05).

The titer was the last dilution with >50% inhibition and in each patient showed the variation of the IFN-ɣ autoAbs titer. For example, the patient titer numbers 1, 6, 14, and 19 were 1:5000, 1:50,000, 1:500,000, and 1:5,000,000, respectively (**FIGURE 4**). The titer of IFN-ɣ autoAbs from the 19 patients with AOID syndrome was equally distributed along the range of 1:5000 to 1:500,000 (4–5 patients per titer) except for the titer >1:5,000,000 (only 2 patients; **TABLE 2**).

Discussion

The standard curve for IFN-ɣ measurement of the BD ELISA and the QuantiFERON ELISA used the different units of concentration (pg/mL and IU/mL); however, IU/mL could be converted to pg/mL by multiplying with 40 (x40).[26] From the results, the efficacy of IFN-ɣ measurement using the QuantiFERON ELISA was not better than the efficacy using the BD ELISA, but the advantage of the QuantiFERON ELISA over the BD ELISA was the quality control system. The quality control system and passing criteria of the QuantiFERON ELISA were defined by the manufacturer as being designed for in vitro diagnostic purposes, whereas the BD ELISA manual does not mention the quality control system and passing criteria because it was designed for the research use only. The quality control system of the QuantiFERON ELISA was based on the passing criteria of the standard curve, as shown in **TABLE 1**. All criteria must pass before an experiment was performed to ensure that no variation of reagent lots or a poor laboratory skill could affect the results. Each criterion of the quality control system had its own purpose. For example, the criterion of the standard IFN-ɣ 0 IU/mL with an OD <0.15 indicated acceptable background signaling. An OD >0.15 could result from an inadequate washing step or from nonspecific absorption of reporting antibodies. The criterion of the standard IFN-ɣ 4 IU/mL with OD ≥0.6 indicated the stability of the reagents (especially the standard IFN-ɣ). An OD <0.6 could result from degraded reagents. In addition, the criterion of the duplicated IFN-ɣ 0 and 0.25 IU/mL with an OD difference ≤0.04 indicated an acceptable variation of a repeated result (precision) when measuring the IFN-ɣ at a low concentration.[27] An OD >0.04 could result from inconsistency in the testing process, such as a pipetting error, over/inadequate washing, or improper time of incubation/stopping reaction.[27] The criterion of IFN-ɣ 1 and 4 IU/mL with a percentage of coefficient of variation (%CV) ≤15 indicated adequate precision when the IFN-ɣ was measured at high concentration; a percentage of coefficient of variation >15 could result from an inconsistency in the testing process. Finally, the criterion of the correlation coefficient ≥0.98 indicated an excellent interpolation of the standard curve. If the correlation coefficient was <0.98, then the standard curve could not correctly predict the concentration of the unknown. The cause could be any of the above errors, and a new standard curve could be generated.

We used IFN-ɣ 2 IU/mL in the neutralizing step of the QuantiFERON ELISA because IFN-ɣ 2 IU/mL was the concentration around the middle of the standard curve (**FIGURE 1**). When IFN-ɣ was neutralized by IFN-ɣ autoAbs, the change in the OD value (percentage of inhibition) was more conspicuous than the concentration at the upper end or the lower end of the standard curve. In addition, IFN-ɣ 100 pg/mL (2.5 IU/mL) was used in the neutralizing step of the BD ELISA for the same reason (**FIGURE 1**). The pooled patient serum (positive control) and the pooled healthy serum (negative control) were used to determine the optimal dilution for IFN-ɣ autoAbs using the neutralizing QuantiFERON ELISA. The serum dilution at 1:5000 was selected because it was the last dilution that could clearly discriminate between the patient serum and the healthy serum (**FIGURE 2**), and this dilution was also utilized in previous research.[25] The serum dilutions at 1:50 and 1:500 could also discriminate between the patient serum and the healthy serum (**FIGURE 2**) but were not used to avoid the false-positive results in some healthy serums.[28] The purpose of the pooled patient serum was only to define the optimal dilution (not for diagnostic purposes)

TABLE 2. Amount of Patients with AOID Syndrome at Each Serum Dilution Titer of IFN-ɣ autoAbs.

Serum Dilutions	Number of Patients
1:5000	4
1:50,000	4
1:500,000	5
1:5,000,000	4
>1:5,000,000	2

AOID, adult-onset immunodeficiency disease; IFN-ɣ autoAbs, interferon-gamma autoantibodies.

FIGURE 4. IFN-ɣ autoAbs titers in patients with AOID syndrome using the neutralizing QuantiFERON ELISA. The graph shows the percentage of inhibition of patient numbers 1, 6, 14, and 19 at serum dilution 1:5000, 1:50,000, 1:500,000, and 1:5,000,000, respectively and * was the titer of each patient. AOID, adult-onset immunodeficiency; ELISA, enzyme-linked immunosorbent assay.

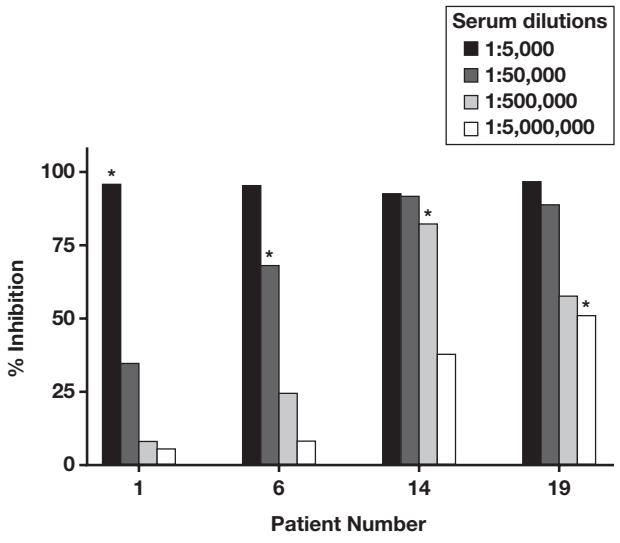

to evaluate the diagnostic performance at this particular dilution; the individual patient serum was measured and interpreted separately. Both the neutralizing BD and the neutralizing QuantiFERON ELISA could discriminate between all the patient serums and all the healthy serums without the false-positive or false-negative results. Moreover, the results from both assays were concordant, with a strong correlation (r = 0.992; **FIGURE 3**). Therefore, the neutralizing QuantiFERON ELISA could be interchangeable with the neutralizing BD ELISA (reference method) for IFN-γ autoAbs detection. The titer of IFN-γ autoAbs was able to monitor and follow up the treatment in patients with AOID syndrome.[8,15,16] The variable of IFN-γ autoAbs titers (ranging from 1:5000 to 1:5,000,000) could be detected using the neutralizing QuantiFERON ELISA (**TABLE 2**). The range of titers corresponded to those in previous studies that ranged from 1:400 to 1:6,553,600.[16] The appropriate range and ratio of dilution were required for further study to validate the severity of the disease and the response to treatment.

The limitation of this study was the small amount of patients with AOID syndrome (because of the rare disease), so the false-positive and the false-negative results were not observed. The blank signals in the ELISA were not measured and were not subtracted from each OD result. However, there was little effect on the percentage of inhibition because it was derived from the difference between the nonneutralizing OD result and the neutralizing OD result (the background signal was partly subtracted). The appropriate range and ratio of dilution were not investigated. Moreover, the 2 patients with AOID syndrome with an IFN-γ autoAbs titer >1:5,000,000 were not defined at the end point titer, because the result may be prone to dilutional error.

Conclusion

Both the commercially available test kits, QuantiFERON ELISA and BD ELISA, can be utilized for IFN-γ autoAbs detection and showed a the strong correlation between the assays. However, the QuantiFERON ELISA was better than the BD ELISA for in vitro diagnosis because of the quality control system that could guarantee the accuracy of the results. Moreover, the QuantiFERON ELISA is available (usually for the diagnosis of latent TB) in many laboratories. Hence, the test is readily accessible without the need to maintain another test kit (especially for a rare disease such as AOID syndrome) and can present the results as a single standard.

Supplementary Data

Supplemental figures and tables can be found in the online version of this article at www.labmedicine.com.

Conflict of Interest

The authors declared that there was no conflict of interest.

REFERENCES

1. Belardelli F. Role of interferons and other cytokines in the regulation of the immune response. *APMIS.* 1995;103(3):161–179.
2. Schroder K, Hertzog PJ, Ravasi T, Hume DA. Interferon-gamma: an overview of signals, mechanisms and functions. *J Leukoc Biol.* 2004;75(2):163–189.
3. Wu UI, Holland SM. Host susceptibility to non-tuberculous mycobacterial infections. *Lancet Infect Dis.* 2015;15(8):968–980.
4. Browne SK. Anticytokine autoantibody-associated immunodeficiency. *Annu Rev Immunol.* 2014;32:635–657.
5. Kampmann B, Hemingway C, Stephens A, et al. Acquired predisposition to mycobacterial disease due to autoantibodies to IFN-gamma. *J Clin Invest.* 2005;115(9):2480–2488.
6. Chetchotisakd P, Kiertiburanakul S, Mootsikapun P, Assanasen S, Chaiwarith R, Anunnatsiri S. Disseminated nontuberculous mycobacterial infection in patients who are not infected with HIV in Thailand. *Clin Infect Dis.* 2007;45(4):421–427.
7. Browne SK, Burbelo PD, Chetchotisakd P, et al. Adult-onset immunodeficiency in Thailand and Taiwan. *N Engl J Med.* 2012;367(8):725–734.
8. Hase I, Morimoto K, Sakagami T, Ishii Y, van Ingen J. Patient ethnicity and causative species determine the manifestations of anti-interferon-gamma autoantibody-associated nontuberculous mycobacterial disease: a review. *Diagn Microbiol Infect Dis.* 2017;88(4):308–315.
9. Aoki A, Sakagami T, Yoshizawa K, et al. Clinical significance of interferon-gamma neutralizing autoantibodies against disseminated nontuberculous mycobacterial disease. *Clin Infect Dis.* 2018:66(8):1239–1245.
10. Kim K, Waterer G, Thomson R, et al. Levels of anti-cytokine antibodies may be elevated in patients with pulmonary disease associated with non-tuberculous mycobacteria. *Cytokine.* 2014;66(2):160–163.
11. Chi CY, Lin CH, Ho MW, et al. Clinical manifestations, course, and outcome of patients with neutralizing anti-interferon-γ autoantibodies and disseminated nontuberculous mycobacterial infections. *Medicine (Baltimore).* 2016;95(25):e3927.
12. Döffinger R, Helbert MR, Barcenas-Morales G, et al. Autoantibodies to interferon-gamma in a patient with selective susceptibility to mycobacterial infection and organ-specific autoimmunity. *Clin Infect Dis.* 2004;38(1):e10–e14.
13. Höflich C, Sabat R, Rosseau S, et al. Naturally occurring anti-IFN-gamma autoantibody and severe infections with Mycobacterium cheloneae and Burkholderia cocovenenans. *Blood.* 2004;103(2):673–675.
14. Wu UI, Hung CC, Chang SY, et al. Neutralizing antiinterferon-γ autoantibodies causing disseminated Mycobacterium avium complex infection in an HIV-infected patient on successful combination antiretroviral therapy. *AIDS.* 2017;31(18):2557–2559.
15. Chang PH, Chuang YC. Anti-interferon-γ autoantibody-associated disseminated Mycobacterium abscessus infection mimicking parotid cancer with multiple metastases: a case report. *Medicine (Baltimore).* 2017;96(39):e8118.
16. Wongkulab P, Wipasa J, Chaiwarith R, Supparatpinyo K. Autoantibody to interferon-gamma associated with adult-onset immunodeficiency in non-HIV individuals in Northern Thailand. *PLoS One.* 2013;8(9):e76371.
17. Rattanathammethee K, Chawansuntati K, Chaiwarith R, Praparattanapan J, Supparatpinyo K, Wipasa J. Dot enzyme-linked immunosorbent assay strip as a screening tool for detection of autoantibody to interferon gamma in sera of suspected cases of adult-onset immunodeficiency. *J Clin Lab Anal.* 2018;32(7):e22460.
18. Lalvani A, Meroni PL, Millington KA, et al. Recent advances in diagnostic technology: applications in autoimmune and infectious diseases. *Clin Exp Rheumatol.* 2008;26(1 Suppl 48):S62–S66.
19. Suárez I, Lehmann C, Gruell H, et al. Repurposing QuantiFERON for detection of neutralizing interferon-γ autoantibodies in patients with nontuberculous mycobacterial infections. *Clin Infect Dis.* 2017;65(3):518–521.
20. Belknap R, Daley CL. Interferon-gamma release assays. *Clin Lab Med.* 2014;34(2):337–349.
21. Shima K, Sakagami T, Tanabe Y, et al. Novel assay to detect increased level of neutralizing anti-interferon gamma autoantibodies in non-tuberculous mycobacterial patients. *J Infect Chemother.* 2014;20(1):52–56.

22. Chi CY, Chu CC, Liu JP, et al. Anti-IFN-γ autoantibodies in adults with disseminated nontuberculous mycobacterial infections are associated with HLA-DRB1*16:02 and HLA-DQB1*05:02 and the reactivation of latent varicella-zoster virus infection. *Blood.* 2013;121(8):1357–1366.
23. Mazurek GH, Jereb J, Vernon A, LoBue P, Goldberg S, Castro K; IGRA Expert Committee; Centers for Disease Control and Prevention (CDC). Updated guidelines for using interferon gamma release assays to detect Mycobacterium tuberculosis infection—United States, 2010. *MMWR Recomm Rep.* 2010;59(RR-5):1–25.
24. Mazurek GH, Villarino ME; CDC. Guidelines for using the QuantiFERON-TB test for diagnosing latent Mycobacterium tuberculosis infection. Centers for Disease Control and Prevention. *MMWR Recomm Rep.* 2003;52(RR-2):15–18.
25. Chetchotisakd P, Anunnatsiri S, Nithichanon A, Lertmemongkolchai G. Cryptococcosis in anti-interferon-gamma autoantibody-positive patients: a different clinical manifestation from HIV-infected patients. *Jpn J Infect Dis.* 2017;70(1):69–74.
26. Desem N, Jones SL. Development of a human gamma interferon enzyme immunoassay and comparison with tuberculin skin testing for detection of Mycobacterium tuberculosis infection. *Clin Diagn Lab Immunol.* 1998;5(4):531–536.
27. Westgard JO. Precision and accuracy: concepts and assessment by method evaluation testing. *Crit Rev Clin Lab Sci.* 1981;13(4):283–330.
28. Watanabe M, Uchida K, Nakagaki K, et al. Anti-cytokine autoantibodies are ubiquitous in healthy individuals. *FEBS Lett.* 2007;581(10):2017–2021.

Tracking Antimicrobial Resistance in *Neisseria gonorrhoeae* from the Molecular Level Using Endocervical Swabs

G. Oree, MSc,[1] M. Naicker, PhD,[1] H. C. Maise, MBChB,[2] P. Tinarwo, MSc,[3] V. Ramsuran, PhD,[4] N.S. Abbai, PhD[1,]*

[1]School of Clinical Medicine Research Laboratory, Nelson R. Mandela School of Medicine, University of KwaZulu-Natal, Durban, South Africa; [2]Department of Obstetrics and Gynaecology, School of Clinical Medicine, Nelson R. Mandela School of Medicine, University of KwaZulu-Natal, Durban, South Africa; [3]Department of Biostatistics, Nelson R. Mandela School of Medicine, University of KwaZulu-Natal, Durban, South Africa; [4]School of Laboratory Medicine and Medical Sciences, College of Health Sciences, University of KwaZulu-Natal, Durban, South Africa; *To whom correspondence should be addressed. ABBAIN@ukzn.ac.za

Keywords: *Neisseria gonorrhoeae*, antimicrobial resistance, pregnant women, endocervical swabs, molecular markers/genes, polymerase chain reaction

Abbreviations: STI, sexually transmitted infection; AMR, antimicrobial resistance; qPCR, quantitative polymerase chain reaction.

Laboratory Medicine 2022;53:18–23; DOI: 10.1093/labmed/lmab037

ABSTRACT

Objective: The global emergence of drug resistance in *Neisseria gonorrhoeae* has resulted in the use of a range of antibiotics and is now a public health concern because this pathogen may become untreatable in the future. This study aimed to detect antimicrobial-resistant determinants in *N. gonorrhoeae* directly from endocervical specimens.

Methods: Three hundred seven pregnant women were enrolled in this study. Endocervical swabs were collected from consenting women and used for the detection of *N. gonorrhoeae.* Molecular indicators associated with penicillin, tetracycline, ciprofloxacin, azithromycin, spectinomycin, cefixime, and ceftriaxone resistance were detected by polymerase chain reaction.

Results: Of the 307 women, 24 (7.8%) tested positive for *N. gonorrhoeae.* The *tetM* gene carried on the American-type plasmid was shown to be present in all the specimens. Approximately 87.5% of the specimens carried the penicillinase-producing African-type plasmid, and the *gyrase A* gene carrying the Ser-91 mutation was shown to be present in 37.5% of the specimens. Mutations associated with azithromycin, spectinomycin, cefixime, and ceftriaxone resistance were not detected in the study specimens.

Conclusion: The detection of resistance determinants without the need for culture may prove to be more feasible for future epidemiological investigations focused on tracking antimicrobial susceptibility patterns in *N. gonorrhoeae.*

Neisseria gonorrhoeae, the etiologic agent of gonorrhea, is reported to be the second most prevalent bacterial sexually transmitted infection (STI) globally.[1] The World Health Organization conducted an STI surveillance in 2018 that revealed an estimated 87 million new gonorrhea infections globally during 2016, with an incidence of 20 infections per 1,000 population (uncertainty interval, 14–28 per 1,000 population) in women.[2] A study conducted in South Africa and Zimbabwe reported an overall prevalence of 0.7% for *N. gonorrhoeae* infections in women from the general population.[3] The same study reported an overall incidence rate of 2.4 per 100 woman-years for *N. gonorrhoeae* infections. A higher incidence rate was observed in South African women (3.7 per 100 woman-years) when compared with women from Zimbabwe (1.3 per 100 woman-years).[3] Other studies conducted in South Africa have reported prevalence rates for *N. gonorrhoeae* ranging from 3% to 11% in women.[4-5]

A population of women attending antenatal care in Shiraz, Iran previously reported a prevalence of *N. gonorrhoeae* of 1.3%.[6] Untreated *N. gonorrhoeae* infections have been reported to have an association with a range of adverse pregnancy outcomes such as conjunctivitis, fetal growth impedance, spontaneous abortion, stillbirth, prematurity, low birth weight, postpartum endometritis, and increased risk of HIV transmission from mother to child during birth.[1-4,7-9] *N. gonorrhoeae* has been reported to be asymptomatic, thereby allowing the survival of this organism to persist because asymptomatic infections are not treated as per standard of care.[7]

The global emergence of the drug resistance of *N. gonorrhoeae* to beta-lactams (including cephalosporins), tetracyclines, and quinolones is a public health concern because this infection may become untreatable in the future.[10,11] A recent study conducted in KwaZulu-Natal, South Africa indicated antimicrobial resistance (AMR) toward ciprofloxacin (70%), penicillin (60%), and tetracycline (100%) for pure isolates of *N. gonorrhoeae*.[9] The South African STI management guidelines use a syndromic approach for the diagnosis and management of STIs.[12]

Gonorrhea is associated with abnormal vaginal discharge, which according to South African guidelines is treated with an intramuscular single dose of 250 mg ceftriaxone and the oral consumption of 1 g azithromycin, together with 12-hour oral doses of 400 mg metronidazole for 7 days.[12] Patients who are allergic to penicillin stop ceftriaxone and are recommended to use a single oral dose (2 g) of azithromycin.[12] A gynecological assessment is suggested if pain persists after 48 to 72 hours of treatment.[12]

Previous AMR studies on *N. gonorrhoeae* have been based on culturing, which was the gold standard against which other diagnostic tests were compared. However, other nonculture tests have been in demand because of the difficulty in maintaining the viability of *N. gonorrhoeae* during transportation and storage.[13] Many countries have now shifted to performing nucleic acid amplification assays for the identification and association of AMR in *N. gonorrhoeae*.[9-11,14] It is highly likely that previous studies that have reported on AMR patterns in *N. gonorrhoeae* may have missed a significant proportion of positive specimens because of the drawbacks of culturing. Therefore, this study was aimed at detecting the resistance determinants associated with penicillin, tetracycline, ciprofloxacin, spectinomycin, cefixime, ceftriaxone, and azithromycin from the molecular level using a primary endocervical swab specimen. There is no published South African study that has used this approach to determine patterns of resistance, especially in pregnant women.

Materials and Methods

Ethics Approval

Full ethics approval for this study was granted by the Biomedical Research Ethics Committee of the University of KwaZulu-Natal (Durban, South Africa; BE355/18).

Study Setting and Population

The study population included 307 pregnant women recruited from the antenatal clinic of the King Edward VIII hospital in Durban, South Africa from November 2018 to July 2019.

Specimen Collection and Processing

Each enrolled woman underwent a pelvic examination during which an endocervical swab specimen was to be collected. The swab was immersed in 2 mL phosphate-buffered saline (pH 7.4) and vortexed to dislodge the specimen material from the swab, and the cervical fluid was stored at –20°C until further molecular analysis. The molecular assays were conducted at the School of Clinical Medicine's Research Laboratory at the University of KwaZuu-Natal.

DNA Isolation from the Endocervical Specimen

The PureLink Microbiome DNA Purification kit (ThermoFisher Scientific) was used for DNA extraction from the swabs. The manufacturer's instructions were followed without any modifications.

Detection of *N. gonorrhoeae* from the Endocervical Specimen

The predesigned commercially available TaqMan quantitative polymerase chain reaction (qPCR) assay, developed specifically for *N. gonorrhoeae* (assay identification number Ba04646252_s; ThermoFisher Scientific), was used. Amplification was performed on a Quant Studio 5 real-time PCR system.

Detection of Molecular Markers/Genes Associated with AMR

Detection of Beta-Lactamase-Producing Plasmid Types

A multiplex PCR was used to detect beta-lactamase-producing plasmid types (Africa, Asia, and Toronto) using specific primers and protocols previously described by Lawung et al[15] and Tanaka et al[16] (**TABLE 1**).

Detection of Tetracycline Resistance

TetM tetracycline resistance plasmid types (American and Dutch) were detected by PCR using the primers shown in **TABLE 1**. Detection of the specific plasmid type was performed by the digestion of the PCR amplicon with *Hinf*I (New England Biolabs,).

TABLE 1. Primer Sequences and Targeted Genes for Antibiotic-Resistant Determinants

Antibiotic	Primer Name	Primer Sequence (5'-3')	Targeted Gene
Azithromycin	gon*rRNA*-F	ACGAATGGCGTAACGATGGCCACA	Point mutations in 23*S rRNA* regions in allele 2[20]
	23*S rRNAR*-allele 2	GCGACCATACCAAACACCCACAGG	
Cefixime and ceftriaxone	PA1	CGATATGATCGAACCTGG	*penA* gene[28]
	PA2	ACAATCTCGTTGATACTCG	
Spectinomycin	5S-F	TGGCAAAACATGA AATTGAAG	*rpsE* gene[29]
	5S-R	GCCATGGTTAACTCCCAAAA	
Penicillin G	GC1F	AACTCACGGACAAAATCACGG	β-lactamase-producing plasmid[14]
	GC2F	CACCTATAAATCTCGCAAGCC	
	GC3R	AACGCAAGCAGGACGAAATC	
	GC4R	CCTCCACCTTCATCCTCAGC	
Tetracycline	TetMF	ACTGTTGAACCGAGYAAACCT	*tetM* gene[14]
	TetMR	TCTATCCGACTATTTGGACGACG	
Ciprofloxacin	GyrAF	CGGCGCGTACTGTACGCGATGCA	*gyrase A* gene[15]
	GyrAR	ATGTCTGCCAGCATTTCATGTGAGA	

Detection of Ciprofloxacin Resistance

The *gyrase A* gene was amplified using the primers described in **TABLE 1**. Detection of the Ser-91 mutation, which confers ciprofloxacin resistance, was performed by the digestion of the PCR amplicon with *Hinf*I (New England Biolabs).

Detection of Azithromycin, Spectinomycin, Cefixime, and Ceftriaxone resistance determinants

The 23*S rRNA* gene was amplified to identify mutations that are responsible for conferring azithromycin resistance, and the *rpsE* gene was amplified to identify spectinomycin-resistant determinants (**TABLE 1**). The *penA* and *por* genes were amplified to identify resistant determinants for cefixime and ceftriaxone. The PA1 and PA2 primers were used for the amplification of the *penA* gene (**TABLE 1**).

Statistical Analysis

The data analysis was performed using R Statistical Computing software, version 3.6.2. Because of the smaller sample size and consequently a low power, the demographic, behavioral and clinical factors were simply described either as overall or stratified by the resistant profiles. Age was the only numerical measure and was skewed, which was suggestive of summarization by minimum, maximum, and quartiles only. The other categorical demographic attributes were summarized in the form of counts and percentage frequencies.

Results

Detection of Resistance Targets

Of the 307 specimens tested, 24 produced positive amplification using the TaqMan qPCR assay. The prevalence of *N. gonorrhoeae* among the participants was 7.8% (24/307). Overall, all the specimens tested produced a PCR product for at least 1 of the target genes. **TABLE 2** shows the results of the PCR assays for the targets investigated.

All 24 positive specimens produced a PCR amplicon of 700 bp corresponding to the *tetM* gene (**TABLE 2**). Sanger sequencing of the PCR amplicons confirmed the identity of the PCR product (99% match with the American-type *tetM* conjugative plasmid; accession number: GU479464.1). The restriction digestion pattern (600 bp and 93 bp) of the *tetM* gene confirmed the presence of the American-type conjugative plasmid in the study specimens (**TABLE 2**).

An amplicon size of 737 bp was obtained using the multiplex PCR for the beta-lactamase-producing plasmid. This amplicon was shown to be present in 87.5% (21/24) of the specimens analyzed (**TABLE 2**). Sanger sequencing confirmed that the specimens carried the *N. gonorrhoeae* strain African-TEM 1-MIC16 plasmid PJD5, complete sequence (accession number: MK973084.1).

A PCR amplicon of 278 bp corresponding to the *gyrase A* gene was amplified in 41.6% (10/24) of the positive specimens (**TABLE 2**). The amplicons were confirmed to be the *gyrase A* gene from *N. gonorrhoeae,* DNA gyrase subunit A, partial (*N. gonorrhoeae*) (accession number: APU93729.1). According to the restriction digestion analysis, the 278 bp fragment remained undigested in 90.0% (9/10) of the *gyrase A*–positive specimens, indicating the presence of the Ser-91 mutation associated with ciprofloxacin resistance (**TABLE 2**).

The *penA* gene, which carries mutations associated with cefixime and ceftriaxone resistance, was detected in 9/24 (37.5%) of the specimens. The *penA* amplicons were confirmed to be the penicillin-binding protein 2 of *N. gonorrhoeae* (GenBank number AFJ54623.1). However, none of the mutations associated with resistance to these antibiotics were detected after the sequencing of the PCR amplicons, indicating a lack of emerging patterns of resistance to ceftriaxone and cefixime. Similarly, mutations associated with resistance to spectinomycin and azithromycin were not detected in the study specimens. The PCR amplicons were confirmed to be *N. gonorrhoeae* strain 32380 23S ribosomal RNA gene, complete sequence (GenBank number KT954110.1) and *N. gonorrhoeae* strain 3mut_SPC 30S subunit ribosomal protein S5 (*rpsE*) gene (GenBank number GU395615.1).

Detection of Dual- and Triple-Resistant Profiles

According to the data, a monoresistance profile was observed for 1 specimen. Only the *tetM* determinant related to tetracycline resistance was identified in this specimen. With respect to the specimens exhibiting a dual-resistance profile, it was shown that 66.6% (16/24) specimens carried at least 2 of the resistant determinants. A lower percentage of the specimens (29.1%; 7/24) carried determinants for all the resistance markers tested (ie, *tetM*, *gyrase A,* and beta-lactamase-producing plasmid; **TABLE 3**).

Description of Behavioral and Clinical Factors by Resistance Profile

A description of the 24 study participants who were positive for *N. gonorrhoeae* stratified by overall resistance in relation to demographics and behavioral and clinical factors is shown in **TABLE 4**. The results showed that the majority were unmarried (91.7%; 22/24), with 79.2% (19/24) of the participants having completed high school. A high proportion (79.2%; 19/24) of the women had their first sexual experience at age 15 to 20 years. Condoms were mostly used "sometimes" by 66.7% (16/24) of participants. The majority (58.3%; 14/24) reported having 2 to 4 lifetime sex partners. The results also showed that a high pro-

TABLE 2. Summary of Antibiotic Resistance Profiles Generated for Endocervical Swab Specimens Testing Positive for *N. gonorrhoeae* in Study Population

Antibiotic	Targeted Gene	Type	n = 24
Penicillin G	β-lactamase-producing plasmid	African	21/24
Tetracycline	*tetM*	American	24/24
Ciprofloxacin	*gyrase A*	Mutation Ser-91	9/24
		Wild-type	1/24
Azithromycin	23S allele 2	N/A	5/24
Spectinomycin	*rpsE*	N/A	5/24
Ceftriaxone and cefixime	*penA*	N/A	9/24

N/A, not applicable.

TABLE 3. Results of PCR Amplification Reactions for Individual Specimens and Resistance Profiles Generated

PCR Results for Resistant Determinants										
Participant Identifier	*gyrase A*	Ser-91 Mutation	*tetM*	Beta-Lactamase-Producing Plasmid	*23SrRNA*	*23SrRNA* Allele 2 Mutation	*penA* Gene	*penA* Mutation	*rpsE* Gene	*rpsE* Mutation
G003	Positive	Yes	Positive	Positive	Negative	Negative	Positive	Positive	Negative	Negative
G007	Negative	…	Positive	Negative	Negative	Negative	Negative	Negative	Negative	Negative
G051	Positive	Yes	Positive	Positive	Positive	Negative	Positive	Positive	Negative	Negative
G061	Positive	Yes	Positive	Positive	Negative	Negative	Positive	Positive	Positive	Negative
G079	Positive	Yes	Positive	Negative	Negative	Negative	Positive	Positive	Negative	Negative
G132	Negative	…	Positive	Positive	Negative	Negative	Negative	Negative	Negative	Negative
G133	Negative	…	Positive	Positive	Negative	Negative	Positive	Positive	Negative	Negative
G134	Negative	…	Positive	Positive	Negative	Negative	Negative	Negative	Negative	Negative
G136	Positive	Yes	Positive	Positive	Negative	Negative	Negative	Negative	Negative	Negative
G138	Negative	…	Positive	Positive	Negative	Negative	Negative	Negative	Negative	Negative
G141	Negative	…	Positive	Positive	Negative	Negative	Negative	Negative	Negative	Negative
G142	Negative	…	Positive	Positive	Negative	Negative	Negative	Negative	Negative	Negative
G143	Positive	Yes	Positive	Negative	Negative	Negative	Negative	Negative	Negative	Negative
G144	Negative	…	Positive	Positive	Negative	Negative	Negative	Negative	Negative	Negative
G145	Negative	…	Positive	Positive	Negative	Negative	Negative	Negative	Negative	Negative
G148	Negative	…	Positive	Positive	Negative	Negative	Negative	Negative	Negative	Negative
G151	Negative	…	Positive	Positive	Negative	Negative	Negative	Negative	Negative	Negative
G153	Negative	…	Positive	Positive	Negative	Negative	Negative	Negative	Negative	Negative
G154	Negative	…	Positive	Positive	Negative	Negative	Negative	Negative	Negative	Negative
G160	Negative	…	Positive	Positive	Negative	Negative	Negative	Negative	Negative	Negative
G176	Positive	Yes	Positive	Positive	Positive	Negative	Positive	Positive	Negative	Negative
G180	Positive	Yes	Positive	Positive	Positive	Negative	Positive	Positive	Positive	Negative
G206	Positive	No	Positive	Positive	Positive	Negative	Positive	Positive	Positive	Negative
G247	Positive	Yes	Positive	Positive	Positive	Negative	Positive	Positive	Positive	Negative

PCR, polymerase chain reaction.
Specimens highlighted in blue indicate dual resistance. Specimens highlighted in red indicate triple resistance.

portion of participants (83.3%; 20/24) were asymptomatic for infection (ie, they did not present with symptoms of abnormal vaginal discharge). A high proportion 18/24 (75%) reported no previous treatment for any STIs; however, 41.7% (10/24) reported past STI symptoms. No woman was reported to have had spontaneous abortion, and most participants (79.2%; 19/24) were reported to be in their third trimester of pregnancy.

Discussion

The worldwide clinical management of *N. gonorrhoeae* infections is becoming increasingly challenging because of resistance to various classes of available antibiotics. These include sulfonamides, beta-lactams, tetracyclines, macrolides, fluoroquinolones, and more recently expanded-spectrum cephalosporins.[17,18] The ability of *N. gonorrhoeae* to exhibit drug resistance to a wide range of antibiotics results from this bacterium's remarkable phenotypic and genotypic variability, which gives it an added advantage in evading host responses.[11] The genotypic variability of *N. gonorrhoeae* has been linked to the acquisition of new genetic material.[7]

The emergence of drug-resistant *N. gonorrhoeae* is a global concern.[19] For pregnant women, this concern is escalated because untreated *N. gonorrhoeae* infections can have severe consequences on reproductive health, such as an increased risk for acquiring HIV and other STIs and obstetric morbidity.[20] Currently, there are limited published data in South Africa on the molecular detection of AMR determinants in *N. gonorrhoeae* from primary genital swab specimens. This study provides evidence for the detection of resistant determinants associated with penicillin, tetracycline, and ciprofloxacin from the molecular level using a primary endocervical swab specimen collected from pregnant women.

In this study, *N. gonorrhoeae* was detected in 24/307 (7.82%) endocervical swab specimens. The *tetM* gene was detected in all 24 specimens. The prevalence of tetracycline resistance in this study population was 100%. Similar findings were reported by Rambaran et al,[9] who found that the prevalence of tetracycline resistance was 100% in a population of men and women from South Africa. Further analysis of the *tetM* gene revealed that the *tetM* gene was carried on the American-type plasmid. The findings of our study are similar to those of other African studies.[14,21] A study conducted in a Moroccan female population revealed a 100% prevalence of the American-type plasmid carrying the *tetM* gene.[21] A study conducted in South African men also reported a high prevalence of the American-type *tetM* plasmid and a lower prevalence of the Dutch-type *tetM* plasmid.[14] Previous studies have suggested that the Dutch-type *tetM* plasmid is more prevalent in Asian countries (such as Thailand, the Philippines, China, and Bangladesh), whereas the American-type *tetM* plasmid is more prevalent in European and African countries.[22-24] A recent study conducted in South Africa showed that the *tetM* gene was detected in 92% of their isolates with a 90% predominance of the American variant, corresponding with previous findings suggesting that the American variant of the *tetM* originated in Africa.[9,25] These studies provide evidence for the

TABLE 4. Demographic, Behavioral, and Clinical Factors of Positive *N. gonorrhoeae* Specimens that Displayed Resistance Profiles

Variables	Overall (n = 24)
Age (y)	
Median (Q1–Q3)	27.5 (24.8–32.3)
Min–max	20.0–40.0
Current abnormal discharge	
No	20 (83.3%)
Yes	4 (16.7%)
Level of education	
Did not attend school	1 (4.2%)
High school	19 (79.2%)
College, university	4 (16.7%)
Marital status	
No	22 (91.7%)
Yes	2 (8.3%)
Has a regular sex partner	
No	11 (45.8%)
Yes	13 (54.2%)
Cohabitating with partner	
No	17 (70.8%)
Yes	7 (29.2%)
Age of first sex (y)	
15–20	19 (79.2%)
21–25	5 (20.8%)
Number of lifetime sex partners	
1	8 (33.3%)
2–4	14 (58.3%)
>4	2 (8.3%)
Condom use	
Sometimes	16 (66.7%)
Never	6 (25%)
Always	2 (8.33%)
Condom used during last sex act	
No	14 (58.3%)
Yes	10 (41.7%)
Trimester of pregnancy	
Second	5 (20.8%)
Third	19 (79.2%)
Past preterm delivery	
No	19 (79.2%)
Yes	5 (20.8%)
Past miscarriage	
No	18 (75.0%)
Yes	6 (25.0%)
Past spontaneous abortion	
No	24 (100%)
Experienced past symptoms of STIs	
No	14 (58.3%)
Yes	10 (41.7%)
Previous treatment for STIs	
No	18 (75.0%)
Yes	6 (25.0%)

STI, sexually transmitted infection.

nonuse of tetracycline for future treatment of *N. gonorrhoeae* infections because of such high levels of resistance to this antibiotic.

Beta-lactamase-producing plasmids were shown to be present in 87.5% of the specimens analyzed in this study. The prevalence of penicillin resistance observed in this study was higher than reports from a recent study conducted in a male population from South Africa in which penicillin resistance was 33%.[26] The African-type plasmid related to penicillin resistance was observed in the current study. A 2010 study conducted in South Africa showed the presence of the African-type (35.2%) and the Toronto-type plasmids (44.4%) and a new Johannesburg-type plasmid (20.3%).[10]

Ciprofloxacin resistance has been increasing and has been reported on a worldwide scale, with locations such as Asia overall (93.8%) and Hefei, China in particular (100%) exhibiting high levels of resistance.[27,28] In this study, the *gyrase A* gene was detected in less than half of the study specimens (41.6%). The sensitivity of the PCR for this gene was shown to be low and will require further optimization to obtain the desired results. Mutations within the *gyrase A* gene (Ser-91) have been linked to ciprofloxacin resistance.[7,29] The mutations associated with ciprofloxacin resistance have been previously described.[10,11,28,30] Despite the limited number of positive amplicons obtained, the Ser-91 mutation that is associated with ciprofloxacin resistance was present in 90% of the specimens analyzed. A Moroccan study conducted from 2013 to 2015 showed an extremely high level of ciprofloxacin resistance, with 77.9% of the specimens exhibiting the Ser-91 mutation.[11] Despite the lack of detection of resistant mutations to ceftriaxone, spectinomycin, and azithromycin, PCR detection and DNA sequencing without the need for culture can be used to track emerging resistance to these antibiotics.

According to the behavioral and sociodemographic data collected in this study, the majority of participants were unmarried, had a secondary level of education, had between 2 and 4 lifetime sex partners, and had sometimes used condoms during sex. In addition, these women who were associated with AMR were predominantly in the third trimester of pregnancy, were asymptomatic, and had not been treated for STIs in the past. There is a lack of published data that have compared sociodemographic and behavioral risk factors in association with AMR patterns. The majority of published studies have focused on demographic, behavioral, and clinical factors associated with the prevalence of *N. gonorrhoeae* infections.[5,29,30] Our study provides data on the demographic, behavioral, and clinical characteristics of pregnant women associated with AMR, thereby adding to the current literature.

Limitations

A major limitation of the study was the inability to amplify the genes associated with ciprofloxacin, azithromycin, cefixime, spectinomycin, and ceftriaxone resistance in all the study specimens tested. To advocate for the use of molecular-based techniques for the detection of emerging patterns of AMR in *N. gonorrhoeae*, the PCR reactions will need to be optimized to conduct mutation screening. Once optimized, molecular-based detection assays for AMR will have a significant impact on the public health responses and clinical management for this pathogen.

Conclusion

Because of the limitations associated with culture-based techniques (such as loss of viability of the gonococcus) for identifying susceptibility/resistance patterns in *N. gonorrhoeae,* the detection of resistance determinants from the

molecular level without the need for culture may prove to be more feasible for future epidemiological investigations focused on tracking antimicrobial susceptibility/resistance patterns for this pathogen.

Acknowledgments

The authors thank all the women who participated in this study, the King Edward VIII Hospital Antenatal Clinic, and Magnus Unemo, PhD from the World Health Organization Collaborating Centre for Gonorrhoeae and other STIs for the World Health Organization reference strains.

The author(s) declare no potential conflicts of interests with respect to the research, authorship, and/or publication of this article.

The authors disclose receipt of the following financial support for the research, authorship, and/or publication of this article. This work was supported by the College of Health Science, University of KwaZulu-Natal (grant number 640603) and the National Research Foundation (grant number: 112555).

REFERENCES

1. Ramjee G, Abbai NS, Naidoo S. Women and sexually transmitted infections in Africa. *Open J Obstet Gyn.* 2015;5:385–399.
2. World Health Organization. Report on global sexually transmitted infection surveillance 2018. https://www.who.int/reproductivehealth/publications/stis-surveillance-2018/en/. Accessed June 3, 2021.
3. Venkatesh KK, van der Straten A, Mayer KH, et al. African women recently infected with HIV-1 and HSV-2 have increased risk of acquiring Neisseria gonorrhoeae and Chlamydia trachomatis in the Methods for Improving Reproductive Health in Africa trial. *Sex Transm Dis.* 2011;38(6):562–570.
4. Abbai NS, Wand H, Ramjee G. Sexually transmitted infections in women participating in a biomedical intervention trial in Durban: prevalence, coinfections, and risk factors. *J Sex Transm Dis.* 2013;2013:358402.
5. Mlisana K, Naicker N, Werner L, et al. Symptomatic vaginal discharge is a poor predictor of sexually transmitted infections and genital tract inflammation in high-risk women in South Africa. *J Infect Dis.* 2012;206(1):6–14.
6. Pourabbas B, Rezaei Z, Mardaneh J, et al. Prevalence of Chlamydia trachomatis and Neisseria gonorrhoeae infections among pregnant women and eye colonization of their neonates at birth time, Shiraz, Southern Iran. *BMC Infect Dis.* 2018;18:1–4.
7. Patel AL, Chaudhry U, Sachdev D, Sachdeva PN, Bala M, Saluja D. An insight into the drug resistance profile and mechanism of drug resistance in Neisseria gonorrhoeae. *Indian J Med Res.* 2011;134:419–431.
8. Calado J, Castro R, Lopes Â, Campos MJ, Rocha M, Pereira F. Antimicrobial resistance and molecular characteristics of Neisseria gonorrhoeae isolates from men who have sex with men. *Int J Infect Dis.* 2019;79:116–122.
9. Rambaran S, Naidoo K, Dookie N, Moodley P, Sturm AW. Resistance profile of Neisseria gonorrhoeae in KwaZulu-Natal, South Africa questioning the effect of the currently advocated dual therapy. *Sex Transm Dis.* 2019;46(4):266–270.
10. Fayemiwo SA, Müller EE, Gumede L, Lewis DA. Plasmid-mediated penicillin and tetracycline resistance among Neisseria gonorrhoeae isolates in South Africa: prevalence, detection and typing using a novel molecular assay. *Sex Transm Dis.* 2011;38(4):329–333.
11. Karim S, Bouchikhi C, Banani A, et al. Molecular antimicrobial resistance of Neisseria gonorrhoeae in a Moroccan area. *Infect Dis Obstet Gynecol.* 2018;2018:7263849.
12. Grossman LC. *Sexually transmitted infections. In Grossman S, Porth CM, eds. Porth's Pathophysiology: Concepts of Altered Health States, 9th ed*. Philadelphia: Lippincott Williams & Wilkins; 2013:1416–1425.
13. Johnson RE, Newhall WJ, Papp JR, et al.; Screening tests to detect Chlamydia trachomatis and Neisseria gonorrhoeae infections—2002. *MMWR Recom Rep.* 2002;51(RR-15):1–38.
14. Moodley P, Pillay C, Goga R, Kharsany AB, Sturm AW. Evolution in the trends of antimicrobial resistance in Neisseria gonorrhoeae isolated in Durban over a 5 year period: impact of the introduction of syndromic management. *J Antimicrob Chemother.* 2001;48(6):853–859.
15. Lawung R, Cherdtrakulkiat R, Charoenwatanachokchai A, Nabu S, Suksaluk W, Prachayasittikul V. One-step PCR for the identification of multiple antimicrobial resistance in Neisseria gonorrhoeae. *J Microbiol Methods.* 2009;77(3):323–325.
16. Tanaka M, Nakayama H, Haraoka M, Saika T. Antimicrobial resistance of Neisseria gonorrhoeae and high prevalence of ciprofloxacin-resistant isolates in Japan, 1993 to 1998. *J Clin Microbiol.* 2000;38(2):521–525.
17. Unemo M, Shafer WM. Antimicrobial resistance in Neisseria gonorrhoeae in the 21st century: past, evolution, and future. *Clin Microbiol Rev.* 2014;27(3):587–613.
18. Harris SR, Cole MJ, Spiteri G, et al.; Euro-GASP study group. Public health surveillance of multidrug-resistant clones of Neisseria gonorrhoeae in Europe: a genomic survey. *Lancet Infect Dis.* 2018;18(7):758–768.
19. Crowther-Gibson P, Govender N, Lewis DA, et al. Part IV. Human infections and antibiotic resistance. *S Afr Med J.* 2011;101(8 Pt 2):567–578.
20. Tapsall JW. Antibiotic resistance in Neisseria gonorrhoeae. *Clin Infect Dis.* 2005;41(Suppl 4):S263–S268.
21. Chisholm SA, Dave J, Ison CA. High-level azithromycin resistance occurs in Neisseria gonorrhoeae as a result of a single point mutation in the 23S rRNA genes. *Antimicrob Agents Chemother.* 2010;54(9):3812–3816.
22. Zheng H, Wu X, Huang J, et al. The prevalence and epidemiology of plasmid-mediated penicillin and tetracycline resistance among Neisseria gonorrhoeae isolates in Guangzhou, China, 2002–2012. *BMC Infect Dis.* 2015;15:1–7.
23. Su X, Jiang F, Dai X, Sun H, Ye S. Surveillance of antimicrobial susceptibilities in Neisseria gonorrhoeae in Nanjing, China, 1999–2006. *Sex Trans Dis.* 2007;34(12):995–999.
24. Turner A, Gough KR, Leeming JP. Molecular epidemiology of tetM genes in Neisseria gonorrhoeae. *Sex Transm Infect.* 1999;75(1):60–66.
25. Van Dyck E, Rossau R, Duhamel M, et al. Antimicrobial susceptibility of Neisseria gonorrhoeae in Zaire: high level plasmid-mediated tetracycline resistance in central Africa. *Genitourin Med.* 1992;68(2):111–116.
26. Maduna LD, Kock MM, van der Veer BMJW, et al. Antimicrobial resistance of Neisseria gonorrhoeae isolates from high-risk men in Johannesburg, South Africa. *Antimicrob Agents Chemother.* 2020;64(11):e00906-20.
27. Chen Y, Gong Y, Yang T, et al. Antimicrobial resistance in Neisseria gonorrhoeae in China: a meta-analysis. *BMC Infect Dis.* 2016;16:1–6.
28. Jiang FX, Lan Q, Le WJ, et al. Antimicrobial susceptibility of Neisseria gonorrhoeae isolates from Hefei (2014–2015): genetic characteristics of antimicrobial resistance. *BMC Infect Dis.* 2017;17:1–6.
29. Deguchi T, Yasuda M, Nakano M, et al. Rapid screening of point mutations of the Neisseria gonorrhoeae parC gene associated with resistance to quinolones. *J Clin Microbiol.* 1997;35(4):948–950.
30. Siedner MJ, Pandori M, Castro L, et al. Real-time PCR assay for detection of quinolone-resistant Neisseria gonorrhoeae in urine samples. *J Clin Microbiol.* 2007;45(4):1250–1254.

Clinical Interpretation Challenges of Germline-Shared Somatic Variants in Cancer

Kyoung-Jin Park, MD, PhD[1,*]

[1]Department of Laboratory Medicine & Genetics, Samsung Changwon Hospital, Sungkyunkwan University School of Medicine, Changwon, Gyeongsangnam-do, Korea; *To whom correspondence should be addressed. unmar21@gmail.com

Keywords: actionability, pathogenicity, germline, somatic, variant, interpretation

Abbreviations: TCGA, The Cancer Genome Atlas; P/LP, pathogenic or likely pathogenic; CS, Costello syndrome; WHO, World Health Organization; COSMIC, The Catalog of Somatic Mutations in Cancer; HGMD, Human Genome Mutation Database; GENIE, Genomics Evidence Neoplasia Information Exchange; ACMG/AMP, American College of Medical Genetics and Genomics and Genomics and the Association of Molecular Pathology; VUS, variant of unknown significance; B/LB, benign/likely benign; AMP/ASCO/CAP, Association of Molecular Pathology, American Society of Clinical Oncology, and College of American Pathologists; CGI, Cancer Genome Interpreter Cancer Biomarkers Database; CIViC, Clinical Interpretation of Variants in Cancer; OncoKb, Precision Oncology KnowledgeBase; JAX-CKB, Jackson Laboratory Clinical Knowledgebase; DEPO, Database of Evidence for Precision Oncology; MCG, My Cancer Genome; PMKB, Precision Medicine Knowledge Base; PharmGKB, Pharmacogenomics KnowledgeBase; JMML, juvenile myelomonocytic leukemia

Laboratory Medicine 2022;53:24–29; DOI: 10.1093/labmed/lmab020

ABSTRACT

Objective: To investigate the interpretation differences of germline-shared somatic variants.

Methods: A total of 123,302 COSMIC variants associated with hematologic malignant neoplasms were used. The pathogenicity and actionability of shared variants were analyzed based on the standardized guidelines.

Results: The overall frequency of variants shared in ClinVar/HGMD and COSMIC was 10%. The pathogenicity of 54 shared variants was pathogenic/likely pathogenic (P/LP; *n* = 30), variants of unknown significance (*n* = 3), and benign/likely benign (*n* = 21). In total, 30 P/LP variants were reclassified to tier I/tier II (83%) and tier III (17%) variants.

Conclusions: This is the first study about different clinical interpretations of shared variants based on the current standard guidelines. This study takes a meaningful step in bridging the interpretation gap between the somatic and germline variants.

Germline and somatic variants have been extensively catalogued in patients with cancer by using genomic technologies such as massively parallel sequencing. The Cancer Genome Atlas (TCGA) project, comprising 9423 tumor exomes across 33 cancer types, has reported that actionable somatic alterations were identified in 57% of tumor specimens.[1] Moreover, it has been reported[2,3] that germline pathogenic or likely pathogenic (P/LP) variants in cancer genes were identified in 4% to 16% of tumor sequencing specimens.

Distinguishing somatic and germline variants is important because of their different clinical meanings. The main purposes of the germline and somatic sequencing are different in the clinical settings. The aims of germline testing for cancer are typically to inform cancer predisposition and to guide therapies in pharmacogenomics. However, tumor testing primarily focuses on the discovery of oncogenic driver mutations and actionable alterations associated with diagnosis, prognosis, and/or therapeutics. Also, there are differences in interpretation between the germline and somatic variants.[4,5]

A recent study report[6] has revealed that a total of 336,987 variants were shared between the germline genome from gnomAD and somatic exomes from TCGA. The investigators have demonstrated that shared variants arise from statistical independence (34%), basic mutation types (50%), extended nucleotide contexts (4%), potential germline leakage (4%), and unexplained reasons (9%).[6] Considering that chemical vulnerabilities to DNA are basically same regardless of the origin, identical variants could have occurred in the germline and somatic setting, despite the differences between the germline and somatic mutation rates.[7]

Several study reports have stated that there is an overlap between somatic driver mutations and germline pathogenic variants in solid cancers, including lung cancer and Costello syndrome (CS)–associated cancers.[8,9] For example, the *EGFR* T790M mutation, which is associated with gefitinib resistance, has been reported as germline mutation and as somatic mutation in lung cancer.[8,10,11] Also, *HRAS* mutations were most commonly identified at codons 12 and 13, regardless of variant origins.[9,12] The *HRAS* G12S, G12A, and G13C are found in patients with CS-associated cancer as oncogenic somatic or germline mutations.[9,12] However, *NRAS* and *KRAS* mutation data have shown that there is little overlap between germline and somatic variants. Somatic *NRAS* mutations have been frequently observed at codons 12, 13, or 61, whereas germline *NRAS* variants in patients with Noonan syndrome–associated malignancy have been commonly identified at codons 24, 34, 50, and 60.

TABLE 1. Germline-shared Somatic Variants with Clinical Significance in Cancer

Gene	Nucleotide	Amino Acid	Germline Interpretation			OMIM	Representative Cancer Type	Drug	Somatic Interpretation (AMP/ASCO/CAP Guideline)[a]		
			ClinVar	HGMD	ACMG/AMP Guideline				Dx	Px	Tx
KRAS	c.*12A > T	NA	P	DM	PS3, PP2, PP3, PM2, PM5, PM6	190070	JMML	NA	Tier I	Tier I	NA
KRAS	c.178G > C	p.G60R	P	DM	PS3, PP2, PP3, PM2, PM1, PM6	190070	JMML	Mab[b]	Tier I	Tier I	Tier II
KRAS	c.173C > T	p.T58I	P	DM	PS3, PP2, PP3, PM1, PM2, PM6	190070	JMML	NA	Tier I	Tier I	NA
KRAS	c.101C > T	p.P34L	P	DM	PS2, PP2, PP3, PM5, PM2	190070	JMML	Mab[b]	Tier I	Tier I	Tier II
KRAS	c.65A > G	p.Q22R	P	DM	PS3, PP2, PP3, PM2, PM6, PS4	190070	JMML	Mab[b]	Tier I	Tier I	Tier II
KRAS	c.40G > A	p.V14I	P	DM	PS3, PP2, PP3, PM1, PS2, PS4	190070	JMML	Mab[b]	Tier I	Tier I	Tier II
KRAS	c.15A > T	p.K5N	P	DM	PP2, PP3, PM2, PS4, PM6	190070	JMML	Mab[b]	Tier I	Tier I	Tier II
PTPN11	c.155C > T	p.T52I	LP	DM	PS4, PP2, PP3, PM6, PM2	176876	JMML	NA	Tier I	Tier I	NA
PTPN11	c.188A > G	p.Y63C	P	DM	PS4, PS3, PP3, PP2, PM1, PP1	176876	JMML	NA	Tier I	Tier I	NA
PTPN11	c.417G > C	p.E139D	P	DM	PS4, PS3, PP2, PP3, PM2, PS2	176876	JMML	NA	NA	Tier II	NA
PTPN11	c.794G > A	p.R265Q	P	DM	PS2, PS3, PP2, PP1, PM1, PS4	176876	JMML	NA	Tier I	Tier I	NA
PTPN11	c.1403C > T	p.T468M	P	DM	PS3, PS4, PP2, PP3, PM1, PM6, PP1	176876	JMML	NA	Tier I	Tier I	NA
PTPN11	c.1510A > G	p.M504V	P	DM	PS3, PP3, PP2, PM6, PS4	176876	JMML	NA	Tier I	Tier I	NA
RUNX1	c.861C > A	p.Y287*	P	DM	PM2, PS4, PVS1, PP1	151385	AML	NA	Tier I	Tier I/Tier II[c]	NA
RUNX1	c.602G > A	p.R201Q	P	DM	PS4, PS3, PP1, PP3, PM2, PM1	151385	AML	NA	Tier I	Tier I/Tier II[c]	NA
RUNX1	c.601C > T	p.R201*	P	DM	PS4, PP1, PM2, PVS1	151385	AML	NA	Tier I	Tier I/Tier II[c]	NA
RUNX1	c.497G > A	p.R166Q	P	DM	PS3, PP1, PP3, PM2, PM1, PS4, PM6	151385	AML	NA	Tier I	Tier I/Tier II[c]	NA
RUNX1	c.400G > C	p.A134P	P	DM	PS3, PP1, PP3, PM1, PM2, PS4	151385	AML	NA	Tier I	Tier I/Tier II[c]	NA
RUNX1	c.352-1G > A	NA	P	DM	PP1, PM2, PVS1, PS4	151385	AML	NA	Tier I	Tier I/Tier II[c]	NA
RUNX1	c.352-1G > T	NA	P	DM	PP1, PM2, PVS1, PS4	151385	AML	NA	Tier I	Tier I/Tier II[c]	NA
RUNX1	c.328A > G	p.K110E	P	DM	PP1, PS3, PP3, PM2, PM1, PS4	151385	AML	NA	Tier I	Tier I/Tier II[c]	NA
RUNX1	c.315C > A	p.H105Q	LP	NA	PS3, PP3, PM2, PM1	151385	AML	NA	Tier I	Tier I/Tier II[c]	NA
BRAF	c.1787G > T	p.G596V	P	DM	PS3, PP2, PP3, PM1, PM2, PM6	164757	CRC	Cetuximab and LSN3074753	NA	NA	Tier II
BRAF	c.1785T > G	p.F595L	P	DM	PP2, PP3, PM1, PM2, PS4, PM6	164757	Advanced solid cancer	Vemurafenib	NA	NA	Tier II
BRAF	c.741T > G	p.F247L	P	NA	PS3, PS2, PP3, PP2, PM1, PM2, PM6, PS4	164757	Advanced solid cancer	Trametinib	NA	NA	Tier II

HGMD, the Human Genome Mutation Database; OMIM, Online Mendelian Inheritance in Man; COSMIC, the Catalog of Somatic Mutations in Cancer; GENIE, Genomics Evidence Neoplasia Information Exchange; ACMG/AMP, the American College of Medical Genetics and Genomics and Genomics and the Association of Molecular Pathology; AMP/ASCO/CAP; the Association of Molecular Pathology, American Society of Clinical Oncology, and College of American Pathologists; Dx, diagnosis; Px, prognosis; Tx, therapeutics; P, pathogenic; LP, likely pathogenic; DM, disease-causing mutation; MAb, multiple monoclonal antibodies; NA, not applicable; JMML, juvenile myelomonocytic leukemia; AML, acute myeloid leukemia; MDS, myelodysplastic syndrome; MPN, myeloproliferative neoplasm; CRC, colorectal cancer.

[a]*Tier I and Tier II variants are defined as variants of strong clinical significance and variants of potential clinical significance, respectively.*

[b]*Multiple monoclonal antibodies include afatinib, dacomitinib, erlotinib, gefitinib, osimertinib, cetuximab, and panitumumab.*

[c]*The variants were classified as Tier I in PV, ET, and MDS and Tier II in AML.*

FIGURE 1. **The overall workflow. COSMIC indicates the Catalog of Somatic Mutations in Cancer; HGMD, Human Genome Mutation Database; P/LP, pathogenic or likely pathogenic; VUS, variant of unknown significance; B/LB, benign/likely benign; AMP/ASCO/CAP, the Association of Molecular Pathology, American Society of Clinical Oncology, and College of American Pathologists; ACMG/AMP, American College of Medical Genetics and Genomics and Genomics and the Association of Molecular Pathology.**

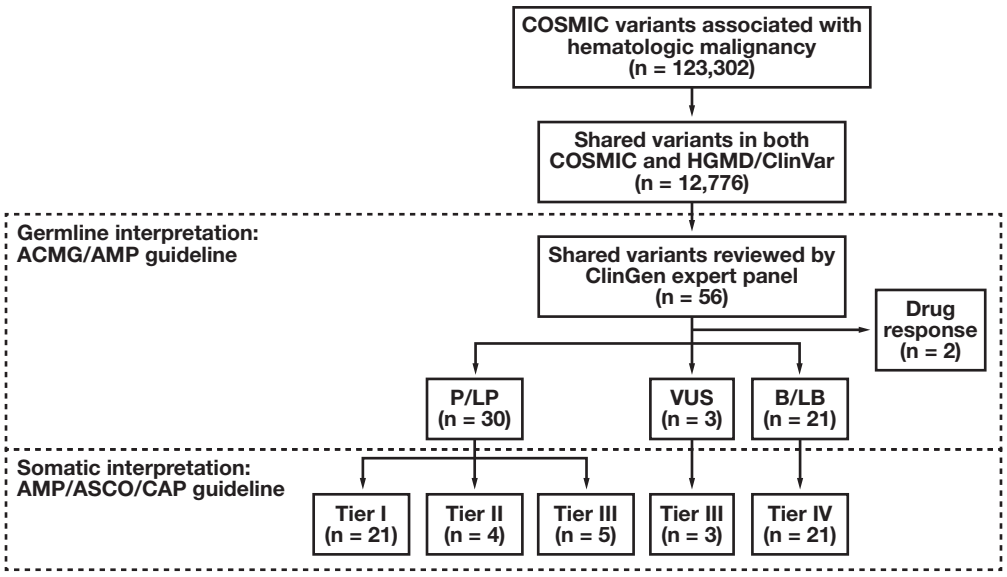

TABLE 2. **Pathogenic Variants of Unknown Clinical Significance in Cancer**

Gene	Nucleotide	Amino Acid	ClinVar	HGMD	Evidences for pathogenecity	COSMIC	GENIE	Oncogenecity	Germline classification	Somatic classification
PTPN11	c.922A > G	p.N308D	Pathogenic	DM	PS2, PS3, PP2, PP3, PM2, PP1	COSM24612	Somatic	Neutral	Pathogenic	Tier III
PTPN11	c.1530G > C	p.Q510H	Pathogenic	DM	PP2, PP3, PM2, PM6, PM5	COSM1318058	Somatic	Not characterized	Pathogenic	Tier III
BRAF	c.1741A > G	p.N581D	Pathogenic	DM	PS3, PP2, PP3, PM1, PM2, PM6	COSM6964515	Somatic	Not characterized	Pathogenic	Tier III
BRAF	c.1406G > A	p.G469E	Pathogenic	DM	PS2, PS3, PP2, PP3, PM2, PM1	COSM461	Somatic	Conflicting evidences	Pathogenic	Tier III
BRAF	c.735A > C	p.L245F	Pathogenic	DM	PS2, PP3, PP2, PM2, PM1, PS4	COSM3634278	Not available	Conflicting evidences	Pathogenic	Tier III

HGMD, the Human Genome Mutation Database; DM, disease-causing mutation; COSMIC, the Catalog of Somatic Mutations in Cancer; GENIE, Genomics Evidence Neoplasia Information Exchange.
[a]*The Tier III variants are defined as variants of unknown clinical significance regarding diagnosis, prognosis, and therapeutics of cancer.*

Hematologic malignant neoplasms were previously considered sporadic rather than inherited. However, in recent studies,[13–15] it has been reported that germline predisposition is associated with approximately 10% of patients with hematologic malignant neoplasms, as a whole. Further, new diagnostic categories, such as *myeloid neoplasms with germline predisposition*, have been added to the revised World Health Organization (WHO) classification.[16] Currently, germline-shared somatic variants have been reported in a small number of genes such as NRAS and EGFR, especially in solid cancer. The study of the shared variants in hematologic malignant neoplasms was previously underappreciated.

Currently, little is known regarding the frequency of specific variant overlapping between the germline and somatic databases. One previous study about shared variants[6] was designed to investigate the questions using a control-population database, such as gnomAD, rather than a disease-associated germline database. Further, there is a lack of data comparing the differences between somatic and germline interpretations of specific variants.[17]

The aim of this study was to investigate the frequency of variants shared between germline databases and somatic databases for hematologic malignant neoplasms. Also, the differences in the clinical interpretations of shared variants were evaluated using the current standard interpretation guidelines in the germline and the somatic contexts, respectively. In particular, the author focused on pathogenicity, oncogenecity, and clinical actionability of the shared variants.

Materials and Methods

The Catalog of Somatic Mutations in Cancer (COSMIC, release v91, April 2020) variants and the Human Genome Mutation Database (HGMD, professional version 2019.01) variants were downloaded. A total of 123,302 variants associated with hematologic malignant neoplasms were used for the analysis of shared variants (**FIGURE 1**).

All studied variants were located in 99 genes associated with hematologic malignant neoplasms according to the WHO classification and National Comprehensive Cancer Network guideline/European LeukemiaNet: *ABL1*, *ABL2*, *ALK*, *ANKRD26*, *ASXL1*, *ATM*, *BCL2*, *BCL6*, *BCOR*, *BCR*, *BIRC3*, *BRAF*, *CALR*, *CBFB*, *CBL*, *CCND1*, *CDKN2A*, *CDKN2B*, *CEBPA*, *CRLF2*, *CSF1R*, *CSF3R*, *DDX41*, *DEK*, *DHX15*, *DKC1*, *DNMT3A*,

EBF1, *EP300*, *ETNK1*, *ETV6*, *EZH2*, *FGFR1*, *FIP1L1*, *FLT3*, *GATA2*, *GATA3*, *IDH1*, *IDH2*, *IKZF1*, *IL3*, *IL7R*, *JAK1*, *JAK2*, *JAK3*, *KDM6A*, *KIT*, *KMT2A (MLL1)*, *KRAS*, *MECOM*, *MGA*, *MKL1*, *MLLT3*, *MPL*, *MTCP1*, *MYC*, *MYD88*, *MYH11*, *NF1*, *NOTCH1*, *NPM1*, *NRAS*, *NTRK3*, *NUP214*, *PBX1*, *PCM1*, *PDGFRA*, *PDGFRB*, *PHF6*, *PML*, *PRPF8*, *PTPN11*, *RAD21*, *RARA*, *RB1*, *RBM15*, *RUNX1*, *RUNX1T1*, *SETBP1*, *SF3B1*, *SH2B3*, *SMC1A*, *SMC3*, *SRSF2*, *STAG2*, *STAT3*, *TAL1*, *TCF3*, *TERC*, *TERT*, *TET2*, *TLX1*, *TLX3*, *TP53*, *TYK2*, *U2AF1*, *WT1*, *ZBTB7A*, *ZRSR2*.[16,18–20] The annotations of COSMIC variants were performed using the ANNOVAR and InterVar software (intervar_20180118).[21]

The HGMD, ClinVar (clinvar_20190305), and Online Mendelian Inheritance in Man (OMIM, 2020.08) were used as germline databases; COSMIC and Genomics Evidence Neoplasia Information Exchange (GENIE, version 8.0, June 2020) were used as somatic databases. A *germline-shared somatic variant* was defined as a variant with identical genomic position and nucleotide alterations in the germline databases and somatic databases.

A *somatic variant* was defined as a variant that is present in tumor specimens but absent from nontumor specimens from the same individuals. To avoid the possibility of spurious shared variants due to the contamination of germline variants into COSMIC databases, the origin of the shared variants was analyzed using GENIE. If COSMIC variants were present in the nontumor and tumor specimens from the GENIE database, the variants were considered to be spurious COSMIC variants with germline nature.

The germline interpretation of shared variants was analyzed based on the American College of Medical Genetics and Genomics and Genomics and the Association of Molecular Pathology (ACMG/AMP) guideline: P/LP, variant of unknown significance (VUS), benign/likely benign (B/LB).[4] To avoid the possibility of subjective interpretation of the variants, selection of germline variants were restricted to previously reported HGMD variants or ClinVar variants reviewed by an expert panel with the definitive evidences based on ACMG/AMP guidelines.[4] The somatic interpretation of the shared variants was classified into 4 tiers based on the Association of Molecular Pathology, American Society of Clinical Oncology, and College of American Pathologists (AMP/ASCO/CAP) guideline: tier I (Variants of Strong Clinical Significance), tier II (Variants of Potential Clinical Significance, tier III (Variants of Unknown Clinical Significance), and tier IV (Benign or Likely Benign Variants).[5]

The evidences of variant oncogenicity and clinical actionability of the shared variants were extracted from the following knowledge bases (assessed in June 2020) and the previous large scale in vitro functional studies: the Cancer Genome Interpreter Cancer Biomarkers Database (CGI), Clinical Interpretation of Variants in Cancer (CIViC), Precision Oncology KnowledgeBase (OncoKB), Jackson Laboratory Clinical Knowledgebase (JAX-CKB), Database of Evidence for Precision Oncology (DEPO), My Cancer Genome (MCG), Precision Medicine Knowledge Base (PMKB), and the Pharmacogenomics KnowledgeBase (PharmGKB).[1,22–30]

Results

The number of germline-shared somatic variants from COSMIC and ClinVar/HGMD was 12,776 (10% of the COSMIC variants and 6% of the HGMD variants) (**FIGURE 1**). Among the shared variants, 2 variants associated with drug response were excluded, and the germline pathogenicity of 54 variants was reviewed based on the ACMG/AMP guideline with definitive evidence (**FIGURE 1**). Further, GENIE dataset analysis revealed that the shared variants were somatic in origin; a total of 30 variants among 54 variants were also identified in GENIE datasets, and there were no spurious COSMIC variants. The variant allele frequency of the shared variants in tumor specimens ranged from 4 to 62% (median, 23%), according to the GENIE database.

Interpretation of a total of 54 shared variants were categorized as follows: 30 P/LP, 3 VUS, and 21 B/LB. A total of 30 P/LP germline variants were reclassified to tier I (21/30 [70%]), tier II (4/30 [13%]), and tier III (5/30 [17%]) somatic variants (**FIGURE 1**, **TABLE 1**, and **TABLE 2**). Three VUS and 21 B/LB germline variants were reclassified to tier III and tier IV, respectively (**FIGURE 1**). Among the shared variants, the germline P/LP and tier III variants include the *PTPN11* c.922A > G (p.N308D) and c.1530G > C (p.Q510H); *BRAF* c.1741A > G (p.N581D), c.1406G > A (p.G469E), and c.735A > C (p.L245F) variants (**TABLE 2**).

Discussion

This study investigated the frequency of germline-shared somatic variants associated with hematologic malignant neoplasms and discovered that 10% of the COSMIC variants and 6% of HGMD variants could be interpreted in germline and somatic contexts. Meyerson et al[6] have reported that 6% of gnomAD variants and 21% of TCGA variants were shared between the germline and somatic databases. The data by Meyerson et al were from control-population databases, such as gnomAD as a germline database, and were not limited to specific cancer type.[6] However, this study was performed using disease-associated databases, such as HGMD as germline database and focused on genetic variants with hematological malignant neoplasms. The differences in frequency of the shared variants could be attributable to the difference of databases, number of analyzed variants, and cancer type. It should be noted that this study focuses on shared variants between disease-associated germline and somatic databases, rather than overlapped variants between germline polymorphisms and somatic databases.

Also, this study directly compared the germline and somatic interpretations of the shared variants according to the current standard guidelines. The author noted that 17% of P/LP variants in germline context were reclassified into tier III somatic variants in terms of clinical actionability. The *PTPN11* c.922A > G (p.N308D), and c.1530G > C (p.Q510H) and the *BRAF* c.1741A > G (p.N581D), c.1406G > A (p.G469E), and c.735A > C (p.L245F), which were interpreted as tier III somatic variants, were also associated with RASopathies, including Noonan syndrome, LEOPARD syndrome, and cardiofaciocutaneous syndrome in the germline context.

RASopathies are a group of developmental disorders with an increased risk of multiple neoplasms, including rhabdomyosarcoma, acute lymphoblastic leukemia, and juvenile myelomonocytic leukemia (JMML).[9,12] This information in the germline setting could inform the risk of hereditary cancer predisposition. However, the clinical significance of these variants would be missed by the single use of the AMP/ASCO/CAP guideline in tumor-only sequencing. Considering the difference in clinical significance between germline and somatic interpretations, distinguishing somatic and germline variants are crucial for shared variant interpretations, especially in tumor-only sequencing.

The AMP/ASCO/CAP interpretation guideline has recommended sequencing of normal tissues for definitive classification of potential

germline variants.[5] In patients with hematologic malignant neoplasms, testing using peripheral blood cannot distinguish germline variants from somatic variants. Although DNA from skin fibroblasts is an ideal source of germline testing for hematologic malignant neoplasms, skin biopsy is impractical due to the invasiveness of the procedures. Currently, family history, clinical features, and certain mutations provide some important clues to genetic predisposition to hereditary hematologic malignant neoplasms.[15] However, negative family history does not exclude the genetic predisposition to hematologic malignant neoplasms.[31] Recognition of the shared variants might be an alternative red flag warning of hereditary hematologic malignant neoplasms in tumor-only sequencing. Future studies regarding the roles of germline-shared somatic variants will be required in the clinical settings.

It should be noted that there was 1 additional interpretation challenge, in *PTPN11* c.417G > C (p.E139D). Considering the alterations of protein binding properties, the variant was determined to be pathogenic in the germline context.[32,33] However, considering no changes in cell proliferation and viability, oncogenecity of the same variant was not established in the somatic context.[30] Although oncogenic impact of the variant was neutral, the same variant was assigned as tier II because the variant was frequently reported in patients with JMML and associated with poor survival.[34,35] This finding suggested that the oncogenecity and clinical actionability should be interpreted in a different aspect in the somatic context.

In this study, the clinical interpretation was performed in a small subset among a total of 12,776 shared variants. Currently, it has been recommended that the interpretation of germline variants identified from tumor sequencing be based on the ACMG/AMP guideline, rather than the AMP/ASCO/CAP guideline.[4,5] However, it has been reported[36] that germline interpretation, even based on the ACMG/AMP guideline, could be different across laboratories; initial concordance of ACMG-AMP guidelines–based variant classification was only 34%. To avoid controversial interpretation of germline variants, this study selected only 54 shared variants that had already been reviewed by expert panels from ClinGen and determined to have definitive evidence of pathogenicity.

Conclusion

This study directly compared the germline and somatic interpretations of variants shared in ClinVar/HGMD and COSMIC. Germline-shared somatic variants should be simultaneously interpreted in germline and somatic contexts. Distinguishing somatic and germline variants is crucial for shared variant interpretations, especially in tumor-only sequencing. This is the first study, to the best of my knowledge, regarding different clinical interpretations of shared variants based on the current standard guidelines. The current study takes a meaningful step in bridging the interpretation gap between the somatic variants and germline variants in cancer. I recommend further prospective clinical studies be conducted to investigate the clinical implications of shared variants.

Personal and Professional Conflicts of Interest

None reported.

REFERENCES

1. Bailey MH, Tokheim C, Porta-Pardo E, et al.; MC3 Working Group; Cancer Genome Atlas Research Network. comprehensive characterization of cancer driver genes and mutations. *Cell.* 2018;173(2):371–385.e18.
2. Huang K-L, Mashl RJ, Wu Y, et al; Cancer Genome Atlas Research Network. Pathogenic germline variants in 10,389 adult cancers. *Cell.* 2018;173(2):355–370.e14.
3. Seifert BA, O'Daniel JM, Amin K, et al. Germline analysis from tumor-germline sequencing dyads to identify clinically actionable secondary findings. *Clin Cancer Res.* 2016;22(16):4087–4094.
4. Richards S, Aziz N, Bale S, et al; ACMG Laboratory Quality Assurance Committee. Standards and guidelines for the interpretation of sequence variants: a joint consensus recommendation of the American College of Medical Genetics and Genomics and the Association for Molecular Pathology. *Genet Med.* 2015;17(5):405–424.
5. Li MM, Datto M, Duncavage EJ, et al. Standards and guidelines for the interpretation and reporting of sequence variants in cancer: A Joint Consensus Recommendation of the Association for Molecular Pathology, American Society of Clinical Oncology, and College of American Pathologists. *J Mol Diagn.* 2017;19(1):4–23.
6. Meyerson W, Leisman J, Navarro FCP, Gerstein M. Origins and characterization of variants shared between databases of somatic and germline human mutations. *BMC Bioinformatics.* 2020;21(1):227.
7. Milholland B, Dong X, Zhang L, Hao X, Suh Y, Vijg J. Differences between germline and somatic mutation rates in humans and mice. *Nat Commun.* 2017;8:15183.
8. Bell DW, Gore I, Okimoto RA, et al. Inherited susceptibility to lung cancer may be associated with the T790M drug resistance mutation in EGFR. *Nat Genet.* 2005;37(12):1315–1316.
9. Dunnett-Kane V, Burkitt-Wright E, Blackhall FH, Malliri A, Evans DG, Lindsay CR. Germline and sporadic cancers driven by the RAS pathway: parallels and contrasts. *Ann Oncol.* 2020;31(7):873–883.
10. Yu HA, Arcila ME, Harlan Fleischut M, et al. Germline EGFR T790M mutation found in multiple members of a familial cohort. *J Thorac Oncol.* 2014;9(4):554–558.
11. Gazdar A, Robinson L, Oliver D, et al. Hereditary lung cancer syndrome targets never smokers with germline *EGFR* gene T790M mutations. *J Thorac Oncol.* 2014;9(4):456–463.
12. Rauen KA. The RASopathies. *Annu Rev Genomics Hum Genet.* 2013;14:355–369.
13. Feurstein S, Drazer MW, Godley LA. Genetic predisposition to leukemia and other hematologic malignancies. *Semin Oncol.* 2016;43(5):598–608.
14. Furutani E, Shimamura A. Germline genetic predisposition to hematologic malignancy. *J Clin Oncol.* 2017;35(9):1018–1028.
15. Kohlmann W, Schiffman JD. Discussing and managing hematologic germ line variants. *Blood.* 2016;128(21):2497–2503.
16. Swerdlow SH, Campo E, Harris NL, et al. *Tumours of Haematopoietic and Lymphoid Tissues*. Revised 4th edition. IARC. 2017;2.
17. Moody EW, Vagher J, Espinel W, Goldgar D, Hagerty KJ, Gammon A. Comparison of somatic and germline variant interpretation in hereditary cancer genes. *JCO Precision Oncol*. 2019;3:1–8.
18. Döhner H, Estey E, Grimwade D, et al. Diagnosis and management of AML in adults: 2017 ELN recommendations from an international expert panel. *Blood.* 2017;129(4):424–447.
19. Heidel FH, Gale RP, Hochhaus A. Managing myeloproliferative neoplasms evidence based on the ELN treatment recommendations 2018. *Leukemia.* 2018;32(5):1055–1056.
20. National Comprehensive Cancer Network. Accessed April 4, 2021. https://www.nccn.org/professionals/physician_gls/default.aspx
21. Liu X, Wu C, Li C, Boerwinkle E. dbNSFP v3.0: a one-stop database of functional predictions and annotations for human nonsynonymous and splice-site SNVs. *Hum Mutat.* 2016;37(3):235–241.
22. Tamborero D, Rubio-Perez C, Deu-Pons J, et al. Cancer Genome Interpreter annotates the biological and clinical relevance of tumor alterations. *Genome Med.* 2018;10(1):25.
23. Griffith M, Spies NC, Krysiak K, et al. CIViC is a community knowledgebase for expert crowdsourcing the clinical interpretation of variants in cancer. *Nat Genet.* 2017;49(2):170–174.

24. Chakravarty D, Gao J, Phillips SM, et al. OncoKB: a precision oncology knowledge base. *JCO Precis Oncol*. 2017;2017:PO.17.00011.
25. Patterson SE, Liu R, Statz CM, Durkin D, Lakshminarayana A, Mockus SM. The clinical trial landscape in oncology and connectivity of somatic mutational profiles to targeted therapies. *Hum Genomics.* 2016;10:4.
26. Sun SQ, Mashl RJ, Sengupta S, et al. Database of evidence for precision oncology portal. *Bioinformatics.* 2018;34(24):4315–4317.
27. Taylor AD, Micheel CM, Anderson IA, Levy MA, Lovly CM. The Path(way) less traveled: a pathway-oriented approach to providing information about precision cancer medicine on My Cancer Genome. *Transl Oncol.* 2016;9(2):163–165.
28. Whirl-Carrillo M, McDonagh EM, Hebert JM, et al. Pharmacogenomics knowledge for personalized medicine. *Clin Pharmacol Ther.* 2012;92(4):414–417.
29. Huang L, Fernandes H, Zia H, et al. The cancer precision medicine knowledge base for structured clinical-grade mutations and interpretations. *J Am Med Inform Assoc.* 2017;24(3):513–519.
30. Ng PK-S, Li J, Jeong KJ, et al. Systematic functional annotation of somatic mutations in cancer. *Cancer Cell.* 2018;33(3):450–462.e10.
31. Zhang J, Walsh MF, Wu G, et al. germline mutations in predisposition genes in pediatric cancer. *N Engl J Med.* 2015;373(24):2336–2346.
32. Keilhack H, David FS, McGregor M, Cantley LC, Neel BG. Diverse biochemical properties of Shp2 mutants. Implications for disease phenotypes. *J Biol Chem.* 2005;280(35):30984–30993.
33. Martinelli S, Torreri P, Tinti M, et al. Diverse driving forces underlie the invariant occurrence of the T42A, E139D, I282V and T468M SHP2 amino acid substitutions causing Noonan and LEOPARD syndromes. *Hum Mol Genet.* 2008;17(13):2018–2029.
34. Yoshida N, Yagasaki H, Xu Y, et al. Correlation of clinical features with the mutational status of GM-CSF signaling pathway-related genes in juvenile myelomonocytic leukemia. *Pediatr Res.* 2009;65(3):334–340.
35. Park H-D, Lee SH, Sung KW, et al. Gene mutations in the Ras pathway and the prognostic implication in Korean patients with juvenile myelomonocytic leukemia. *Ann Hematol.* 2012;91(4):511–517.
36. Amendola LM, Jarvik GP, Leo MC, et al. Performance of ACMG-AMP variant-interpretation guidelines among nine laboratories in the Clinical Sequencing Exploratory Research Consortium. *Am J Hum Genet.* 2016;98(6):1067–1076.

Association of Plasma Fibrinogen Levels on Postoperative Day 1 with 2-Year Survival of Orthotopic Liver Transplantation for HBV-Related HCC

Xia Liu, MM,[1] *Renyong Guo, MM,*[2,*] *Jie Tian, MM*[1]

[1]Department of Intensive Care Unit, First Affiliated Hospital, College of Medicine, Zhejiang University, Hangzhou, Zhejiang, China; [2]Department of Laboratory Medicine, First Affiliated Hospital, College of Medicine, Zhejiang University, Key Laboratory of Clinical In Vitro Diagnostic Techniques of Zhejiang Province, Hangzhou, Zhejiang, China; *To whom correspondence should be addressed. zygry@zju.edu.cn

Keywords: fibrinogen, hepatocellular carcinoma, survival, liver transplantation, hepatitis B virus, postoperative day

Abbreviations: OLT, orthotopic liver transplantation; HBV, hepatitis B virus; HCC, hepatocellular carcinoma; POD, postoperative day; PLT, platelet; AFP, alpha fetoprotein; TB, total bilirubin; WBC, white blood cells; Hb, hemoglobin; PT, prothrombin time; INR, international normalized ratio; APTT, activated partial thromboplastin time; MELD, model for end-stage liver disease; ROC, receiver operating characteristic; NLR, neutrophil-lymphocyte ratio.

Laboratory Medicine 2022;53:30–38; DOI: 10.1093/labmed/lmab052

ABSTRACT

Objective: To clarify the prognostic values of hemostatic parameters to predict the survival of patients undergoing orthotopic liver transplantation (OLT) for hepatitis B virus (HBV)-related hepatocellular carcinoma (HCC).

Methods: The data of 182 consecutive adult patients who underwent OLT for HBV-related HCC were subjected to univariate and multivariate analyses.

Results: Ascites and fibrinogen levels on postoperative day (POD) 1 were independent predictors of postoperative 2-year mortality (both P <.05). Kaplan-Meier survival analysis showed that the higher the fibrinogen level on POD 1, the better the 1- and 2-year survival of patients with ascites (P <.05), whereas the fibrinogen level on POD 1 was associated with 1-year (P <.05) but not 2-year survival of patients without ascites.

Conclusion: Fibrinogen on POD 1 is a predictor of 2-year post-OLT survival of patients with HBV-related HCC with ascites.

Hepatocellular carcinoma (HCC) is a leading cause of cancer-related death worldwide.[1] Epidemiological studies have shown that hepatitis B virus (HBV) infection is the main cause of HCC, especially in regions throughout Asia.[2,3] Furthermore, HBV-related HCC is more common in male than in female patients.[4] Because the liver is the major organ that synthesizes coagulation, anticoagulation, and fibrinolytic factors, patients with HCC usually present with decreased synthesis of pro- and antihemostatic proteins by the diseased liver, reduced platelet (PLT) levels, and altered structures of synthesized coagulation factors and inhibitors. These changes are correlated with the degree of hepatocellular damage.[5]

Orthotopic liver transplantation (OLT) has become the optimal treatment option for unresectable HCC and liver cirrhosis. Most patients have multifactorial hemostatic disorders during liver transplantation.[6] Concomitantly, the simultaneous decreases in procoagulant and anticoagulant factors create a state of so-called rebalanced hemostasis. However, this rebalanced hemostatic system is more fragile than that of healthy individuals, resulting in either hypocoagulability or hypercoagulability.[5,7] Because the liver is the primary organ regulating hemostasis, pre- or postoperative hemostatic parameters can be used to monitor patients undergoing OLT.[8] Furthermore, depending on the function of the transplanted liver, post-OLT hemostatic parameters may be more useful to predict patient survival. However, relatively few studies have investigated hemostasis parameters in the post-OLT period.[8-11] A study by Novaković-Anucin et al[6] showed that investigated laboratory parameters normalized within 7 to 14 days after transplantation, whereas Moia et al[8] observed that the activated partial thromboplastin time at day 8 post-OLT was an independent predictor of 6-month survival.

The aim of this retrospective analysis of short-term dynamic changes in the hemostatic system after OLT in patients with HBV-related HCC was to determine the predictive value of hemostatic parameters during the early postoperative period as markers of survival after OLT.

Patients and Methods

Study Patients

The study cohort consisted of 276 consecutive patients with HBV-related HCC who underwent OLT from June 2012 to May 2017 at the Depart-

ment of Hepatic Surgery of the First Affiliated Hospital of Zhejiang University (Hangzhou, China). Transplants were performed using the classic or modified piggyback technique[5] with a strict anesthetic protocol. All patients received homogeneous treatment in the intensive care unit after surgery. Patients aged <18 years (n=3) and those with diabetes mellitus (n=15), acute inflammatory disease (n=18), a second primary tumor (n=3), or complications such as thrombosis (n=36), along with those who underwent surgery within 3 months before enrollment (n=4), underwent a second or subsequent OLT (n=8), or had died during surgery (n=7) were excluded from the analysis. In total, 182 patients were included in the study. All patients were followed up until the date of death, loss to follow-up, or July 10, 2019. The study protocol was approved by the Institutional Research Ethics Committee of the First Affiliated Hospital of Zhejiang University and performed in accordance with the principles embodied in the Declaration of Helsinki. Written informed consent was obtained from all patients before surgery.

Clinical and Laboratory Variables

Preoperative characteristics, laboratory variables, perioperative management, surgical procedures, and postoperative laboratory test results (postoperative day [POD] 1 to POD 7) from all patients were retrieved from the hospital electronic medical record system. The laboratory variables included serum levels of alpha fetoprotein (AFP), creatinine, total bilirubin (TB), white blood cells (WBCs), neutrophils, lymphocytes, hemoglobin (Hb), PLTs, plasma fibrinogen, and D-dimer in addition to prothrombin time (PT), international normalized ratio (INR), and activated partial thromboplastin time (APTT).

Serum levels of creatinine (enzymatic method) and TB (colorimetric diazo method) were measured using a Hitachi 7600 analyzer (Hitachi Ltd., Tokyo, Japan) with commercial kits (Roche Diagnostics, Mannheim, Germany). The levels of PT (coagulation method), INR (coagulation method), APTT (coagulation method), fibrinogen (Clauss method), and D-dimer (immunoturbidometric method) were measured using the Sysmex CS 5100 coagulation analyzer (Sysmex Corporation, Kobe, Japan) with dedicated reagents (Siemens AG, Marburg, Germany). Serum levels of AFP were determined using a chemiluminescent microparticle immunoassay with the ARCHITECT i2000SR System (Abbott Laboratories, Chicago, IL). Serum levels of WBCs, neutrophils, lymphocytes, Hb, and PLTs were measured with a Sysmex XE-2100 automatic hematologic analyzer with reagents and protocols from the manufacturer (Sysmex, Kobe, Japan). The model for end-stage liver disease (MELD) score was obtained using the following formula: $R = 3.8 \times \ln$ [TB (mg/dl)] + 11.2 × ln (INR) + 9.6 × ln [Cr (mg/dl)] + 6.4 × cause (cause: 0 for cholesteric cirrhosis and alcoholic cirrhosis, 1 for virus and other reasons).[12]

Statistical Analyses

Data are expressed as the mean ± standard deviation or the median and interquartile range if the distribution of the continuous variables was skewed. Categorical variables are expressed as numbers with percentages. The time-series laboratory data were compared between groups by 2-way repeated-measures analysis of variance. Cox regression analysis (stepwise forward method) was performed to analyze the relationship between patients' clinical characteristics, perioperative management, laboratory variables, and risk of death after OLT. Spearman's rank correlation coefficient was used to evaluate the relationships between parameters. The optimal cutoff value and diagnostic performance of the laboratory variables were determined using the area under the receiver operating characteristic (ROC) curve. The sensitivity and specificity of laboratory variables to predict survival after OLT were calculated. Patient survival was compared using Kaplan-Meier curves, and statistical significance was assessed with the log-rank test. GraphPad Prism 5 software (San Diego, CA) and SPSS software version 16.0 (SPSS Inc., Chicago, IL) were used for analyses. A probability (P) value of ≤.05 was considered statistically significant.

Results

Patient Characteristics

The final cohort consisted of 173 (95.1%) men and nine (4.9%) women with a mean age of 51.3 years. All patients were diagnosed with HBV-related HCC. The patients' preoperative characteristics and laboratory variables, in addition to perioperative transfusion management, are presented in **TABLE 1**. Tumor recurrence was observed in 28 (15.4%) patients. The 1- and 2-year postoperative survival rates of all 182 patients were 65.9% and 50.5%, respectively.

Dynamics of Fibrinogen Levels After OLT

Longitudinal analysis of fibrinogen levels was carried out at 1, 3, 5, and 7 days after OLT according to survival at postoperative years 1 and 2 and HCC recurrence. As shown in **FIGURE 1**, fibrinogen levels gradually increased from the day before surgery to POD 7 in the >1 year and >2 year survival time groups and the non-HCC recurrence group, but they were significantly decreased on POD 1 as compared with preoperative levels in the ≤1 year and ≤2 year survival time groups and the HCC recurrence group (all P <.01). Furthermore, there were significant differences in fibrinogen levels at each observation point from the day before surgery to POD 7 between the >1 year and ≤1 year survival time groups (all P <.05), on POD 1 and POD 5 between the >2 year and ≤2 year survival time groups, and on the day before surgery between the HCC and non-HCC recurrence groups (all P <.05). Finally, there were significant differences in the dynamic changes of fibrinogen levels from the day before surgery to POD 7 between the >1 year and ≤1 year survival time groups, the >2 year and ≤2 year survival time groups, and the HCC and non-HCC recurrence groups (all P <.05).

Independent Prognostic Factors for Death

The median values were used to dichotomize the levels of age, body mass index, AFP, intraoperative blood loss, creatinine, TB, INR, MELD score, WBCs, neutrophil-lymphocyte ratio (NLR), Hb, PLTs, PT, APTT, fibrinogen, and D-dimer on POD 1. The results of univariate analysis revealed that the size of the largest tumor, ascites, intraoperative blood loss, intraoperative transfusion of fibrinogen concentrate, and fibrinogen levels on POD 1 were associated with postoperative death. The results of multivariate analysis showed that ascites and fibrinogen levels on POD 1 were independent predictors of postoperative death (both P <.05; **TABLE 2**). **FIGURE 2** shows the survival rates of the 182 patients undergoing OLT according to the range of fibrinogen levels on POD 1. As the fibrinogen level on POD 1 increased, the 1- and 2-year survival rates both gradually increased.

Correlation Between Fibrinogen Levels and Clinical Parameters on POD 1

Potential correlations between several clinical parameters and fibrinogen levels on POD 1 were also investigated. As shown in **FIGURE 3**,

TABLE 1. Demographic and Clinical Characteristics of 182 Participants

Variables	Patients Undergoing OLT (n=182)
Sex (M/F)	173/9
Age (y)	51.3 ± 8.8
BMI (kg/m^2)	22.1 (20.2–23.9)
AFP (μg/mL)	31.3 (4.3–581.2)
Size of largest tumor (>5 cm/≤5 cm)	49/133
Tumor numbers (>3/≤3)	77/105
Vascular invasion, n (%)	75 (41.2)
Complications	
Ascites, n (%)	121 (66.5)
HE, n (%)	28 (15.4)
SBP, n (%)	11 (6.0)
HRS, n (%)	11 (6.0)
EGV, n (%)	25 (13.7)
Laboratory assessment	
Creatinine (μmol/L)	68.5 (56.0–83.0)
TB (μmol/L)	37.5 (19.0–72.3)
INR	1.29 (1.15–1.47)
MELD score	9.6 (5.9–13.9)
WBCs (×10^9/L)	5.4 (3.5–7.6)
NLR	4.46 (2.25–10.35)
Hb (g/L)	113.4 ± 21.2
PLTs (×10^9/L)	83.0 (53.5–126.0)
PT (s)	15.0 (13.2–17.0)
APTT (s)	42.4 (33.6–56.0)
Fibrinogen (g/L)	1.97 (1.50–2.76)
D-dimer (mg/L FEU)	2.69 (1.23–7.56)
Intraoperative blood loss (L)	1.10 (0.80–2.00)
Intraoperative transfusion	
FFP (L, n*P* = 137 [75.3%])	0.54 (0.29–1.04)
RBCs (units, n*P* = 70 [38.5%])	5.0 (2.0–9.1)
PLTs (units, n*P* = 15 [8.2%])	14.0 (11.0–28.0)
Fibrinogen concentrate (g, n*P* = 23 [12.6%]) [12.6%])	2.0 (1.5–2.5)
Postoperative outcomes	
Tumor recurrence, n (%)	28 (15.4)
Survival at 1 y, n (%)	120 (65.9)
Survival at 2 y, n (%)	92 (50.5)

AFP, alpha fetoprotein; APTT, activated partial thromboplastin time; BMI, body mass index; EGV, esophageal and gastric varices; FEU, fibrinogen-equivalent units; FFP, fresh-frozen plasma; Hb, hemoglobin; HE, hepatic encephalopathy; HRS, hepatorenal syndrome; INR, international normalized ratio; MELD, model for end-stage liver disease; NLR, neutrophil-lymphocyte ratio; PLTs, platelets; PT, prothrombin time; RBCs, red blood cells; SBP, spontaneous bacterial peritonitis; SD, standard deviation; TB, total bilirubin; WBCs, white blood cells.
Data are expressed as mean ± SD, medians with interquartile ranges, or the number of patients (%).

FIGURE 1. Dynamics of fibrinogen levels in patients undergoing OLT according to postoperative survival time and HCC recurrence. The error bars represent standard deviations. HCC, hepatocellular carcinoma; OLT, orthotopic liver transplantation.

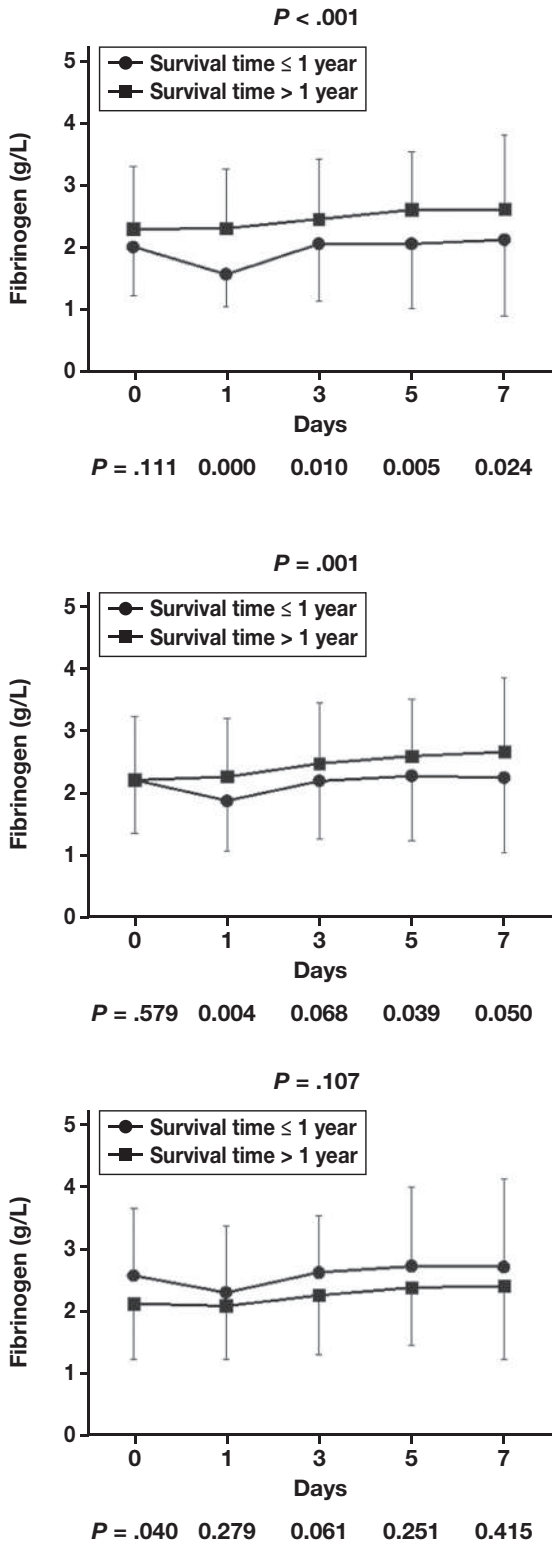

fibrinogen levels on POD 1 were positively correlated with WBCs, NLR, Hb, and PLTs but negatively correlated with the MELD score, PT, APTT, and D-dimer (all $P < .05$).

Determination of Cutoff Values

The fibrinogen levels on POD 1 were significantly higher in patients who survived for 1 year (2.31 ± 0.94 g/L vs 1.58 ± 0.52 g/L; $P < .001$) and

TABLE 2. Cox Regression Analyses of Coagulative Parameters on POD 1 After OLT for Prediction of Death at Year 2

Variables	Univariate Analysis		Multivariate Analysis	
	HR (95% CI)	*P* Value	HR (95% CI)	*P* Value value
Sex (F vs M)	1.701 (0.742–3.898)	.209		
Age (>51.0 y vs ≤51.0 y)[a]	1.200 (0.793–1.815)	.388		
BMI (>22.1 kg/m^2 vs ≤22.1 kg/m^2)[a]	0.777 (0.506–1.193)	.249		
AFP (>31.3 µg/mL vs ≤31.3 µg/mL)[a]	1.443 (0.951–2.192)	.085	1.430 (0.933–2.193)	.101
Size of largest tumor (>5 cm vs ≤5 cm)[a]	1.704 (1.098–2.644)	.017	1.479 (0.943–2.320)	.088
Tumor numbers (>3 vs ≤3)[a]	0.883 (0.580–1.344)	.562		
Vascular invasion (Y vs N)[a]	0.892 (0.584–1.363)	.597		
Complications				
Ascites (Y vs N)[a]	1.840 (1.145–2.959)	.012	**1.682 (1.037–2.730)**	**.035**
HE (Y vs N)[a]	1.023 (0.579–1.810)	.937		
SBP (Y vs N)[a]	1.691 (0.781–3.664)	.183		
HRS (Y vs N)[a]	1.447 (0.63203.313)	.382		
EGV (Y vs N)[a]	0.582 (0.292–1.159)	.124		
Intraoperative blood loss (>1.10 L vs ≤1.10 L)	1.621 (1.068–2.462)	.023	1.300 (0.835–2.022)	.245
Intraoperative transfusion				
FFP (Y vs N)	1.016 (0.632–1.632)	.948		
RBCs (Y vs N)	1.283 (0.841–1.955)	.247		
PLTs (Y vs N)	1.822 (0.914–3.630)	.088	0.919 (0.386–2.190)	.849
Fibrinogen concentrate (Y vs N)	2.355 (1.307–4.243)	.004	1.693 (0.939–3.053)	.080
Creatinine (>89.5 µmol/L vs ≤89.5 µmol/L)	0.910 (0.597–1.386)	.660		
TB (>78.5 µmol/L vs ≤78.5 µmol/L)	1.199 (0.787–1.826)	.397		
INR (>1.36 vs ≤1.36)	1.116 (0.738–1.687)	.603		
MELD score (>15.3 vs ≤15.3)	1.286 (0.844–1.958)	.242		
WBCs (>9.8 × 10^9/L vs ≤9.8 × 10^9/L)	1.213 (0.794–1.853)	.373		
NLR (>28.83 vs ≤28.83)	0.808 (0.531–1.232)	.322		
Hb (>96 g/L vs ≤96 g/L)	0.755 (0.476–1.199)	.234		
PLTs (>72 × 10^9/L vs ≤72 × 10^9/L)	1.418 (0.928–2.166)	.107		
PT (>15.8 s vs ≤15.8 s)	1.032 (0.682–1.560)	.883		
APTT (>42.6 s vs ≤42.6 s)	1.258 (0.831–1.903)	.278		
Fibrinogen (>1.87 g/L vs ≤1.87 g/L)	0.478 (0.314–0.729)	.001	**0.499 (0.321–0.773)**	**.002**
D-dimer (>6.62 mg/L FEU vs ≤6.62 mg/L) FEU)	0.785 (0.510–1.208)	.271		

AFP, alpha fetoprotein; APTT, activated partial thromboplastin time; BMI, body mass index; CI, confidence interval; EGV, esophageal and gastric varices; FEU, fibrinogen-equivalent units; FFP, fresh-frozen plasma; Hb, hemoglobin; HE, hepatic encephalopathy; HR, hazard ratio; HRS, hepatorenal syndrome; INR, international normalized ratio; MELD, model for end-stage liver disease; NLR, neutrophil-lymphocyte ratio; OLT, orthotopic liver transplantation; PLTs, platelets; POD, postoperative date; PT, prothrombin time; RBCs, red blood cells; SBP, spontaneous bacterial peritonitis; TB, total bilirubin; WBCs, white blood cells.

[a]*Clinical characteristics at baseline.*

2 years (2.25 ± 0.93 g/L vs. 1.87 ± 0.80 g/L, *P* = .004) as compared with those who did not. The ROC curve analysis determined that the fibrinogen levels on POD 1 were significantly correlated with 1- and 2-year survival of patients with ascites (**FIGURE 4A and 4B**) and with 1-year survival of patients without ascites (**FIGURE 4C**), whereas no correlation was observed between fibrinogen levels on POD 1 and 2-year survival of patients without ascites (**FIGURE 4D**).

Survival Rates According to Fibrinogen Levels on POD 1

To determine the ability of fibrinogen levels on POD 1 to predict 2-year postoperative survival, the median values of patients with ascites (n=121) and without ascites (n=61) were used to dichotomize the levels of fibrinogen on POD 1. The Kaplan-Meier curve showed that survival at 1 year and 2 years was significantly correlated with fibrinogen levels of ≥1.82 g/L as compared to <1.82 g/L (72.1% and 50.8% vs 40.0% and 38.3%, respectively; *P* <.001 and *P* =.011) in patients with ascites (**FIGURE 5A**). However, in patients without ascites (**FIGURE 5B**), survival at 1 year but not at 2 years was significantly correlated with fibrinogen levels of ≥2.18 g/L as compared to <2.18 g/L (93.8% and 65.6% vs 75.9% and 58.6%, respectively; *P* =.049 and *P* =.390).

Discussion

It is widely known that HCC is associated with severe hemostatic defects.[5] Although several studies have shown that the transplanted liver has sufficient synthetic capacity early after OLT,[6,13] marked

FIGURE 2. Distribution of 1-year and 2-year survival rates according to fibrinogen levels on POD 1. POD, postoperative date.

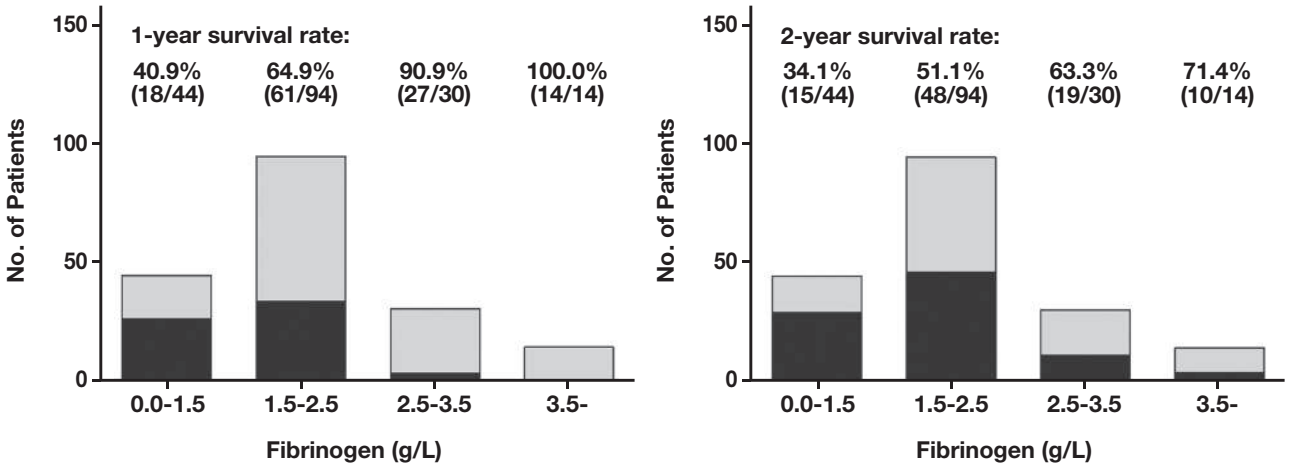

differences in hemostatic capacity have still been observed as compared to that of healthy individuals.[14] An imbalance in hemostasis was even observed in patients at 1 year after liver transplantation.[9] Previous studies have reported correlations between preoperative fibrinogen levels and tumor recurrence and clinical outcomes in patients with HCC after liver transplantation, although the results were inconsistent.[15-18] The results of the present study were in agreement with the findings by Mao et al[16] and Ayala et al,[17] showing that no significant associations were observed between preoperative fibrinogen levels and overall survival after OLT. However, relatively few studies have focused on the relationships between hemostatic parameters in the immediate postoperative period and the outcomes of patients with HCC after OLT. Therefore, in the present study, the values of hemostatic parameters to predict the survival of patients after OLT were further investigated.

Of the 182 patients with HBV-related HCC who were included for analysis, there were obvious discrepancies between men and women, because men are more likely to develop HCC among patients with chronic hepatitis B infection.[19] The results of this study showed that fibrinogen levels on POD 1 were significantly higher in patients with 1- and 2-year survivals, as compared with those of patients who died. The results of multivariate analysis revealed that ascites and plasma levels of fibrinogen on POD 1 were independent predictors of postoperative death. Wang, Zhao, et al[20] and Novaković-Anucin et al[6] found that fibrinogen levels significantly decreased during OLT but gradually returned to normal during postoperative week 1. Moia et al[8] found no association between fibrinogen levels on POD 8 and survival at 6 months. However, the latest findings by Groeneveld et al[21] showed that lower fibrinogen levels on POD 1 were associated with higher incidences of postoperative liver dysfunction and mortality within 90 days after liver resection. The findings of the present study revealed a similar prognostic value of fibrinogen on POD 1 in patients undergoing OLT. This report is the first study to show a close relationship between fibrinogen levels on POD 1 and the prognosis of patients with HBV-related HCC undergoing OLT.

Fibrinogen is a soluble plasma glycoprotein synthesized by hepatocytes that plays important roles in thrombosis, inflammatory responses, and immune regulation.[22,23] The negative correlations of fibrinogen levels with the MELD score, PT, APTT, and D-dimer on POD 1 indicated that fibrinogen levels on POD 1 partially reflected the postoperative recovery of liver function and deficiencies in hemostatic components after OLT. As important effectors of immunity and inflammation, both fibrinogen and NLR partly reflect the dynamic homeostasis of the immuno-inflammation system during OLT. However, there was no association between NLR on POD 1 and 2-year postoperative death by Cox regression analysis, suggesting that NLR on POD 1 might not be the proinflammatory factor affecting the prognoses of HCC patients undergoing OLT. Fibrinogen levels may increase in any form of inflammation as an acute-phase protein and play a proinflammatory role in cancer.[24] By serving as an extracellular matrix, fibrinogen deposition in tumor tissues enhances the interactions between PLTs and tumor cells and protects tumor cells from natural killer cytotoxicity, which may facilitate the recurrence and metastasis of HCC.[25] Several studies have shown close relationships between high plasma fibrinogen levels and tumor progressions and poor patient outcomes in several cancers, including HCC.[15,26] Notably, inconsistent with previous reports, we found no significant association between preoperative fibrinogen levels and 1- and 2-year survival after OLT but significant associations between low fibrinogen levels on POD 1 and mortality after OLT, which may indicate that the predictive potentials of fibrinogen for patient outcomes after OLT were not exclusively attributed to its association to proinflammatory roles.

Accumulating evidence from in vitro and in vivo studies suggests that an impairment of hepatic regeneration after liver surgery is associated with liver dysfunction and postoperative mortality in patients undergoing liver resection.[27,28] During initiation of liver regeneration, fibrinogen and "platelet-coagulation cross-talk" seem to be of crucial relevance. The mechanism may be that coagulation-dependent intrahepatic fibrinogen deposition drives PLT accumulation and liver regeneration after partial hepatectomy.[29] Low postoperative fibrinogen levels, resulting in the lack of intrahepatic fibrinogen deposition in the regenerating liver, may be linked to liver dysfunction and mortality after OLT.[21] In fact, except for fibrinogen, von Willebrand factor and tissue factors are also required for adequate PLT accumulation and concomitant liver regeneration after liver surgery.[30] Our results suggested that fibrinogen induced both regeneration of the transplanted liver and tumor progression. With respect to the current literature, this led us to hypothesize that the stimulating effect of fibrinogen on liver regeneration may be of greater significance than that on tumor progression, at least during the early postoperative phase

FIGURE 3. Correlations of fibrinogen levels with clinical parameters on POD 1. Data are shown as scatterplots and 95% confidence intervals. The coefficient *r* was derived from the Spearman's correlation test. APTT, activated partial thromboplastin time; Hb, hemoglobin; MELD, model for end-stage liver disease; NLR, neutrophil-lymphocyte ratio; PLTs, platelets; POD, postoperative date; PT, prothrombin time; WBCs, white blood cells.

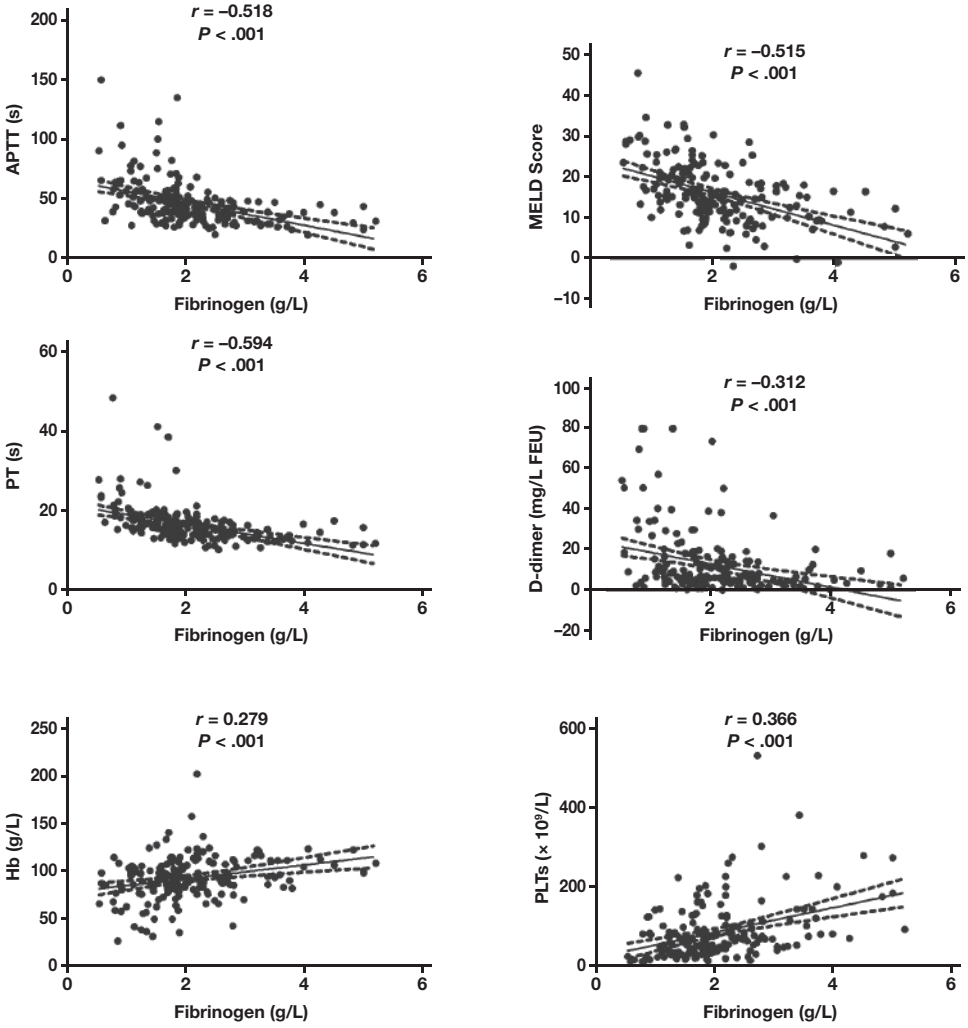

for patient outcome after OLT. Even so, crucial details regarding the mechanisms by which fibrinogen stimulates liver regeneration are as yet not fully understood. More research on this topic and large clinical examinations need to be performed to validate this hypothesis. Moreover, given the central role of fibrinogen in both hemostasis and thrombosis, little is known about whether or how plasma fibrinogen or intrahepatic fibrinogen deposits contribute to the progression of liver disease through mechanisms traditionally linked to thrombosis.[31] Further data are also needed to clarify the close associations of the hemostatic system with liver regeneration and postoperative outcomes in patients undergoing OLT.[32]

Low perioperative fibrinogen levels are associated with massive bleeding and the need for transfusion,[33] which have been controversially shown to be risk factors for postoperative death.[34] Several studies have found that the use of fibrinogen concentrate was beneficial for massive bleeding during liver transplantation.[11,35] Researchers have even supposed that supplementation with fibrinogen concentrate before or during resection may be a novel clinical approach to target failing regenerative responses for patients undergoing liver resection.[36,37] Despite this hypothesis, an imbalance between coagulation and fibrinolysis early after liver transplantation may exist because of the relatively slow recovery of depleted anticoagulant proteins, such as proteins C and S, and antithrombin. Therefore, patients tend to be in a hypercoagulable state even with decreased fibrinogen levels.[38] It is plausible that anticoagulant administration early after liver transplantation may be important for the prevention of thrombus formation after OLT.[39,40] Unfortunately, the patients included in this study did not undergo comprehensive examinations of blood clotting or the anticoagulation system. Thus, we were unable to assess changes in coagulation factors and the anticoagulation system after OLT.

Ascites is a well-known predictor of cirrhosis-related mortality.[41] However, relatively few studies have investigated the effect of preoperative ascites on mortality after liver transplantation. Ling et al[42] reported that moderate ascites was an independent risk factor of 3-month mortality after liver transplantation. Similarly, Somsouk et al[43] found that preoperative ascites was associated with a higher mortality rate after liver transplantation, consistent with the findings of the present study. Because ascites is a crude indica-

FIGURE 4. ROC curve of fibrinogen levels on POD 1 to predict 1- and 2-year survival of patients with ascites (A and B) and without (C and D) ascites. POD, postoperative date; ROC, receiver operating characteristic.

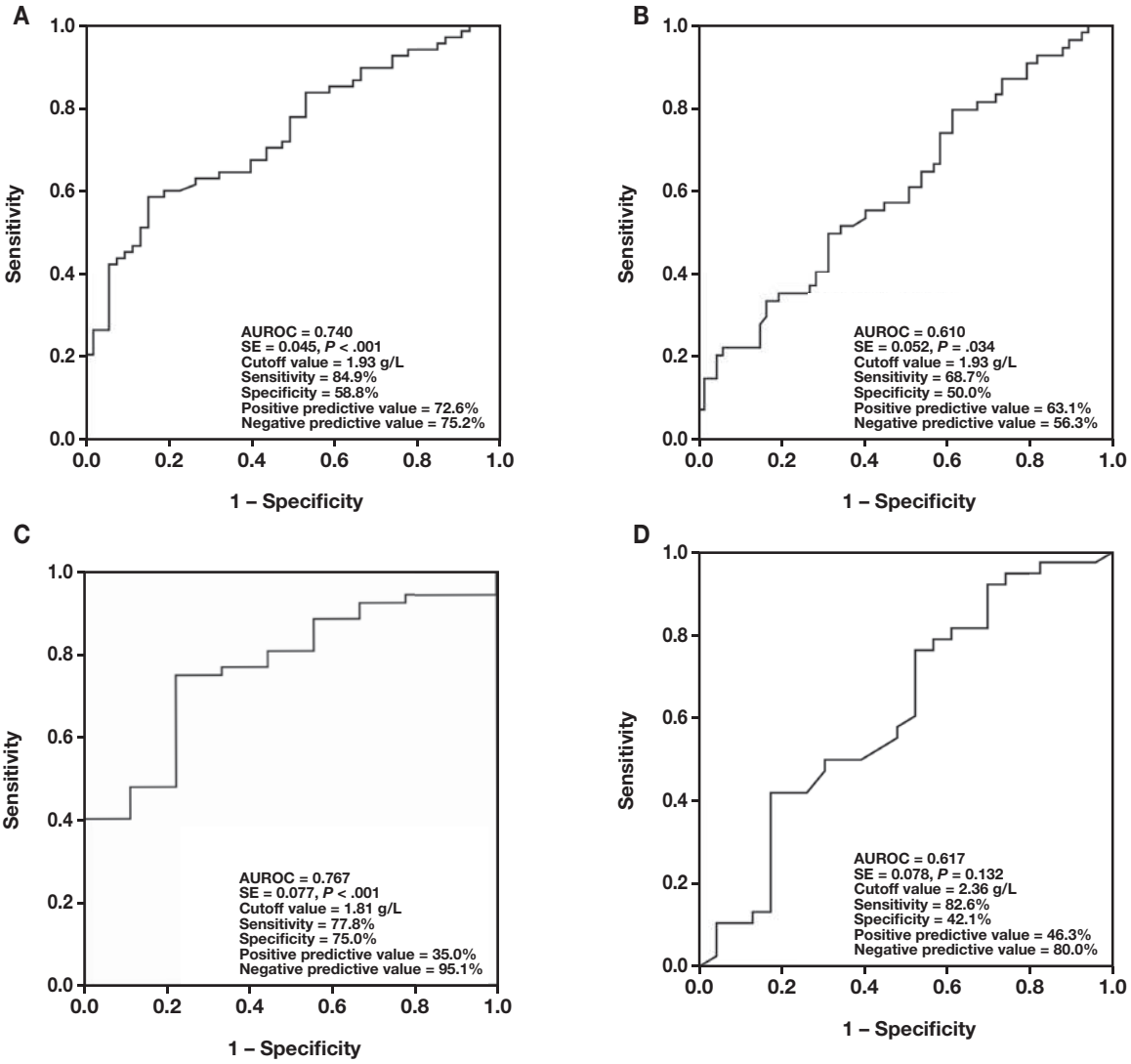

FIGURE 5. Kaplan-Meier survival curves of patients undergoing OLT with high or low plasma fibrinogen levels on POD 1. The median values in patients with ascites (A) and without (B) ascites were used to dichotomize fibrinogen levels on POD 1. OLT, orthotopic liver transplantation; POD, postoperative date.

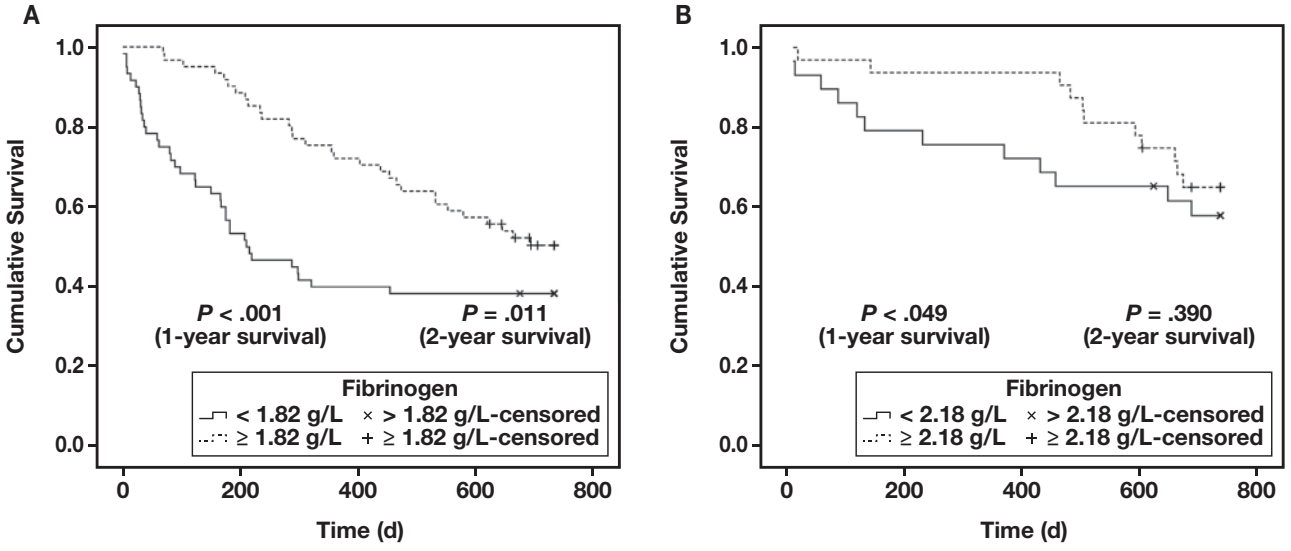

tor of underlying circulatory dysfunction, it is likely that the patients with ascites were compromised by more severe end-stage liver disease and may be temporarily contraindicated for liver transplantation.[44,45] Clinicians should therefore carefully consider the timing of liver transplantation, because patients with ascites may require more aggressive monitoring.

Several limitations to this study should be noted. First, the retrospective, single-center design of this study may have introduced bias; thus a prospective, randomized controlled trial is needed to validate the results. Second, note that surgical duration, anesthesia time, wound healing, and other factors such as anticoagulant factors, which may influence clinical outcome, were not included because of the lack of sufficient data. Third, because of the small sample size, the results need to be interpreted with caution.

Conclusion

The results of this study suggested that ascites and fibrinogen levels on POD 1 were independent predictors of postoperative death after OLT. Furthermore, fibrinogen on POD 1 was a predictor of 2-year post-OLT survival of patients with HBV-related HCC with ascites. The results of the present study may help guide the management of coagulation during and after OLT and to predict the outcome of surgery. Further studies are required to confirm and increase our knowledge of the effect of fibrinogen on liver regeneration and tumor progression and its predictive impact in patients undergoing OLT.

Acknowledgments

The authors thank all those who participated in the recruitment of patients and helped gather patient information. This work was supported by the Medical Science and Technology Project of Zhejiang Province (2017KY337). The authors declare that they have no competing interests.

REFERENCES

1. Yang JD, Heimbach JK. New advances in the diagnosis and management of hepatocellular carcinoma. *BMJ.* 2020;371:m3544.
2. Zheng B, Zhu YJ, Wang HY, Chen L. Gender disparity in hepatocellular carcinoma (HCC): multiple underlying mechanisms. *Sci China Life Sci.* 2017;60(6):575–584.
3. Xie DY, Ren ZG, Zhou J, Fan J, Gao Q. 2019 Chinese clinical guidelines for the management of hepatocellular carcinoma: updates and insights. *Hepatobiliary Surg Nutr.* 2020;9(4):452–463.
4. Buettner N, Thimme R. Sexual dimorphism in hepatitis B and C and hepatocellular carcinoma. *Semin Immunopathol.* 2019;41(2):203–211.
5. Lisman T, Porte RJ. Rebalanced hemostasis in patients with liver disease: evidence and clinical consequences. *Blood.* 2010;116(6):878–885.
6. Novaković-Anucin S, Gnip S, Canak V, et al. Laboratory monitoring of the haemostatic system changes during orthotopic liver transplantation. *Srp Arh Celok Lek.* 2013;141(9–10):608–614.
7. Chow JH, Lee K, Abuelkasem E, Udekwu OR, Tanaka KA. Coagulation management during liver transplantation: use of fibrinogen concentrate, recombinant activated factor VII, prothrombin complex concentrate, and antifibrinolytics. *Semin Cardiothorac Vasc Anesth.* 2018;22(2):164–173.
8. Moia M, Martinelli I, Gridelli B, Langer M, Galmarini D, Mannucci PM. Prognostic value of hemostatic parameters after liver transplantation. *J Hepatol.* 1992;15(1–2):125–128.
9. Arshad F, Adelmeijer J, Blokzijl H, van den Berg A, Porte R, Lisman T. Abnormal hemostatic function one year after orthotopic liver transplantation can be fully attributed to endothelial cell activation. *F1000Res.* 2014;3:103.
10. Martinelli I, Moia M, Panzeri D, Tondo L, Mannucci PM. Prognostic value of the activated partial thromboplastin time after orthotopic liver transplantation: a prospective study. *J Hepatol.* 1994;21(5):917.
11. Kirchner C, Dirkmann D, Treckmann JW, et al. Coagulation management with factor concentrates in liver transplantation: a single-center experience. *Transfusion.* 2014;54(10 Pt 2):2760–2768.
12. Kamath PS, Wiesner RH, Malinchoc M, et al. A model to predict survival in patients with end-stage liver disease. *Hepatology.* 2001;33(2):464–470.
13. Thai C, Oben C, Wagener G. Coagulation, hemostasis, and transfusion during liver transplantation. *Best Pract Res Clin Anaesthesiol.* 2020;34(1):79–87.
14. Lisman T, Bakhtiari K, Pereboom IT, Hendriks HG, Meijers JC, Porte RJ. Normal to increased thrombin generation in patients undergoing liver transplantation despite prolonged conventional coagulation tests. *J Hepatol.* 2010;52(3):355–361.
15. Wang GY, Jiang N, Yi HM, et al. Pretransplant elevated plasma fibrinogen level is a novel prognostic predictor for hepatocellular carcinoma recurrence and patient survival following liver transplantation. *Ann Transplant.* 2016;21:125–130.
16. Mao JX, Guo WY, Guo M, Liu C, Teng F, Ding GS. Acute rejection after liver transplantation is less common, but predicts better prognosis in HBV-related hepatocellular carcinoma patients. *Hepatol Int.* 2020;14(3):347–361.
17. Ayala R, Martínez-López J, Cedena T, et al. Recipient and donor thrombophilia and the risk of portal venous thrombosis and hepatic artery thrombosis in liver recipients. *BMC Gastroenterol.* 2011;11:130.
18. Fu SJ, Ji F, Han M, et al. Prognostic value of combined preoperative fibrinogen and neutrophil-lymphocyte ratio in patients with hepatocellular carcinoma after liver transplantation. *Oncotarget.* 2017;8(3):4301–4312.
19. Sun J, Robinson L, Lee NL, Welles S, Evans AA. No contribution of lifestyle and environmental exposures to gender discrepancy of liver disease severity in chronic hepatitis B infection: observations from the Haimen City cohort. *PLoS One.* 2017;12(4):e0175482.
20. Wang HY, Zhao QY, Yuan YF. Perioperative changes of coagulation functions in the local advanced liver cancer patients receiving liver transplantation. Article in Chinese. *Ai Zheng.* 2008;27(7):743–747.
21. Groeneveld D, Pereyra D, Veldhuis Z, et al. Intrahepatic fibrin(ogen) deposition drives liver regeneration after partial hepatectomy in mice and humans. *Blood.* 2019;133(11):1245–1256.
22. Luyendyk JP, Schoenecker JG, Flick MJ. The multifaceted role of fibrinogen in tissue injury and inflammation. *Blood.* 2019;133(6):511–520.
23. Acharya SS, Dimichele DM. Rare inherited disorders of fibrinogen. *Haemophilia.* 2008;14(6):1151–1158.
24. Davalos D, Akassoglou K. Fibrinogen as a key regulator of inflammation in disease. *Semin Immunopathol.* 2012;34(1):43–62.
25. Zheng S, Shen J, Jiao Y, et al. Platelets and fibrinogen facilitate each other in protecting tumor cells from natural killer cytotoxicity. *Cancer Sci.* 2009;100(5):859–865.
26. Lee JH, Hyun JH, Kim DY, et al. The role of fibrinogen as a predictor in preoperative chemoradiation for rectal cancer. *Ann Surg Oncol.* 2015;22(1):209–215.
27. Gruttadauria S, Pagano D, Luca A, Gridelli B. Small-for-size syndrome in adult-to-adult living-related liver transplantation. *World J Gastroenterol.* 2010;16(40):5011–5015.

28. Starlinger P, Pereyra D, Haegele S, et al. Perioperative von Willebrand factor dynamics are associated with liver regeneration and predict outcome after liver resection. *Hepatology.* 2018;67(4):1516–1530.
29. Beier JI, Guo L, Ritzenthaler JD, Joshi-Barve S, Roman J, Arteel GE. Fibrin-mediated integrin signaling plays a critical role in hepatic regeneration after partial hepatectomy in mice. *Ann Hepatol.* 2016;15(5):762–772.
30. Kirschbaum M, Jenne CN, Veldhuis ZJ, et al. Transient von Willebrand factor-mediated platelet influx stimulates liver regeneration after partial hepatectomy in mice. *Liver Int.* 2017;37(11):1731–1737.
31. Kopec AK, Luyendyk JP. Role of fibrin(ogen) in progression of liver disease: guilt by association? *Semin Thromb Hemost.* 2016;42(4):397–407.
32. Lisman T. Platelets and fibrin in progression of liver disease: friends or foes? *J Thromb Haemost.* 2015;13(1):54–56.
33. Gallagher TK, Thomas KA, Ladner DP, et al. Incidence and risk factors of intracranial hemorrhage in liver transplant recipients. *Transplantation.* 2018;102(3):448–453.
34. Bezinover D, Dirkmann D, Findlay J, et al. Perioperative coagulation management in liver transplant recipients. *Transplantation.* 2018;102(4):578–592.
35. Sabate A, Dalmau A, Koo M, Aparicio I, Costa M, Contreras L. Coagulopathy management in liver transplantation. *Transplant Proc.* 2012;44(6):1523–1525.
36. Dickneite G, Pragst I, Joch C, Bergman GE. Animal model and clinical evidence indicating low thrombogenic potential of fibrinogen concentrate (haemocomplettan P). *Blood Coagul Fibrinolysis.* 2009;20(7):535–540.
37. Donohue CI, Mallett SV. Reducing transfusion requirements in liver transplantation. *World J Transplant.* 2015;5(4):165–182.
38. Blasi A, Beltran J, Pereira A, et al. An assessment of thromboelastometry to monitor blood coagulation and guide transfusion support in liver transplantation. *Transfusion.* 2012;52(9):1989–1998.
39. Flynn E, Huang JY, Hardikar W, Herd L, Hodgson A, Monagle P. Antithrombotic management and thrombosis rates in children post-liver transplantation: a case series and literature review. *Pediatr Transplant.* 2019;23(4):e13420.
40. Ziaziaris WA, Darani A, Holland AJA, et al. Reducing the incidence of hepatic artery thrombosis in pediatric liver transplantation: effect of microvascular techniques and a customized anticoagulation protocol. *Pediatr Transplant.* 2017;21(4):e12917.
41. Garbuzenko DV, Arefyev NO. Current approaches to the management of patients with cirrhotic ascites. *World J Gastroenterol.* 2019;25(28):3738–3752.
42. Ling Q, Dai H, Zhuang R, et al. Predicting short-term survival after liver transplantation on eight score systems: a national report from China Liver Transplant Registry. *Sci Rep.* 2017;7:42253.
43. Somsouk M, Kornfield R, Vittinghoff E, Inadomi JM, Biggins SW. Moderate ascites identifies patients with low model for end-stage liver disease scores awaiting liver transplantation who have a high mortality risk. *Liver Transpl.* 2011;17(2):129–136.
44. Heuman DM, Abou-Assi SG, Habib A, et al. Persistent ascites and low serum sodium identify patients with cirrhosis and low MELD scores who are at high risk for early death. *Hepatology.* 2004;40(4):802–810.
45. Endo K, Iida T, Yagi S, et al. Impact of preoperative uncontrollable hepatic hydrothorax and massive ascites in adult liver transplantation. *Surg Today.* 2014;44(12):2293–2299.

LINC00205 Promotes Tumor Malignancy of Lung Adenocarcinoma Through Sponging miR-185-5p

Yongqiang Li, MM,[1,a] Yahui Hu, MM,[2,a] Yuting Wu, MD,[1] Deming Zhang, MD,[2] Dongwei Huang, MM[2,]*

[1]Department of Respiratory Medicine, PLA General Hospital of Southern Theatre Command, Guangzhou, Guangdong, China; [2]Department of Geriatric Respiratory Medicine, PLA General Hospital of Southern Theatre Command, Guangzhou, Guangdong, China; *To whom correspondence should be addressed. huangdongwei6@163.com; [a]These authors made equal contributions to this article.

Keywords: LINC00205, lung adenocarcinoma, tumor malignancy, miR-185-5p

Abbreviations: lncRNA, long noncoding RNA; LUAD, lung adenocarcinoma; NSCLC, non-small cell lung cancer; miRNA, micro RNA; ceRNAs, competing endogenous RNAs; FBS, fetal bovine serum; qPCR, quantitative polymerase chain reaction; WT, wild type; MUT, mutant.

Laboratory Medicine 2022;53:39–46; DOI: 10.1093/labmed/lmab041

ABSTRACT

The emerging role of long noncoding RNAs (lncRNAs) in cancer, especially in lung adenocarcinoma (LUAD), is attracting increasingly more attention as a potential therapeutic target. However, whether lncRNA LINC00205 regulates the malignancy of LUAD has not been characterized. In this study, we discovered that LINC00205 was markedly upregulated in LUAD tissues and cell lines and correlated with poor prognosis of patients with LUAD. Our data showed that LINC00205 promoted the migration and proliferation of LUAD cells in vitro and tumor growth in vivo. Notably, the tumor suppressor miR-185-5p was found to be a direct target of LINC00205. In addition, miR-185-5p diminished the promotion of cell proliferation and migration mediated by LINC00205, whereas miR-185-5p inhibition had the opposite effect. In summary, our results show that LINC00205 contributes to LUAD malignancy by sponging miR-185-5p, which provides new insight into LUAD progression.

Lung cancer is the leading cause of cancer-related mortality worldwide, and non-small cell lung cancer (NSCLC) accounts for approximately 80% of newly diagnosed patients with lung cancer.[1,2] According to the World Health Organization classification, the main histologic types of NSCLC include lung adenocarcinoma (LUAD), lung squamous cell cancer, and large cell carcinoma, and LUAD is the most common histologic type of lung cancer.[3,4] Despite the advantages achieved in the treatment of LUAD, because most patients with LUAD are diagnosed at a late stage and with metastasis, the overall 5-year survival rate of LUAD patients is low.[5,6] However, the precise molecular mechanisms leading to tumor malignancy of LUAD remains incompletely understood, limiting the development for effective drugs and therapies against LUAD.

With the rapid development of multiple computational tools, an increasing number of noncoding RNAs have been widely applied to the detection of coding driver mutations in lung cancer.[7,8] The lncRNAs are a subtype of noncoding RNAs of >200 nucleotides in length without protein coding capacity.[9] Over the previous decade, an increasing amount of evidence has indicated that lncRNAs play critical roles in modulating gene expression, epigenetics, RNA processing, and chromatin structure, along with protein activities and multiple cellular processes, including proliferation, cell cycle progression, invasion, and migration.[10-12] Notably, emerging evidence has shown that these lncRNAs participate in the initiation and progression of cancer, and several cancer-associated lncRNAs have been proven as potential biomarkers and therapeutic targets in the pathology of lung cancer.[13,14] For example, previous studies found that lncRNA AK126698 inhibits NSCLC cell proliferation and migration by repressing the Wnt/β-catenin signaling pathway,[15] and some lncRNAs such as MALAT1, SCAL1, and LINC00301 are considered important regulators of lung cancers.[16-18] Hence, the identification of lung cancer–associated lncRNAs and the investigation of their biological functions and molecular mechanisms are vital for obtaining a better understanding of lung cancer.

Micro RNAs (miRNAs) are a class of post-transcriptional regulators and exert crucial effects in tumor progression, including lung cancer.[19] In addition, an increasing number of studies has indicated that the functional regulation that lncRNAs exert is to affect target protein expression by miRNAs as molecular sponges, or competing endogenous RNAs (ceRNAs). For instance, the lncRNA DGCR5 mediates cancer stem cell (CSC)-like properties through regulating miR-330-5p/CD44 in NSCLC and LINC00319 aggravates LUAD carcinogenesis by regulating the miR-450b-5p/EZH2 signal pathway.[20,21] This study aims to reveal potential lncRNAs and miRNAs that may lead to tumor malignancy of LUAD, and to explore their role in the pathogenesis of LUAD.

In the present study, we observed that the expression of LINC00205 was upregulated in LUAD-derived cell lines as compared with normal cells and that the increased LINC00205 expression was positively correlated with a poorer prognosis for patients with LUAD. Moreover, our data revealed that the aberrant expression of LINC00205 promoted cell proliferation and migration in LUAD cells through interaction with miR-185-5p. Overall, we reveal the role that LINC00205 plays in

LUAD and provide a novel target for further development of biological diagnostics and therapeutics.

Materials and Methods

Online Data Mining

The expression data of LINC00205 in LUAD tissues were obtained and analyzed using starBase.[22] The survival analysis was performed on the TANRIC platform.[23] The prediction of lncRNA-miRNA binding was performed using LncBase Experimental v.2 and starBase3.[22,24]

Cell Lines and Human Specimens

The LUAD cell lines (A549, PC9, H1975, and H1993) and a normal human bronchial epithelial cell line (BEAS-2B) were originated from ATCC. The cells were cultured in Roswell Park Memorial Institute 1640 or Dulbecco's Modified Eagle's Medium (Gibco, Life Technology) supplemented with 10% fetal bovine serum (FBS), 100 μg/mL penicillin, and 100 μg/mL streptomycin. All cells were incubated in a humidified incubator at 37°C with an atmosphere of 5% CO_2. Paired LUAD and adjacent nontumor tissues were obtained from 36 patients undergoing open or thoracoscopic surgery. None of the patients had received radiotherapy or systemic chemotherapeutic treatment before the surgery. Tissue specimens were collected, then immediately snap-frozen in liquid nitrogen and stored at –80°C for RNA extraction.

Vector Construction

The LINC00205 was cloned into the pSIN-EF2-puro vector using the following oligos. LINC00205 F: 5'-CCCGGACGAATTCTTCGAACCGCAGCGGCTAGAGGTT-3'; LINC00205 R:5'-TGCGGATCACTAGTGCTAGCTGATGCTGACATATTATTTATAATAGGGATGTAATTACCCAAAA-3'. The *AKT1* was cloned into the pSIN-EF2-puro vector using the following oligos. *AKT1* F: 5'-CCCGGACGAATTCTTCGAAATGAGCGACGTGGCTATTGTGAAG-3'; *AKT1* R:5'-TGCGGATCACTAGTGCTAGCTCAGGCCGTGCCGCT-3'. The short hairpin RNA (shRNAs) targeting LINC00205 was cloned into the PLKO.1-puro vector using the following oligos. ShRNA#1 F: 5'-CCGGGAGGGCTGTATCTAGAATATACTCGAGTATATTCTAGATACAGCCCTCTTTTTG-3';ShRNA#1 R: 5'-AATTCAAAAAGAGGGCTGTATCTAGAATATACTCGAGTATATTCTAGATACAGCCCTC-3'. ShRNA#2 F: 5'-CCGGTTCCAGCTCTCAACGAATTTACTCGAGTAAATTCGTTGAGAGCTGGAATTTTTG-3'. ShRNA#2 R: 5'-AATTCAAAAATTCCAGCTCTCAACGAATTTACTCGAGTAAATTCGTTGAGAGCTGGAA-3'.

Transfection and Generation of Stable Expression Cell Lines

The mimics and inhibitor of miR-185-5p were obtained from RiboBio (Guangzhou, People's Republic of China). Transfections of the mimics and inhibitor were performed using Lipofectamine 2000 reagent (Invitrogen, Carlsbad, CA) per the instructions. Vectors for the overexpression of LINC00205 and *AKT1* and vectors of shRNAs were introduced using lentivirus. To generate stable expression cell lines, the infected cells were cultured in a medium containing 1.0 μg/mL puromycin.

Quantitative Real-Time Polymerase Chain Reaction

Total RNA was extracted from cells using TRIZOL reagent (Invitrogen), following the manufacturer's protocol. The RNA was reverse-transcribed by the Prime Script TM RT Master Mix (TaKaRa Bio Technology, Dalian, China), and quantitative polymerase chain reaction (qPCR) was detected by qPCR kits (Invitrogen). The gene *GAPDH* was used as an internal control. Primer sequences used for quantitative real-time PCR analysis were as follows: LINC00205 F 5'-TGTCAAGACCCACAGCAGTC-3', LINC00205 R 5'-ATGAGCACATCGGACATCAA-3',GAPDH F 5'-CCTGCACCACCAACTGCTTA-3',GAPDH R 5'-GGCCATCCACAGTCTTCTGAG-3'. The miRNA was isolated using the miRNeasy Mini Kit (Qiagen, Duesseldorf, Germany), and cDNA was synthesized using the Mir-X miRNA First-Strand Synthesis Kit (Takara, Japan). MiR-185-5p F 5'-TGGAGAGAAAGGCAGTTCCTGA-3',miR-185-5p R 5'-GGCCAACCGCGAGAAGATGTTTTTTTTT-3'.U6 F5'-CTCGCTTCGGCAGCACATATACT-3',U6 R 5'-ACGCTTCACGAATTTGCGTGTC-3'. The $2^{-\Delta\Delta Ct}$ method was used for quantification, and the fold change for the target genes was normalized by internal control.

MTT Proliferation Assay

A Cell Proliferation Reagent Kit I (methylthiazolyldiphenyl-tetrazolium bromide [MTT]) assay was used to monitor cell proliferation according to the manufacturer's protocol. Cells were seeded in 96-well plates and MTT solution was added to the plates 24, 48, 72, and 96 hours later. The cells were cultured for 4 hours at 37°C. Then the medium was discarded and dimethyl sulfoxide (DMSO) was added and oscillated for 15 minutes. Optical density was detected using an enzyme-labeled analyzer. The experiment was performed in triplicate and repeated 3 times.

Colony Formation Assay

For the colony formation assay, the containing approximately pretreated cells were placed in 6-well plates for approximately 14 days, and the medium was replaced every 4 days. After 14 days of culture, the cells were fixed in methanol and stained with crystal violet, and colony formation was determined by counting the number of stained colonies. The experiment was repeated 3 times independently for each group.

Transwell Migration Assay

Cell migration was detected using transwell chambers (8 μm pore size; Millipore). A total of 1×10^5 cells in serum-free medium was seeded in the upper chamber of an insert. Medium containing 10% FBS was added to the lower chamber. After incubating for 24 hours at 37°C, the migrated cells were fixed with 4% methanol and stained with 0.1% crystal violet. The cell numbers were determined by counting the migrated cells under a microscope at 200× magnification in random fields in each well. The experiment was performed in triplicate and repeated 3 times.

Luciferase Reporter Assay

The human lncRNA LINC00205 was amplified and cloned into the pGL3-reporter luciferase vector. The cells were subjected to cotransfection with either the miR-185-5p mimics or mimics-negative control (NC) and pmirGL3-wild type (WT) LINC00205 or pmirGL3-mutated type (MUT) LINC00205 plasmids for 48 hours. The luciferase activities were detected using the dual-luciferase reporter assay kit (Promega, Madison, WI) according to the manufacturer's instructions. Experiments were performed in triplicate.

Western Blot

The treated cells were collected and boiled in standard sodium dodecyl sulfate (SDS) specimen buffer and Western blot for detection of the following antigens: antibodies against *AKT1,* cyclin D1, CDK2, and MMP2/9 (Cell signaling technology). After incubation with a secondary

antibody, the immunoreactive bands were exposed to the Odyssey CLx Imager for image capture.

Mouse Model

The LINC00205 overexpression or knockdown LUAD cells were subcutaneously injected into the flanks of male BALB/c-nude mice (4–5 weeks old). Tumor volumes were measured every 3 days, and tumor volumes were calculated as length × width^2 × 0.5 (mm^3). At the indicated time point, mice were killed, and the subcutaneous growth of each tumor was examined. All experiments were conducted under the guidelines outlined by the committee on the use and care of animals. Standard guidelines for laboratory animal care followed the Guide for the Care and Use of Laboratory Animals.

Statistical Analysis

Statistical analysis was performing using the SPSS (version 19.0) software package. The variables were expressed as mean ± standard deviation. One-way analysis of variance and Student's *t*-test were utilized to compare differences among groups. Overall survival curves were generated using the Kaplan-Meier method, and the log-rank test was performed. Values of $P < .05$ were considered statistically significant.

Results

LINC00205 Overexpressed in LUAD and Correlated with Poor Prognosis of Patients with LUAD

Bioinformatics databases (starBase) were used to predict putative lncRNAs that might regulate LUAD tumorigenesis. In this study, we analyzed the expression levels of LINC00205 in human LUAD tissues using sequencing data downloaded from starBase and found that LINC00205 expression levels were significantly upregulated in LUAD tissues compared with normal tissues (**FIGURE 1A**). To verify this finding, we measured the expression of LINC00205 in 36 paired LUAD tissues and adjacent normal tissues. The expression of LINC00205 was consistently upregulated in LUAD tissues (**FIGURE 1C**). Next, we examined the LINC00205 expression level in 4 human LUAD cell lines and 1 human bronchial epithelial cell line (BEAS-2B), and we found a higher level of LINC00205 expression in the LUAD cell lines than in BEAS-2B (**FIGURE 1D**). Further, we conducted the Kaplan-Meier survival analysis in patients with LUAD based on LINC00205 expression. Notably, the results showed that high expression of LINC00205 was correlated with worse overall survival (**FIGURE 1B**). These results indicate that LINC00205 may represent a potential oncogene and a novel indicator of poor prognosis for LUAD.

LINC00205 Promoted Migration and Proliferation of LUAD Cells and Tumorigenesis In Vivo

To further investigate the role of LINC00205 in the oncogenesis of LUAD, we generated stable-expression A549 cells with LINC00205 and H1993 cells with LINC00205 knockdown. The expression of LINC00205 in these stable-expression cells was detected by quantitative real-time PCR (**FIGURE 2A** and **2C**). First, to investigate the effect of LINC00205 on LUAD cell migration, the transwell migration assay was used. As shown in **FIGURE 2B** and **2D**, the upregulation of LINC00205 promoted the migration of LUAD cells, whereas the knockdown of LINC00205 suppressed this process. We further examined whether LINC00205 regulated the proliferation of LUAD cells. A cell-counting assay revealed that the upregulation of LINC00205 improved the growth of A549 cells (**FIGURE 2E**), whereas the downregulation of LINC00205 significantly repressed the proliferation of H1993 cells (**FIGURE 2F**). In addition, data from the colony formation assay also revealed that LINC00205-overexpressing A549 cells formed more colonies than the control group (**FIGURE 2G**); however, the colony formation was inhibited in shRNA-LINC00205-treated H1993 cells (**FIGURE 2H**). Taken together, these data indicated that LINC00205 promoted migration and proliferation ability in the LUAD cell lines.

Then, to further verify whether LINC00205 could impact tumorigenesis, we performed an in vivo tumorigensis assay in nude mouse models in which LINC00205 overexpression or knockdown LUAD cells were introduced. The results showed that overexpression of LINC00205 increased tumor growth of LUAD cells whereas the knockdown of LINC00205 decreased the growth (as valuated by monitoring the tumor volume; **FIGURE 2I** and **2J**). These in vivo data supported the in vitro findings and showed that LINC00205 can increase the tumor growth of LUAD cells in vivo by accelerating cell proliferation. To further identify our findings, we performed Western blot and found that upregulation of LINC00205 increased the expressions of cyclin D1, CDK2, and MMP2/9 in LUAD cells whereas the knockdown of LINC00205 decreased this expression (**FIGURE 2K**). These data indicated that LINC00205 promotes the migration and proliferation of LUAD cells and tumorigenesis in vivo.

LINC00205 Served as a Sponge for miR-185-5p in A549 and H1993 Cells

An increasing number of studies have indicated that lncRNAs, as molecular sponges or ceRNAs, regulate miRNAs and downstream protein-coding genes. The prediction of lncRNA-miRNA binding was performed using LncBase Experimental v.2 and starBase3. It was predicted that miR-26a-5p, miR-26b-5p, and miR-185-5p were the potential interacting miRNAs of LINC00205 (**FIGURE 3A**). Among these 3 miRNAs, miR-185-5p was able to reduce at least half of the luciferase activities of LINC00205 (**FIGURE 3B**). The predicted binding sites of miR-185-5p to the LINC00205 sequence are illustrated in **FIGURE 3C**. In addition, a dual-luciferase reporter assay indicated that miR-185-5p impeded the luciferase activity of WT LINC00205 rather than that of the MUT in the A549 and H1993 cells (**FIGURE 3D**). We then detected the expression of LINC00205 and miR-185-5p in LUAD tissues and found that the expression of LINC00205 and miR-185-5p was significantly negatively correlated (**FIGURE 3E**). Meanwhile, our results also showed that the upregulation of LINC00205 decreased the expression of miR-185-5p in A549 and that the knockdown of LINC00205 increased the expression of miR-185-5p in H1993 cells (**FIGURE 3F and 3G**). These results suggest that LINC00205 may function as a sponge to miR-185-5p.

LINC00205 Regulated the miR-185-5p/*AKT1* Pathway to Promote Migration and Proliferation of A549 and H1993 Cells

First, we found that the overexpression of LINC00205 elevated the expression of *AKT1* in A549 cells and that miR-185-5p mimics reduced LINC00205-induced *AKT1* expression (**FIGURE 4A**). Meanwhile, the knockdown of LINC00205 in H1993 cells treated with shRNA decreased the expression of *AKT1*, whereas the miR-185-5p inhibitor abolished this effect (**FIGURE 4B**). To further validate whether the effects of LINC00205 on LUAD were mediated by miR-185-5p/*AKT1*, we performed rescue assays. In brief, the miR-185-5p mimics were transfected in LINC00205-

FIGURE 1. **LINC00205 was overexpressed in LUAD and correlates with poor prognosis of patients with LUAD. (A) LINC00205 expression levels in LUAD tissues and normal tissues were analyzed using starBase. (B) Association of LINC00205 expression with overall survival of patients with LUAD. (C)The expression of LINC00205 in LUAD tissues relative to adjacent normal tissues in 36 patients. (D) The expression of LINC00205 in LUAD cell lines and human bronchial epithelial cell line. LUAD, lung adenocarcinoma.**

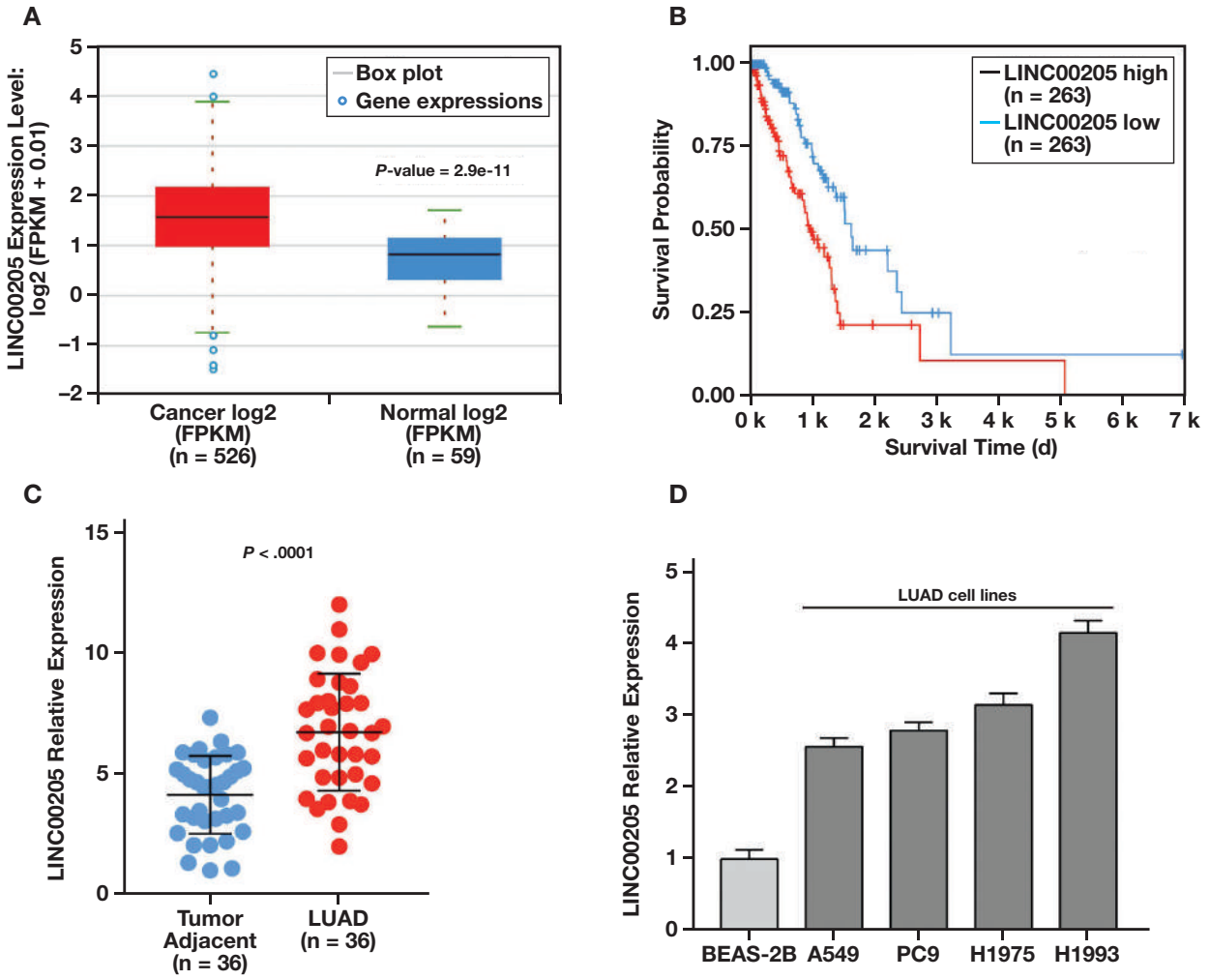

upregulated A549 cells with or without the overexpression of ATK1, whereas the miR-185-5p inhibitor was transfected in LINC00205-downregulated H1993 cells with or without the overexpression of *AKT1*. First, we found that miR-185-5p mimics suppressed the expression of *AKT1* that was upregulated by LINC00205 overexpression (**FIGURE 4A**), whereas the miR-185-5p inhibitor partially recovered the expression of *AKT1* that was downregulated by LINC00205 knockdown (**FIGURE 4B**). To further verify the rescue effect, we examined the proliferation and migration of these cells and related control cells. Data from these experiments showed that the miR-185-5p mimics partially suppressed the effect of LINC00205 on cell proliferation and migration, whereas the expression of *AKT1* recovered this effect of LINC00205 (**FIGURES 4C**, **4E** and **4G**). Meanwhile, the miR-185-5p inhibitor erased the effect of LINC00205 shRNA on cell proliferation and migration, whereas the expression of *AKT1* recovered this effect (**FIGURES 4D**, **4F** and **4H**). The above results suggest that LINC00205 promotes the migration and proliferation of A549 and H1993 cells by regulating the miR-185-5p/*AKT1* pathway.

Discussion

Recent studies have suggested that the dysregulation of lncRNAs is involved in the development of human disease, especially cancer, and that many lncRNAs can be used as a cancer therapeutic or prognostic biomarker.[25,26] In lung cancer, an increasing quantity of lncRNAs has been reported to participate in cancer progression and tumorigenesis. Recent studies have shown that LINC00205 modulates the expression of *EPHX1* through the inhibition of miR-184 in hepatocellular carcinoma as a ceRNA.[27] However, whether and how LINC00205 functions in LUAD progression remains unknown. In the present study, we explored the role of LINC00205 in LUAD and its underlying mechanism.

We determined that lncRNA LINC00205 is an oncogene that is overexpressed in LUAD tissues and cell lines. More important, a high level of LINC00205 expression in patients with LUAD was positively correlated with a poor prognosis. This is the first report of a relationship between LINC00205 expression and LUAD. We also detected the expression levels of LINC00205 in several LUAD cell lines to select certain cell lines for use in subsequent experiments and found that LINC00205 was increased in LUAD cell lines (A549, PC9, H1975, and H1993) compared

2022;53;39–46 | DOI: 10.1093/labmed/lmab041

FIGURE 2. **LINC00205-promoted migration and proliferation of A549 and H1993 cells. (A) The expression of LINC00205 was evaluated after cells were transfected with pcDNA LINC00205 in A549 cells. (B) Transwell migration assays were performed, and the numbers of cells that migrated were calculated in A549 cells. (C) The expression of LINC00205 was evaluated after cells were transfected with 2 shRNAs individually in H1993 cells. (D) Transwell migration assays were performed, and the numbers of cells that migrated were calculated in H1993 cells. (E and F) An MTT assay was used to evaluate the proliferation of A549 and H1993 cell lines. (G and H) Colony formation assay was used to evaluate the colony formation of A549 and H1993 cell lines. (I) Tumors and the tumor volume curve from mice injected with lentiviral vector (LV)-LINC00205 or LV-vector A549 cells. (J) Tumors and the tumor volume curve from mice injected with LINC00205 shRNA (sh-LINC00205) or empty-vector H1993 cells. (K) The expression of cyclin D1, CDK2, and MMP2/9 was measured by Western blot analysis in a different group of A549 and H1993 cells. ***$P < .001$, ****$P < .0001$.**

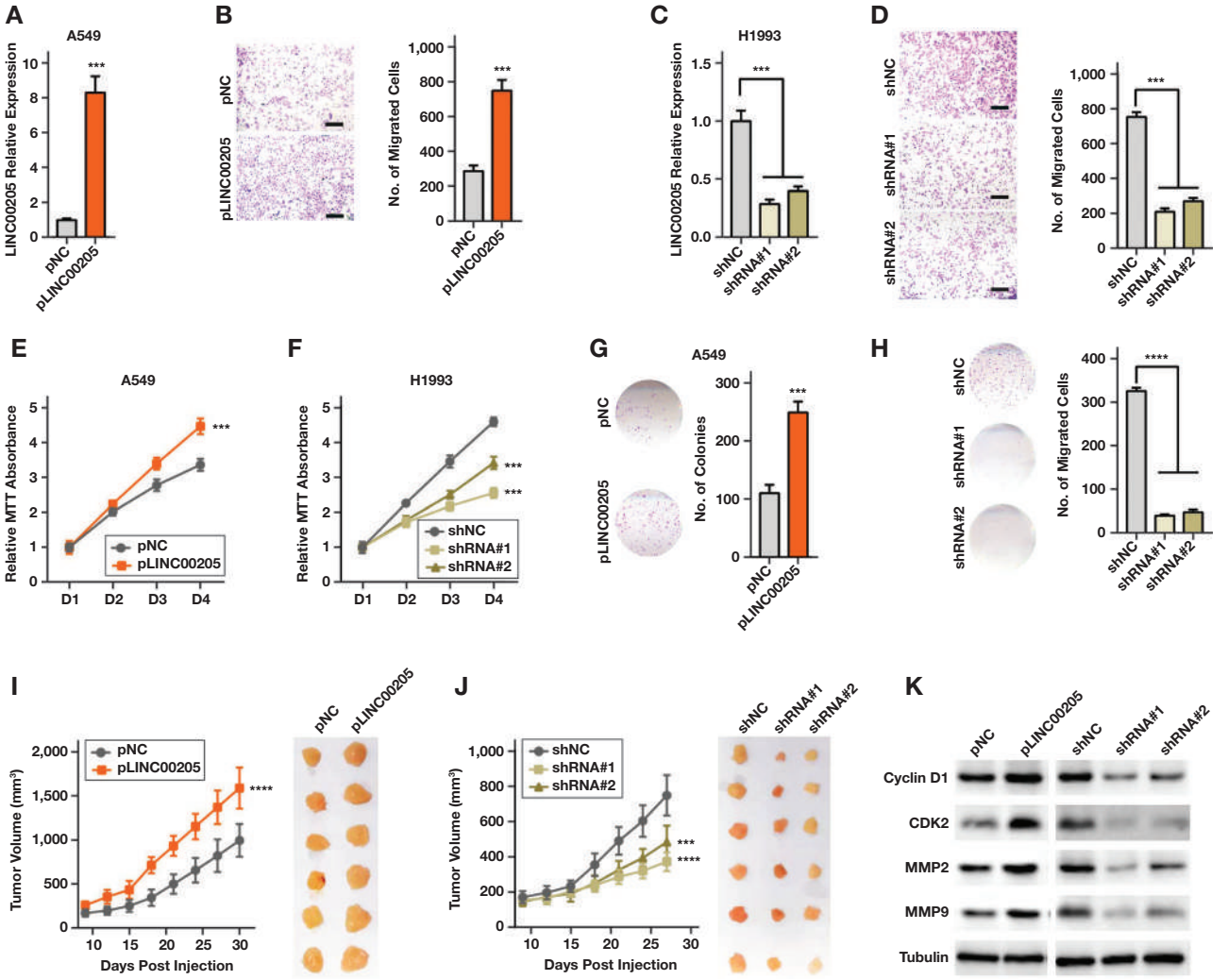

with the normal human bronchial epithelial cell line BEAS-2B. Meanwhile, we identified the expression of LINC00205 in 36 pairs of LUAD and adjacent normal tissues and found that the level of LINC00205 was significantly upregulated in LUAD tissues. These findings indicated that LINC00205 may function in an oncogenic role in LUAD progression.

Adenocarcinoma of the lung, the most common subtype of NSCLC (approximately 50% of all NSCLCs), is the leading cause of cancer death worldwide.[28] It is characterized by high infiltration and destructive growth, the invasion of blood vessels and lymphatic vessels, and blood and lymph metastasis.[29] The function of lncRNAs, including transcriptional and post-transcriptional control, covers the series of proliferation, apoptosis, invasion, and metastasis in cancer.[30] We therefore speculated that LINC00205 may play an important role in tumor cell proliferation and migration in LUAD. To better understand the biological functions of LINC00205 in LUAD, we detected cell proliferation and migration by the knockdown and overexpression of LINC00205 in LUAD cells and tumor growth in vivo. Moreover, because LINC00205 was more highly expressed in H1993 cells and less expressed in A549 cells, we selected H1993 cells to establish a knockdown cell line and A549 cells to establish a overexpression cell line. Subsequently, we found that LINC00205 overexpression in A549 enhanced proliferation and migration abilities, tumor growth in vivo, and the expression of cyclin D1, CDK2, and MMP2/9, whereas LINC00205 knockdown with shRNA inhibited the proliferation and migration activity of H1993 cells, tumor growth in vivo, and the expression of cyclin D1, CDK2, and MMP2/9. The above findings indicate that LINC00205 could enhance the proliferation and

FIGURE 3. **LINC00205 served as a sponge for miR-185-5p in A549 and H1993 cells. (A) The prediction of lncRNA-miRNA binding was performed by using LncBase Experimental v.2 and starBase3. (B) Luciferase reporter assay for identifying miRNAs that were able to bind to the LINC00205 sequence. (C) The predicted binding sites of miR-185-5p to the LINC00205 sequence. (D) A549 and H1993 cells were cotransfected with miR-185-5p mimics or mimics NC and a PGL3 vector (pmirGL3)-LINC00205-WT or pmirGL3-LINC00205-MUT. Luciferase activity was detected using the dual luciferase assay. (E) The expression of LINC00205 and miR-185-5p in LUAD tissues was measured by quantitative real-time PCR. The correlation of the expression of LINC00205 and miR-185-5P was analyzed. (F and G) The expression of miR-185-5p in LINC00205 overexpression and knockdown cells was measured by quantitative real-time PCR. ***P* < .01, ****P* < .001, *****P* < .0001. LUAD, lung adenocarcinoma; MUT, mutant; PCR, polymerase chain reaction; WT, wild type.**

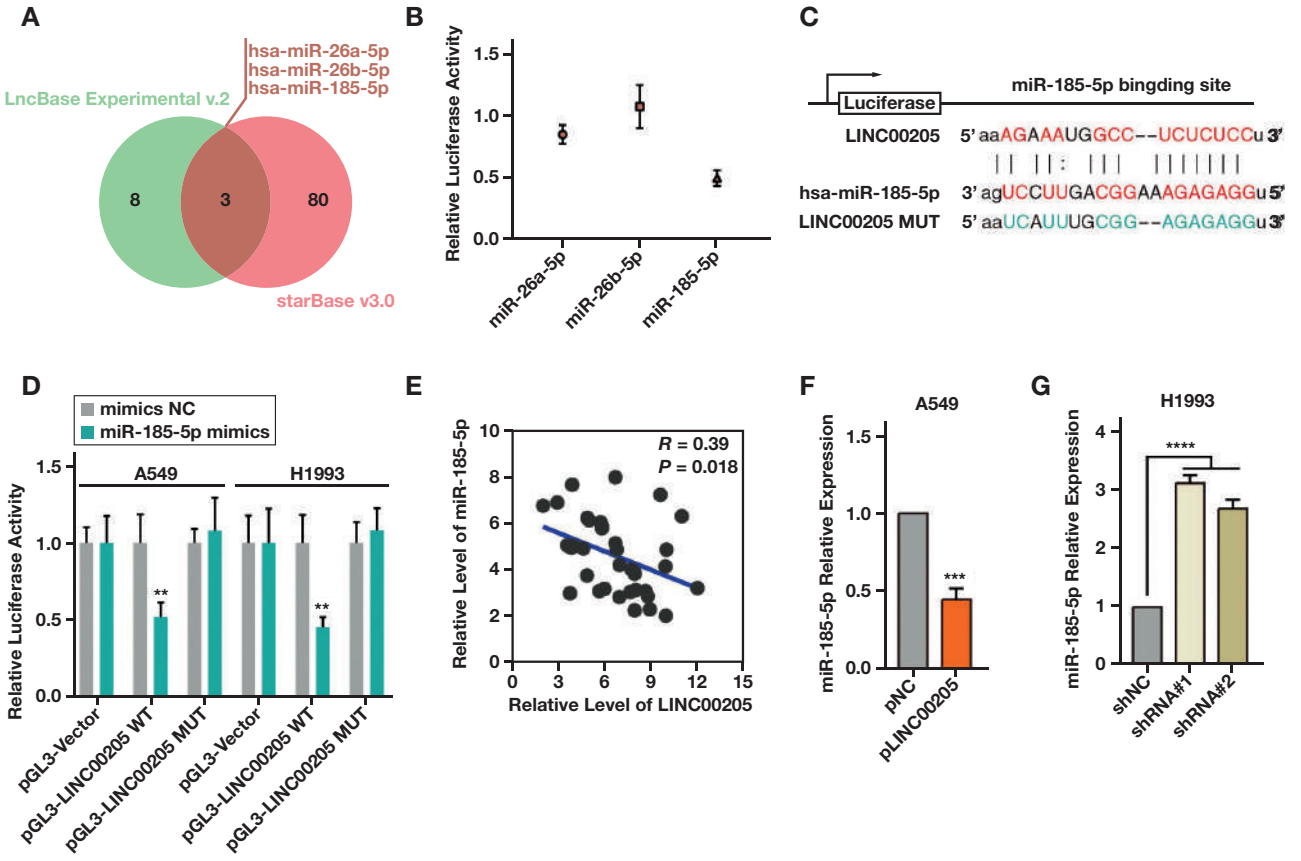

migration activity of LUAD cells. However, the molecular mechanism through which LINC00205 contributes to proliferation and migration in LUAD still requires further investigation.

Despite lacking protein coding ability, lncRNAs indeed orchestrate protein levels and thus modulate abundant signaling pathways. Consistent with previous reports, evidence from this study shows that sponging miRNA is an important regulatory mechanism of lncRNA functions and indirectly promotes target protein expression through an miRNA/protein axis.[31,32] For instance, overexpression of lncRNA SNHG1 has been involved in regulating NSCLC progression by directly binding to miR-145-5p,[32] and lncRNA TP73-AS1 promotes NSCLC progression by competitively sponging miR-449a/EZH2.[33] Another example is that miR-184 represses the luciferase activity of WT LINC00205, and miR-184 and LINC00205 may affect each other in the progression of hepatocellular carcinoma.[27] Through investigation, we predicted that miR-26a-5p, miR-26b-5p, and miR-185-5p were the potential interacting miRNAs of LINC00205, and the luciferase reporter assay validated the prediction. Meanwhile, the luciferase reporter assay also found that miR-185-5p could reduce at least half of the luciferase reporter activities, suggesting that miR-185-5p and LINC00205 could affect each other. Moreover, we also showed that miR-185-5p mimics repress the luciferase activity of WT LINC00205 in A549 and H1993 cells and found that the expression of LINC00205 and miR-185-5p was significantly negatively correlated, implying a direct interaction between miR-185-5p and LINC00205. To further elucidate the relationship between the LINC00205-promoted cell proliferation and migration and miR-185-5p in LUAD cells, we treated A549 cells with LINC00205 overexpression in the presence of the miR-185-5p mimics and treated H1993 cells with shRNA LINC00205 in the presence of the miR-185-5p inhibitor. We found that miR-185-5p reversed the LINC00205-mediated cell proliferation and migration.

Research has shown that *AKT* is a serine/threonine protein kinase that plays a significant role in the regulation of cell functions.[34] The activation of *AKT* isoforms is responsible for inducing tumorigenesis and development by affecting different hallmarks of cancer such as lung and breast cancer.[35,36] Furthermore, some recent reports have shown that *AKT* was the target gene of miR-185 in some cell lines.[37] Interestingly, in the current study miR-185-5p reversed the LINC00205-mediated expression of *AKT1*, indicating that *AKT1* may be responsible, at least in

FIGURE 4. **LINC00205 regulated the miR-185-5p/*AKT1* pathway to promote the migration and proliferation of A549 and H1993 cells. (A and B) The expression of *AKT1* was measured by Western blot analysis in different groups of A549 and H1993 cells. (C and D) Transwell migration assays were performed, and the numbers of cells that migrated were calculated in different group of A549 and H1993 cells. (E and F) An 3-(4,5)-dimethylthiahiazo (-z-y1)-3,5-di- phenytetrazoliumromide (MTT) assay was used to evaluate the cell viability of A549 and H1993 cell lines in different groups. (G and H) Colony formation assay was used to evaluate the colony formation of A549 and H1993 cell lines in different groups. ***$P < .001$, ****$P < .0001$.**

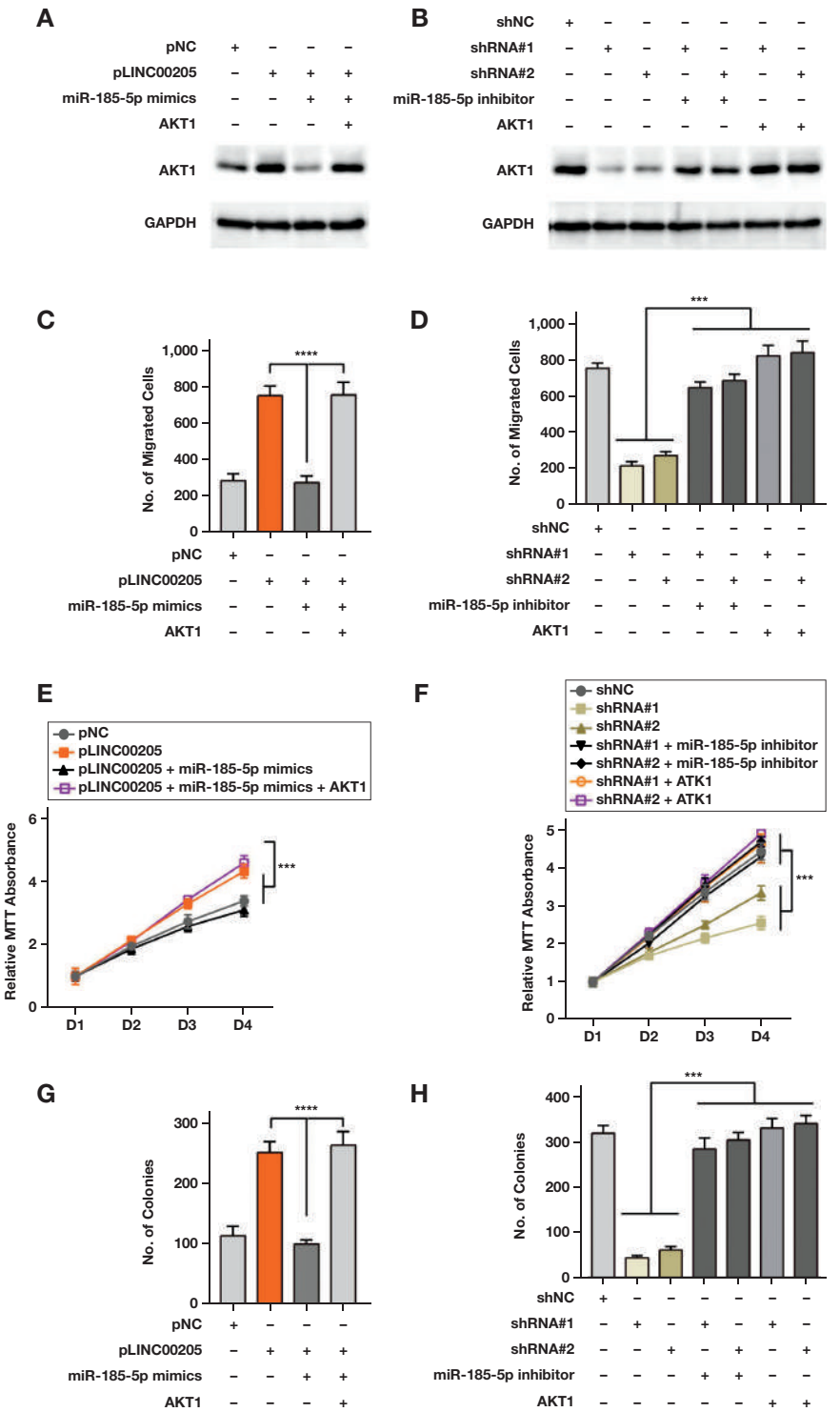

part, for the effects of LINC00205. Furthermore, the overexpression of *AKT1* could negate the effect of miR-185-5p on cell proliferation and migration. It is conceivable that LINC00205 may regulate cell proliferation and migration via the miR-185-5p/*AKT1* axis in LUAD cells. However, further investigation is needed to better understand the specific mechanism of *AKT1* and activity changes of other *AKT* family members.

Conclusion

In summary, our results show that lncRNA LINC00205 is aberrantly overexpressed in LUAD tissues and cell lines, which contributes to the tumor malignancy of LUAD by acting as a sponge of the tumor suppressor miR-185-5p. Notably, these findings provide additional insights into the importance of LINC00205 in LUAD and point out that LINC00205 could be developed as a potential therapeutic target for LUAD.

Acknowledgments

We thank the TCGA and starBase research network for providing the data analyzed in this study.

REFERENCES

1. Jemal A, Bray F, Center MM, et al. Global cancer statistics. *CA A Cancer J Clin*. 2011;6(2):169–190.
2. Välk K, Vooder T, Kolde R, et al. Gene expression profiles of non-small cell lung cancer: survival prediction and new biomarkers. *Oncology*. 2010;79(3–4):283–292.
3. Teng XD. World Health Organization classification of tumours, pathology and genetics of tumours of the lung. *Zhonghua Bing Li Xue Za Zhi.* 2005;34(8):544–546.
4. Selvaggi G, Scagliotti GV. Histologic subtype in NSCLC: does it matter? *Oncology (Williston Park).* 2009;23(13):1133–1140.
5. Somaiah N, Simon GR. Molecular targeted agents and biologic therapies for non-small cell lung cancer. *J Thoracic Oncol.* 2010;5(12):S434–S454.
6. Chheang S, Brown K. Lung cancer staging: clinical and radiologic perspectives. *Sem Intervent Radiol.* 2013;30(02):099–113.
7. Djebali S, Davis CA, Merkel A, et al. Landscape of transcription in human cells. *Nature*. 2012;489(7414):101–108.
8. Nagano T, Fraser P. No-nonsense functions for long noncoding RNAs. *Cell*. 2011;145(2):0–181.
9. Mercer TR, Dinger ME, Mattick JS. Long non-coding RNAs: insights into functions. *Nat Rev Genet.* 2009;10(3):155–159.
10. Gutschner T, Diederichs S. The hallmarks of cancer: a long non-coding RNA point of view. *RNA Biol.* 2012;9(6):703–719.
11. Sun M, Nie F, Wang Y, et al. LncRNA HOXA11-AS promotes proliferation and invasion of gastric cancer by scaffolding the chromatin modification factors PRC2, LSD1, and DNMT1. *Cancer Res.* 2016;76(21):6299–6310.
12. Lin R, Roychowdhury-Saha M, Black C, et al. Control of RNA processing by a large non-coding RNA over-expressed in carcinomas. *FEBS Lett.* 2011;585(4):671–676.
13. Qiu MT, Hu JW, Yin R, et al. Long noncoding RNA: an emerging paradigm of cancer research. *Tumor Biol.* 2013;34(2):613–620.
14. Tsai M-C, Spitale RC, Chang HY. Long intergenic noncoding RNAs: new links in cancer progression. *Am Assoc Cancer Res.* 2011;71(1):3–7.
15. Fu X, Li H, Liu C, Hu B, Li T, Wang Y. Long noncoding RNA AK126698 inhibits proliferation and migration of non-small cell lung cancer cells by targeting Frizzled-8 and suppressing Wnt/β-catenin signaling pathway. *Onco Targets Ther.* 2016;9:3815–3827.
16. Ji P, Diederichs S, Wang W, et al. MALAT-1, a novel noncoding RNA, and thymosin beta4 predict metastasis and survival in early-stage non-small cell lung cancer. *Oncogene.* 2003;22(39):8031–8041.
17. Thai P, Statt S, Chen CH, Liang E, Campbell C, Wu R. Characterization of a novel long noncoding RNA, SCAL1, induced by cigarette smoke and elevated in lung cancer cell lines. *Am J Respir Cell Mol Biol.* 2013;49(2):204–211.
18. Sun C, Zhu W, Li S, et al. FOXC1-mediated LINC00301 facilitates tumor progression and triggers an immune-suppressing microenvironment in non-small cell lung cancer by regulating the HIF1α pathway. *Genome Med.* 2020;12(1):77.
19. Joshi P, Middleton J, Jeon YJ, et al. MicroRNAs in lung cancer. *World J Methodol.* 2014;8(2):81679.
20. Wang R, Dong HX, Zeng J, Pan J, Jin XY. LncRNA DGCR5 contributes to CSC-like properties via modulating miR-330-5p/CD44 in NSCLC. *J Cell Physiol.* 2018;233(9):7447–7456.
21. Zhang ZW, Chen JJ, Xia SH, et al. Long intergenic non-protein coding RNA 319 aggravates lung adenocarcinoma carcinogenesis by modulating miR-450b-5p/EZH2. *Gene.* 2018;650:60–67.
22. Li JH, Liu S, Zhou H, Qu LH, Yang JH. starBase v2.0: decoding miRNA-ceRNA, miRNA-ncRNA and protein-RNA interaction networks from large-scale CLIP-Seq data. *Nucleic Acids Res.* 2014;42(Database issue):D92–D97.
23. Li J, Han L, Roebuck P, et al. TANRIC: an interactive open platform to explore the function of lncRNAs in cancer. *Cancer Res.* 2015;75(18):3728–3737.
24. Paraskevopoulou MD, Vlachos IS, Karagkouni D, et al. DIANA-LncBase v2: indexing microRNA targets on non-coding transcripts. *Nucleic Acids Res.* 2016;44(D1):D231–D238.
25. Li H, Lv X. Functional annotation of noncoding variants and prioritization of cancer-associated lncRNAs in lung cancer. *Oncol Lett.* 2016;12(1):222–230.
26. Huarte M. The emerging role of lncRNAs in cancer. *Nat Med.* 2015;21(11):1253–1261.
27. Long X, Li Q, Zhi LJ, Li JM, Wang ZY. LINC00205 modulates the expression of EPHX1 through the inhibition of miR-184 in hepatocellular carcinoma as a ceRNA. *J Cell Physiol.* 2020;235(3):3013–3021.
28. Yun-Yong P, Sung PE, Bae KS, et al. Development and validation of a prognostic gene-expression signature for lung adenocarcinoma. *PLoS One*. 2012;7(9):e44225.
29. Chen G, Gharib TG, Huang CC, et al. Discordant protein and mRNA expression in lung adenocarcinomas. *Mol Cell Proteomics.* 2002;1(4):304–313.
30. Zeng HF, Qiu HY, Feng FB. Long noncoding RNA LINC01133 sponges miR-422a to aggravate the tumorigenesis of human osteosarcoma. *Oncol Res.* 2017;25(9):405–416.
31. Sun CC, Zhang L, Li G, et al. The lncRNA PDIA3P interacts with miR-185-5p to modulate oral squamous cell carcinoma progression by targeting cyclin D2. *Mol Ther Nucleic Acids.* 2017;9:100–110.
32. Lu Q, Shan S, Li Y, et al. Long noncoding RNA SNHG1 promotes non-small cell lung cancer progression by up-regulating MTDH via sponging miR-145-5p. *FASEB J.* 2018;32(7):3957–3967.
33. Lin Z, Fang F, Xin H. Long noncoding RNA TP73-AS1 promotes non-small cell lung cancer progression by competitively sponging miR-449a/EZH2[J]. *Biomed Pharmacother*. 2018;104:705–711.
34. Hanada M, Feng J, Hemmings BA. Structure, regulation and function of PKB/AKT—a major therapeutic target. *Biochim Biophys Acta.* 2004;1697(1–2):3–16.
35. Qiu ZX, Zhang K, Qiu XS, Zhou M, Li WM. The prognostic value of phosphorylated AKT expression in non-small cell lung cancer: a meta-analysis. *PLoS One.* 2013;8(12):e81451.
36. Iacovides DC, Johnson AB, Wang N, Boddapati S, Korkola J, Gray JW. Identification and quantification of AKT isoforms and phosphoforms in breast cancer using a novel nanofluidic immunoassay. *Mol Cell Proteomics.* 2013;12(11):3210–3220.
37. Chen Z, Zhang Z, et al. Long noncoding RNA (lncRNA) FOXD2-AS1 promotes cell proliferation and metastasis in hepatocellular carcinoma by regulating MiR-185/AKT axis. *Med Sci Monit.* 2019;25:9618–9629.

Development of an LC-MS/MS Method for Measurement of Irinotecan and Its Major Metabolites in Plasma: Technical Considerations

Zineb Aoullay, PhD,[1,2,,a] Xander M.R. Van Wijk, PhD,[2,3,a] Ma Yanhui, MD,[2,4] Bouchra Meddah, PharmD,[1] Kara L. Lynch, PhD,[2] Yahia Cherrah, PharmD,[1] Alan H.B. Wu, PhD[2]*

[1]Laboratory of Pharmacology and Toxicology, Faculty of Medicine and Pharmacy of Rabat, University Mohamed V Rabat, Rabat, Morocco; [2]Department of Laboratory Medicine, University of California and Zuckerberg San Francisco General Hospital, San Francisco, CA, US; [3]Department of Pathology, University of Chicago, Chicago, IL, US; [4]Department of Laboratory Medicine, Shanghai Jiao Tong University School of Medicine, Shanghai, China; *To whom correspondence should be addressed. zinebaoullay@gmail.com; [a]These authors contributed equally.

Keywords: CPT-11, mass spectrometry, liquid chromatography, therapeutic drug monitoring, internal standard, in-source fragmentation

Abbreviations: CPT-11, irinotecan; SN-38G, SN-38-glucuronide; LC-MS/MS, liquid chromatography-tandem mass spectrometry; MS, mass spectrometry; TDM, therapeutic drug monitoring; LC, liquid chromatography; IS, internal standard; DMSO, dimethyl sulfoxide; MPA, 0.1% acetic acid/water; MPB, 0.1% acetic acid/acetonitrile; QC, quality control; LLMI, lower limit of the measurement interval.

Laboratory Medicine 2022;53:47–52; DOI: 10.1093/labmed/lmab059

ABSTRACT

Objective: Irinotecan (CPT-11) is an important drug used in the treatment of several solid tumor types. To minimize its toxicity, therapeutic drug monitoring of CPT-11 and its major metabolites (SN-38, SN-38-glucuronide [SN-38G], and APC) has been proposed. We aimed to develop a liquid chromatography-tandem mass spectrometry (LC-MS/MS) method for the quantification of CPT-11 and its major metabolites in plasma.

Methods: Specimen preparation consisted of protein precipitation, evaporation, and reconstitution. Analyses were performed on a C18 column using reverse-phase gradient elution. Electrospray ionization and multiple reaction monitoring in positive mode were used for MS. The following heavy isotope–labeled internal standards were used: CPT-11 D10, SN-38 D3, SN-38G D3, and APC D3.

Results: We found that CPT-11, SN-38G, and APC eluted at ~4.6 to 4.7 minutes, and SN-38 eluted at ~5.1 to 5.2 minutes. A second peak for SN-38 was detected at ~4.6 to 4.7 minutes. Given that the structure of SN-38 is found in CPT-11, SN-38G, and APC, and in the CPT-11 D10 used here, in-source fragmentation was the likely cause. In addition, we found that a low-level SN-38 impurity was present in CPT-11 D10 and to a lesser extent in SN-38 D3.

Conclusion: When developing methods for CPT-11 and its metabolites, it is important to consider the effects of in-source fragmentation and the choice of internal standards.

Irinotecan (CPT-11) is a semisynthetic water-soluble derivative of the natural product camptothecin used in the treatment of several solid tumor types, mainly colorectal cancer.[1] It is a prodrug and is converted to its active metabolite SN-38 by liver carboxylesterases; SN-38 is converted into SN-38-glucuronide (SN-38G), an inactive metabolite, by *UGT1A1* and excreted into the bile. Research has shown that SN-38G may be converted back into SN-38 in the intestine by bacterial β-glucuronidases. Cytochrome P450 3A4/5 enzymes convert CPT-11 directly into inactive metabolites, the major one being APC.[2]

Accumulation of SN-38 because of polymorphic variances in *UGT1A1* is thought to be responsible for the gastrointestinal and hematopoietic toxicity of CPT-11.[3,4] Patients with a higher biliary index, ie, [CPT11] × [SN-38]/[SN-38G], which reflects a lower rate of SN-38 glucuronidation, presumably have higher biliary SN-38 concentrations, and it has been shown that higher biliary indices correlate with gastrointestinal toxicity (diarrhea).[5] To minimize toxicity, in addition to *UGT1A1* genotyping, it has been proposed to measure CPT-11 and metabolite concentrations and adjust CPT-11 dosing for individual patients if required, a process known as therapeutic drug monitoring (TDM).[6]

There are no commercial immunoassays for monitoring concentrations of CPT-11 or its metabolites. Given their structural similarity, it would be difficult to construct an immunoassay specific for CPT-11 that would not react with metabolites or vice versa. Liquid chromatography (LC) with fluorescence detection has been used to measure CPT-11 and metabolites[7,8]; however, with excellent sensitivity and specificity, LC-tandem mass spectrometry (LC-MS/MS) has become the method of choice.

We aimed to develop an LC-MS/MS method for the quantification of CPT-11 and its major metabolites in plasma. In contrast to previous methods,[9-11] we used stable heavy isotope–labeled internal standards (ISs), which are generally thought to be superior to structural analogs.

Methods

Standards and Reagents

We purchased CPT-11, SN-38, and SN-38G from Cayman Chemical and APC, CPT-11 D10, SN-38 D3, SN-38G D3, and APC D3 from Toronto Research Chemicals. Dimethyl sulfoxide (DMSO), LC-MS–grade acetonitrile, methanol, and acetic acid were purchased from Sigma-Aldrich. The LC-grade water was from Honeywell.

Instruments and Analytical Conditions

Analyses were carried out on an Agilent Autosampler and Binary Pump 1260 Infinity coupled with an AB SCIEX API 3200 triple quadrupole mass spectrometer.

Chromatographic Conditions

A C18 reverse-phase 2.6 µm, 50 × 4.6 mm column (Phenomenex) was used for chromatography. Specimens were eluted with 0.1% acetic acid/water (MPA) and 0.1% acetic acid/acetonitrile (MPB) at a flow rate of 0.3 mL/min and a linear gradient separation as follows: 95% MPA for 0.5 minutes; to 5% MPA over 5.0 minutes; constant for 0.5 minutes; to the initial condition of 95% MPA over 0.5 minutes and a 2.5 minute hold reconditioning step. The total run time was 9 minutes.

MS Conditions

Electrospray ionization in positive mode was used. The TurboIonSpray source was operated at 750°C with an ion spray voltage of 5500 V. Curtain gas was set at 20 psi, nebulizer and heater gas were set at 45 psi, and collision gas was set at medium intensity. The monitored transitions (quantifier and qualifier) are shown in **TABLE 1**. Data acquisition and processing was performed by Analyst and PeakView (SCIEX).

TABLE 1. Monitored Ion Transitions for Each Analyte and IS

Analyte	Precursor Ion (m/z)	Daughter Ions (m/z)
CPT-11	587.2	124.3
		167.1
SN-38	393.3	349.2
		249.1
SN-38G	569.2	393.3
		349.2
APC	619.2	393.3
		227.2
CPT-11 D10	597.3	133.3
		177.3
SN-38 D3	396.2	352.3
		249.3
SN-38G D3	572.1	396.2
		352.3
APC D3	622.3	396.2
		227.2

CPT-11, irinotecan; IS, internal standard; SN-38G, SN-38-glucuronide.

Calibrators and Quality Control

Stock solutions were prepared at concentrations of 1000 µg/mL for CPT-11, CPT-11 D10, SN-38, and SN-38 D3 in DMSO, and at 500 µg/mL for APC, APC D3, SN-38G, and SN-38G D3 in 50% DMSO/50% methanol. All stock solutions were stored at −80°C. Calibration curve standards and quality controls (QCs) were prepared in drug-free EDTA plasma pooled from 5 healthy volunteers. The standard curve for CPT-11 ranged from 4.9 to 2500 ng/mL, from 1.0 to 500 ng/mL for SN-38/SN-38G, and from 2.4 to 1250 ng/mL for APC. Three QCs were prepared at different concentrations; CPT-11: 100, 400, and 1000 ng/mL; SN-38/SN-38G: 40, 100, and 400 ng/mL; APC: 40, 200, and 400 ng/mL.

Specimen Preparation

Specimen preparation was performed by protein precipitation, evaporation, and reconstitution. Briefly, 745 µL of 0.1% acetic acid/methanol solvent solution spiked with 5 µL IS mix (CPT-11 D10, SN-38 D3, SN-38G D3, and APC D3 at final concentrations of 100, 50, 200, and 100 ng/mL, respectively) was added to 250 µL of standard or QC. This mixture was vortexed for 10 seconds, followed by centrifugation for 10 minutes at 4°C at 16,000 g. Supernatant (900 µL) was transferred, evaporated to dryness for 30 minutes under nitrogen flow, and then reconstituted with 100 µL of mobile phase mix: 70% MPA/30% MPB. This combination was centrifuged at 16,000 g for 10 minutes, after which 90 µL was transferred to an autosampler vial and 10 µL was injected into the high performance liquid chromatography system.

Performance Metrics Evaluation

Method performance was evaluated with respect to linearity, matrix effect, recovery, accuracy, intra- and interday precision, and carryover. The calibration curve was constructed by plotting the analyte concentration vs the analyte-IS peak area ratio. Assay linearity was determined on 5 different days, and mean calibrator concentrations were graphed with standard deviation. Matrix effect and extraction recovery were determined according to Matuszewski et al.[12] as follows: Matrix effects were evaluated by comparing peak area ratios obtained from 6 different blank human plasma specimens to a mobile phase solution, both spiked with standards and IS postextraction, at 3 different concentrations (CPT-11: 100, 400, and 1000 ng/mL; SN-38 and SN-38G: 40, 100, and 400 ng/mL; APC: 40, 200, and 400 ng/mL). The relative extraction recovery was calculated for all compounds at these 3 concentrations by comparing the peak area ratio of each analyte from the same plasma spiked with standards and IS postextraction to pre-extraction. Spike-recovery accuracy of QC specimens and intra- and interday precision were evaluated by triplicate analysis of QCs on 5 different days. Carryover was determined by injection of a blank specimen after each calibrator.

Results

The total method run time was 9 minutes, of which the last 3 were for reconditioning. When analyzing QC specimens, we noted that there were 2 peaks for SN-38 and SN-38 D3, one peak eluting after ~4.6 minutes and one after ~5.1 minutes (**FIGURE 1A**). Given that the

FIGURE 1. Analysis of QC specimen with standards and ISs. A, For both the standards and the ISs, 2 peaks are present for SN-38 (D3). The arrow marks the peak that likely results from the in-source fragmentation of other standards and ISs. CPT-11: 100 ng/mL; SN-38, SN-38G, and APC: 40 ng/mL; CPT-11 D10: 500 ng/mL; SN-38 D3 and SN-38G D3: 50 ng/mL; and APC D3: 200 ng/mL. B, Structures of standards and ISs used in this study. CPT-11, irinotecan; IS, internal standard; SN-38G, SN-38-glucuronide; QC, quality control.

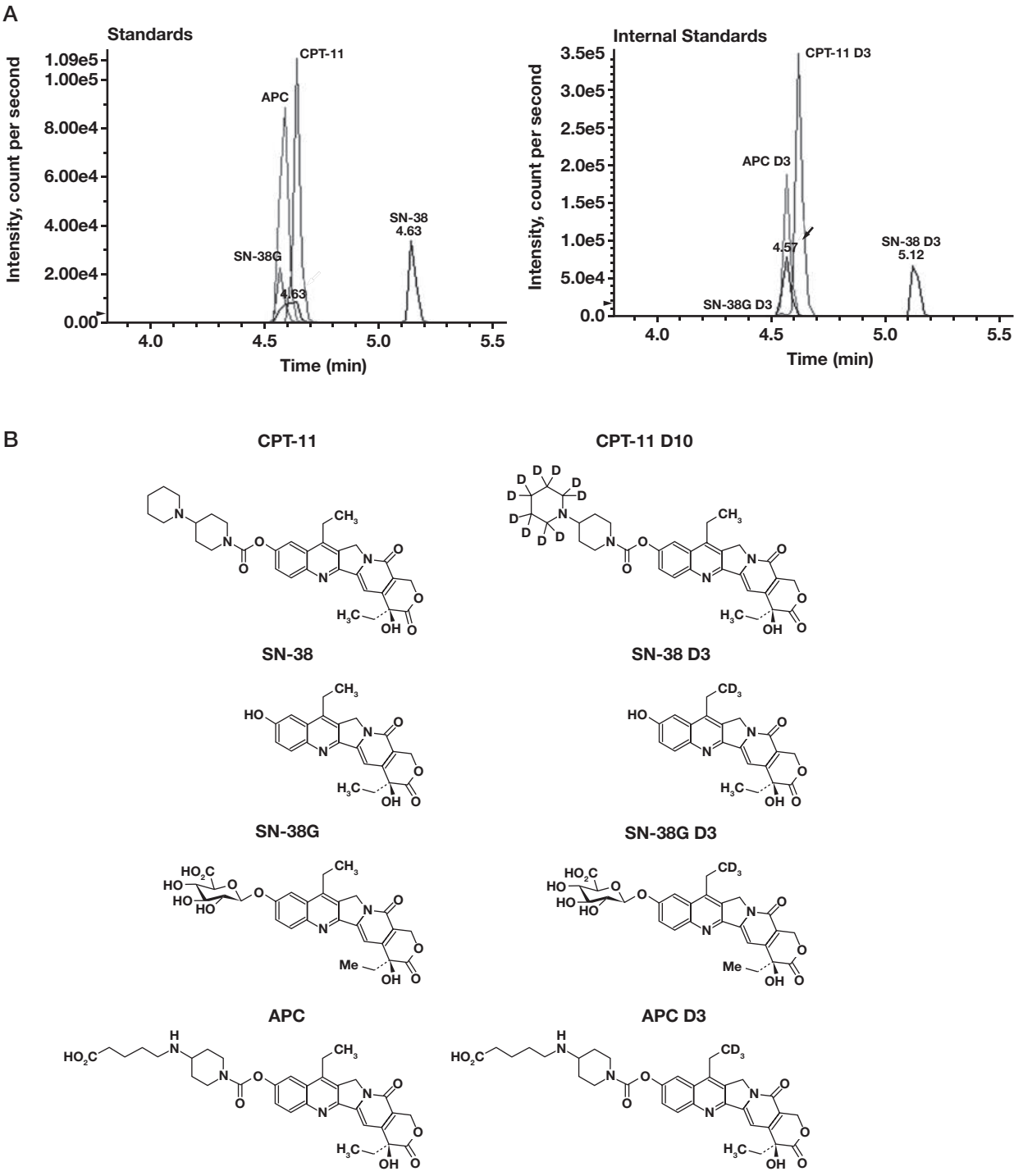

structure of SN-38 is found within SN-38G, APC, CPT-11, and CPT-11 D10 (**FIGURE 1B**), and because all these compounds eluted at ~4.6 to 4.7 minutes, the additional peak for SN-38 likely resulted from in-source fragmentation of these compounds. The structure of SN-38 D3 is found within APC D3 and SN-38G D3, and similarly the additional peak for SN-38 D3 likely resulted from in-source fragmentation of these compounds.

When analyzed by themselves, SN-38 and SN-38 D3 eluted at ~5.1 to 5.2 minutes, with no additional peak at ~4.6 minutes (**FIGURE 2A**). Analysis of the ISs individually confirmed in-source frag-

FIGURE 2. Individual analysis of SN-38 and ISs reveals in-source fragmentation and pre-LC existence of SN-38 in ISs. A, Separate analysis for SN-38 (left panel) and SN-38 D3 (right panel) shows that only 1 peak is present. SN-38 D3 contains a minor quantity of SN-38 (inset). B, Analysis of SN-38G D3 (left panel), APC D3 (middle panel), and CPT-11 D10 (right panel) shows in-source fragmentation of these compounds and the presence of SN-38 D3 and SN-38 before LC separation. The inset shows a zoom-in of SN-38 in CPT-11 D10 analysis. C, Estimation of SN-38 in a blank specimen spiked with ISs. SN-38 concentration was estimated using a small low-end calibration curve (right panel) with specimens spiked with 0 (left panel), 1, 2, and 4 (middle panel) ng/mL SN-38. CPT-11 D10 and APC D3: 100 ng/mL; SN-38 D3: 50 ng/mL; and SN-38G D3: 200 ng/mL. CPT-11, irinotecan; IS, internal standard; LC, liquid chromatography; SN-38G, SN-38-glucuronide.

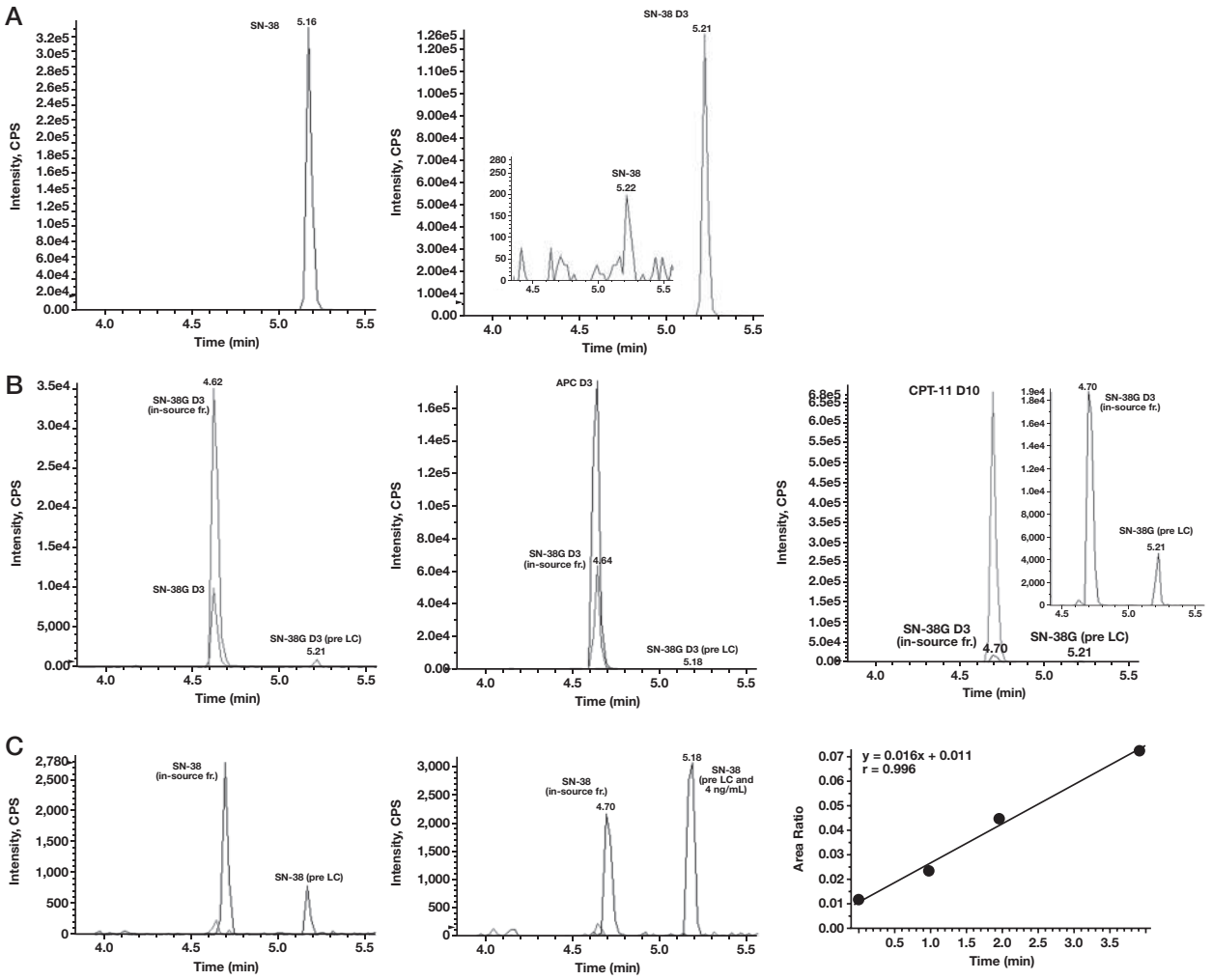

mentation for SN-38G D3, APC D3, and CPT-11 D10 (**FIGURE 2B**). In addition, SN-38 D3 found at ~5.2 minutes was present in SN-38G D3 and APC D3, indicating that it was present before LC separation and present within the IS. Similarly, SN-38 found at ~5.2 minutes was present in CPT-11 D10 and to a lesser extent in SN-38 D3 (insets in **FIGURE 2A and 2B**), indicating that it was present before LC separation.

Because SN-38 and SN-38 D3 are chromatographically well separated from the other compounds, the additional peak at ~4.6 to 4.7 minutes did not cause quantification issues. The pre-LC existence of SN-38 D3 in SN-38G D3 and APC D3 was not a problem because the quantity of SN-38 D3 far exceeded the quantity of what were likely impurities in these ISs. However, the presence of SN-38 in CPT-11 D10 (and to a lesser extent in SN-38 D3) may be an issue when analyzing low SN-38 concentrations. Even after reducing CPT-11 D10 5-fold (from 500 to 100 ng/mL), there was still a detectable SN-38 peak at ~5.2 minutes when a blank plasma specimen was spiked with ISs (CPT-11 D10 and APC D3: 100 ng/mL; SN-38 D3: 50 ng/mL; and SN-38G D3: 200 ng/mL; **FIGURE 2C**, left panel). Using a small low-end calibration curve (**FIGURE 2C**, middle and right panels), we found that the concentration of SN-38 in an IS spiked sample was ~0.7 (0.011/0.016) ng/mL. Calculated from the relative peak areas as shown in **FIGURE 2A and 2B**, >90% to 95% originated from CPT-11 D10. Based on these results, we decided to change the lower limit of the measurement interval (LLMI) for SN-38 from 1.0 to 2.0 ng/mL (area ratio approximately 4 times over blank) and omit the lowest calibrator in subsequent experiments.

Other than the described issue with SN-38 at the low end, we found no major issues in the experiments evaluating performance metrics. Standard curves for CPT-11, SN-38, SN-38G, and APC with a concentration range of 9.8 to 2500 ng/mL, 2.0 to 500 ng/mL, 2.0 to 500 ng/mL, and 4.8 to 1250 ng/mL, respectively, were used. For APC, the calculated calibrator concentration based on the calibration curve was 79%

FIGURE 3. Linearity for CPT-11 and its main metabolites SN-38, SN-38G, and APC. Measured concentrations were the mean of 5 different days and were calculated from the calibration curve. Inset: linearity for APC after removal of the highest calibrator. CPT-11, irinotecan; SN-38G, SN-38-glucuronide.

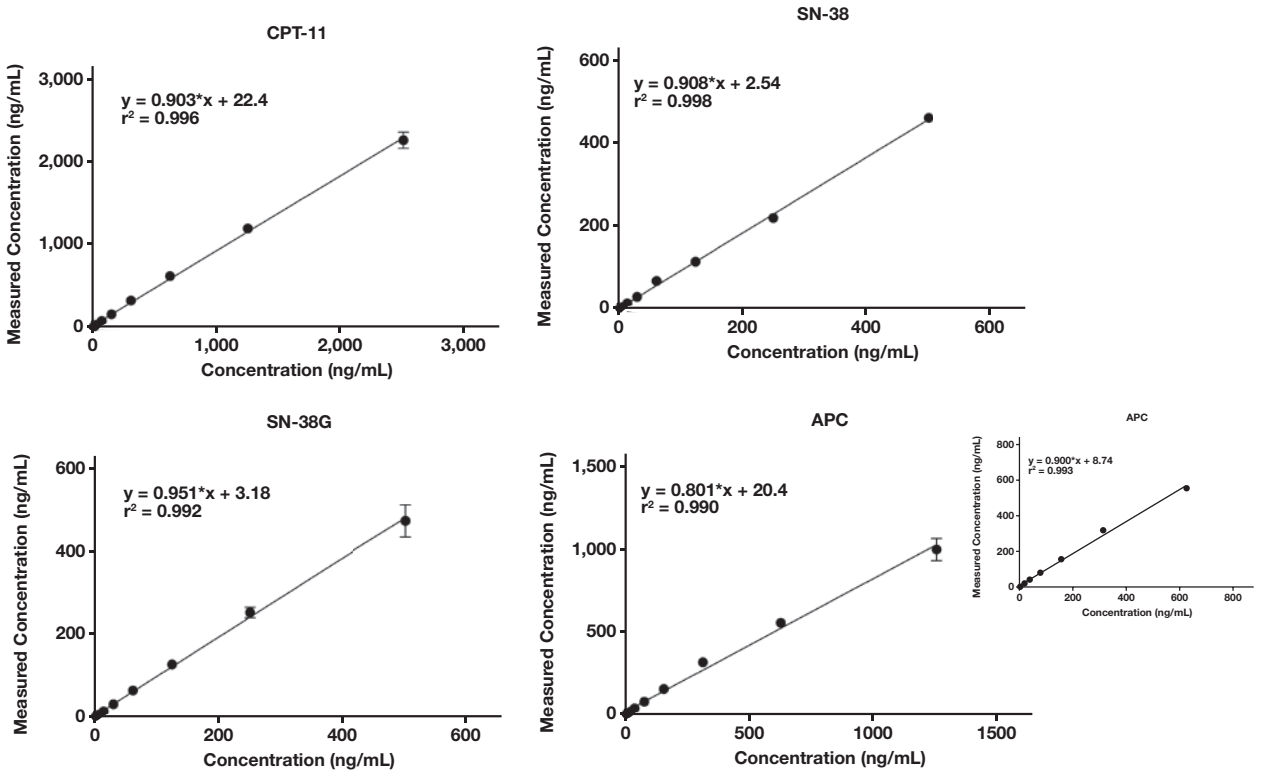

at 1250 ng/mL. After the removal of the highest calibrator for APC, calibrator concentrations for all analytes were within 15% deviation and the r^2 was >.99 (**FIGURE 3**). Notably, these measurement intervals cover a large range of the expected concentrations in human plasma specimens for up to 50 hours after administration (CPT-11: ~10 to 3000 ng/mL; SN-38: ~1 to 30 ng/mL; SN-38G: ~5 to 200 ng/mL; APC: ~2 to 250 ng/mL[5,9,13]). Intra- and interday precision coefficient of variations (CVs) of QC specimens were all below 10%, except for the interprecision of SN-38 at the lowest concentration (40 ng/mL), for which the CV was 11.3%. Spike-recovery accuracy of QC specimens was 85% to 115%, except for APC at the lowest concentration (40 ng/mL), for which it was 120%. The mean extraction recovery was in the range of 85% to 115% for all analytes, except for APC at the middle concentration (200 ng/mL), at which it was 116%. Similarly, the mean matrix effects were between 85% and 115%, except for SN-38G, for which it was 118% and 117% at the middle and high concentrations (100 and 400 ng/mL), respectively (the CVs for the matrix effects were not greater than 10%). There was no carryover for any of the analytes (0 ng/mL results for blank specimens after injection of the highest calibrator).

Discussion

Our study shows that LC-MS/MS assays for the quantification of CPT-11 and its major metabolites can potentially be used in pharmacokinetic and pharmacodynamic studies, to evaluate CPT-11 in clinical trials for novel anti-tumor applications, and for TDM for individuals taking CPT-11.

We used heavy isotope–labeled ISs and found that relatively small quantities of SN-38 were present in CPT-11 D10 and to a lesser extent in SN-38 D3. The concentration of SN-38 in a blank specimen spiked with ISs was ~0.7 ng/mL. When a criterion of an area ratio 4 times over blank was used, it constrained the LLMI for SN-38 to ~2.0 ng/mL; for 5 times over blank, this result was ~2.5 to 3.0 ng/mL. Using the structural analog camptothecin as an IS[9-11] would solve this issue. Detection and/or correction of matrix effects may be less efficient using camptothecin; however, we have not evaluated this hypothesis.

Given that the structure of SN38 is found in CPT-11, SN-38G, and APC, and in the CPT-11 D10 IS used here, the in-source fragmentation of these compounds can lead to interference in the SN-38 channel. Chromatographic separation of SN-38 from CPT-11, SN-38G, and APC is important if in-source fragmentation is present. We used a relatively high source temperature of 750°C, as determined during compound optimization in method development, which is a possible reason for the observed in-source fragmentation. By comparison, Marangon et al.[9] used a source temperature of 650°C (AB Sciex 4000 API), and Zhang et al[10] and Atasilp et al[11] used a source temperature of 550°C (AB Sciex 4000 Q-Trap, AB Sciex 3200 API, respectively).

Conclusion

When developing methods for CPT-11 and its metabolites, it is important to consider the effects of in-source fragmentation and the choice of internal standards.

Funding

Zineb Aoullay is a Fulbright Scholar. This research did not receive any other specific grant from funding agencies in the public, commercial, or not-for-profit sectors.

Conflicts of Interest

We wish to confirm that there are no known conflicts of interest associated with this publication and there has been no significant financial support for this work that could have influenced its outcome.

REFERENCES

1. Cunningham D, Maroun J, Vanhoefer U, Van Cutsem E. Optimizing the use of irinotecan in colorectal cancer. *Oncologist.* 2001;6 Suppl 4:17–23.
2. de Man FM, Goey AKL, van Schaik RHN, Mathijssen RHJ, Bins S. Individualization of irinotecan treatment: a review of pharmacokinetics, pharmacodynamics, and pharmacogenetics. *Clin Pharmacokinet.* 2018;57(10):1229–1254.
3. Innocenti F, Undevia SD, Iyer L, et al. Genetic variants in the UDP-glucuronosyltransferase 1A1 gene predict the risk of severe neutropenia of irinotecan. *J Clin Oncol.* 2004;22(8):1382–1388.
4. Innocenti F, Ratain MJ. Pharmacogenetics of irinotecan: clinical perspectives on the utility of genotyping. *Pharmacogenomics.* 2006;7(8):1211–1221.
5. Gupta E, Lestingi TM, Mick R, Ramirez J, Vokes EE, Ratain MJ. Metabolic fate of irinotecan in humans: correlation of glucuronidation with diarrhea. *Cancer Res.* 1994;54(14):3723–3725.
6. Di Paolo A, Bocci G, Danesi R, Del Tacca M. Clinical pharmacokinetics of irinotecan-based chemotherapy in colorectal cancer patients. *Curr Clin Pharmacol.* 2006;1(3):311–323.
7. de Jong FA, Mathijssen RH, de Bruijn P, Loos WJ, Verweij J, Sparreboom A. Determination of irinotecan (CPT-11) and SN-38 in human whole blood and red blood cells by liquid chromatography with fluorescence detection. *J Chromatogr B Analyt Technol Biomed Life Sci.* 2003;795(2):383–388.
8. Owens TS, Dodds H, Fricke K, Hanna SK, Crews KR. High-performance liquid chromatographic assay with fluorescence detection for the simultaneous measurement of carboxylate and lactone forms of irinotecan and three metabolites in human plasma. *J Chromatogr B Analyt Technol Biomed Life Sci.* 2003;788(1):65–74.
9. Marangon E, Posocco B, Mazzega E, Toffoli G. Development and validation of a high-performance liquid chromatography-tandem mass spectrometry method for the simultaneous determination of irinotecan and its main metabolites in human plasma and its application in a clinical pharmacokinetic study. *PLoS One.* 2015;10(2):e0118194.
10. Zhang W, Dutschman GE, Li X, Ye M, Cheng YC. Quantitation of irinotecan and its two major metabolites using a liquid chromatography-electrospray ionization tandem mass spectrometric. *J Chromatogr B Analyt Technol Biomed Life Sci.* 2009;877(27):3038–3044.
11. Atasilp C, Chansriwong P, Sirachainan E, et al. Determination of irinotecan, SN-38 and SN-38 glucuronide using HPLC/MS/MS: application in a clinical pharmacokinetic and personalized medicine in colorectal cancer patients. *J Clin Lab Anal.* 2018;32(1):e22217.
12. Matuszewski BK, Constanzer ML, Chavez-Eng CM. Strategies for the assessment of matrix effect in quantitative bioanalytical methods based on HPLC-MS/MS. *Anal Chem.* 2003;75(13):3019–3030.
13. D'Esposito F, Tattam BN, Ramzan I, Murray M. A liquid chromatography/electrospray ionization mass spectrometry (LC-MS/MS) assay for the determination of irinotecan (CPT-11) and its two major metabolites in human liver microsomal incubations and human plasma samples. *J Chromatogr B Analyt Technol Biomed Life Sci.* 2008;875(2):522–530.

To Reflex or Not to Reflex: A Time and Cost-Effectiveness Analysis of Autocontrol with Reflex DAT versus Direct DAT

Trang Lollie, MD,[1]✉ Voicu Suciu, BB(ASCP)[CM]SBB,[1] Dawn C. Ward, MD,[1] Alyssa Ziman, MD,[1] Andrea M. McGonigle, MD[1,]*

[1]Wing-Kwai and Alice Lee-Tsing Chung Transfusion Service, Department of Pathology and Laboratory Medicine, University of California, Los Angeles, Los Angeles, California, US; *To whom correspondence should be addressed. amcgonigle@mednet.ucla.edu

Keywords: transfusion medicine, immunology, blood banking/transfusion medicine, clinical pathology, autocontrol, pretransfusion testing, laboratory utilization, DAT (direct antiglobulin test)

Abbreviations: DAT, direct antiglobulin test; ABID, antibody identification; RBC, red blood cell; C3, third component of complement; PS, polyspecific; IAT, indirect antiglobulin test.

Laboratory Medicine 2022;53:53–57; DOI: 10.1093/labmed/lmab056

ABSTRACT

Objective: Performing autocontrol with a reflex direct antiglobulin test (DAT) or directly performing IgG DAT only for alloantibody detection has been a matter of institutional preference. The aim of this study is to evaluate antibody identification (ABID), local cost, and staff time savings of both processes.

Methods: We retrospectively reviewed all positive indirect antiglobulin tests with corresponding ABID, DAT, autocontrol, and patients with newly identified antibodies in 2014 and 2016. The number of tests performed, ABID, and the cost differences between methods were compared. Cost analysis was estimated from direct material costs, labor costs, and time spent per ABID workup.

Results: Annual costs and time saved by performing direct IgG DAT only were $8460 and 180 hours, respectively. The percentage of new ABID in 2014 and 2016 was identical (3.3%).

Conclusion: Removing autocontrol with reflex DATs at our center reduced costs and staff time while maintaining a comparable rate of positivity of ABID.

Pretransfusion testing for allogeneic transfusion is vital to patient safety.[1] A significant component of pretransfusion testing is to identify red blood cell (RBC) alloantibodies, which are demonstrable in approximately 2% to 9% of transfused individuals.[2-4] It is estimated that only 30% of induced RBC alloantibodies are detected, given alloantibody production and evanescence, different test methodologies with varying sensitivities, and the absence of a centralized antibody registry in the United States.[5] These alloantibodies may clinically impact future transfusion, forcing a need for alloantibody testing to be completed in advance of planned procedures that may require blood, increasing the amount of time needed to complete antibody testing, possibly requiring antigen-negative blood to be ordered from a community donor center at an increased cost, and potentially resulting in hemolytic transfusion reactions.

The AABB Standards for Blood Banks and Transfusion Services stipulate requirements for pretransfusion testing to detect the presence and identification of newly formed clinically significant antibodies.[6] The most recent edition of the AABB Technical Manual lists the autologous control (autocontrol) and direct antiglobulin test (DAT) as important components of basic antibody identification.[7] In the autocontrol, a patient's own plasma (which contains any autologous or allogeneic red blood cell antibodies the patient has) is added to a patient's own RBCs. If the patient has autologous RBC antibodies, then they will bind to their own RBCs, causing the autocontrol to be positive in vitro. In a DAT, anti-IgG or an antibody against the third component of complement (C3) are combined with a patient's RBCs to detect whether IgG or C3 have been bound to the RBCs in vivo.

There is no prescribed standard testing protocol, and specifics are determined by individual institutional policy and available testing platforms. Autocontrol and DAT were routinely included in pretransfusion testing algorithms historically, based on the premise that these tests would identify early manifestations of alloantibody production.[7,8] By the early 1980s, the utility of the autocontrol for routine pretransfusion testing was being questioned and the use of an IgG DAT was suggested in lieu of polyspecific (PS) DAT for the purposes of alloantibody detection.[9] In a review of more than 65,000 pretransfusion blood specimens, Judd, Barnes, and colleagues[8] argued that the use of monospecific DAT without autocontrol for early alloantibody detection would be clinically equivalent and cost effective. It became a matter of

institutional preference whether to perform autocontrol with reflex to DAT or DAT alone as a part of antibody screening; the routine use of an autocontrol, a DAT test, or both decreased from 58.8% in 1995 to 54% in 1998.[10] As of 2001, Shulman and colleagues[10] reported that only 36.3% of laboratories included autocontrol and DAT tests in antibody screening procedures.[11]

For those laboratories that have ceased the use of autocontrol and DAT as a part of their routine antibody screening, we suspect that many continue to use both to evaluate positive antibody screens. We theorized that this practice represents an inefficient and clinically unnecessary process and considered whether we could show equivalent antibody detection and cost and time savings with the removal of autocontrol with reflex DAT for ABID. In 2014, our pretransfusion testing policy outlined 2 pathways for antibody identification after a positive antibody screen. The policy stated that technologists should preferably perform antibody identification using the same method that had returned the initial positive indirect antiglobulin test (IAT). If they performed antibody identification in tube or by gel, then a PS DAT including IgG and C3 was performed reflexively with a concurrent positive autocontrol. Alternatively, if antibody identification was performed with solid phase, then autocontrol testing was bypassed using PS DAT alone. If the PS DAT was positive, then monospecific testing with IgG and C3 was subsequently performed. In 2016, our institution stopped routinely performing autocontrols with reflex DAT, alternatively switching to performing an IgG DAT only with each positive antibody screen. We anticipated that our simplified workflow would reduce overall costs and time while maintaining a comparable rate of positivity of ABID for new (not previously identified) RBC alloantibodies.

Materials and Methods

Workflow

In 2014, a positive IAT (solid phase or column agglutination) resulted in the performance of either a PS DAT (tube) or an autocontrol (column agglutination). The PS DAT was performed if the initial positive IAT was performed in solid phase. The autocontrol was performed if the initial IAT was performed in column agglutination. If the PS DAT was positive, then the monospecific IgG DAT and monospecific C3 DAT were performed by tube. If the autocontrol was positive, then the PS DAT (tube) was performed with reflex to tube IgG DAT and C3 DAT if positive. In 2016, a positive IAT (solid phase or column agglutination) resulted in an IgG DAT alone (solid phase or column agglutination; see **FIGURE 1**).

Data Collection, Calculations, and Estimation

We retrospectively reviewed blood bank records to collect data on the total number of ABIDs, DATs, autocontrols, and patients with newly identified antibodies from 2014 and 2016. Patients from 2015 were excluded because we began to switch processes in mid-2015 and wanted to compare 2 full years of data right before and after switching processes. Newly identified antibodies were defined as antibodies not identified historically and identified by ABID and/or elution from a positive DAT. At our institution, DATs are performed not only as a part of ABID workup but also for a physician order and for transfusion reactions. Physician-ordered DATs and those performed for transfusion reactions were excluded from the data set to ensure that the time and cost differentials calculated were only for those tests associated with ABID workups.

The total number of DATs during the study period was extracted from our blood bank operating system. In 2016, test names for a physician-ordered DAT and an ABID-associated DAT were available. In 2014, there was no discriminator between physician-ordered DATs and ABID-associated DATs in the blood bank operating system. Therefore, the number of ABID-associated DATs that were deemed positive in 2014 was estimated by the total number of positive PS DATs minus the estimated number of positive physician-ordered DATs. The number of positive physician-ordered DATs in 2014 was estimated by using the percentage of positive physician-ordered DATs in 2016 multiplied by the total number of physician-ordered DATs performed in 2014. In 2014 and 2016, the number of monospecific C3 tests was used as a proxy for the number of positive PS DATs because this test was only performed when a PS DAT was deemed positive.

Time and Cost Calculations

The unit cost to perform 1 ABID was calculated from direct labor costs and the costs of the direct materials required for each workup. The costs of materials for automated solid-phase technology (NEO, Immucor Inc., Norcross, GA), column agglutination (Ortho Workstation, Ortho-Clinical Diagnostics, Raritan, NJ), and tube testing (reagents by Immucor Inc., Norcross, GA), including reagents and controls, were compared and broken down by cost per individual ABID workup. Labor costs were determined by the average hourly rate for technical staff (which was the same in 2014 and 2016) and the average hands-on time necessary to perform testing. Equipment cost was excluded. This included the Immucor Echo Calileo on which IAT and ABIDs were performed, the Immucor Neo that performed all the same tests as the Echo plus IgG DAT, and the Ortho Workstation, on which IAT, ABIDs, and autocontrols were performed. The costs of direct labor and materials were summed and averaged by the total number of ABIDs per year.

Time was compared for each individual testing modality performed in 2014 and 2016. Hands-on time was estimated using time measurements of staff performing each type of test in 2018 and defined as the time during which the technologist was performing the test (did not include the time waiting for the test to run, when the technologist might be working on other tasks). Two time measurements were taken for each test, after which direct measurements were averaged and used to calculate the total time to perform ABID workups. Annual time savings were calculated by multiplying the total automated solid-phase technology and column-agglutination DATs in 2016 by the difference of the average time per ABID in 2014 and 2016. All calculations were performed in a spreadsheet (Excel, Microsoft Office).

Results

Process 1 (2014): Autocontrol with Reflex PS IgG and C3 DAT

In our 2014 process, a positive antibody screen (n = 1185) led to the performance of an autocontrol in 69.8% (n = 828) of workups, with the remainder of positive ABIDs (n = 357) leading to the direct performance of a PS DAT (**FIGURE 1**). Of the 828 autocontrols performed, 54.5% (n = 452) were positive and resulted in the performance of a PS DAT in addition to the autocontrol. Of the estimated 809 total PS DATs performed either as a direct result of a positive antibody screen or as a result of a positive autocontrol, 440 (54.3%) were positive and required

FIGURE 1. Workflow of pretransfusion workup in patients with positive IAT results in 2014 vs 2016. In 2014, workups for positive IAT were chosen at the discretion of the technician using either PS DAT by the tube method or autocontrol by the column agglutination method. Of the 828 autocontrols performed in 2014, 452 reactive specimens triggered a reflex PS DAT (highlighted by red arrow), along with 357 workups that bypassed autocontrol for a sum of 809 PS DATs. Positive PS DATs triggered a reflex monospecific IgG and C3 tube DAT testing, resulting in the detection of 39 new antibodies in 2014. In 2016, the new policy required only an IgG DAT to be performed, either by SPRCA or the column agglutination method, resulting in the detection of 30 new antibodies in 2016. C3, third component of complement; IAT, indirect antiglobulin test; PS DAT, polyspecific direct antiglobulin test; SPRCA, solid-phase red-cell adherence.

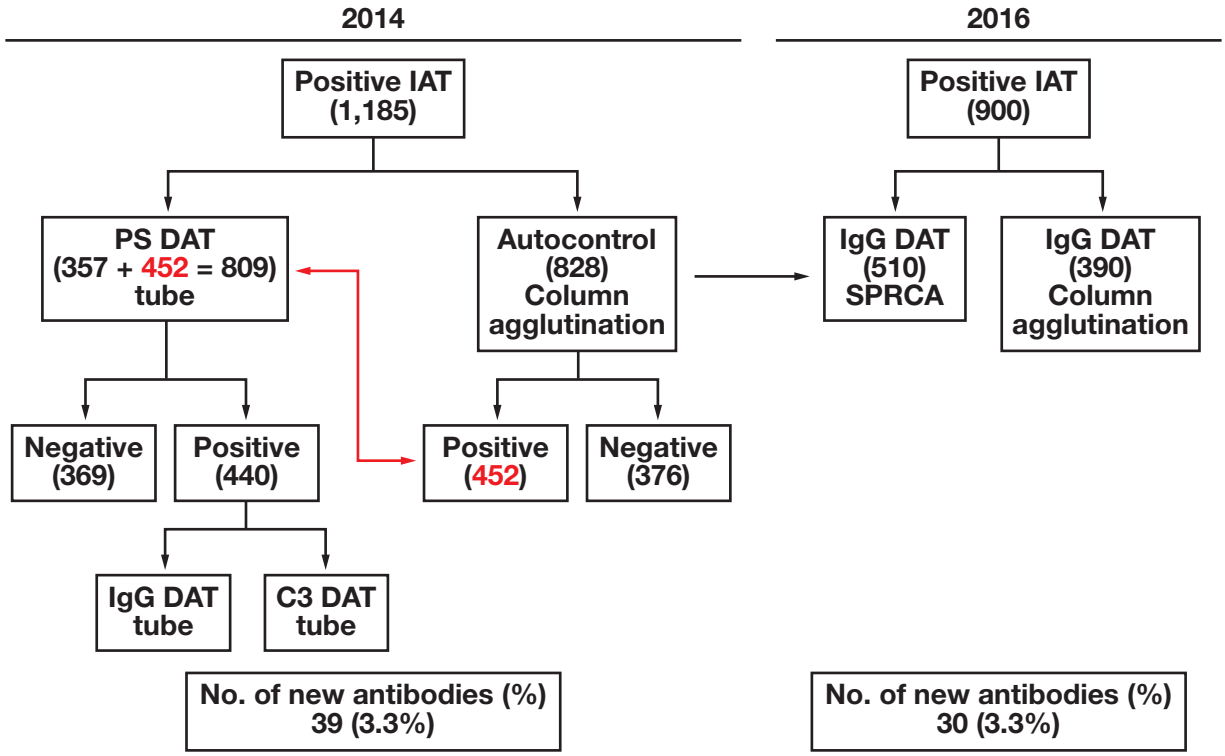

additional monospecific IgG and C3 testing. In 2014, the number of new RBC antibodies identified by the serological workup was 39 (representing a 3.3% rate of new RBC antibodies found per ABID workup; **FIGURE 1**).

Process 2 (2016): IgG DAT only

In the 2016 process, a total of 900 IgG DATs were performed as a result of a positive antibody screen, and there were 30 new RBC antibodies identified (representing a 3.3% rate of new RBC antibodies found per ABID workup; **FIGURE 1**).

Cost and Time Savings

All costs were calculated in U.S. dollars. The total costs of 828 autocontrols, an estimated 440 positive PS tube DATs, and an estimated 369 negative PS tube DATs in 2014 were $2070.00, $11,000.00, and $4059.00, respectively, with a sum of $17,129.00, resulting in a calculated average cost of $14.45 per ABID in 2014. In contrast, the total costs of 510 automated DATs and an estimated 390 column-agglutination DATs in 2016 amounted to $4545.00, resulting in an average cost of $5.05 per ABID in 2016 (**TABLE 1**). Time measurements are also shown in **TABLE 1**.

The total hands-on time of performing 828 autocontrols, an estimated 440 positive PS tube DATs, and an estimated 369 negative PS tube DATs in 2014 accumulated to 1656; 10,120; and 4797 minutes, respectively, with a sum of 16,573 minutes. The calculated average time per ABID workup in 2014 was 14 minutes. The total hands-on time of the 510 automated DATs and 390 gel DATs in 2016 amounted to 1800 minutes. The average time per ABID in 2016 for the 900 DATs, performed by either automated solid-phase technology or manual column agglutination, was 2 minutes.

Discussion

Pretransfusion compatibility testing has been shown to comprise as much as 3% to 11% of laboratory costs.[12,13] In our center, we found that the small change of performing an IgG DAT with each positive antibody screen rather than a PS DAT or an autocontrol with reflex to additional DAT testing saved money and technologist time. The cost savings from reduced technologist time between 2014 and 2016 primarily resulted from the transition from manual tube DATs performed in 2014 for all positive ABIDs or positive autocontrols to automated (solid phase) or semi-automated (column agglutination) testing. Although not directly measured in our study, we hypothesize that the saved technologist time allowed for the reallocation of staff and resources to other functions such as blood component processing, testing, clerical checks, or administrative duties. Thus, periodic review of the necessity, efficiency, and efficacy of routine testing could be of value to individual laboratories.

TABLE 1. Cost and time savings of performing DAT only (2016) instead of autocontrol with reflex to DAT (2014)

Variable	2014	Time and cost difference (2016–2014)	2016
Number of ABID workups	1185		900
Autocontrol			
Number	828		N/A
Cost per test	$2.50		N/A
Time per test	2 min		N/A
PS DAT			
Number	809		N/A
Cost per positive test	$25.00		N/A
Cost per negative test	$11.00		N/A
Time per positive test	23 min		N/A
Time per negative test	13 min		N/A
Monospecific IgG DAT—Gel			
Number	N/A		390
Cost per test	N/A		$2.50
Time per test	N/A		2 min
Monospecific IgG DAT—SPRCA			
Number	N/A		510
Cost per test	N/A		$7.00
Time per test	N/A		2 min
Average cost per ABID workup	$14.45		$5.05
ABID total cost per year	$17,129.00		$4545.00
ABID total cost savings per workup		$8.95	
Annual cost savings estimate		$8460	
Average time per ABID workup	14		2
Annual time savings estimate		10,800 min (or 180 h or ~4.5 wks/y)	

ABID, antibody identification; DAT, direct antiglobulin test; PS, polyspecific; SPRCA, solid-phase red-cell adherence.
Cost and time per test, quantity of each test performed per year, and cost and time-savings estimate of performing direct antiglobulin test (DAT) only (2016 process) instead of autocontrol with reflex to DAT (2014 process), are shown. For 2016, cost and time values were calculated using an estimated number of DATs performed as a reflex from of positive antibody identification (ABID). For 2014, the average cost for polyspecific (PS) DAT calculated based on whether the test resulted as positive or negative. The positive PS DAT test reflexed to a monospecfic C3 DAT (tube) and monospecific IgG DAT (tube). The negative PS DAT resulted in performance of IgG check cells.

One of the significant limitations of this study was that the number of positive PS DATs resulting in monospecific IgG and C3 DATs performed in 2014 as a part of ABID (as opposed to physician-ordered DATs) was not known. We therefore had to assume that the percentage of positive physician-ordered DATs in 2014 would be the same as in 2016 and used that percentage to estimate the number of positive DATs performed for a physician order in 2014. We then utilized that estimation to calculate the number of positive PS DATs and the resulting monospecific IgG and C3 DATs performed as a part of ABID workups in 2014. The direction of bias on the number of DATs performed as a part of ABID workup in 2014 was unknown. However, the general rate of positive DATs ordered by physicians was expected to show minimal fluctuation in 2014 vs 2016.

There were also limitations with the cost savings calculation. These cost savings were relative to local labor costs and institution-specific reagent contracts that are not generalizable to other institutions but could serve as sn impetus for others to review their own potential cost savings from adopting an IgG DAT–only workflow. Data on the volume of each test performed in 2014 vs 2016 were acquired from a retrospective review of paper and electronic records. Based on the volume derived from the retrospective review, the automated solid-phase technology DAT cost was calculated based on the worst-case assumption that only 1 DAT was run per DAT strip. At maximum, 4 DATs and 4 controls can be performed on a single strip (8 wells per strip). This process would result in underestimating the cost savings if a strip was used to run more than 1 DAT for at least some of the tests and would bias the calculations toward the null hypothesis and likely have a minimal effect on the cost calculations. Data for the exact average hands-on time necessary to perform testing for each ABID workup performed in 2014 and 2016 was unavailable for evaluation. Therefore, the average hands-on time for each test was utilized instead. The effect on time savings would be expected to influence both the 2014 and 2016 calculations because averages were used for all tests. In addition, the cost of equipment wear and tear was excluded, possibly leading to overestimation of cost savings, which would affect both the 2014 and 2016 calculations. In the 2014 calculations, the instrument was used exclusively to complete autocontrol results. In 2016, approximately 75% of the process was completely automated on the instrument. However, this finding was expected to affect the calculations minimally. There were also limitations to the time calculation savings. The reduced technologist time mostly

resulted from the transition from manual tube DATs to automated and semi-automated (gel) testing.

In our institution, moving to an IgG DAT–only workflow was easy to implement and reduced pretransfusion antibody identification resource utilization. The annual costs and time saved after switching to the new model were calculated as $8460 and 180 hours, respectively. The percentages of new antibody identification in 2014 and 2016 were identical (3.3%), suggesting that the new process does not compromise patient safety. In addition, our new workflow eliminates technologist variability and the ambiguity of decision-making by improving standard operative procedures.

Conclusion

In conclusion, we observed that removing autocontrol with reflex DAT in favor of an IgG DAT alone reduced laboratory costs and saved employee time while maintaining patient safety at our institution.

Acknowledgments

The authors declare they have no conflicts of interest relevant to the manuscript submitted to *Laboratory Medicine*. The manuscript has been seen and approved by all authors; it is not under active consideration for publication, has not been accepted for publication, and has not been published, in full or in part.

REFERENCES

1. Forbes JM, Anderson MD, Anderson GF, Bleecker GC, Rossi EC, Moss GS. Blood transfusion costs: a multicenter study. *Transfusion.* 1991;31(4):318–323.
2. Heddle NM, Soutar RL, O'Hoski PL, et al. A prospective study to determine the frequency and clinical significance of alloimmunization post-transfusion. *Br J Haematol.* 1995;91(4):1000–1005.
3. Redman M, Regan F, Contreras M. A prospective study of the incidence of red cell allo-immunisation following transfusion. *Vox Sang.* 1996;71(4):216–220.
4. Tormey CA, Fisk J, Stack G. Red blood cell alloantibody frequency, specificity, and properties in a population of male military veterans. *Transfusion.* 2008;48(10):2069–2076.
5. Tormey CA, Hendrickson JE. Transfusion-related red blood cell alloantibodies: induction and consequences. *Blood.* 2019;133(17):1821–1830.
6. American Association of Blood Banks. *Standards for Blood Banks and Transfusion Services*, 32nd ed. Bethesda, MD: American Association of Blood Banks; 2020.
7. Cohn C, ed. *Technical Manual*, 20th ed. Bethesda, MD: American Association of Blood Banks; 2020.
8. Judd W, Barnes B, Steiner E, et al. The evaluation of a positive direct antiglobulin test (autocontrol) in pretransfusion testing revisited. *Transfusion*. 1986;26(3):220–224.
9. Judd WJ, Butch SH, Oberman HA, Steiner EA, Bauer RC. The evaluation of a positive direct antiglobulin test in pretransfusion testing. *Transfusion.* 1980;20(1):17–23.
10. Shulman IA, Downes KA, Sazama K, Maffei LM. Pretransfusion compatibility testing for red blood cell administration. *Curr Opin Hematol.* 2001;8(6):397–404.
11. Padget BJ, Hannon JL. Variations in pretransfusion practices. *Immunohematology.* 2003;19(1):1–6.
12. Stokes EA, Wordsworth S, Staves J, et al. Accurate costs of blood transfusion: a microcosting of administering blood products in the United Kingdom National Health Service. *Transfusion.* 2018;58(4):846–853.
13. Shander A, Hofmann A, Ozawa S, Theusinger OM, Gombotz H, Spahn DR. Activity-based costs of blood transfusions in surgical patients at four hospitals. *Transfusion.* 2010;50(4):753–765.

MiR-150 Expression in Chronic Myeloid Leukemia: Relation to Imatinib Response

Eman M. Habib, MSc,[1] Nahla A. Nosiar, MD,[1] Manal A. Eid, MD,[2] Atef M. Taha, MD,[3] Dalia E. Sherief, MSc,[1] Asmaa E. Hassan, MSc,[1] Muhammad T. Abdel Ghafar, MD[2,]*

[1]Department of Clinical Pathology, Faculty of Medicine, Kafr El-Sheikh University, Kafr El-Sheikh, Egypt; [2]Department of Clinical Pathology, Faculty of Medicine, Tanta University, Tanta, Egypt, and; [3]Department of Internal Medicine, Faculty of Medicine, Tanta University, Tanta, Egypt; *To whom correspondence should be addressed. mohamed.abdelghafar@med.tanta.edu.eg; mohammedtarek5514@yahoo.com

Keywords: chronic myeloid leukemia, miR-150, *BCR-ABL1*, imatinib, prediction, early treatment response

Abbreviations: CML, chronic myeloid leukemia; miR-150, micro-RNA-150; ETR, early treatment response; TKI, tyrosine kinase inhibitor; rt-PCR, real-time polymerase chain reaction; Ct, cycle threshold; ROC, receiver operating characteristic; WBC, white blood cell; OR, odds ratio; CI, confidence interval; IQR, interquartile range; AUC, area under the curve.

Laboratory Medicine 2022;53:58–64; DOI: 10.1093/labmed/lmab040

ABSTRACT

Objective: To assess the circulating micro-RNA-150 (miR-150) expression in patients with chronic myeloid leukemia (CML) in relation to imatinib response.

Methods: Sixty patients with CML and 20 age- and sex-matched control subjects were enrolled. Circulating miR-150 levels were assessed by quantitative real-time polymerase chain reaction on days 0, 14, and 90 of imatinib therapy for patients and once for control subjects.

Results: The baseline miR-150 expression was significantly lower in patients with CML than in control subjects with subsequent elevation at 14 and 90 days after the start of imatinib treatment. Early treatment response (ETR) at 90 days was the main study outcome. The miR-150 expression had a significantly higher level in patients with CML with ETR. On multivariate analysis, miR-150 on day 14 was significantly related to ETR in patients with CML with predictive efficacy (area under the curve = 0.838, 72.9% sensitivity, and 84.2% specificity).

Conclusion: We found that miR-150 expression on day 14 of imatinib treatment is a useful early predictive candidate for imatinib response in patients with CML.

Chronic myeloid leukemia (CML) is a chronic myeloproliferative disorder with an estimated annual incidence of 0.78 patients/100,000 worldwide.[1] The condition is caused by a chimeric fusion protein known as BCR-ABL. This protein is involved in the activation of ABL tyrosine kinase, which mediates the uncontrolled cellular proliferation in CML.[2] The recent introduction of tyrosine kinase inhibitors (TKIs) has dramatically changed the course of CML, and most patients are now able to enjoy a normal life expectancy.[3]

Among others, the earliest target of TKI treatment is to achieve major molecular response after 90 days of treatment. Patients who fail to achieve the therapeutic target can use another TKI. In fact, resistance to TKIs is not an uncommon event. It can affect ~10% of patients and is usually associated with poor outcomes. Early identification of patients susceptible to TKI resistance can minimize treatment costs and improve treatment outcomes.[4,5]

Micro-RNAs (miRs) are small noncoding RNA fragments that serve as epigenetic regulators of gene expression and cellular signaling pathways. They are commonly dysregulated in human malignancies.[6] In CML, miRs can modulate the expression of BCR-ABL, Crk family proteins, SOS proteins, K-Ras proteins, Raf-1 protein, and mitogen-activated protein kinases/extracellular signal–regulated kinase proteins.[7]

Research has shown that miR-150 is known for its role in hematopoiesis, and its dynamic expression changes play a major role in myeloid, B-, and T-cell differentiation.[8] The genetic pathways involved in miR-150 actions include eukaryotic translation Initiation Factor 4B, forkhead box protein O4, and protein kinase C alpha pathways.[9] Furthermore, miR-150 is repressed by BCR-ABL with subsequent upregulation of its target, oncogenic transcription factor MYB, resulting in the progression of CML.[10] Therefore, miR-150 has been found to be downregulated at CML diagnosis[11,12] and has been implicated in treatment response to imatinib therapy.[13,14] Normalization of miR-150 expression levels after treatment has resulted in the marked inhibition of leukemic growth and the induction of leukemia cell apoptosis. The present study aimed to assess the levels of circulating miR-150 in a cohort of Egyptian patients with CML and to uncover their relation to treatment outcome in response to imatinib.

Methods

Study Cohort

In this study, 60 patients with newly diagnosed CML in the chronic phase were recruited from Kafr El-Sheikh University Hospital, Egypt

as the CML group (group 1). They were diagnosed based on the revised World Health Organization criteria for CML from 2016.[15] Patients with synchronous malignancy or hepatic or renal diseases were excluded (n = 15). In addition, 20 healthy participants were recruited and served as control subjects (group 2). The study cohort was recruited as illustrated in **FIGURE 1**.

Clinical and Laboratory Assessment

The included participants were asked about their personal history and underwent complete clinical examination and ultrasonography to assess the presence and extent of splenomegaly. Complete blood count with blast cell count and quantitative estimation of *BCR-ABL1* by quantitative real-time polymerase chain reaction (rt-PCR) at days 0 and 90 of imatinib therapy were performed. The Sokal score was calculated, and patients were defined as low (<0.8), intermediate (0.8–1.2), and high risks (>1.2).[16] The Sokal score is a prognostic score that is used to determine the relative risk and decide on therapy based on the National Comprehensive Cancer Network guidelines for CML.[17] It is calculated using simple clinical and hematological data such as age, splenic size, platelet count, and blast cell percentage.[16] Circulating miR-150 levels were relatively quantified at day 0 (baseline), day 14, and day 90 of imatinib therapy for patients with CML and once for control subjects using rt-PCR.

Relative Quantitation of miR-150 Expression

We obtained 3 mL of venous blood under complete aseptic conditions from both patients with CML and control subjects and delivered them into a K3EDTA vacutainer tube. The plasma was separated by centrifugation and total RNA, including miR isolation, was carried out using the miRNeasy Mini Kit (Qiagen, catalog number 217004) according to the manufacturer's protocols. The RNA yields were measured using the NanoDrop2000 Spectrophotometer (Thermo Scientific), and RNA purity was further determined by dividing the absorbance at 260/280 nm. The purified RNA was reversely transcribed into cDNA using a small RNA-specific, stem-loop reverse transcription primer from the TaqMan Small RNA Assays and reagents from the TaqMan MicroRNA Reverse Transcription Kit. The expression level of miR-150 was assessed by relative quantitation PCR on the Stratagene Mx3000p real-time instrument using the TaqMan Small RNA Assay together with the TaqMan Universal PCR Master Mix II. An internal control (RNU48) was used for normalization. The cycle threshold (Ct) of miR-150 and RNU48 in both patients with CML and control subjects was detected, and miR-150a expression was relatively quantified using an arithmetic formula ($2^{-\Delta Ct}$) where $\Delta Ct = Ct_{\text{miR-150—Ct RNU48}}$.[18]

FIGURE 1. Study flow chart according to the international Standards for Reporting of Diagnostic Accuracy Studies guidelines.

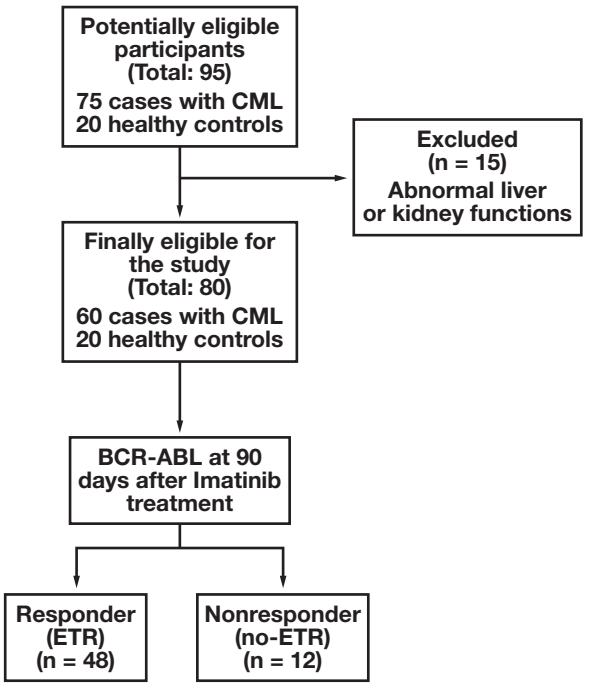

Study Outcomes

Achievement of early treatment response (ETR) at day 90 was the main outcome in this study. The criteria of ETR were early molecular response (3-month *BCR-ABL1* transcript <10%).[19] The included patients with CML were divided according to ETR at day 90 into 2 groups: (i) group 1A: those who achieved ETR, and (ii) group 1B: those who failed to achieve ETR.

Ethical Statement

This study was approved by the ethics committee of the Faculty of Medicine, Kafr El-Sheikh University, and performed in accordance with the 1964 Declaration of Helsinki and its later amendments. All participants in this study signed informed consents.

Statistical Analysis

Statistical analysis of data was carried out using IBM SPSS software package version 22.0 (IBM Corp.) and GraphPad Prism 7.0 software (GraphPad Software, San Diego, CA). The normal distribution of variables was analyzed using the Kolmogorov-Smirnov test. For normally distributed variables, the Student's *t*-test and an analysis of variance were used for comparing 2 groups and more than 2 groups, respectively; otherwise, the skewed data were compared between 2 groups or more than 2 groups using the Mann-Whitney *U* test and the Kruskal-Wallis test, respectively. Qualitative data were described as number and percentage and compared using the χ^2 test. Independent predictors for imatinib response were assessed by univariate analysis; significant variables with $P < .05$ were included in multivariate logistic regression models. The predictive value of miR-150 in imatinib response was determined by receiver operating characteristic (ROC) curve analysis, and the maximal Youden's index was used for determining the optimal cutoff value. All analyses were 2-sided; a P value of <.05 was considered statistically significant.

Results

Basic Group Characteristics

In this study, 60 patients with CML were recruited (group 1) and comprised 33 women (55.0%) and 27 men (45.0%) with a mean age of 55.15 ± 10.95 years. Their hematological profile revealed a mean hemoglobin level of 10.95 g/dL (range, 9.0–12.0 g/dL), a mean platelet count of 430.75 × 10^9/L (range, 250.0–600.0 × 10^9/L), a mean white blood cell

(WBC) count of 91.23 × 10^9/L (range, 50.0–164.0 × 10^9/L), and median blast cells of 2.0% (range, 0%–6.0%). Their mean Sokal score was 1.08 (range, 0.7–1.53). Ultrasonographic findings revealed a mean splenic size of 12.2 ± 3.35 cm. In addition, 20 healthy subjects were recruited as a healthy control group (group 2) and comprised 10 men and 10 women with a mean age of 51.2 ± 9.25 years. They were age- and sex-matched with the CML group.

Predictors of ETR in Patients with CML

Patients with CML were divided according to ETR at day 90 based on *BCR-ABL1* transcript level results into group 1A—patients with CML with ETR (n = 48)—and group 1B—patients with CML with no ETR (n = 12). As shown in **FIGURE 2**, there was a significant difference between both groups regarding the baseline WBC count, splenic size, Sokal score, and *BCR-ABL1* transcript level at day 90 (P <.001), with no significant difference regarding patients' age, baseline hemoglobin level, platelet count, blast cell count, and baseline *BCR-ABL1* transcript level (P >.05). Patients' age and Sokal score were significantly related to ETR in univariate analysis; however, in multivariate analysis, the Sokal score (odds ratio [OR], 18.6; 95% confidence interval [CI], 2.14–37.0) was the only independent significant predictor of ETR in patients with CML (**TABLE 1**).

MiR-150 as a Predictor for ETR in Patients with CML

A comparison between the patients and the control subjects regarding baseline circulating miR-150 levels revealed a significantly higher expression of miR-150 in the control subjects (**FIGURE 3A**). Subsequent evaluation of miR-150 levels at day 14 and day 90 after the start of imatinib treatment revealed a significant elevation of miR-150 levels (median and interquartile range [IQR], 0.0046; range, 0.000002–0.1989 at baseline; median and IQR, 0.1698; range, 0.0002–8.574 after 14 days; and median and IQR, 0.9372; range, 0.11–12.55 after 90 days of treatment, respectively (**FIGURE 3B**). The miR-150 expression level at day 90 was inversely correlated with the *BCR-ABL1* expression level (r = −.344; P = .007). The miR-150 expression level was significantly higher in group 1A than in group 1B

FIGURE 2. Clinical, ultrasonographic, and hematological characteristics in ETR group (group 1A) vs no ETR group (group 1B) of patients with CML. CML, chronic myeloid leukemia; ETR, early treatment response; Hb, hemoglobin; WBCs, white blood cells. ns: P-value is non significant. *P-value <.05 and >.01 ***P-value <.001.

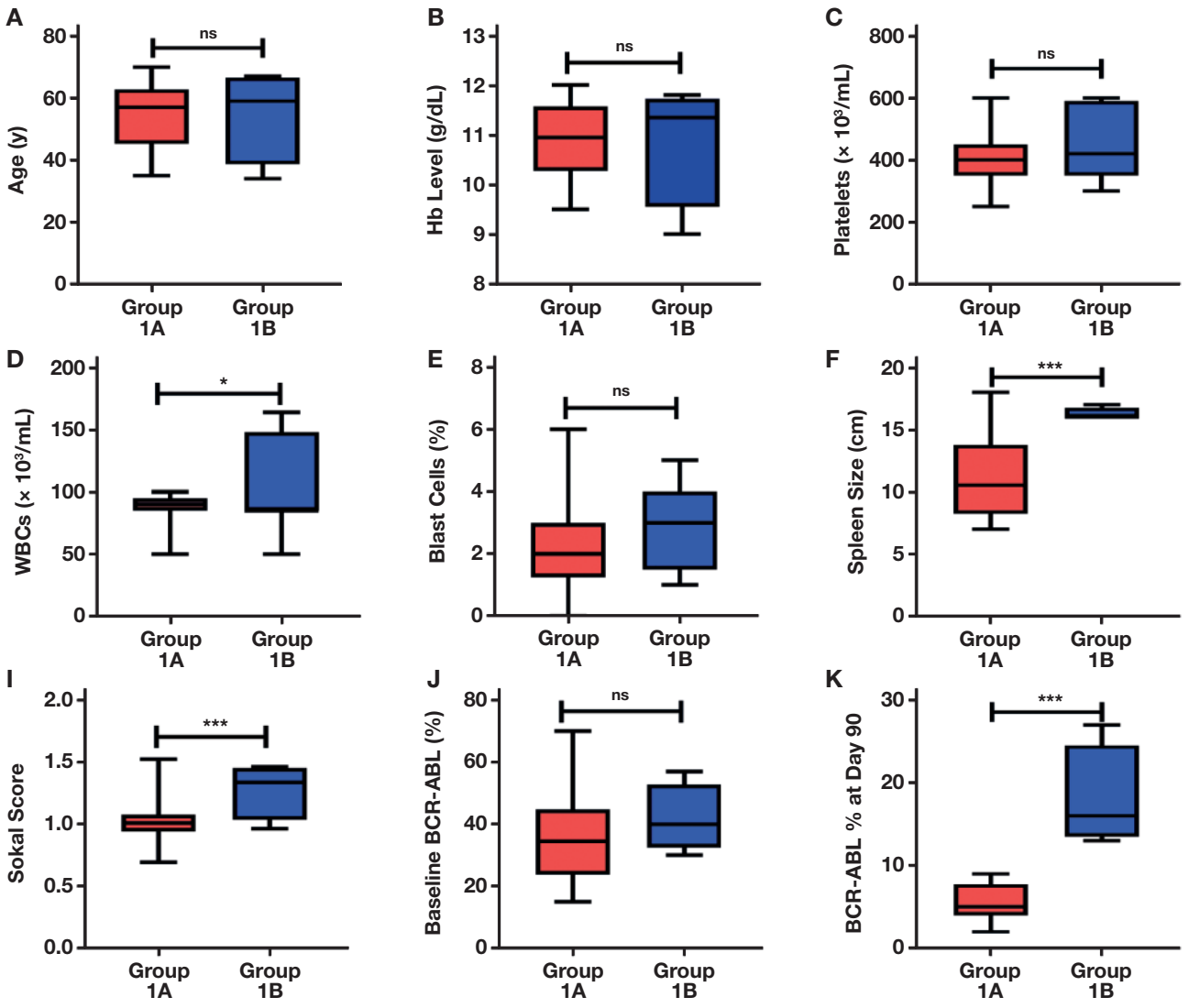

TABLE 1. Predictors of Imatinib Response in Patients with CML

	Univariate Analysis		Multivariate Analysis	
	OR (95% CI)	*P* Value	OR (95% CI)	*P* Value
Age	0.99 (0.94–1.06)	.885	…	…
Sex	5.0 (1.19–20.92)	.028[a]	2.63 (0.43–16.33)	.298
Hb	0.87 (0.40–1.87)	.718	…	…
Platelets	1.01 (0.99–1.01)	.075	…	…
WBCs	1.03 (0.99–1.06)	.072	…	…
Blast cells%	1.38 (0.91–2.11)	.132	…	…
Sokal score	38.4 (11.1–44.2)	.001[a]	18.6 (2.14–37.0)	.040[a]
Baseline *BCR-ABL1*	1.03 (0.99–1.08)	.188	…	…
miR-150 at 14 days	0.0 (0.0–0.13)	.022[a]	0.0 (0.0–0.924)	.029[a]
miR-150 at 90 days	0.51 (0.24–1.11)	.090	…	..

[a]P *<.05 was significant. CI, confidence interval; CML, chronic myeloid leukemia; Hb, hemoglobin; miR-150, micro-RNA-150; OR, odds ratio; WBCs, white blood cells.*

FIGURE 3. Relative miR-150 expression in patients with CML vs healthy control subjects (A), baseline vs day 14 and day 90 of imatinib treatment (B), in ETR group (group 1A) vs no-ETR group (group 1B) of patients with CML at day 14 (C), and at day 90 of imatinib treatment (D). CML, chronic myeloid leukemia; Ct, cycle threshold; ETR, early treatment response; miR-150, micrp-RNA-150. ******P*-value <.001.

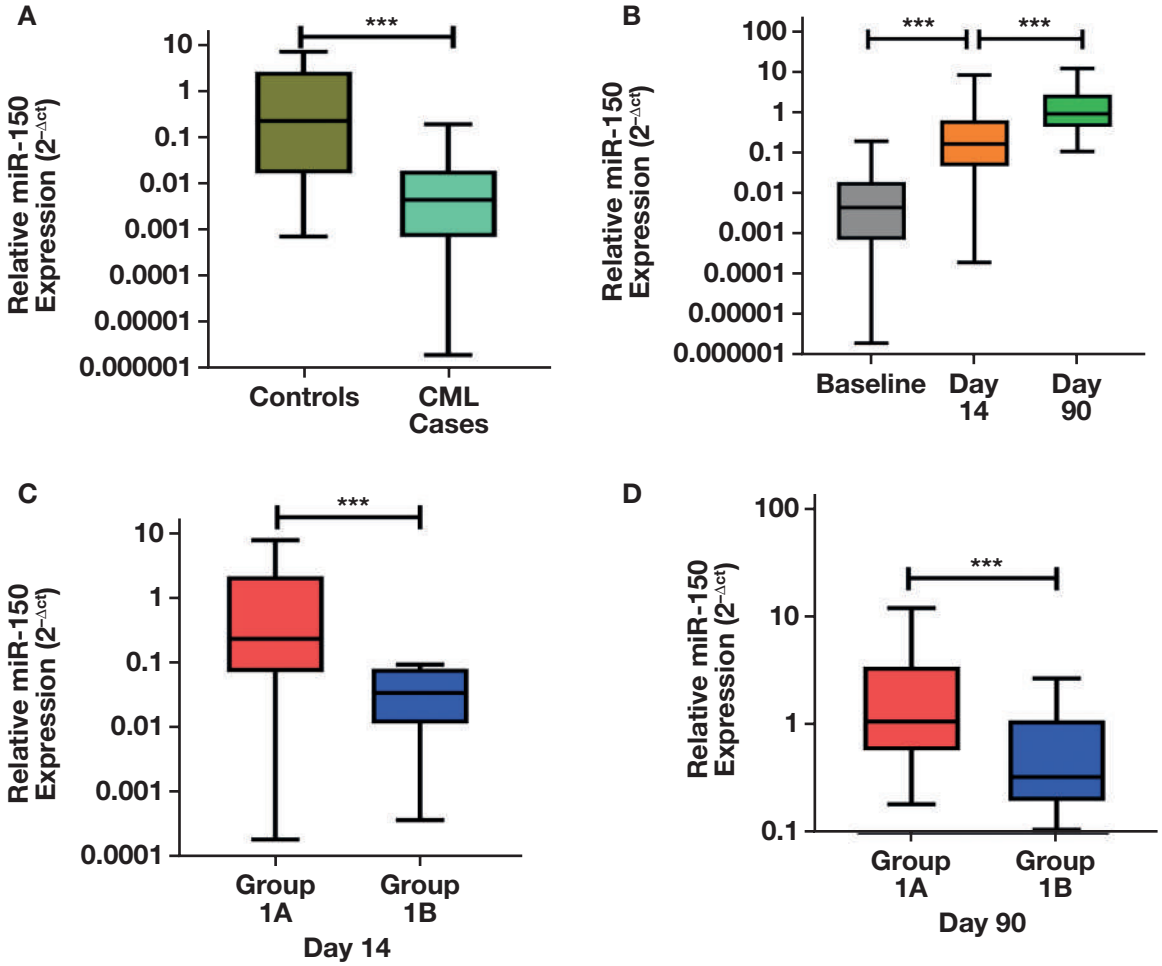

FIGURE 4. ROC curve analysis of miR-150 at day 14 and day 90 of imatinib treatment in patients with CML. CML, chronic myeloid leukemia; miR-150, micro-RNA-150; ROC, receiver operating characteristic.

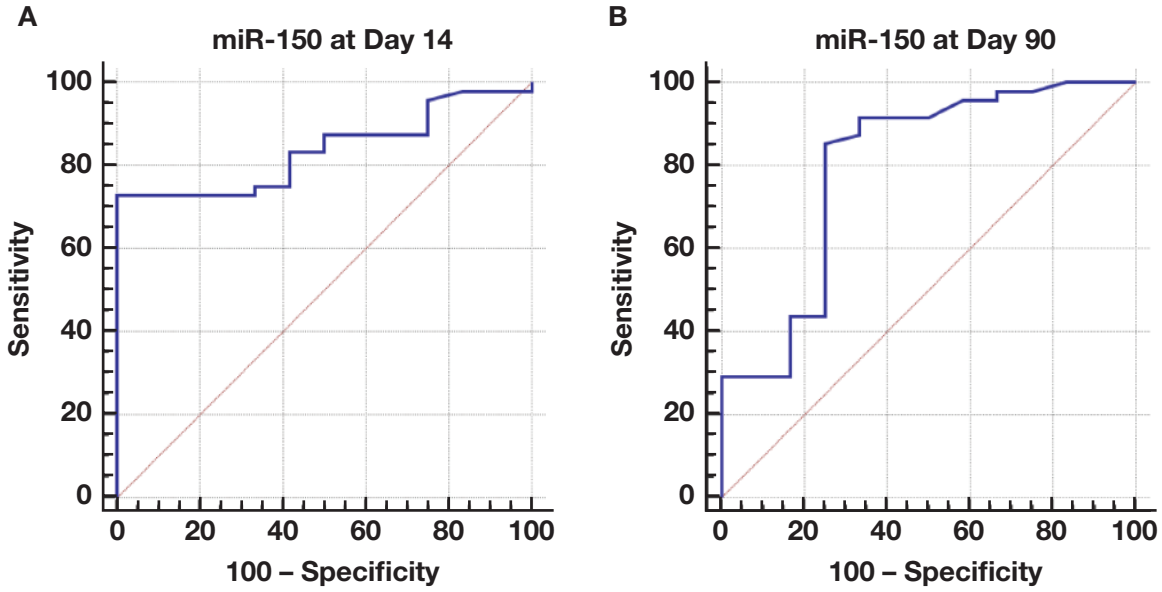

at day 14 (**FIGURE 3C**) and day 90 (**FIGURE 3D**). The miR-150 expression level at day 14 was detected to be a significant predictor of ETR in patients with CML in univariate and in multivariate analysis (OR, 0.0; 95% CI, 0.0–0.924; **TABLE 1**).

The predictive value of miR-150 in the detection of ETR in patients with CML was further evaluated using ROC curve analysis (**FIGURE 4**) and revealed that the area under the curve (AUC) of miR-150 at day 14 was 0.838 (95% CI, 0.720–0.920) with 72.9% sensitivity and 84.2% specificity at a cutoff value >0.088, whereas the AUC of miR-150 at day 90 was 0.799 (95% CI, 0.675–0.891) with 72.9% sensitivity and 75.0% specificity at a cutoff value >0.61.

Discussion

Although CML is characterized by a distinct cytogenetic feature, the underlying molecular mechanisms of its progression remain to be elucidated.[12] The achievement of early molecular response is crucial in predicting the prognosis and determining the treatment plan for patients with CML. In this study, 12 out of 60 patients (20%) who received imatinib therapy failed to achieve ETR. The response rate to imatinib varies greatly among studies. Similar findings to our study were reported by Marin et al[20] in 282 consecutive newly diagnosed patients with chronic-phase CML treated using frontline imatinib; they found that 68 patients (24%) failed to achieve ETR. A similar figure was reported by Hanfstein et al,[21] in a cohort of 1303 patients as part of the German CML IV study, and found that 28% of the patient group had a *BCR-ABL1* transcript level >10%. In addition, Vieira-Mion et al[22] reported that in a study of 1403 patients, 80.8% of patients achieved the optimal response (*BCR-ABL1* < 10%) from 3 to 5 months after beginning imatinib treatment. In contrast, Shao et al,[23] found that 24 out of 40 (60%) patients with CML failed to achieve ETR. In addition, in another study, only 21 out of 70 patients with CML achieved molecular response at or before 18 months of treatment.[24] Moreover, 281 out of 412 patients with CML (68.2%) achieved a <10% *BCR-ABL1* transcript level at 3 months.[25] This discrepancy among studies seems to be caused by differences in sample size and follow-up duration.

Recently, molecular markers have been introduced in the field of cancer diagnosis, prognosis, and precision medicine.[26–29] The miRs have a major role in regulating cellular functions including growth, differentiation, migration, and apoptosis, and they are also involved in cancer progression.[30] The present study aimed to explore the role of circulating miR-150 expression in the treatment outcomes of patients with CML under imatinib therapy. At baseline, patients had significantly lower miR-150 expression in comparison to control subjects. The low or absent expression of miR-150 in patients with CML was previously reported.[12,13,31] Those earlier studies suggested that miR-150 promotes myeloid differentiation and that its low or absent expression may result in blocking myeloid differentiation with subsequent myeloid neoplasm progression such as acute myeloid leukemia and the blastic crisis of CML.[31]

Research has shown that miR-150 mediates myeloid differentiation by several mechanisms. It activates transcription factors, cytokines, and growth factors that are implicated in myeloid differentiation such as C/EBPA, C/EBPE, interleukin 1B, and granulocyte-macrophage colony-stimulating factor.[32] In addition, miR-150 inhibits MYB, an oncogenic transcription factor that blocks myeloid cell differentiation and mediates *BCR-ABL1*-dependent leukemogenesis.[33] Moreover, miR-150 may induce other miRNA expression such as miR-223 to promote myeloid differentiation.[34]

In fact, the role of miR-150 in CML extends beyond the diagnostic implications. It has been suggested that the alteration of miR-150 expression can be used as a treatment approach in CML.[35] Furthermore, miR-150 expression had a significant increase 2 weeks after imatinib treatment in this study. This finding is concordant with Flamant et al,[13] who reported similar observations. Moreover, the present study revealed that miR-150 expression showed sustained elevation at day 90 of imatinib therapy, which is negatively correlated with *BCR-ABL1* transcript levels as reported in Machová Poláková et al.[11]

Interestingly, the present study identified miR-150 expression at 14 days after imatinib treatment as a significant predictor of treatment response in patients with CML. These conclusions are supported by Yurt et al,[14] who reported significantly lower miR-150 expression in their patients who were nonresponsive to imatinib treatment in comparison to their responsive counterparts. We found that measuring miR-150 expression at day 14 of imatinib treatment could be a valuable early predictor of imatinib response in patients with CML with an AUC of 0.838, 72.9% sensitivity, and 84.2% specificity. Notably, our study reports for the first time that the elevated miR-150 expression levels at day 14 are of high predictive value for ETR in patients with CML patients.

The significant elevation of miR-150 after treatment by TKIs is attributed to their inhibition of *c-MYC*. Increased *c-MYC* expression results in genomic instability and promotes error-prone repairs through an augmented expression of the alternative form of the nonhomologous end-joining pathway.[36] More specifically, it has been shown that c-MYC occupies the regulatory regions –11.7 kb and –0.35 kb in the *miR-150* gene. This occupancy is markedly enhanced through *BCR-ABL1* activity, resulting in the downregulation of miR-150 expression in the CD34+ and CD34– cells of patients with CML.[37]

The results of the present study are limited by the relatively small size and short follow-up period. However, this study was conducted at only 1 center. Future multicentric studies with longer follow-up are advocated.

Conclusion

The present study suggests that miR-150 expression at day 14 of imatinib treatment may be a useful predictive candidate of imatinib response in patients with CML.

Acknowledgments

The authors confirm that the data supporting the findings of this study are available within the article. This study was approved by the ethics committee of the Faculty of Medicine, Kafr El-Sheikh University. Informed consent was obtained from all individual participants included in the study.

EMH, NAN, MAE, AEH, DES, and MTA contributed to study designing, retrieving the literature, performing routine and molecular investigations, and analyzing data. AMT contributed to patient selection and follow-up. All authors contributed to writing the original draft, reviewing, and final manuscript approval.

REFERENCES

1. Hoffmann VS, Baccarani M, Hasford J, et al. The EUTOS population-based registry: incidence and clinical characteristics of 2904 CML patients in 20 European countries. *Leukemia.* 2015;29(6):1336–1343.
2. Singh VK, Coumar MS. Chronic myeloid leukemia: existing therapeutic options and strategies to overcome drug resistance. *Mini Rev Med Chem.* 2019;19(4):333–345.
3. Aladağ E, Haznedaroğlu İC. Current perspectives for the treatment of chronic myeloid leukemia. *Turk J Med Sci.* 2019;49(1):1–10.
4. Baccarani M, Rosti G, Soverini S. Chronic myeloid leukemia: the concepts of resistance and persistence and the relationship with the BCR-ABL1 transcript type. *Leukemia.* 2019;33(10):2358–2364.
5. Izzo B, Gottardi EM, Errichiello S, Daraio F, Baratè C, Galimberti S. Monitoring chronic myeloid leukemia: how molecular tools may drive therapeutic approaches. *Front Oncol.* 2019;9:833.
6. Yeh CH, Moles R, Nicot C. Clinical significance of microRNAs in chronic and acute human leukemia. *Mol Cancer.* 2016;15(1):37.
7. Chakraborty C, Sharma AR, Patra BC, Bhattacharya M, Sharma G, Lee SS. MicroRNAs mediated regulation of MAPK signaling pathways in chronic myeloid leukemia. *Oncotarget.* 2016;7(27):42683–42697.
8. Undi RB, Kandi R, Gutti RK. MicroRNAs as haematopoiesis regulators. *Adv Hematol.* 2013;2013:695754.
9. Fang ZH, Wang SL, Zhao JT, et al. miR-150 exerts antileukemia activity in vitro and in vivo through regulating genes in multiple pathways. *Cell Death Dis.* 2016;7(9):e2371.
10. He Y, Jiang X, Chen J. The role of miR-150 in normal and malignant hematopoiesis. *Oncogene.* 2014;33(30):3887–3893.
11. Machová Poláková K, Lopotová T, Klamová H, et al. Expression patterns of microRNAs associated with CML phases and their disease related targets. *Mol Cancer.* 2011;10:41.
12. Zhu X, Lin Z, Du J, Zhou X, Yang L, Liu G. Studies on microRNAs that are correlated with the cancer stem cells in chronic myeloid leukemia. *Mol Cell Biochem.* 2014;390(1-2):75–84.
13. Flamant S, Ritchie W, Guilhot J, et al. Micro-RNA response to imatinib mesylate in patients with chronic myeloid leukemia. *Haematologica.* 2010;95(8):1325–1333.
14. Yurt M, Ayyildiz O, Karakus A, Nursal AF, Isi H. MicroRNAs expression profiles as biomarkers and therapeutic tools in Turkish patients with chronic myeloid leukemia. *Bratisl Lek Listy.* 2020;121(2):159–163.
15. Swerdlow SH, Campo E, Pileri SA, et al. The 2016 revision of the World Health Organization classification of lymphoid neoplasms. *Blood.* 2016;127(20):2375–2390.
16. Sokal JE, Cox EB, Baccarani M, et al. Prognostic discrimination in "good-risk" chronic granulocytic leukemia. *Blood.* 1984;63(4):789–799.
17. Radich JP, Deininger M, Abboud CN, et al. Chronic Myeloid Leukemia, Version 1.2019, NCCN Clinical Practice Guidelines in Oncology. *J Natl Compr Canc Netw.* 2018;16(9):1108–1135. https://www.nccn.org/store/login/login.aspx?ReturnURL=https://www.nccn.org/professionals/physician_gls/pdf/cml.pdf.
18. Schmittgen TD, Livak KJ. Analyzing real-time PCR data by the comparative C(T) method. *Nat Protoc.* 2008;3(6):1101–1108.
19. Hochhaus A, Saussele S, Rosti G, et al.; ESMO Guidelines Committee. Chronic myeloid leukaemia: ESMO clinical practice guidelines for diagnosis, treatment and follow-up. *Ann Oncol.* 2017;28(suppl_4):iv41–iv51.
20. Marin D, Ibrahim AR, Lucas C, et al. Assessment of BCR-ABL1 transcript levels at 3 months is the only requirement for predicting outcome for patients with chronic myeloid leukemia treated with tyrosine kinase inhibitors. *J Clin Oncol.* 2012;30(3):232–238.
21. Hanfstein B, Müller MC, Hehlmann R, et al.; SAKK; German CML Study Group. Early molecular and cytogenetic response is predictive for long-term progression-free and overall survival in chronic myeloid leukemia (CML). *Leukemia.* 2012;26(9):2096–2102.
22. Vieira-Mion AL, Pereira NF, Funke VAM, Pasquini R. Molecular response to imatinib mesylate of Brazilian patients with chronic myeloid leukemia. *Rev Bras Hematol Hemoter.* 2017;39(3):210–215.
23. Shao H, Zeng Z, Cen J, et al. The impact of early molecular response in children and adolescents with chronic myeloid leukemia treated with imatinib: a single-center study from China. *Leuk Lymphoma.* 2018;59(9):2152–2158.

24. Bee PC, Sekaran V, Ng RR, Kweh TY, Gan GG. The predictive value of early molecular response in chronic myeloid leukaemia patients treated with imatinib in a single real-world medical centre in a developing country. *Singapore Med J.* 2017;58(3):150–154.
25. Zhang J, Wang Y, Wang J, et al. Early BCR-ABL1 decline in imatinib-treated patients with chronic myeloid leukemia: results from a multicenter study of the Chinese CML alliance. *Blood Cancer J.* 2018;8(7):61.
26. Abdel Ghafar MT, Gharib F, Abdel-Salam S, et al. Role of serum metadherin mRNA expression in the diagnosis and prediction of survival in patients with colorectal cancer. *Mol Biol Rep.* 2020;47(4):2509–2519.
27. Abdel Ghafar MT, Gharib F, Al-Ashmawy GM, Mariah RA. Serum high-temperature-required protein A2: a potential biomarker for the diagnosis of breast cancer. *Gene Rep.* 2020;20:100706.
28. Abdel Ghafar M, Allam A, Darwish S. Serum HOX transcript antisense RNA expression as a diagnostic marker for chronic myeloid leukemia. *Egypt J Haematol.* 2019;44:91–97.
29. El-Guindy DM, Wasfy RE, Abdel Ghafar MT, Ali DA, Elkady AM. Oct4 expression in gastric carcinoma: association with tumor proliferation, angiogenesis and survival. *J Egypt Natl Canc Inst.* 2019;31(1):3.
30. Baskerville S, Bartel DP. Microarray profiling of microRNAs reveals frequent coexpression with neighboring miRNAs and host genes. *RNA.* 2005;11(3):241–247.
31. Morris VA, Zhang A, Yang T, et al. MicroRNA-150 expression induces myeloid differentiation of human acute leukemia cells and normal hematopoietic progenitors. *PLoS One.* 2013;8(9):e75815.
32. Halene S, Gaines P, Sun H, et al. C/EBPepsilon directs granulocytic-vs-monocytic lineage determination and confers chemotactic function via Hlx. *Exp Hematol.* 2010;38(2):90–103.
33. Lidonnici MR, Corradini F, Waldron T, Bender TP, Calabretta B. Requirement of c-Myb for p210(BCR/ABL)-dependent transformation of hematopoietic progenitors and leukemogenesis. *Blood.* 2008;111(9):4771–4779.
34. Fazi F, Rosa A, Fatica A, et al. A minicircuitry comprised of microRNA-223 and transcription factors NFI-A and C/EBPalpha regulates human granulopoiesis. *Cell.* 2005;123(5):819–831.
35. Biray Avcı Ç, Özcan İ, Balcı T, Özer Ö, Gündüz C. Design of polyethylene glycol-polyethylenimine nanocomplexes as non-viral carriers: mir-150 delivery to chronic myeloid leukemia cells. *Cell Biol Int.* 2013;37(11):1205–1214.
36. Muvarak N, Kelley S, Robert C, et al. c-MYC generates repair errors via increased transcription of alternative-NHEJ factors, LIG3 and PARP1, in tyrosine kinase-activated leukemias. *Mol Cancer Res.* 2015;13(4):699–712.
37. Srutova K, Curik N, Burda P, et al. BCR-ABL1 mediated miR-150 downregulation through MYC contributed to myeloid differentiation block and drug resistance in chronic myeloid leukemia. *Haematologica.* 2018;103(12):2016–2025.

Diagnostic Value of Circular RNA hsa_circ_0002874 Expression in Peripheral Blood of Patients with Gastric Cancer

Xiaoye Sun, MD,[1] Shang Kong, MD,[2] Chen Jiang, MD,[1] Rongrong Jing, PhD,[2] Shaoqing Ju, PhD,[2,] Hui Cong, MD[1,2,*]*

[1]Department of Blood Transfusion, Affiliated Hospital of Nantong University, Nantong, Jiangsu, China; [2]Department of Laboratory Medicine, Affiliated Hospital of Nantong University, Nantong, Jiangsu, China; *To whom correspondence should be addressed. huicjs@163.com

Keywords: hsa_circ_0002874, gastric cancer, qRT-PCR, biomarker, ROC, circular RNA

Abbreviations: GC, gastric cancer; IQR, interquartile range; ROC, receiver operating characteristic; circRNA, circulating RNA; PCR, polymerase chain reaction; RT-qPCR, real-time quantitative polymerase chain reaction; CV, coefficient of variation; AUC, area under the curve.

Laboratory Medicine 2022;53:65–70; https://doi.org/10.1093/labmed/lmab062

ABSTRACT

The purpose of this study was to determine whether circular RNA hsa_circ_0002874 could serve as a novel biomarker for the diagnosis of gastric cancer (GC). The expression level of hsa_circ_0002874 mean (interquartile range [IQR]) in the plasma of patients with GC, patients with benign gastric lesions, and healthy individuals was 3.482 (IQR, 1.524–9.048), 1.261 (IQR, 0.817–2.000), and 1.00 (IQR, 0.726–1.382), respectively, whereas there was no significant difference between the latter 2 groups. The plasma expression level of hsa_circ_0002874 was significantly correlated with tumor stage ($U = 234.0$; $P < .001$) and lymph node metastasis ($U = 240.0$; $P < .001$). The receiver operating characteristic (ROC) curve showed that the sensitivity of the combined determination of hsa_circ_0002874 and the serum markers CEA and CA19-9 was 95.8% in patients with GC compared with that of the healthy group and 93.0% compared with that of patients with benign gastric tumor lesions. The specificity of hsa_circ_0002874 in differentiating GC from benign lesions was 98.3%. The results showed that plasma hsa_circ_0002874 may prove to be a useful biomarker for auxiliary diagnosis, the grading of malignant neoplasms, and the prognostic prediction of GC.

Gastric cancer (GC) is one of the most common malignant tumors. Statistics show that the mortality rate of GC ranks third worldwide, with a tendency to increase gradually yearly. Because of the insidiousness of symptoms in the early stages, most patients with GC are already in an advanced stage at the time of diagnosis[1]; in these patients, the 5-year survival is only 25% to 30%.[2] Therefore, early detection and treatment are primarily important to improve the prognosis of patients with GC. Currently, early screening of GC is mainly through endoscopic examination. But because endoscopy is invasive, it is difficult for it to be generally accepted as a routine screening method. Some serological tumor markers such as CEA and CA19-9 currently used in clinical practice are likely to cause missed detection or misdiagnosis because of insufficient sensitivity and specificity. It is therefore necessary and urgent to find a more sensitive, more specific, and less invasive marker for early diagnosis, prognostic prediction, and therapeutic monitoring of patients with GC.

Circular RNA (circRNA) is a type of new noncoding RNA molecule discovered in recent years that extensively exists in eukaryotic cytoplasm. Most circRNAs are generated from exons without containing the 5' and 3' ends. They are closed in a circular form with stable properties and high conservation and can regulate the expression of target genes through the "sponge effect" of microRNA.[3–5] Studies have shown that circRNA plays a role in many diseases and shows a close association with cancer development and progression. The characteristic properties of circRNA make it a new potential molecular marker for the diagnosis of malignant tumors. However, few studies have reported the use of circRNA as a biomarker for the diagnosis of GC. Research has shown that hsa_circ_0002874, also known as hsa_circ_GLIS3_003, is derived from the *GLIS3* gene, a member of the Gli-like zinc finger protein family. The *GLIS3* gene plays a dual role in organisms, both inhibiting and activating protein transcription. The aim of the present study was to explore the feasibility and clinical value of hsa_circ_0002874 as a new molecular biomarker for the diagnosis of GC by detecting its expression level and analyze its association with malignant behavior in patients with GC.

Materials and Methods

Patients

Plasma specimens were collected from 71 patients (49 male and 22 female; ages 43–86 years) who were pathologically confirmed as having GC and had not received radiochemotherapy before admission to the affiliated hospital of Nantong University (Nantong, China), 59 patients

with benign gastric lesions (19 male and 40 female; ages 43–85 years), and 60 healthy individuals (23 male and 37 female; ages 40–89 years) as the control patients.

In addition, we collected 48 pairs of cancer and para-cancer tissues from patients (36 male and 12 female; ages 44–85 years) who were pathologically confirmed as having GC between January 2018 and November 2019 and had not received any radiochemotherapy or other adjuvant therapies before surgery. Three GC cell strains (HGC-27, BGC-823, and MKN-45) and a normal gastric epithelial cell strain (GES-1) were used in this study.

This research protocol was approved by the Ethics Committee of Nantong University Affiliated Hospital (Nantong University Affiliated Hospital Ethical Approval for Scientific Research number 2016–061). Informed consent was obtained from all participants in the study.

Specimen Collection

Peripheral blood (3–5 mL) was collected from each participant, immediately placed in a tube containing EDTA-K_2, and centrifuged at room temperature and 3000 g for 10 minutes. The plasma (300 μL) in the upper layer was sucked and placed in a 1.5 mL eppendorf tube for RNase inactivation and stored at –80°C for use. Surgically resected GC tissues and gastric mucosa tissues 5 cm from the tumor with a thickness <0.5 cm were placed immediately in 1 mL RNA Fixer solution and stored at –80°C for use.

Expression of Hsa_circ_0002874

Total RNA (10 μL) was extracted and reverse-transcribed. Briefly, total RNA was extracted from the plasma specimens, tissues, and cell strains according to the protocols of the RNA reagent kits. The RNA was reverse-transcribed into cDNA according to the kit instructions under the following conditions: reaction buffer 4 μL, deoxyribonucleotide triphosphate mix (10 mM) 2 μL, random primer 1 μL, RevertAid RT 1 μL, and RiboLock RI 1 μL, then add RNase-free H2O to make up to 20uL with total RNA 500 ng at 42°C for 60 minutes and at 70°C for 5 minutes. The complementary DNA thus obtained was used for the polymerase chain reaction (PCR) assay.

Fluorescence real-time quantitative PCR (RT-qPCR) was as follows: hsa_circ_0002874-F: 5'-AATCCTGGGAAAGGCTTATA-3', hsa_circ_0002874-R: 5'-GTCCGGTGGAGACTCATGCT-3', 18s-F: 5'-CGGCTACCACATCCAAGGAA-3', 18s-R:5'-GCTGGAATTACCGCGGCT-3'. The reaction system was as follows: SYBR (sybr green I nucleic acid gel stain) Green I Master mix (Rox) 10 μL, diethypyrocarbonate 3 μL, forward primer 0.5 μL, reverse primer 0.5 μL, and complementary DNA 6 μL, totaling 20 μL at 95°C for 5 minutes, 95°C for 15 seconds, 58°C for 30 seconds, and 72°C for 30 seconds, totaling 45 cycles. The relative quantity of hsa_circ_0002874 expression was calculated using the $2^{-\Delta\Delta Ct}$ method: ΔΔCt = mean value of study group ($Ct_{hsa\_circ\_0002874}$-Ct_{18s})–mean value of control group ($Ct_{hsa\_circ\_0002874}$-Ct_{18s}). Reagents used in this study included reverse transcription kit (Thermo Fisher), hsa_circRNA_0002874 primer and 18s primer (Shanghai Sangon Biotech).

Detection of Serum CEA and CA19-9

Serum expression levels of CEA and CA19-9 were detected using the ARCHITET I2000 SR (Abbott, Chicago, IL).

Statistical Analysis

Statistical analysis was performed using SPSS 25.0 and GraphPad Prism7. Data for normal distribution were analyzed using the K-S test and were expressed as mean ± standard deviation. Nonnormally distributed data were expressed as the median (IQR). Comparison of 2 independent specimens was performed using the Mann-Whitney *U* test, and the comparison of multiple specimens was performed using the Kruskal-Wallis *H* test. Correlations between variables were analyzed using Spearman correlation analysis. The statistically significant difference was set at P <.05.

Results

Methodological Evaluation of miR-92a-3p in Plasma Exosomes

For better clinical application, we first evaluated the RT-qPCR method, which is generally used to detect hsa_circ_0002874 expression. The hsa_circ_0002874 was constructed, the linearity of which was assessed by using serial 10-fold dilutions of complementary DNA. The R^2 of the hsa_circ_0002874 standard curve was 0.9992, and the regression equation was $Y = -2.942X + 25.598$.

In addition, we evaluated the coefficient of variation (CV) of hsa_circ_0002874 between the intra-assay and the interassay. As expected, the interassay CV and intra-assay CV were <5%. The amplification curve was unimodally specific, meaning that the results were representative (**TABLE 1**).

Expression of Hsa_circ_0002874 in GC Cell Strains, GC Plasma, and Pathologic Tissues

Microassay analysis revealed several differentially expressed circRNAs, among which hsa_circ_0002874 was highly and differentially expressed. The RT-qPCT showed that hsa_circ_0002874 expression in HGC-27, BGC-823, and MKN-45 was significantly different from that in GES-1 expression (P <.05). The expression of hsa_circ_0002874 in MKN-45 was the highest among the 3 GC cell lines (**FIGURE 1A**). The relative expression of hsa_circ_0002874 in the 71 patients with GC, 59 patients with benign lesions, and 60 healthy control patients was 3.482 (IQR, 1.524–9.048), 1.261 (IQR, 0.817–2.000), and 1.00 (IQR, 0.726–1.382) respectively, showing significant differences between the GC group and the benign and healthy groups (both P <.001) and no significant difference between the benign and healthy groups (P =.077; **FIGURE 1B**). The relative expression of hsa_circ_0002874 in the GC and para-GC tu-

TABLE 1. The Intra- and Interassay Repeatability of hsa_circ_0002874 and Reference

	Hsa_circ_0002874	18s[a]
Intra-assay		
Mean ± SD	35.78 ± 0.923	11.94 ± 0.335
CV, %	2.58	2.81
Interassay		
Mean ± SD	36.03 ± 0.537	11.49 ± 0.343
CV, %	1.49	2.99

[a]18S was selected as the internal reference for RT-PCR to remove some systematic errors. 18S is rich in content and stable in any case, so it is less affected by external regulation, and the background is more stable in semi-quantification.
CV, coefficient of variation; SD, standard deviation.

mor tissues was 2.892 (IQR, 1.814–4.808) and 0.977 (IQR, 0.479–2.376), respectively, showing a significant difference between the 2 groups ($P < .001$; **FIGURE 1C**).

Correlations Between Relative hsa_circ_0002874 Expression and Clinical Characteristics of Patients with GC

(1) Analysis of correlations between hsa_circ_0002874 expression and clinicopathological parameters in patients with GC showed that the relative expression of hsa_circ_0002874 in the plasma of the 71 patients with GC was not significantly correlated with sex ($P = .296$), age ($P = .639$), or tumor size ($P = .988$) but was significantly correlated with TNM stage ($P < .001$) and lymph node metastasis ($P < .001$; **TABLE 2**).

(2) Analysis of correlations between hsa_circ_0002874 expression in GC tumor tissues and clinicopathologcial characteristics in the 48 patients with GC showed that the relative expression of hsa_circ_0002874 was not significantly correlated with sex ($P = .153$), age ($P = .131$), or tumor size ($P = .107$) but was significantly correlated with TNM stage ($P = .009$) and lymph node metastasis ($P < .001$; **TABLE 3**).

Correlation Between Relative Plasma hsa_circ_0002874 Expression and CEA and CA19-9 in Patients with GC

The concentration of CEA and CA19-9 in patients with GC, patients with benign gastric lesions, and healthy control patients are shown in **FIGURE 2**. Nonparametric Spearman correlation analysis showed that the relative expression of hsa_circ_0002874 in the plasma of patients with

FIGURE 1. Expression of hsa_circ_0002874 in GC cell strains, plasma, and pathological tissues of patients with GC. A, hsa_circ_0002874 expression in GC cell strains. B, Relative expression of hsa_circ_0002874 in initially diagnosed patients with GC, patients with benign gastric lesions, and healthy control patients. C, Relative expression of hsa_circ_0002874 in GC and para-GC tumor tissues. *P <.05, ***P <.001, ****P <.0001.

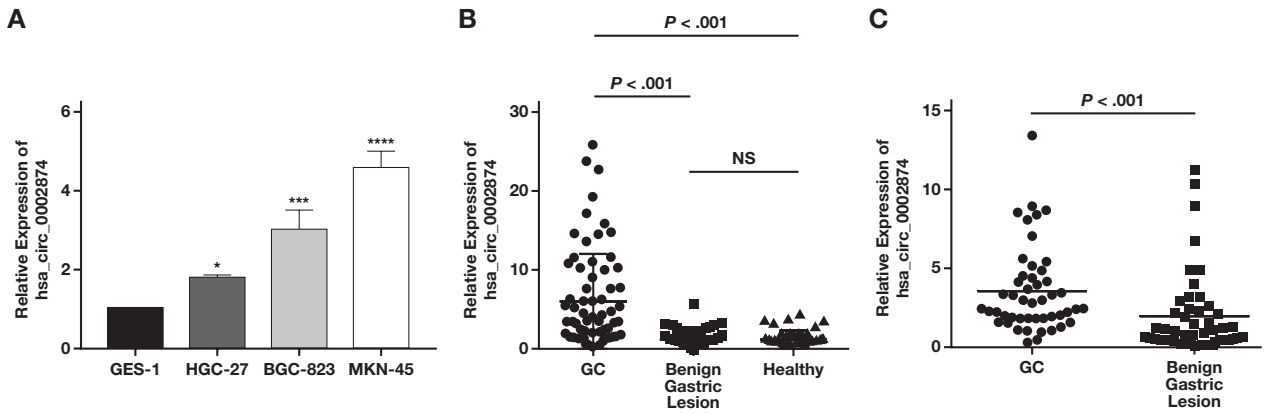

TABLE 2. Correlation Between Relative Expression of Plasma hsa_circ_0002874 and Clinical Characteristics of Patients with GC

Clinicopathological Characteristics	n	Hsa_circ_0002874 Expression, Mean (IQR)	*U* Value	*P* Value
Sex			455.0	.296
M	49	3.681 (1.608–9.517)		
F	22	2.392 (1.454–7.395)		
Age (y)			536.0	.639
≤60	25	2.549 (1.454–10.541)		
>60	46	3.544 (1.566–7.710)		
Size (cm)			376.0	.988
≥5	13	2.549 (1.504–14.103)		
<5	58	3.544 (1.524–8.125)		
Tumor stage			234.0	<.001
I + II	40	1.791 (1.430–3.871)		
III + IV	31	6.255 (3.605–14.470)		
Metastasis			240.0	<.001
Yes	50	5.028 (2.115–10.431)		
No	21	1.524 (0.649–3.117)		

GC, gastric cancer; IQR, interquartile range.

TABLE 3. Correlation Between Relative Expression of hsa_circ_0002874 in GC Tissues and Clinical Characteristics of Patients with GC

Clinical Characteristics	n	Hsa_circ_0002874 Expression, Mean (IQR)	*U* Value	*P* Value
Sex			156.0	.153
M	36	2.344 (1.797–4.117)		
F	12	3.789 (2.059–7.606)		
Age (y)			142.0	.131
≤60	11	3.967 (2.990–5.440)		
>60	37	2.287 (1.799–4.250)		
Size (cm)			203.0	.107
≥5	20	2.166 (1.206–3.927)		
<5	28	3.336 (1.981–4.808)		
TNM stage			151.00	.009
I + II	18	1.970 (1.057–3.359)		
III + IV	30	3.337 (2.089–5.525)		
Metastasis			61.000	<.001
Yes	38	3.164 (1.997–5.237)		
No	10	1.319 (0.850–2.319)		

GC, gastric cancer; IQR, interquartile range.

FIGURE 2. Correlation between the relative expression of plasma hsa_circ_0002874 and CEA and CA19-9 in patients with GC.

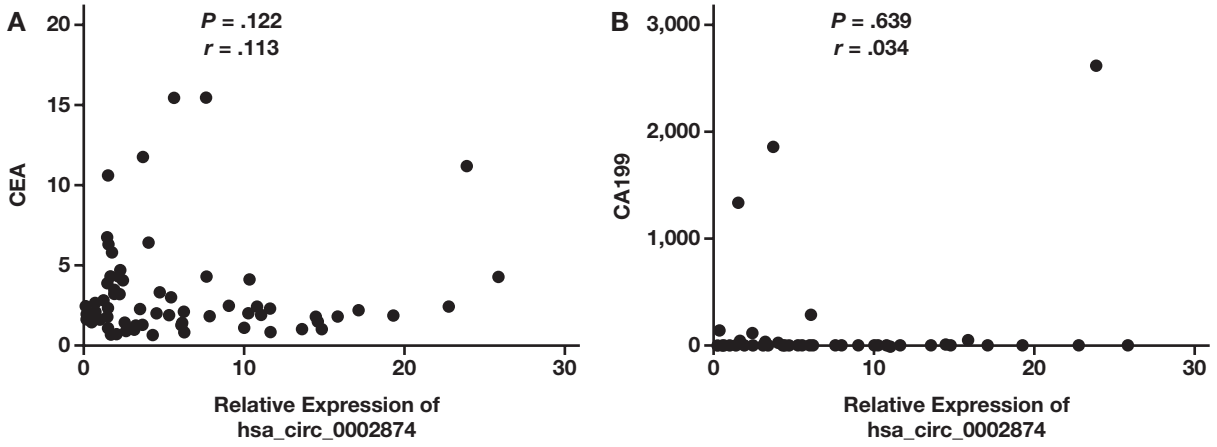

GC was not significantly correlated with CEA (P = .122; r = 0.113) and CA19-9 (P = .639; r = −0.034).

ROC Curve Analysis

The ROC curve analysis of the relative expression of hsa_circ_0002874 and the concentration of CEA and CA19-9 in the plasma of patients with GC vs healthy control patients showed that the area under the curve (AUC) of the relative expression of hsa-circ-0002874 in patients with GC was 0.836 (IQR, 0.764–0.908), using 1.402 as the cutoff value; 0.686 (IQR, 0.595–0.777) for CEA, using 1.850 ng/mL as the cutoff value; and 0.537 (IQR, 0.437–0.636) for CA19-9, using 6.15 U/mL as the cutoff value. These results indicate that the diagnostic value of hsa-circ-0002874 was the highest in the hsa-circ-0002874, CEA and CA19-9.

The ROC curve analysis of the relative expression of hsa_circ_0002874 and the content of CEA and CA19-9 in the plasma of patients with GC vs patients with benign gastric lesions showed that the AUC of the relative expression of hsa-circ-0002874 in patients with GC was 0.792 (IQR, 0.714–0.870), using 3.373 as the cutoff value; 0.620 (IQR, 0.524–0.717) for CEA, using 8.300 U/mL as the cutoff value; and 0.572 (IQR, 0.474–0.670) for CA19-9, using 22.4 U/mL as the cutoff value. These results indicate that the diagnostic efficacy of hsa-circ-0002874 was superior to that of the other 2 (**FIGURES 3** and **4**).

Diagnostic Efficacy of Plasma Hsa_circ_0002874, CEA, or CA19-9 Alone and in Combination

Analysis of the sensitivity, specificity, accuracy, positive predictive value, and negative predictive value of hsa_circ_0002874, CEA, or CA19-9 both alone and in combination showed that the sensitivity of hsa_circ_0002874 in differentiating the healthy control group was 87.3%, which was higher than that of CEA and CA19-9. In addition, the sensitivity of two (CEA + CA19-9, hsa_circ_0002874 + CEA or hsa_circ_0002874 + CA19-9) and three-combination (hsa_circ_0002874 + CEA + CA19-9) was higher than either of the three indices alone, and when the 3 indices were detected in combination, the sensitivity was 95.8%. The diag-

FIGURE 3. ROC curves differentiating the healthy control group.

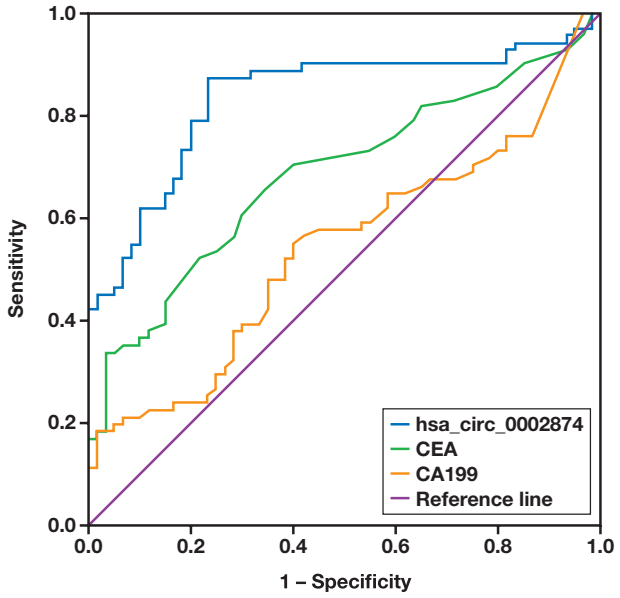

FIGURE 4. ROC curves differentiating the benign gastric lesion group.

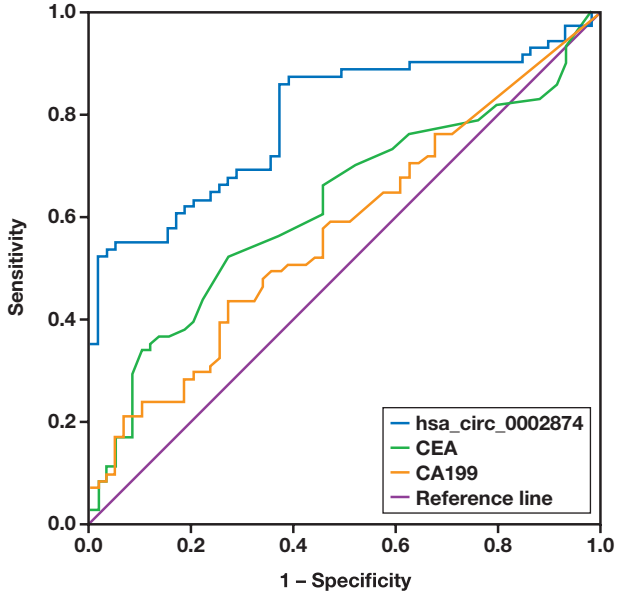

nostic efficacy of two- and three-combination in differentiating patients with benign gastric lesions from the other 2 patient groups was higher than that of either of the three alone, and three-combination offered the highest value (93.0%). The specificity of hsa_circ_0002874 was high as 98.3% (**TABLE 4** and **TABLE 5**).

Discussion

Early diagnosis and treatment are extremely important to improve the prognosis of patients with GC. Gastroscopy is one of the common methods for the clinical screening of GC, but its application is limited by invasiveness.[6] The detection of biomarkers in peripheral blood is less invasive, more convenient, and less expensive, but its clinical value is mainly reflected in monitoring therapeutic efficacy rather than in diagnosis.[7] Cancer diagnosis and classification have entered a molecular era.[8,9] Most recent studies have reported the participation of circRNA and other noncoding RNAs as oncogenes or tumor suppressor genes in the development and progression of cancer and that they are promising as tools for the diagnosis and prognostic prediction of tumors.[10,11]

In the present study, we used microarray screening to identify differentially expressed circRNAs in GC tissues and found that hsa_circ_0002874 was most differentially expressed in GC tissues as compared with that in normal tissues. There is no study reporting the correlation between hsa_circ_0002874 expression and tumors. In addition, we found that hsa_circ_0002874 was highly expressed in the GC cell strains HGC-27, BGC-823, and MKN-45. Subsequently, we detected the relative expression of hsa_circ_0002874 in the plasma of 71 patients with GC, 59 patients with benign gastric lesions, and 60 healthy patients and found that the expression level of hsa_circ_000287 in the plasma of patients with GC was significantly higher than that in the other two groups. In addition, we detected the relative expression of hsa_circ_0002874 in 48 pairs of GC and para-GC tissues in patients who were confirmed as having GC by the department of pathology of our hospital and found that the relative expression of hsa_circ_0002874 in GC tissues was significantly higher than that in para-GC normal tissues.

Furthermore, we grouped the patients with GC and analyzed the correlation between the relative expression of plasma hsa_circ_0002874 and their clinicopathological characteristics. The results showed that the relative expression of hsa_circ_0002874 in plasma was not correlated with sex, age, or tumor size but was significantly correlated with TNM stage and lymph node metastasis. In addition, the later the TNM stage the higher the expression level of hsa_circ_0002874 in plasma. The lack of correlation between tumor size and plasma hsa_circ_0002874 level may be related to the small sample size, pathological grossing error, or

TABLE 4. Diagnostic Efficacy of Plasma Hsa_circ_0002874, CEA, and CA19-9 in Differentiating Healthy Control Patients

Molecular Markers	Sensitivity (%)	Specificity (%)	Accuracy (%)	PPV (%)	NPV (%)
hsa_circ_0002874	87.3 (62/71)	76.7 (46/60)	82.4 (108/131)	81.6 (62/76)	83.6 (46/55)
CEA	66.2 (47/71)	65.0 (39/60)	65.6 (86/131)	69.1 (47/68)	61.9 (39/63)
CA19-9	18.3 (13/71)	96.7 (58/60)	54.2 (71/131)	86.7 (13/15)	50.0 (58/116)
CEA + CA19-9	71.8 (51/71)	63.3 (38/60)	67.9 (89/131)	69.9 (51/73)	65.5 (38/58)
hsa_circ_0002874 + CEA	95.8 (68/71)	45.0 (27/60)	72.5 (95/131)	67.3 (68/101)	90.0 (27/30)
hsa_circ_0002874 + CA19-9	88.7 (63/71)	73.3 (44/60)	81.7 (107/131)	79.7 (63/79)	84.6 (44/52)
hsa_circ_0002874 + CEA + CA19-9	95.8 (68/71)	43.3 (26/60)	71.8 (94/131)	66.7 (68/102)	89.7 (26/29)

NPV, negative predictive value; PPV, positive predictive value.

TABLE 5. Diagnostic Efficacy of Plasma Hsa_circ_0002874, CEA, and CA19-9 in Differentiating Benign Gastric Lesion Group

Molecular Markers	Sensitivity (%)	Specificity (%)	Accuracy (%)	PPV (%)	NPV (%)
hsa_circ_0002874	52.1 (37/71)	98.3 (58/59)	73.1 (95/130)	97.4 (37/38)	63.0 (58/92)
CEA	52.1 (37/71)	72.9 (43/59)	61.5 (80/130)	69.8 (37/53)	55.8 (43/77)
CA19-9	43.7 (31/71)	74.6 (44/59)	57.7 (75/130)	67.4 (31/46)	52.4 (44/84)
CEA + CA19-9	71.8 (51/71)	54.2 (32/59)	63.8 (83/130)	65.4 (51/78)	61.5 (32/52)
hsa_circ_0002874 +CEA	80.3 (57/71)	71.2 (42/59)	76.2 (99/130)	77.0 (57/74)	75.0 (42/56)
hsa_circ_0002874 +CA19-9	77.5 (55/71)	72.9 (43/59)	75.4 (98/130)	77.5 (55/71)	72.9 (43/59)
hsa_circ_0002874 +CEA + CA19-9	93.0 (66/71)	52.5 (31/59)	74.6 (97/130)	70.2 (66/94)	86.1 (31/36)

NPV, negative predictive value; PPV, positive predictive value.

size by imaging only. Similarly, we analyzed the correlation between the relative expression of hsa_circ_0002874 in the GC tissue of the patients from whom the 48 pairs of GC and para-GC tissues were collected and their clinicopathological characteristics. The results were the same as those obtained from the plasma. All these results clearly show the potential of using the plasma level of hsa_circ_0002874 expression as a molecular marker of GC tumors.

In addition, in this study, we found that there was no statistically significant difference in the plasma hsa_circ_0002874 between men and women but that the median of men was higher than that of women. In future studies, we will further expand the sample size for further study.

The ROC curve analysis differentiating the healthy control group showed that the AUC of hsa_circ_0002874 was significantly higher than that of CEA and CA19-9, and the sensitivity was higher than that of CEA and CA19-9. In addition, the combination of these 3 factors offered the highest sensitivity (95.8%). The specificity of hsa_circ_0002874 reached 98.3%, which was higher than that of CEA and CA19-9.

Conclusion

In summary, the detection of the relative expression of hsa_circ_0002874 in plasma may prove to be a new less invasive and traumatic biomolecular marker for the diagnosis of GC. The action mechanism of hsa_circ_0002874 as a brand-new circRNA in tumors is not clear, nor is there a study reporting its association with GC. In our ongoing study, we plan to further confirm the application value of hsa_circ_0002874 in GC in larger patient samples by focusing on seeking target mRNAs and signaling pathways of hsa_circ_0002874 and analyzing its action mechanism in GC to provide evidence-based clues for finding new therapeutic targets of GC.

Acknowledgments

The National Natural Science Foundation of China (program numbers 81271920, 81871720), the Jiangsu Provincial Funds for Six Categories of Top Talents (program number WS-066), the Research Project of the Jiangsu Provincial Health and Family Planning Commission (program number H201526), and the Nantong Technology Project (numbers MS12017008-1, MS12020007). We have declared that no competing interests exist.

REFERENCES

1. Bray F, Ferlay J, Soerjomataram I, Siegel RL, Torre LA, Jemal A. Global cancer statistics 2018: GLOBOCAN estimates of incidence and mortality worldwide for 36 cancers in 185 countries. *CA Cancer J Clin.* 2018;68(6):394–424.
2. Allemani C, Weir HK, Carreira H, et al. Global surveillance of cancer survival 1995–2009: analysis of individual data for 25,676,887 patients from 279 population-based registries in 67 countries (CONCORD-2). *Lancet.* 2015;385(9972):977–1010.
3. Qu S, Zhong Y, Shang R, et al. The emerging landscape of circular RNA in life processes. *RNA Biol.* 2017;14(8):992–999.
4. Hsiao KY, Sun HS, Tsai SJ. Circular RNA—new member of noncoding RNA with novel functions. *Exp Biol Med.* 2017;242(11):1136–1141.
5. Lacazette É, Diallo LH, Tatin F, Garmy-Susini B, Prats AC. Do circular RNAs play tricks on us? *Med Sci.* 2020;36(1):38–43.
6. Badurdeen DS, Kumbhari V. Endoscopic sleeve gastroplasty and its application to China. *J Dig Dis.* 2017;18(10):551–555.
7. Shen M, Wang H, Wei K, Zhang J, You C. Five common tumor biomarkers and CEA for diagnosing early gastric cancer: a protocol for a network meta-analysis of diagnostic test accuracy. *Medicine.* 2018;97(19):e0577.
8. Anderson KJ, Cormier RT, Scott PM. Role of ion channels in gastrointestinal cancer. *World J Gastroenterol.* 2019;25(38):5732–5772.
9. Wang Y, Guan J, Wang Y. Could microRNA be used as a diagnostic tool for lung cancer? *J Cell Biochem.* 2019;120(11):18937–18945.
10. Zhang HD, Jiang LH, Sun DW, Hou JC, Ji ZL. CircRNA: a novel type of biomarker for cancer. *Breast Cancer.* 2018;25(1):1–7.
11. Kristensen LS, Hansen TB, Venø MT, Kjems J. Circular RNAs in cancer: opportunities and challenges in the field. *Oncogene.* 2018;37(5):555–565.

Clinical Value of Pepsinogen in the Screening, Prevention, and Diagnosis of Gastric Cancer

Xiao-Lei Han, MM,[1,2,†] Chang-Lin Yi, MBBS,[3] Jin-Dan Ma, MD,[1] Yanhong He, MBBS,[1] La-Mei Wu, MM,[1] Yun-Feng Wang, MM,[4] Hui-Jian Yang, MM,[5] Dong-Yu Liang, MM,[6] Jin-Fang Shi, MD[2,]*

[1]Department of Clinical Laboratory, Anting Hospital, Jiading District, Shanghai, China; [2]Department of Clinical Laboratory, The First Affiliated Hospital of Soochow University, Suzhou, China; [3]Department of Clinical Laboratory, Ruijin Hospital Affiliated to Shanghai Jiao Tong University, Shanghai, China; [4]Digestive Internal Medicine, Kunshan Branch of Shanghai Cancer Hospital, Shanghai, China; [5]Department of Clinical Laboratory, Dongfang Hospital affiliated to Tongji University, Shanghai, China; [6]Department of Clinical Laboratory, Jiading District Central Hospital Affiliated Shanghai University of Medicine & Health Sciences, Shanghai, China; *To whom correspondence should be addressed. 344783222@qq.com
[†]First author (mali0105@163.com)

Keywords: gastric cancer, screening, prevention, pepsinogen, diagnosis, clinical value

Laboratory Medicine 2022;53:71–77; https://doi.org/10.1093/labmed/lmab035

ABSTRACT

Objectives: To compare the levels of serum pepsinogen (PG) in patients with gastric cancer (GC), patients with atrophic gastritis (AG), and healthy donors. Also, we explored the clinical value of PG detection for the diagnosis and treatment of GC.

Methods: The PG level in peripheral blood from patients and heathy donors was determined using an Abbott automatic chemiluminescence instrument. The study included 117 patients with GC confirmed by gastroscopy and histopathology, of whom 13 patients had cancer at stage I, 47 at stage II, 41 at stage III, and 16 at stage IV. The AG group included 122 patients, and the control group had 120 healthy donors. The relationship between serum PG levels and the occurrence and development of GC, as well as the evaluation of the clinical value of diagnostic tests based on serum PG detection, were investigated by receiver operating characteristic (ROC) curve analyses.

Results: Pepsinogen I (PGI) levels gradually decreased from the control group, the AG group, and the GC group.

PGI exhibited high diagnostic value for GC (area under the curve [AUC], 0.834; cutoff, 51.2 ng/mL, sensitivity, 81.7%; specificity, 68.4%), PGII (AUC, 0.587; cutoff value, 13.05 ng/mL; sensitivity, 65.8%; specificity, 53.8%), and PGR (AUC, 0.752; cutoff, 5.65; sensitivity, 54.2%; specificity, 87.2%). The occurrence of GC was negatively correlated with serum levels of PGI (B = –0.054; OR = 0.947; 95% confidence interval [CI], 0.925–0.970; P <.001) and PGR (B = –0.420; OR = 0.657; 95% CI, 0.499–0.864; P = .003).

Conclusions: The combined detection of PGI, PGII, and PGR has important clinical value for the screening, prevention, and diagnosis of GC and could allow for earlier detection, diagnosis, and treatment of GC.

Gastric cancer (GC) has a high incidence in China. Patients with GC tend to be young; the incidence of GC is typically due to stress, diet, and *Helicobacter pylori* (HP) infection. Reducing the incidence of and mortality from GC is a major public health issue; early diagnosis and treatment remain the best strategies.[1,2] Identification of new diagnostic markers that can rapidly translate into clinical applications and meet the needs for diagnosis and treatment has become a highly dynamic and cutting-edge field in biomedical sciences.

Many studies aim to provide a simple, sensitive, and specific method for the early diagnosis of GC. To date, a range of tumor-related factors have been adopted in clinical practice and have become important assets to tumor diagnosis and treatment. However, their sensitivity and specificity have not reached sufficient reliability.[3–5]

Pepsinogen (PG), an aspartic protein enzyme secreted by gastric mucosa cells, is an inactive precursor of pepsin in gastric juice. It is composed of 375 amino acids, has a molecular weight of approximately 42 kDa, and can be divided into 2 subgroups according to differences in biochemical and immune characteristics: PGI (groups 1–5) and PGII (groups 6 and 7). Gene expression sites of PGI and PGII are different, located on chromosomes 11 and 6, respectively.

After synthesis, PG is primarily released into the gastric cavity, with a small proportion entering the blood circulation through the capillary of gastric mucosa.[6,7] PG can reflect the function and state of the gastric mucosa and is closely related to gastric lesions. Xingjie S et al[8] studied the serum PG content of patients with GC before and after endoscopic treatment and found that PG content after treatment was higher than before the operation. Chunchun C et al[9] reported that the serum PG content of patients with gastric ulcers was relatively high.

Serological testing of PG has the advantages of being noninvasive and inexpensive, allowing for convenient and dynamic monitoring, and being well accepted by the patients. It also has cost-effectiveness compatible with large-scale screening in areas with high incidence of atrophic gastritis (AG) and GC.[10] To assess the clinical value of tests based on serum PG measurement, we investigated the diagnostic accuracy of these tests for GC diagnosis, the relationship between serum PG levels and the occurrence and development of GC, and the feasibility of implementing a dynamic detection to perform serological monitoring.

Using the pathological examination of gastric mucosal biopsy as a diagnostic reference standard, we compared PG levels in healthy donors and patients with precancerous lesions or GC and explored the relationship between serum PG levels and the occurrence and development of GC. Although previous publications have reported the clinical value of serum PG measurement, most studies were single-centered and lacked validation. Therefore, we conducted a multicenter study to provide a stronger reference for clinical diagnosis and treatment.

Materials and Methods

Inclusion Criteria

Patients with GC were diagnosed by combining clinical symptoms, endoscopy, and histopathology. A specimen of the cancer tissue and its surrounding tissues were taken with forceps and stained with hematoxylin-eosin (H&E), observed under a microscope, and diagnosed according to the morphology and structure of tissues and cells (loss of polarity, disordered arrangement, nuclear atypia, increased nucleoplasmic ratio, and condensed chromatin). The diagnosis of GC, AG, and other related diseases met the consensus for pathological diagnosis of chronic gastritis and epithelial tumor gastric mucosa biopsy.[11–13]

No patient experienced serious disease such as liver or kidney failure, other tumors, or had a history of chemotherapy or gastrointestinal surgery, radical treatment of HP, pernicious anemia, intake of drugs acting on the digestive system, or anticancer drugs during the 2 weeks preceding the test.[14] All of the procedures complied with medical ethics requirements. For healthy donors, routine blood tests and liver and kidney function were normal (test results were within the normal ranges: total protein [TP], 65–85 g/L; alanine aminotransferase [ALT], 8–40 u/L; aspartate aminotransferase (AST), 15–35 u/L; total bilirubin [TBIL], 3.5–19 μmol/L; creatinine [CREA], 60–80 μmol/L; uric acid [UA], 202–339 μmol/L; blood urea nitrogen [BUN], 3.0–8.2 mmol/L). There were no space-occupying lesions in any organ, liver, kidney, or digestive tract diseases.

Tumor-node metastasis (TNM) staging of patients with GS was divided into 4 groups according to the latest cancer-staging standard of the American Joint Committee on Cancer (stage I group, stage II group, stage III group, and stage IV group).[15,16] On gastroscopy AG showed a pale mucosa, vascular permeability, small folds or rough surface, erythema, and mucus. Pathological examination showed gland atrophy and hyperplasia. Combined symptoms, such as gastric distension and anemia, completed the diagnosis.[17,18]

Cases and Grouping

In total, 117 patients with GC confirmed by gastroscopy and pathological examination between February 2017 and October 2018 were selected from the Anting Hospital of Shanghai, Ruijin Hospital of Shanghai, The First Affiliated Hospital of Suzhou University, and the Kunshan Branch of Shanghai Cancer Hospital. The GC group included 59 men and 58 women aged 32 to 81 years with a median age of 64 years. Amongst these patients, 13 had GC stage I, 47 patients had stage II, 41 patients had stage III, and 16 patients had stage IV. During the same period, 120 donors (including 60 men and 60 women; age, 24–72 years; median age, 47 years) with normal physical examination indices were enrolled in the healthy control group. There were no significant differences in age and sex composition of the groups ($P > .05$).

Equipment and Methods

The tests were run on an Abbott ARCHITECT i-2000sr automatic chemiluminescence immunoassay system (AbbVie Inc.) that had passed performance verification. The reagents were provided in the kit associated with the instrument. The ARCHITECT Pepsinogen assay is a 2-step immunoassay for the quantitative determination of PG in human serum using chemiluminescent microparticle immunoassay (CMIA) technology with flexible assay protocols, referred to as Chemiflex. In the first step, specimen, assay-specific diluent and antihuman PG antibody-coated paramagnetic microparticles are combined. PG present in the specimen binds to the antihuman PG antibody-coated microparticles. After washing, anti–human PG antibody-acridinium–labeled conjugate is added in the second step. Following another wash step, pretrigger and trigger solutions are added to the reaction mixture. The resulting chemiluminescent reaction is measured as relative light units (RLUs).

A direct relationship exists between the amount of PG in the specimen and the RLUs detected by the ARCHITECT i optical system. The concentration of PG in the specimen is determined using a previously generated ARCHITECT pepsinogen-calibration curve. Interlaboratory quality assessment and indoor quality control were conducted, to ensure the results were controlled. The reportable range was as follows: PGI, 0 to 1000 ng/mL; PGII, 0 to 500 ng/mL. The uncertainty of calibration is 1.99 when PGI is between 0 and 70. When PGII is between 0 and 5, the uncertainty of calibration is 0.13.

The batch numbers of the PGI kits were 73266LI00 and 80439LI00, with the respective expiration dates as April 12, 2018, and January 12, 2019. The batch numbers of the PGII kits were 73371LI00 and 79586LI00, with the respective expiration dates of April 17, 2018 and December 22, 2018.

Fasting venous blood was collected using disposable evacuated blood-collection tubes (BD vacuum red cap [Becton, Dickinson and Company]), and centrifuged at 2664*g* for 10 minutes. After centrifugation, the serum was collected and stored at −20°C for later use. Hemolysis, lipemic, and other specimens that may affect the results were excluded to eliminate the influence of interfering substances such as bilirubin, hemoglobin, albumin, and triglycerides. Before testing, the specimens were allowed to reach room temperature and centrifuged at 2664*g* for 10 minutes. Serum PGI and PGII concentrations were determined with an Abbott ARCHITECT i-2000sr automatic chemiluminescence analyzer, and the PGI/PGII ratio (PGR) was calculated. Results were available within 2 hours.

Statistical Analysis

SPSS statistical software, version 21.0, was used to analyze the results. Serum PGI and PGII levels were expressed as mean (SD). The Student *t* test was used for comparison between 2 groups with normal

distributions, and ANOVA was used for comparison between multiple groups. Bivariate correlation analysis was conducted between the 2 variables. The data were compared by X^2 testing. P <.05 was considered statistically significant. The diagnostic efficacy of PG was evaluated by receiver operating characteristic (ROC) curve.

Results

Serum PGI, PGII, and PGR Levels

Serum PGI and PGII levels in the specimens from 120 healthy donors, 122 patients with AG, and 117 patients with GC were determined, and the PGRs were calculated. Levels from the AG and GC groups were compared with levels from the control group, as well as to each other (**TABLE 1**, **FIGURE 1** and **FIGURE 2**).

As shown in **TABLE 1**, PGI levels between the AG and control groups were significantly different (P = .003). Although the difference in PGII level was not statistically significant between the 2 groups (P = .21), PGR was significantly lower in the AG group (P = .005). Similarly, PGI levels and PGR were significantly lower in the GC, compared with the control group (P <.001) where the PGII levels were not significantly different between the 2 groups (P = .07). Comparison between the GC and AG groups showed significant differences in PGI levels and PGR (P <.001), but no differences were observed in PGII levels (P = .46).

As shown in **FIGURE 1**, levels of PGI and PGII and PGR decreased gradually. The highest values were in the control group, intermediate values in the AG group, and lowest values in the GC group. As depicted in **FIGURE 2**, PGI levels and PGR showed a decreasing trend from the control group to the AG group to the GC group, with no significant difference in PGII levels across the 3 groups.

ROC Curve Evaluating the Diagnostic Efficacy of PG Measurement in GC

Using pathological diagnoses as the most reliable reference standard, we conducted a comparative analysis between the GC and the control groups and created the corresponding ROC curves (**FIGURE 3**). The area under the curve (AUC) was the largest for PGI levels (0.834), followed by PGR (0.752), and PGII levels (0.587), suggesting that serum PGI level and PGR have high diagnostic value for GC detection (**FIGURE 3** and **TABLE 2**).

The point of an ROC curve closest to the top left corner represents the optimal cutoff value for the diagnosis of GC based on serum PG level. The cutoff values obtained with this method for the diagnosis of GC are shown in **TABLE 3**.

The cutoff values of PGI, PGII, and PGR were 51.2 ng/mL, 13.05 ng/mL, and 5.65, respectively. These corresponded to detection sensitivities and specificities of 81.7% and 65.8% for PGI levels, 54.2% and 68.4% for PGII levels, and 53.8% and 87.2% for PGR, demonstrating the clinical value of PG for the diagnosis of GC.

To improve the sensitivity and specificity of the test, we performed parallel and serial multiple judging. With the parallel method, multiple results are run at the same time. If a specimen scores positive in 1 result, it is considered positive. This method improves the sensitivity of the diagnostic test. Conversely, serial judging consists in performing multiple results successively. Only the cases repeatedly positive are considered true positives. This method improves the specificity of the diagnosis. The results of these combined approaches are shown in **TABLE 4**.

When PGI and PGR were combined to detect GC, the sensitivity of parallel judgment was significantly higher than that of serial judgement, and the number of false negatives was reduced. Conversely, the specificity was higher with serial judgements.

Correlation Between GC and Serum PGI and PGR Levels

To further evaluate the value of PG for the diagnosis of GC, we set the control group as the reference. We also used serum PGI and PGR levels as variables for logistic regression analysis (**TABLE 5**).

Discussion

In the early stages, GCs are easy to miss because they do not manifest any obvious symptoms or because symptoms are nonspecific (upper abdominal discomfort and fever) and similarly found in other chronic diseases such as gastritis and gastric ulcers. Therefore, the discovery of highly sensitive and specific screening methods is crucial to improving the early diagnosis of and remission in patients with GC.[19,20] Although endoscopic biopsy is regarded as the criterion standard, it is not suitable for screening and early diagnosis because of its low sensitivity and the possible occurrence of trauma and complications such as pneumothorax or cancer-cell proliferation and transplantation. Because of these associated risks, patients tend to avoid this procedure, an attitude that affects the diagnosis and treatment of the disease.[21–24]

Serological examination is not only convenient but also noninvasive and could provide early warning of tumor occurrence. Still, there is still not enough positive evidence to prove that PG can be used for mass censuses.[11] However, screening for high-risk individuals can not only overcome the shortcomings of pathological diagnosis such as trauma but can also detect lesions early, which is conducive to diagnosis. In 2009, the Chinese Technical Plan for Cancer Screening, Early Diagnosis and Treatment, issued by the Bureau of Disease Control and Prevention of the Ministry of Health of the People's Republic of China, recommended the use of PG serological tests as a primary screening method in GC.[25,26]

By comparing the levels of serum PGI and PGII and PGR from 117 patients with GC, 122 patients with AG, and 120 healthy donors, we found that serum PGI level and PGR in the AG group were significantly lower than in the control group (P <.01), whereas there was no difference in PGII level between these 2 groups (P> .05). Similarly, comparison between the GC and the AG groups showed a significant difference in serum PGI level and PGR (P <.01), but no difference in PGII level (P = .46). The differences in serum PGI level and PGR between the GC and the control groups were also statistically significant (P <.01), contrary to the difference in serum PGII level (P = .07).

The decrease in serum PGI levels in AG and GC may be explained by long-term atrophy or damage of the gastric glands, resulting in decreased number and quality of mucosal cells secreting PGI. Another explanation could be that damaged glandular cells lead to decreased gastric-acid secretion, resulting in decreased serum PGI.

In contrast, PGII is more broadly secreted by different gastric areas, including the main cells of the fundus gland, the mucous neck cells,

TABLE 1. Serum Concentrations of PGI, PGII, and PGR in Control, AG, and GC Groups

Group	Cases, no.	Mean (SD)		
		PGI (ng/mL)	PGII (ng/mL)	PGR
Healthy control	120	89.24 (39.42)	17.64 (11.27)	6.03 (2.59)
AG	122	75.40 (32.79)[a]	15.84 (9.02)	5.25 (1.86)[a]
GC	117	47.74 (20.18)[a,b]	14.87 (10.99)	3.85 (1.70)[a,b]

PG, pepsinogen; PGR, pepsinogen I/II ratio; AG, atrophic gastritis; GC, gastric cancer.
[a]*Comparison with the healthy control group;* P *<.01.*
[b]*Comparison with AG group;* P *<.01.*

FIGURE 1. Histogram showing the levels of serum pepsinogen (PG)I, PGII, and pepsinogen I/II ratio (PGR) in the healthy control, atrophic gastritis (AG), and gastric cancer (GC) groups.

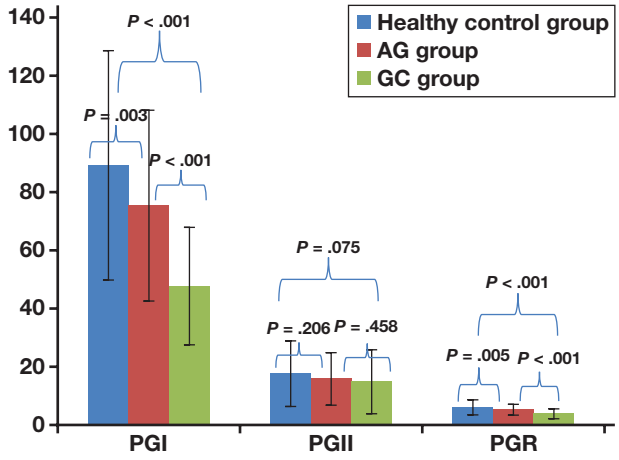

FIGURE 2. Scatterplot showing serum levels of pepsinogen (PG)I and PGII, and pepsinogen I/II ratio (PGR) in the control, atrophic gastritis (AG), and gastric cancer (GC) groups.

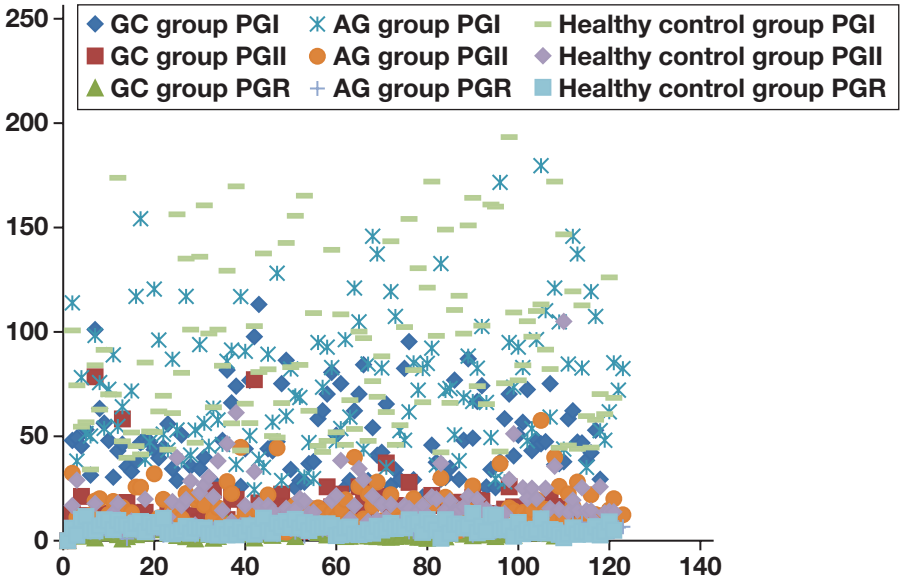

the mucous cells of the cardiac and pyloric glands, and the upper duodenum. The secretion of PGII is associated with atrophy of the gastric basal-gland duct, metaplasia of the gastric upper dermis or the pseudopyloric gland, and hyperplasia. Local lesions or pathologic magnification caused by single etiologies do not significantly modify the level of secreted PGII. Thus, although changes in PGII levels in GC are

FIGURE 3. Receiver operating characteristic (ROC) curves for the evaluation of gastric cancer (GC) diagnosis based on measurement of serum pepsinogen (PG) concentration.

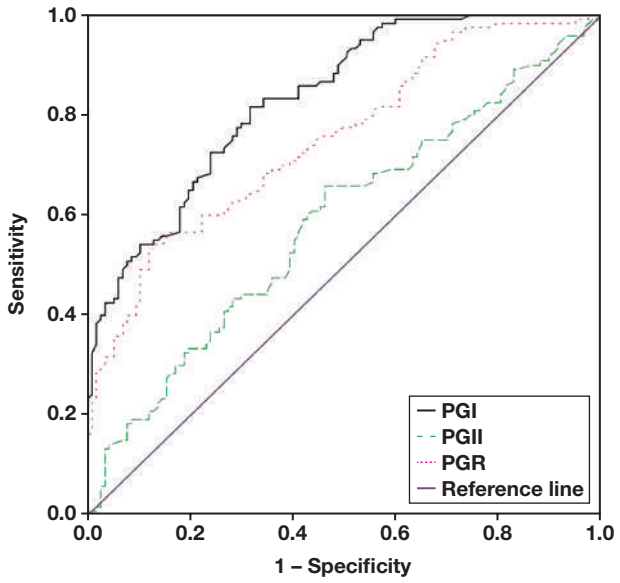

TABLE 2. ROC Curves for PGI, PGII, and PGR in the GC Group

Group	Area	SE	*P* Value	95% CI
PGI	0.843	0.025	<.001	.78–.88
PGII	0.587	0.037	.02	.51–.66
PGR	0.752	0.031	<.001	.69–.81

ROC, receiver operating characteristic; PG, pepsinogen; PGR, pepsinogen I/II ratio; GC, gastric cancer; CI, confidence interval.

TABLE 3. Cutoff Values, Sensitivity, and Specificity for Levels of PGI, PGII, and PGR in GC Diagnosis

Group	Cutoff	Sensitivity, %	Specificity, %
PGI	51.20 ng/mL	81.7	68.4
PGII	13.05 ng/mL	65.8	53.8
PGR	5.65	54.2	87.2

PG, pepsinogen; PGR, pepsinogen I/II ratio; GC, gastric cancer.

minor, the concentration of serum PGI decreases, resulting in decrease of PGR. These results are consistent with those in the study report by Miki et al,[27] which showed that changes in the serum levels of PGI and PGII reflect the degree of gastric mucosal atrophy, and that PGR diminishes as gastric mucosal-gland atrophy progresses. Thus, serum PGI level and PGR can be used as indicators of the degree of gastric mucosal-gland atrophy,[27–30] and serum PGI, PGII, and PGR can be used as detectors of AG.

There is an irreversible point in the development of GC (**FIGURE 4**), past which it becomes difficult to effectively control the progression of GC.[31–33] The risk of developing cancer in patients with AG is 4 times higher than that of healthy individuals, and in severe cases of AG, this risk factor can be as great as 90 times higher.[34,35] Therefore, early screening of precancerous gastric mucosal lesions and identification of gastric mucosal diseases are important to preventing the occurrence of GC. The most effective way to do this is to make a clear diagnosis that enables early treatment and intervention in patients with AG, thereby preventing the development of GC.

FIGURE 3 shows that the AUC for PGI was the largest (0.834), followed by the AUC for PGR (0.752), and the AUC for PGII (0.587). The cutoff values of serum PGI, PGII, and PGR were 51.2 ng per mL, 13.05 ng per mL, and 5.65 ng per mL, respectively. The sensitivities of tests based on PGI, PGII, and PGR were 81.7%, 65.8%, 54.2%, respectively, and their specificity was 68.4%, 53.8%, and 87.2%, respectively. In the literature,[36] the diagnostic sensitivities of tests based on quantification of CA724, CEA, and CA199 are 60%, 76%, and 68%, respectively, with corresponding specificities of 74%, 53%, and 69%. These data suggest that diagnostic sensitivity based on serum PG is higher than those based on CEA, CA724, and CA199, which already have high predictive values in GC diagnosis.

Shikata et al[37] followed up with more than 2000 community residents in Japan for an average period of 10 years and identified cutoff values for GC screening of PGI of 59 ng/mL or less and PGR of 3.9 or less. By this standard, the sensitivity and specificity, compared with the actual incidence of GC, were 71.0% and 69.2%, respectively. In their study of a sample population of Kazakhs in Xinjiang, China, Juan et al[38] reported cutoff values for GC screening of PGI of 64 ng/mL or less and PGR of 4.5 or less, corresponding to a sensitivity and specificity of 80.5% and 89.8%, respectively. Fariborz et al[39] reported good sensitivity and specificity for cutoff values of 70.95 ng/mL for PGI levels and 2.99 for PGR.

Finally, Li et al[40] used ROC curves to determine cutoff values for GC screening in the Liaoning Province of China, and found PGI 94.3 ng/mL or less and PGR of 9.3 or less, conferring sensitivity and specificity of 81.4% and 35.0%, respectively, to the initial screening of GC. Overall, these results are in a similar range as our findings. The differences across the different studies may reflect regional and population variability, among other factors. Therefore, for practical implementation, the screening criteria should be adjusted according to the local clinical specifics of each population.

TABLE 4 shows that for the diagnosis of GC, the combined use of PGI and PGR is more valuable than single indicators for reducing the time before GC diagnosis and improving prognosis. For GC screening, early detection and diagnosis are crucial for treatment success. Therefore, lowering diagnostic criteria to improve the sensitivity would be the best option to reduce the chance of false negatives.

The quality of a diagnostic test also relies on its specificity. Parallel judging improves the sensitivity of the predictive test and reduces the rate of false negatives, but it also reduces the specificity and increases the rate of false positives. Serial judging improves the specificity but decreases the sensitivity, thereby increasing the rate of false negatives and reducing the rate of false positives. Combined approaches help to balance sensitivity and specificity according to different priorities, and to achieve comprehensive testing.

After excluding confounding factors such as sex and age, analysis by logistic regression indicated that the occurrence of GC was negatively correlated with serum PGI level and PGR. PG levels can also be affected by gastric mucosal damage, gland atrophy, ethnicity, cancer cells, and HP, among other factors. We hypothesize that atrophy of the gastric glands leads to a decrease in the production of PG. Gastric ulcer or gastrectomy may lead to gastric mucosal damage and promote the release of more PG into the peripheral blood, thus affecting the content of PG in the peripheral blood. It is unknown whether sex, age, smoking status, al-

TABLE 4. Sensitivity and Specificity of Serum PGI and PGR in the Detection of GC

Type of Test	Decision Thresholds	Sensitivity	Specificity
Parallel	PGI <51.2 ng/mL or PGR <5.65	91%	60%
Series	PGI <51.2 ng/mL and PGR <5.65	45%	94%

PG, pepsinogen; PGR, pepsinogen I/II ratio.

TABLE 5. Logistic Regression Analysis Results of the Relationship Between GC and PG[a]

Variable	Regression Coefficient	SE	*P* Value	OR	95% CI
PGI	–0.054	0.012	<.001	0.947	0.925–0.970
PGR	–0.420	0.140	.003	0.657	0.499–0.864

GC, gastric cancer; PG, pepsinogen; CI, confidence interval; PG, pepsinogen; PGR, pepsinogen I/II ratio.
[a]*This analysis showed negative correlations between the occurrence of GC and the level of serum PGI (B = –0.054; odds ratio [OR] = 0.947; 95% CI, 0.925–0.970;* P *<.001), and the PGR (B = –0.420; OR = 0.657; 95% CI, 0.499–0.864;* P *= .003).*

FIGURE 4. Progression of gastric mucosal pathology.

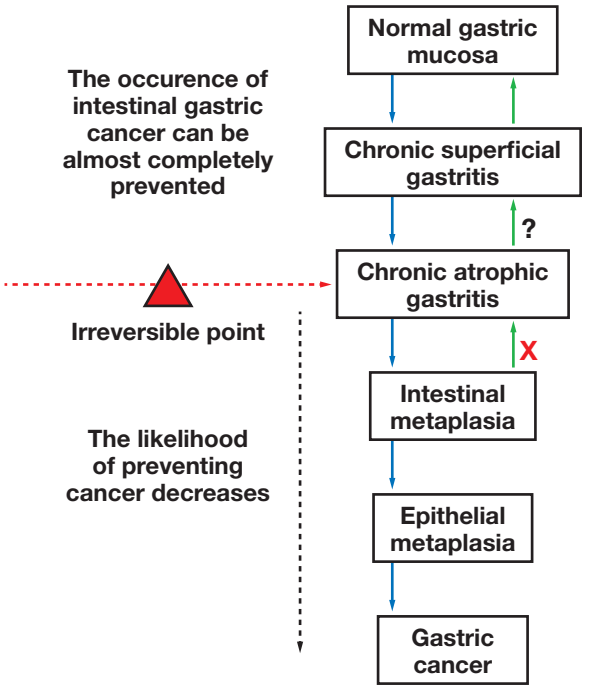

cohol consumption, or dietary habits influence PG levels and how these various factors affect PG levels. Answering these questions requires further study to more accurately and comprehensively assess the relationship between changes in serum PG level and GC progression.[41,42]

In conclusion, serum PGI and the PGR levels showed a gradual decrease from the healthy control group to the AG group to the GC group. The differences in PGI level and PGR between the GC and the control groups were significant, suggesting that tests based on PGI level and PGR have good clinical application value and can be used as indicators for the early diagnosis of GC. Moreover, detection of PG level can be indicative of precancerous diseases such as AG. This diagnostic tool is a feasible way to prevent GC and reduce its incidence and mortality rate by detecting PG abnormalities before the irreversible point of GC development is reached.

Conclusion

This study established the clinical value of PG as a biological marker for the prevention, diagnosis, and prediction of GC. This method is convenient, rapid, inexpensive, noninvasive, and easily accepted by patients. It can be used for auxiliary diagnosis, as an effective supplement to endoscopy and X-ray examination, and is worthy of popularization and broader application.

Acknowledgments: We thank the following persons for their guidance and help: Shunchang Sun, from the Hospital of Shanghai, Jiao Tong University Ruijin Hospital; Tao Li, from The First Affiliated Hospital of Anhui Medical University; experts Chen Yang, Jundong Zhou, and Ping Xu, from Suzhou Hospital; and Hong Du, Xuejun Shao, Hong Zhu, Xuefeng Qian, Qingzhen Han, Yang He, and Yimin Zhao, from Suzhou University. Funding was provided by the National Natural Science Foundation of China (81401937) and the Shanghai Science and Technology Project Fund (19ZR1444800, 2020-KY-ZYY-02).

REFERENCES

1. Bray F, Ferlay J, Soerjomataram I, Siegel RL, Torre LA, Jemal A. Global cancer statistics 2018: GLOBOCAN estimates of incidence and mortality worldwide for 36 cancers in 185 countries. *CA Cancer J Clin*. 2018;68(6):394–424.
2. Chen W, Zheng R, Baade PD, et al. Cancer statistics in China, 2015. *CA Cancer J Clin.* 2016;66(2):115–132.
3. Norollahi SE, Alipour M, Rashidy-Pour A, Samadani AA, Larijani LV. Regulatory fluctuation of WNT16 gene expression is associated with human gastric adenocarcinoma. *J Gastrointest Cancer.* 2019;50(1):42–47.
4. Kosari-Monfared M, Nikbakhsh N, Fattahi S, et al. *CTNNBIP1* downregulation is associated with tumor grade and viral infections in gastric adenocarcinoma. *J Cell Physiol.* 2019;234(3):2895–2904.
5. Rossi T, Tedaldi G, Petracci E, et al. E-cadherin downregulation and microRNAs in sporadic intestinal-type gastric cancer. *Int J Mol Sci.* 2019;20(18):4452.
6. Ikeda F, Shikata K, Hata J, et al. Combination of *Helicobacter pylori* antibody and serum pepsinogen as a good predictive tool of gastric cancer incidence: 20-year prospective data from the Hisayama Study. *J Epidemiol.* 2016;26(12):629–636.
7. Bang CS, Lee JJ, Baik GH. Diagnostic performance of serum pepsinogen assay for the prediction of atrophic gastritis and gastric neoplasms. *Medicine*. 2019;98(4):1–4.
8. Xingjie S, Liang LIU, Jingyu Z, et al. Changes and significance of serum pepsinogen levels in patients with early gastric cancer before and after endoscopic therapy. *Med Philos*. 2017;2(38):52–54.
9. Chunchun C, Hesheng L, Plating C, et al. Clinical study of serum pepsinogen in chronic gastric disease. *J. Gastroenterol Hepatol.* 2012;11(27):1265–1269.

10. Ju YL, Kim N, Lee HS, et al. Correlations among endoscopic, histologic and serologic diagnoses for the assessment of atrophic gastritis. *J Cancer Prev.* 2014;19(1):47–55.
11. Hamashima C. Cancer screening guidelines and policy making: 15 years of experience in cancer screening guideline development in Japan. *Jpn J Clin Oncol.* 2018;48(3):278–286.
12. Preparation Group of Digestive Pathology Group of Pathology Branch of Chinese Medical Association. Consensus on pathological diagnosis of chronic gastritis and epithelial tumor by gastric mucosal biopsy. *Chin J Pathol.* 2017;46(5):289–293.
13. Jun JK, Choi KS, Lee H-Y, et al. Effectiveness of the Korean National Cancer Screening Program in reducing gastric cancer mortality. *Gastroenterology.* 2017;152(6):1319–1328.
14. Lundell L, Vieth M, Gibson F, Nagy P, Kahrilas PJ. Systematic review: the effects of long-term proton pump inhibitor use on serum gastrin levels and gastric histology. *Aliment Pharmacol Ther.* 2015;7(6):649–663.
15. Rugge M, Genta RM, Mario FD, et al. Gastric cancer as preventable disease. *Clin Gastroenterol Hepatol.* 2017;15(12):1833–1843.
16. Choe J, Kim KW, Kim HJ, et al. What Is New in the 2017 World Health Organization Classification and 8th American Joint Committee on Cancer Staging System for Pancreatic Neuroendocrine Neoplasms? *Korean J Radiol*. 2019;20(1).
17. Lomba-Viana R, Dinis-Ribeiro M, Fonseca F, et al. Serum pepsinogen test for early detection of gastric cancer in a European country. *Eur J Gastroenterol Hepatol.* 2012;24(1):37–41.
18. Masuyama H, Yoshitake N, Sasai T, et al. Relationship between the degree of endoscopic atrophy of the gastric mucosa and carcinogenic risk. *Digestion.* 2015;91(1):30–36.
19. Wei ZJ, Zhang XY. Clinical application of serum gastric function detection in early gastric cancer screening. *Int J Lab Med.* 2017;38(16):2240–2242.
20. Niu L, Liang SH, Wu KC. Advances in study on endoscopic diagnosis of early gastric cancer. *Chin J Gastroenterol*. 2016;21(12):752–754.
21. Lansdorp-Vogelaar I, Kuipers EJ. Screening for gastric cancer in Western countries. *Gut*. 2016;65(4):543–544.
22. Parthasarathy G, Maroju NK, Kate V, Ananthakrishnan N, Sridhar MG. Serum pepsinogen I and II levels in various gastric disorders with special reference to their use as a screening test for carcinoma stomach. *Trop Gastroenterol*. 2007;28(4):166–170.
23. Kawai T, Gotoda T, Moriyasu F. Pepsinogen and atrophic gastritis. *Nihon Shokakibyo Gakkai Zasshi.* 2013;110(2):203–209.
24. Lizbeth RK, Augustine D, Rao RS, Sowmya SV, Patil S. Biomarkers in tumorigenesis using cancer cell lines: a systematic review. *Asian Pac J Cancer Prev.* 2017;18(9):2329–2337.
25. Yiqi D, Quancai C, Zhuan L, et al. Expert consensus on the screening process for early gastric cancer in China (draft)(2017, Shanghai). *Gastroenterology.* 2018;23(2):92–97.
26. Iino C, Shimoyama T, Sasaki Y, et al. Influence of endoscopic submucosal dissection on serum levels of pepsinogens in patients with early gastric cancer. *Dig Endosc.* 2012;24(5):339–342.
27. Miki K. Gastric cancer screening using the serum pepsinogen test method. *Gastric Cancer.* 2016;9(4):245–253.
28. Park YH, Kim N. Review of atrophic gastritis and intestinal metaplasia as a premalignant lesion of gastric cancer. *J Cancer Prev*. 2015;20(1):25–40.
29. Kato M, Ota H, Okuda M, et al. Guidelines for the management of *Helicobacter pylori* infection in Japan: 2016 Revised Edition. *Helicobacter.* 2019;24(4):e12597.
30. Yanaoka K, Oka M, Mukoubayashi C. Cancer high-risk subjects identified by serum pepsinogen tests: outcomes after 10-year follow-up in asymptomatic middle-aged males. *Cancer Epidemiol Biomarkers Prev.* 2008;17(4):838–845.
31. Fattahi S, Nikbakhsh N, Taheri H, et al. Prevalence of multiple infections and the risk of gastric adenocarcinoma development at earlier age. *Diagn Microbiol Infect Dis.* 2018;92(1):62–68.
32. Chang M, Zhang JC, Zhou Q, Sun D, Wang Y. Research progress of clinical epidemiology of gastric cancer [in Chinese]. *Chin J Gastroenterol Hepatol*. 2017;26(9):966–969.
33. Li XB, Liu WZ, Ge ZZ, et al. Clinical value of warning symptoms and signs in the diagnosis of gastrointestinal diseases. *Chin J Gastroenterol.* 2005;10(4):198–202.
34. Jencks DS, Adam JD, Borum ML, et al. Overview of current concepts in gastric intestinal metaplasia and gastric cancer. *Gastroenterol Hepatol (NY).* 2018;14(2):92–101.
35. Mansour-Ghanaei F, Joukar F, Rajpout Y, Hasandokht T. Screening of precancerous gastric lesions by serum pepsinogen, gastrin-17, anti-helicobacter pylori and anti-CagA antibodies in dyspeptic patients over 50 years old in Guilan Province, north of Iran. *Asian Pac J Cancer Prev.* 2014;15(18):7635–7638.
36. Gu ZD, Qu CY, Feng XJ, et al. Clinical significance of serum PGI, II and their ratio in the diagnosis and treatment of gastric cancer. In: the Ninth National Academic Conference on Laboratory Medicine of Chinese medical association and the Sixth National Academic Conference on Clinical Laboratory Management of Chinese Hospital Association; Beijing, China; May 24–27, 2011.
37. Shikata K, Ninomiya T, Yonemoto K, et al. Optimal cutoff value of the serum pepsinogen level for prediction of gastric cancer incidence: the Hisayama Study. *Scand J Gastroenterol.* 2012;47(6):669–675.
38. Juan Cai W, Yin L, Kang Q, et al. The serum pepsinogen test as a predictor of Kazakh gastric cancer. *Sci Rep.* 2017;2(7):435–436.
39. Mansour-Ghanaei F, Joukar F, Baghaee M, Sepehrimanesh M, Hojati A. Only serum pepsinogen I and pepsinogen I/II ratio are specific and sensitive biomarkers for screening of gastric cancer. *BioMol Concepts.* 2019;10(1):82–90.
40. Li YK, Lu BL, Liu HD, et al. The latest diagnostic threshold of gastric cancer screening by "serological biopsy" of gastric mucosa in Liaoning province. *Chin Health Stat.* 2016;33(4):697–700.
41. Chisato H. Systematic review group and guideline development group for gastric cancer screening guidelines. Updated version of the Japanese guidelines for gastric cancer screening. *Japn J Clin Oncol.* 2018;7(7):1–11.
42. Samadani AA, Noroollahi SE, Mansour-Ghanaei F, Rashidy-Pour A, Joukar F, Bandegi AR. Fluctuations of epigenetic regulations in human gastric Adenocarcinoma: how does it affect? *Biomed Pharmacother.* 2019;109: 144–156.

Association Between Graft Function and Urine CXCL10 and Acylcarnitines Levels in Kidney Transplant Recipients

Saniye Başak Oktay, MD,[1,] Sadıka Halide Akbaş, MD,[2] Vural Taner Yilmaz, MD,[3] İkbal Özen Küçükçetin, MD,[2] Havva Serap Toru, MD,[4] Süleyman Gültekin Yücel, MD[2]*

[1]Department of Biochemistry, Adıyaman University Education and Research Hospital, Adıyaman, Turkey; [2]Department of Biochemistry, Faculty of Medicine; [3]Division of Nephrology, Department of Internal Medicine, and [4]Department of Pathology, Faculty of Medicine, Akdeniz University, Antalya, Turkey; *To whom correspondence should be addressed. snybasak@gmail.com

Keywords: kidney transplantation, graft function, CXCL10, metabolome, ELISA, Tandem mass spectrometry

Abbreviations: RKFPs, routine kidney-function parameters; BUN, blood urea nitrogen; GFR, glomerular filtration rate; CXCL10, C-X-C motif chemokine 10; IFN-γ, interferon gamma; NK, natural killer; OCTN2, sodium-dependent carnitine transporter; UTI, urinary tract infection; CAD, chronic allograft dysfunction; AMR, antibody-mediated/humoral allograft rejection; IF/TA, interstitial fibrosis/tubular atrophy; PENIA, particle-enhanced immunonephelometric; MS/MS, tandem mass spectrometry; LC, liquid chromatography; eGFR, estimated glomerular filtration rate; eGFRCKD-EPI Cr, serum creatinine–based Chronic Kidney Disease Epidemiology Collaboration formula; eGFRCKD-EPI Cr-CysC, serum creatinine-cystatin C–based Chronic Kidney Disease Epidemiology Collaboration formula; HT, hypertension; DM, diabetes mellitus; HLA, human leukocyte antigen; RRT, renal replacement therapy

Laboratory Medicine 2022;53:78–84; https://doi.org/10.1093/labmed/lmab049

ABSTRACT

Objective: To evaluate post-transplantation graft functions noninvasively by using urine C-X-C motif chemokine 10 (CXCL10) and metabolome analysis.

Methods: The 65 living-donor kidney-transplant recipients in our cohort underwent renal biopsy to investigate possible graft dysfunction. The patients were divided into 2 groups, according to pathology reports: chronic allograft dysfunction (CAD; *n* = 18) and antibody-mediated/humoral allograft rejection (AMR; *n* = 16). The control group was composed of renal transplant recipients with stable health (*n* = 33). We performed serum creatinine, blood urea nitrogen (BUN), cystatin C, urine protein, CXCL10, and metabolome analyses on specimens from the patients.

Results: BUN, creatinine, cystatin C, urine protein, leucine + isoleucine, citrulline, and free/acetyl/propionyl carnitine levels were significantly higher in patients with CAD and AMR, compared with the control individuals. CXCL10 levels were significantly elevated in patients with AMR, compared with patients with CAD and controls. CXCL10 (AUC = 0.771) and cystatin C (AUC = 0.746) were significantly higher in the AMR group, compared with the CAD group (*P*<.02).

Conclusions: CXCL10 and metabolome analyzes are useful for evaluation of graft functions. Also, CXCL10 might be useful as a supplementary noninvasive screening test for diagnosis of allograft rejection.

The best choice for the treatment of end-stage kidney disease is kidney transplantation. However, despite the current use of strong immunosuppressant drugs, a frequent complication is allograft rejection in the posttransplantation period.[1] Allograft rejection is the most common cause of chronic graft dysfunction and subsequent graft loss when untreated.[2] Routine kidney-function parameters (RKFPs), used in the evaluation and monitoring of graft function are serum creatinine, serum blood urea nitrogen (BUN), serum cystatin C, urine total protein, and glomerular filtration rate (GFR).

The gold standard diagnostic method for the diagnosis, typing, and differentiation of allograft rejection from chronic allograft damage or other pathologic manifestations is biopsy. However, due to the invasive nature of biopsy, new noninvasive genomic, proteomic, and metabolomic analysis studies have been conducted to identify biomarkers that can detect the graft damage and its causes at an early stage.[3–8]

The C-X-C motif chemokine 10 (CXCL10) is a cytokine belonging to the CXC chemokine family that is secreted by activated B lymphocytes, monocytes/macrophages, endothelial cells, and fibroblasts in response to interferon gamma (IFN-γ). It is also known in the literature as *small-inducible cytokine B10* and *interferon gamma–induced protein 10*. CXCL10 has chemoattractive effects for monocytes/macrophages, T cells, natural killer (NK) cells, and dendritic cells via cell surface chemokine receptor CXCR3. Urinary chemokines have been evaluated as noninvasive inflammatory markers for rejection.[5] Study results[9,10] have shown that urinary levels of CXCL10 are associated with renal injury, allograft rejec-

tion, and subclinical tubulitis, compared with normal graft function. According to the gene list published in the 2017 Banff Classification,[11] the results of certain studies have shown increased urinary CXCL10 levels in antibody-mediated and T-cell-mediated rejections.

Carnitine (3-hydroxy-4-N-trimethylamine butyrate) is a metabolite that regulates translocation of long-chain fatty acids into the mitochondrial matrix for β-oxidation. L-carnitine is a small, polar, and non–protein-binding molecule, so it is eliminated from the body via glomerular filtration. In total, 95% of the carnitine in the glomerular ultrafiltrate is reabsorbed by the sodium-dependent carnitine transporter (OCTN2) from the proximal tubule.[12]

Also, the kidney has a major role in the homeostasis and metabolism of plasma amino acids. This role is ensured by the synthesis, degradation, filtration, reabsorption, and urinary excretion of amino acids. Proximal tubules recover 50 g to 70 g of amino acids in 1 day by reabsorption of almost all (97%–98%) filtered amino acids.[13] The results of multiple studies[8,14,15] have revealed that the levels of urinary metabolites (amino acids and free/acyl carnitines) increased significantly in graft inflamation, cellular/humoral rejection, and chronic allograft dysfunction. In this study, we aimed to evaluate post-transplantation graft functions noninvasively by using urine CXCL10 and metabolome analysis (amino acids and free/acyl carnitines) in addition to the routine renal function parameters that are currently evaluated.

Materials and Methods

In this prospective study, we studied 65 living-donor renal-transplant recipients, who had undergone renal biopsy and were older than 18 years, in our transplant center from May 2017 to October 2018. Renal biopsy indications were performed based on suspicion of graft dysfunction, in accordance with laboratory (serum creatinine level >25% of the patient's basal level, >3.5 g of urine protein/day) and clinical evaluations. Spot midstream urine and venous blood specimens were collected from all kidney-transplant recipients before biopsy. Twenty-one of the 65 recipients, who had urinary tract infection (UTI), a history of malignant neoplasms, and who had started rejection treatment before we had collected their specimens, were excluded from the study.

According to pathology reports that used the Banff Classification, the patients were divided into 2 groups: those with chronic allograft dysfunction (CAD) and those with antibody-mediated/humoral allograft rejection (AMR). Other than these 2 groups, 10 patients with other pathological diagnoses (BK-virus infection, focal segmental glomerulosclerosis, cellular rejection, etc) were also excluded from the study.

In the remaining 34 recipients, the CAD group (3 women, 15 men; mean age, 41.50 years) consisted of patients with mild (n = 10) and moderate (n = 8) interstitial fibrosis/tubular atrophy (IF/TA). Also, the AMR group (7 women, 9 men; mean age, 39 years) consisted of individuals with $C4d^+$ acute/active humoral rejection (n = 4) and $C4d^+$ chronic active humoral rejection (n = 12). The control group consisted of 33 living-donor renal-transplant recipients in stable health (13 women, 20 men; mean age, 40.97 years) with paired urine and blood specimens, without suspicion of any health problems or and graft dysfunction.

Blood and urine specimens collected from all participants were centrifuged for 5 minutes at 1792g and for 5 minutes at 448g, respectively. All specimens were stored at −80°C until analysis. Serum and urine creatinine, serum BUN, and urine total protein levels (mg/dL) were analyzed by using original commercial kits with a Siemens ADVIA Chemistry XPT autoanalyzer (Siemens Healthineers Diagnostics Ltd). Serum cystatin C levels (mg/L) were analyzed by using the particle-enhanced immunonephelometric (PENIA) method in a BN II Nephelometer (Siemens Healthcare Diagnostics Ltd). Urine CXCL10 levels (pg/mL) were analyzed using the ELISA method (Human CXCL10/IP-10; Quantikine ELISA R&D Systems). The minimum detectable dose of human CXCL10/IP-10 ranged from 0.41 to 4.46 pg/mL.

Urine metabolome analyses (μmol/L) were performed by tandem mass spectrometry (MS/MS) method on a Shimadzu 8040 model liquid chromatography (LC)––MS analyzer (Shimadzu Corporation). The results of metabolome analysis, consisting of 13 amino acids and 28 carnitine derivatives, are shown in **TABLE 1**. Urine specimens were thawed on ice at room temparature, vortexed, and then centrifuged at 18,920g. We loaded 20 μL of urine supernatant onto the kit's filter paper and dried it overnight. After taking 1 punch (3.1-mm diameter = 3 μL) from the urine specimens to the plate wells, we added 200 μL of deuterium-marked internal standard (Immuchrom GmbH) and mixed the contents in a shaker for 26 minutes at 37°C. After adding 60 μL butanolic HCL, the contents were dried using nitrogen gas, dissolved into a 100 μL acetonitrile-water mixture, and analyzed using the MS/MS method.[8,16]

Urine total protein, CXCL10, and metabolite concentrations were normalized by urine creatinine for dilutional correction. Estimated glomerular filtration rates (eGFR) were calculated using the serum creatinine–based Chronic Kidney Disease Epidemiology Collaboration ($eGFR_{CKD\text{-}EPI\ Cr}$) and the serum creatinine-cystatin C–based Chronic Kidney Disease Epidemiology Collaboration ($eGFR_{CKD\text{-}EPI\ Cr\text{-}CysC}$) formulas (mL/Dk/1.73m^2).[17]

We analyzed the study data using SPSS software, version 23.0, for Windows (IBM Corporation), MedCalc software, version 18.11.3 (MedCalc Software Ltd); P =.05 was considered to be statistically significant. Next, we performed Kolmogorov-Smirnov testing to assess the deviation from normal distribution. Quantitative variables were summarized as mean (SD) for parametric data, or as median (minimum-maximum) for nonparametric data.

Parametric continuous data were analyzed using ANOVA and Student t testing. We analyzed nonparametric continuous data using Kruskal-Wallis and Mann-Whitney U testing. P values were corrected according to the Bonferroni method; P = .02 was considered statistically significant in binary group comparisons. We performed analysis of correlation via Spearman or Pearson testing. ROC analysis was performed to estimate the sensitivities and specificities of parameters in evaluation of CAD and AMR.

The study has been approved by the Institutional Clinical Research Ethics Committee (Approval No. 2017/5–327) of Akdeniz University and conducted in accordance with the Helsinki Declaration. Written informed consent was obtained from all participants included in this study.

Results

General patient characteristics and demographic features are shown in **TABLE 2**. There was no statistically significant difference between the groups in terms of age, sex, body weight, months after transplantation, and immunosuppressant agent. **TABLE 3** summarizes the parameters, showing significant differences in serum BUN, creatinine, cystatin C, $eGFR_{CKD\text{-}EPI\ Cr}$, $eGFR_{CKD\text{-}EPI\ Cr\text{-}CysC}$, and urine total protein, CXCL10,

TABLE 1. Amino Acids and Acyl Carnitines Analyzed in the Study

Amino Acid	Free/Acyl Carnitine
Valine	C0 (free carnitine)
Leucine + isoleucine	C2 (acetyl-L-carnitine)
Methionine	C3 (propionyl-L-carnitine)
Phenylalanine	C4 (malonil-L-carnitine)
Arginosuccinic acid	C4-DC (succinyl-L-carnitine)
Tyrosine	C5 (isovaleryl-L-carnitine)
Aspartic acid	C5:1 (tigyl-L-carnitine)
Alanine	C5-OH (3 hydroxy isovaleryl-L-carnitine)
Arginine	C5-DC (glutalyl-L-carnitine)
Citrulline	C6 (hexanoyl-L-carnitine)
Glycine	C6-DC (adipil-L-carnitine)
Ornithine	C8 (octanoyl-L-carnitine)
Glutamic acid	C8:1 (octenoyl-L-carnitine)
	C8-DC (suberyl-L-carnitine)
	C10 (decanoyl-L-carnitine)
	C10:1 (decenoyl-L-carnitine)
	C10-DC (sebasil-L-carnitine)
	C12 (dodecanoil-L-carnitine)
	C14 (myristoyl-L-carnitine)
	C14:1 (tetradecanoyl-L-carnitine)
	C14:2 (tetradecadienyl-L-carnitine)
	C16 (hexadecanoyl-L-carnitine)
	C16:1 (hexadecenoyl-L-carnitine)
	C18 (octadecanoyl-L-carnitine)
	C18:1 (octadecenoyl-L-carnitine)
	C18:2 (octadecadienyl-L-carnitine)
	C18:1-OH (hydroxioctadecenoyl-L-carnitine)
	C5-M-DC (methyl glutalyl carnitine)

amino acids, and carnitine-derivatives levels, among the CAD, AMR, and control groups.

Serum BUN, serum creatinine, cystatin C, and urine total protein levels were significantly higher in patients (CAD and AMR groups) compared with the control group, as we had expected. However, the eGFR values in the patient groups were significantly lower ($P<.001$).

Urine C0, C2, C3, leucine + isoleucine, and citrulline levels were found to be significantly higher in the CAD group, compared with the control group ($P<.005$). Urine C0, C2, C3, leucine + isoleucine, citrulline, and CXCL10 levels were found to be significantly higher in the AMR group, compared with the control group ($P<.01$). Urine C10 vs C10:1 levels were significantly lower in the AMR group, compared with the control group ($P = .002$ and $P = .006$, respectively); we observed and no significant differences between the CAD and control groups.

When we compared the CAD and AMR groups, we found cystatin C and CXCL10 levels to be significantly higher in the AMR group ($P = .02$ and $P = .007$, respectively); however, no significant differences were observed for other RKFPs and metabolome parameters. Correlation results of the parameters that showed statistically significant differences among the CAD, AMR, and control groups with RKFP in all patients were presented in **TABLE 4**. Urine CXCL10 and leucine + isoleucine values showed moderate significant correlation between all RKFPs.

ROC analysis was performed for all parameters that differed significantly between the AMR and control groups; all results are given in **TABLE 5**. Among the RKFPs, $eGFR_{CKD\text{-}EPI\ Cr\text{-}CysC}$ had the highest AUC value (AUC = 0.968; $P<.001$), and among the other parameters, CXCL10 had the highest AUC value (AUC = 0.805; $P<.001$). ROC analysis was performed for all parameters that differed significantly between the CAD and control groups.

Among the RKFPs, cystatin C had the highest AUC value (AUC = 0.922; $P<.001$). Also, among the metabolome parameters, leucine + isoleucine had the highest AUC value (AUC = 0.835; $P<.001$). In the AMR group, CXCL10 and cystatin C levels were significantly higher than in CAD group as mentioned earlier herein (**TABLE 3**).

The sensitivities and specificities of both parameters were calculated to predict AMR, and the cutoff values were determined by ROC analysis. For predicting AMR, the optimal cutoff level for CXCL10 was found to be greater than 0.928 pg/mL; for this value, the sensitivity was 81.25%, the specificity was 72.22%, and the AUC was 0.771 (95% CI, 0.595–0.897; $P<.001$). The optimal cutoff level for cystatin C was found to be greater than 2.31 mg/L; for this value, the sensitivity was 68.75%, the specificity was 76.47%, and the AUC was 0.746 (95% CI, 0.565–0.881; $P=.001$) for the differentiation of AMR from CAD (**TABLE 6**).

Also, we evaluated the correlation of cystatin C and CXCL10 with $GFR_{CKD\text{-}EPI\ Cr}$ in both groups separately. Although there was a significant correlation for cystatin C in both groups (CAD: $r = -0.504$, $P = .04$; AMR: $r = -0.847$, $P<.001$), there was no significant correlation for CXCL10 in either group (CAD: $r = -0.147$, $P = .57$; AMR: $r = -0.035$, $P = .90$).

Discussion

In our study findings, cystatin C and $eGFR_{CDK\text{-}EPI\ Cr\text{-}CysC}$ were revealed to be the parameters with the highest diagnostic performance among the all RKFPs in differentiating the control group from the patient groups. In the study findings published by Christensson et al,[18] in the renal-transplant recipients with stable health, serum cystatin C showed a significantly higher correlation with iohexol clearance than did serum creatinine. In Rodrigo et al,[19] dynamic follow-up of renal-transplant recipients revealed that serum cystatin C levels are more robust predictor than creatinine in evaluating graft loss. Also, in another study to evaluate the clinical significance of serum cystatin C for the diagnosis of acute rejection after renal transplantation,[20] cystatin C was found to be a more sensitive marker than serum creatinine for detecting changes in kidney function.

Our results were compatible with those in the literature. Also, cystatin C was significantly higher in patients with AMR, compared with CAD, and was found to be a promising parameter in the distinction of those pathological groups. However, there was a high negative correlation of serum cystatin C levels with $GFR_{CKD\text{-}EPI\ Cr}$ in the AMR group and also a moderate negative correlation in the CAD group. In addition, $GFR_{CKD\text{-}EPI\ Cr}$ levels was lower in the AMR group, compared with the CAD group, although the value was not significant. Thus, higher cystatin C levels could reflect reduced kidney function.

CXCL10 levels, measured in spot urine specimens, were significantly elevated in the AMR group, compared with the CAD and control groups ($P = .007$ and $P = .001$, respectively). According to our ROC-analysis results, CXCL10 had the highest diagnostic performance after RKFP in differentiating the AMR group from the control group (AUC = 0.805).

TABLE 2. General Characteristics and Demographics Features of Patients[a]

Characteristic	All Patients (*n* = 67)	Group 1: CAD (*n* = 18)	Group 2: AMR (*n* = 16)	Group 3: Control (*n* = 33)	*P* Value
Age (y), mean (SD)	40.49 (13.22)	41.50 (12.99)	39.00 (11.97)	40.97 (14.70)	.47
Sex, no. (%)					.17
Female	23 (34%)	3 (17%)	7 (44%)	13 (39%)	
Male	44 (66%)	15 (83%)	9 (56%)	20 (61%)	
Body weight (kg), mean (SD)	72.89 (15.31)	73.17 (15.75)	69.59 (15.96)	74.41 (14.97)	.28
Etiologies of End-Stage Renal Disease					
HT	17 (25%)	6 (33%)	2 (13%)	9 (27%)	
DM	5 (8%)	2 (11%)	0	3 (9%)	
HT + DM	5 (8%)	1 (6%)	2 (13%)	2 (6%)	
Other	16 (24%)	5 (28%)	5 (31%)	6 (18%)	
Unknown	24 (36%)	4 (22%)	7 (44%)	13 (39%)	
HLA Matches					
0	4 (6%)	1 (6%)	0	3 (9%)	
1–5	54 (81%)	14 (78%)	13 (81%)	27 (82%)	
6	9 (13%)	3 (17%)	3 (19%)	3 (9%)	
RRT time (mo), mean (SD)	68.34 (116.39)	41.22 (52.72)	54.92 (54.87)	108.88 (241.59)	.43
Immunosuppressant Therapy					.38
Tacrolimus	58 (87%)	15 (83%)	13 (81%)	30 (91%)	
Cyclosporine	6 (9%)	2 (11%)	3 (19%)	1 (3%)	
Sirolimus	3 (5%)	1 (6%)	0	2 (6%)	

CAD, chronic allograft dysfunction; AMR, antibody-mediated allograft rejection; HT, hypertension; DM, diabetes mellitus; HLA, human leukocyte antigen; RRT, renal replacement therapy.
[a]Percentages may not total 100 because of rounding.

TABLE 3. Study-Parameter Values Among the CAD, AMR, and Control Groups

Analyte	Median (minimum–maximum)			*P* Value			
	Group 1: CAD (*n* = 18)	Group 2: AMR (*n* = 16)	Group 3: Control (*n* = 33)	Groups 1–2–3[a]	Groups 1–2[b]	Groups 1–3[b]	Groups 2–3[b]
Serum BUN, mg/dL	29.355 (12.86–8.91)	36.67 (20.7–83.98)	15.77 (11.35–87.00)	<.05	NS	<.001	<.001
Serum creatinine, mg/dL	1.78 (0.90–3.24)	2.06 (1.09–5.54)	1.02 (0.61–2.96)	<.05	NS	<.001	<.001
Serum cystatin C, mg/L	2.04 (1.19–4.26)	2.49 (1.41–5.12)	1.26 (0.80–3.9)	<.05	.02	<.001	<.001
Urine total protein, mg/dL	26.65 (3.60–171.00)	76.15 (7.0–364.7)	8.50 (1.70–307.10)	<.05	NS	<.001	<.001
$eGFR_{CKD\text{-}EPI\ Cr}$, mL/Dk/1.73 m2	45.50 (18.00–104.00)	37.50 (9.00–64.00)	79.00 (22.00–125.00)	<.05	NS	<.001	<.001
$eGFR_{CKD\text{-}EPI\ Cr\text{-}CysC}$	36 (14–82)	30 (9–51)	69 (16–108)	<.05	NS	<.001	<.001
CXCL10, pg/mL	0.81 (0.27–1.44)	1.22 (0.37–2.68)	0.57 (0.15–2.30)	<.05	.007	NS	.001
C0	0.795 (0.016–0.356)	0.581 (0.014–3.482)	0.119 (0.005–1.784)	<.05	NS	.001	.005
C2	0.341 (0.003–1.28)	0.190 (0.005–1.137)	0.041 (0.002–0.715)	<.05	NS	.002	.007
C3	0.090 (0.010–0.681)	0.071 (0.004–0.424)	0.026 (0.004–0.193)	<.05	NS	.002	.008
C10	0.002 (0.001–0.01)	0.0010 (0.0004–0.0050)	0.0020 (0.0004–0.1250)	<.05	NS	NS	.002
C10:1	0.005 (0.001–0.007)	0.002 (0.001–0.011)	0.005 (0.001–0.028)	<.05	NS	NS	.006
Leucine + isoleucine	0.571 (0.139–1.200)	0.386 (0.076–2.811)	0.138 (0.023–3.478)	<.05	NS	<.001	.007
Citrulline	0.121 (0.021–0.591)	0.095 (0.024–1.300)	0.043 (0.005–0.381)	<.05	NS	.005	.01

CAD: chronic allograft dysfunction; AMR, antibody mediated allograft rejection; BUN, blood urea nitrogen; NS, nonsignificant; $eGFR_{CKD\text{-}EPI\ Cr}$, serum creatinine–based Chronic Kidney Disease Epidemiology Collaboration formula; $eGFR_{CKD\text{-}EPI\ Cr\text{-}CysC}$, serum creatinine-cystatin C–based Chronic Kidney Disease Epidemiology Collaboration formula; CXCL10, C-X-C motif chemokine 10.
[a]When comparing among the 3 groups, P<.05 was considered statistically significant.
[b]According to Bonferroni correction, P<.02 was considered statistically significant in binary group comparisons.

TABLE 4. Correlation Results of the Parameters Among the CAD, AMR, and Control Groups with Routine Renal Function Parameters

Analyte	Serum Creatinine (mg/dL)	Serum BUN (mg/dL)	Serum Cystatin C (mg/L)	Urine Total Protein (mg/dL)	$GFR_{CKD\text{-}EPI\ Cr}$ (mL/Dk/1.73m^2)	$GFR_{CKD\text{-}EPI\ Cr\text{-}CysC}$ (mL/Dk/1.73m^2)
CXCL10	0.317[a]	0.426[a]	0.434[a]	0.377[a]	−0.358[a]	−0.421[a]
C0	0.274[b]	0.492[a]	0.327[a]	NS	−0.303[b]	−0.328[a]
C2	0.254[b]	0.457[a]	0.322[a]	NS	−0.289[b]	−0.316[a]
C3	0.279[b]	0.534[a]	0.368[a]	NS	−0.314[a]	−0.357[a]
C10	−0.307[b]	NS	−0.311[b]	NS	0.303[b]	0.303[b]
C10:1	−0.361[a]	NS	−0.375[a]	−0.316[a]	0.342[a]	0.359[a]
Leucine + isoleucine	0.362[a]	0.462[a]	0.471[a]	0.247[b]	−0.380[a]	−0.460[a]
Citrulline	0.378[a]	0.466[a]	0.470[a]	NS	−0.402[a]	−0.463[a]

CAD, chronic allograft dysfunction; AMR, antibody mediated allograft rejection; BUN, blood urea nitrogen; $eGFR_{CKD\text{-}EPI\ Cr}$, serum creatinine–based Chronic Kidney Disease Epidemiology Collaboration formula; $eGFR_{CKD\text{-}EPI\ Cr\text{-}CysC}$, serum creatinine-cystatin C–based Chronic Kidney Disease Epidemiology Collaboration formula; CXCL10, C-X-C motif chemokine 10; NS, nonsignificant.
[a]P<.001 was considered statistically significant.
[b]P<.05 was considered statistically significant.

TABLE 5. ROC Analysis Results of All Parameters That Differed Significantly Between the AMR and Control Groups, and the CAD and Control Groups

	Parameter	Cutoff	AUC (95% CI)	Sensitivity	Specificity	*P* Value
For AMR	$eGFR_{CDK\text{-}EPI\ Cr\text{-}CysC}$	≤51	0.968 (0.873–0.997)	100	87.88	<.001
	Serum cystatin C	>1.84	0.962 (0.865–0.996)	93.75	96.97	
	$eGFH_{CDK\text{-}EPI\ CR}$	≤54	0.948 (0.844–0.991)	93.75	87.88	
	Serum creatinine	>1.6	0.939 (0.832–0.987)	81.25	96.97	
	BUN	>20.6	0.936 (0.827–0.986)	100.0	84.85	
	Urine total protein	>0.339	0.896 (0.775–0.965)	87.50	81.82	
	CXCL10	>0.819	0.805 (0.667–0.904)	87.50	69.70	
	C10	≤0.002	0.773 (0.631–0.880)	93.75	57.58	
	C0	>0.256	0.748 (0.604–0.861)	75.00	72.73	.002
	C10:1	≤0.004	0.746 (0.602–0.860)	93.75	51.52	.001
	Leucine + isoleucine	>0.285	0.741 (0.595–0.855)	68.75	72.73	.002
	C2	>0.135	0.739 (0.593–0.854)	75.00	72.73	.003
	C3	>0.028	0.737 (0.591–0.852)	87.50	60.61	.006
	Citrulline	>0.179	0.723 (0.577–0.842)	43.75	96.97	
For CAD	Serum cystatin C	>1.62	0.922 (0.810–0.979)	88.24	90.91	<.001
	$eGFR_{CDK\text{-}EPI\ Cr\text{-}CysC}$	≤54	0.911 (0.796–0.973)	94.12	87.88	
	Serum creatinine	>1.53	0.865 (0.738–0.945)	76.47	93.94	
	$eGFR_{CDK\text{-}EPI\ Cr}$	≤57	0.854 (0.726–0.937)	83.33	87.88	
	BUN	>23.77	0.840 (0.711–0.928)	77.78	93.94	
	Leucine + isoleucine	>0.431	0.835 (0.705–0.924)	61.11	90.91	
	Urine total protein	>0.162	0.800 (0.664–0.899)	88.89	66.67	
	C0	>0.381	0.790 (0.653–0.891)	77.78	78.79	
	C2	>0.171	0.769 (0.630–0.876)	66.67	81.82	.001
	C3	>0.034	0.763 (0.623–0.870)	83.33	66.67	
	Citrulline	>0.159	0.737 (0.595–0.851)	50.00	93.94	.002

AMR, antibody mediated allograft rejection, CAD, chronic allograft dysfunction; $eGFR_{CKD\text{-}EPI\ Cr\text{-}CysC}$, serum creatinine-cystatin C–based Chronic Kidney Disease Epidemiology Collaboration formula; $eGFR_{CKD\text{-}EPI\ Cr}$, serum creatinine–based Chronic Kidney Disease Epidemiology Collaboration formula; BUN, blood urea nitrogen; CXCL10, C-X-C motif chemokine 10.

CXCL10 and cystatin C were 2 parameters found to be significant in the distinction of AMR from CAD. The diagnostic power of CXCL10 was higher than that of cystatin C, according to our ROC-analysis results. Also, CXCL10 did not show a significant correlation with $GFR_{CKD\text{-}EPI\ Cr}$ in either of the pathological groups when evaluated separately. This finding suggests that unlike cystatin C, the increase of CXCL10 in AMR could be

TABLE 6. Predicting Performances of the Parameters with Significant Difference Between the CAD and AMR Groups, for Predicting AMR

Parameter	Cutoff	AUC (95% CI)	Sensitivity	Specificity	*P* Value
CXCL10	>0.928	0.771 (0.595–0.897)	81.25	72.22	.002
Serum cystatin C	>2.31	0.746 (0.565–0.881)	68.75	76.47	.006

CAD, chronic allograft dysfunction; AMR, antibody-mediated allograft rejection; CXCL10, C-X-C motif chemokine 10.

due to inflammation independent of eGFR levels. CXCL10 is an inflammatory marker that is released from leukocytes as a result of developed inflammatory process.[10,21]

In a prospective study in 137 renal-transplant recipients by Ho et al,[8] there was a gradual increase in urinary CXCL10 levels parallel to the severity of the graft inflammation in patients who developed graft rejection. In another study conducted by Ho et al,[21] of CXCL10 in renal-transplant recipients, there was no significant difference between transplant recipients with normal histology and the IF/TA groups. However, there was a significant difference between transplant recipients with normal histology and the tubulitis groups. In another study report in the literature, it was revealed that CXCL10 was markedly elevated in adults and children experiencing acute rejection, compared with allograft recipients in stable health and allograft recipients with IF/TA.[22] All of those study findings are consistent with our results.

Our metabolome analysis results showed that leucine + isoleucine, citrulline, C0, C2, and C3 levels were significantly higher in both patient groups, compared with the control group ($P<.02$). Also, among the metabolome results, only leucine + isoleucine showed significant correlation with all RKFPs.

Leucine and isoleucine are reabsorbed via the SCL6A19 receptor in the proximal tubule. Because the expression of the SCL6A19 receptors decreases in the case of tubular damage, the reabsorption of leucine and isoleucine decreases, and their amount in the urine increases.[23,24]

There are many studies in the literature regarding metabolome analysis in transplant recipients. In the results of the study conducted by Landsberg et al,[14] some amino acids (especially leucine, ornithine, and arginine) and acyl carnitine (especially C4:1, C5:1, and C6:1) urinary levels were found to be elevated in transplant recipients with IF/TA. In the study by Ho et al[8] in renal-transplant recipients, urinary hexose, C2, C8:1, and C3-DC/C4-OH levels were found to be significantly higher in the group with graft inflammation, compared with the group without graft inflammation. There are some differences in significant parameters between our study and those in other studies in the literature; we believe that this difference is due to differences in pathological groupings, evaluated metabolites, and analytical processes.

The relatively small number of patients was the key limitation in our study. Second, due to having few patients in the cohort, our pathological subgroups were limited. For instance, cellular rejection, viral infections (such as BK virus), and systemic inflammatory diseases were not included due to insufficient number of patients having those conditions. The inclusion of these pathologic manifestations, in which increased inflammation is observed, may affect the sensitivity and specificity values of CXCL10 in pathological differentiation.

Third, our patients could not be evaluated with long-term dynamic follow-up, and concurrent serum levels of parameters measured in urine were not analyzed. Further studies are needed to confirm our preliminary study results by cross-validation in different centers with larger patient numbers and pathological subgroups. CXCL10 analysis in spot urine testing with ELISA method and metabolome analysis using the MS/MS method in dried spot urine yield same-day results. Last, for CXCL10 analysis, although the ELISA method with assay procedures can provide same-day results, separate analysis for each patient is impractical and not cost-effective in routine practice. In the future, it will be appropriate to develop immunoassay methods that yield results within a shorter turnaround time and that can be applied in a more practical manner.

In conclusion, high levels of leucine + isoleucine, citrulline, C0, C2, and C3 in urine, along with RKFPs, are significant in diagnosis of graft dysfunction although inadequate in pathological distinction. In pathological distinction, serum cystatin C and urinary CXCL10 levels were found to be significant for AMR; also, the diagnostic performance of CXCL10 was higher. This result has potential as a noninvasive differentiator of the causes of graft dysfunction.

Acknowledgments

We thank Sibtain Ahmed, PhD, for his help in performing data analysis. This research was supported by the Institutional Scientific Research Fund of Akdeniz University (TTU-2018–2883).

Personal and Professional Conflicts of Interest

None reported.

REFERENCES

1. Budak D, Yilmaz VT, Akbas H, Suleymanlar G, Yucel G. Association between graft function and serum TNF-α, TNFR1 and TNFR2 levels in patients with kidney transplantation. *Ren Fail.* 2015;37(5):871–876.
2. Sancho A, Pastor MC, Bayés B, et al. Posttransplant inflammation associated with onset of chronic kidney disease. *Transplant Proc.* 2010;42(8):2896–2898.
3. Roshdy A, El-Khatib MM, Rizk MN, El-Shehaby AM. CRP and acute renal rejection: a marker to the point. *Int Urol Nephrol.* 2012;44(4):1251–1255.
4. Reinhold SW, Straub RH, Krüger B, et al. Elevated urinary sVCAM-1, IL6, sIL6R and TNFR1 concentrations indicate acute kidney transplant rejection in the first 2 weeks after transplantation. *Cytokine.* 2012;57(3):379–388.
5. Hancock WW, Gao W, Faia KL, Csizmadia V. Chemokines and their receptors in allograft rejection. *Curr Opin Immunol.* 2000;12(5):511–516.
6. Yang JL, Hao HJ, Zhang B, Liu YX, Chen S, Na YQ. Level of soluble CD30 after kidney transplantation correlates with acute rejection episodes. *Transplant Proc.* 2008;40(10):3381–3383.
7. Malyszko J, Malyszko JS, Bachorzewska-Gajewska H, Poniatowski B, Dobrzycki S, Mysliwiec M. Neutrophil gelatinase-associated lipocalin is a new and sensitive marker of kidney function in chronic kidney disease patients and renal allograft recipients. *Transplant Proc.* 2009;41(1):158–161.

8. Ho J, Sharma A, Mandal R, et al. Detecting renal allograft inflammation using quantitative urine metabolomics and CXCL10. *Transplant Direct.* 2016;2(6):e78.
9. Hancock WW, Lu B, Gao W, et al. Requirement of the chemokine receptor CXCR3 for acute allograft rejection. *J Exp Med.* 2000;192(10):1515–1520.
10. Schaub S, Nickerson P, Rush D, et al. Urinary CXCL9 and CXCL10 levels correlate with the extent of subclinical tubulitis. *Am J Transplant.* 2009;9(6):1347–1353.
11. Haas M, Loupy A, Lefaucheur C, et al. The Banff 2017 Kidney Meeting Report: revised diagnostic criteria for chronic active T cell-mediated rejection, antibody-mediated rejection, and prospects for integrative endpoints for next-generation clinical trials. *Am J Transplant.* 2018;18(2):293–307.
12. Reuter SE, Evans AM. Carnitine and acylcarnitines: pharmacokinetic, pharmacological and clinical aspects. *Clin Pharmacokinet.* 2012;51(9):553–572.
13. Garibotto G, Sofia A, Saffioti S, Bonanni A, Mannucci I, Verzola D. Amino acid and protein metabolism in the human kidney and in patients with chronic kidney disease. *Clin Nutr.* 2010;29(4):424–433.
14. Landsberg A, Sharma A, Gibson IW, Rush D, Wishart DS, Blydt-Hansen TD. Non-invasive staging of chronic kidney allograft damage using urine metabolomic profiling. *Pediatr Transplant.* 2018;22(5):e13226.
15. Suhre K, Schwartz JE, Sharma VK, et al. Urine metabolite profiles predictive of human kidney allograft status. *J Am Soc Nephrol.* 2016;27(2):626–636.
16. Metz TF, Mechtler TP, Merk M, et al. Evaluation of a novel, commercially available mass spectrometry kit for newborn screening including succinylacetone without hydrazine. *Clin Chim Acta.* 2012;413(15-16):1259–1264.
17. Inker LA, Schmid CH, Tighiouart H, et al; for the CKD-EPI Investigators. Estimating glomerular filtration rate from serum creatinine and cystatin C. *N Engl J Med.* 2012;367(1):20–29.
18. Christensson A, Ekberg J, Grubb A, Ekberg H, Lindström V, Lilja H. Serum cystatin C is a more sensitive and more accurate marker of glomerular filtration rate than enzymatic measurements of creatinine in renal transplantation. *Nephron Physiol.* 2003;94(2):p19–p27.
19. Rodrigo E, Ruiz JC, Fernández-Fresnedo G, et al. Cystatin C and albuminuria as predictors of long-term allograft outcomes in kidney transplant recipients. *Clin Transplant.* 2013;27(2):E177–E183.
20. Liu J. Evaluation of serum cystatin C for diagnosis of acute rejection after renal transplantation. *Transplant Proc.* 2012;44(5):1250–1253.
21. Ho J, Rush DN, Karpinski M, et al. Validation of urinary CXCL10 as a marker of borderline, subclinical, and clinical tubulitis. *Transplantation.* 2011;92(8):878–882.
22. Jackson JA, Kim EJ, Begley B, et al. Urinary chemokines CXCL9 and CXCL10 are noninvasive markers of renal allograft rejection and BK viral infection. *Am J Transplant.* 2011;11(10):2228–2234.
23. Kostidis S, Bank JR, Soonawala D, et al. Urinary metabolites predict prolonged duration of delayed graft function in DCD kidney transplant recipients. *Am J Transplant.* 2019;19(1):110–122.
24. Bröer S. Apical transporters for neutral amino acids: physiology and pathophysiology. *Physiology.* 2008;23(2):95–103.

Stat Laboratory Interventions to Improve Patient Management in the Emergency Department and Resource Expenditure: A 10-Year Study

Maria Salinas, PhD,[1,] Emilio Flores, PhD,[1,2] Maite López Garrigós, PhD,[1,3,4] Alvaro Blasco, PhD,[1] Elena Diaz, MD,[5] Carlos Leiva-Salinas, MD, PhD, MBA[6]*

[1]Clinical Laboratory, Hospital Universitario de San Juan, San Juan de Alicante, Spain; [2]Department of Clinical Medicine, Universidad Miguel Hernandez, Elche, Spain; [3]Department of Biochemistry and Molecular Pathology, Universidad Miguel Hernandez, Elche, Spain; [4]CIBER de Epidemiología y Salud Pública (CIBERESP), Madrid, Spain; [5]Department of Emergency Medicine, Hospital Universitario de San Juan, San Juan de Alicante, Spain; [6]Department of Radiology, University of Missouri, Columbia, Missouri, US; *To whom correspondence should be addressed. salinas_mar@gva.es

Keywords: management, stat laboratory, expenditure, interventions, technology, knowledge

Abbreviations: ED, emergency department; TAT, turnaround time; tBil, total bilirubin; tProt, total protein.

Laboratory Medicine 2022;53:85–90; https://doi.org/10.1093/labmed/lmab030

ABSTRACT

Objective: To illustrate the changes in stat laboratory procedures over a 10 year period.

Materials and Methods: We implemented 5 different interventions: reporting total bilirubin through the icteric index, replacing total proteins for albumin, reporting albumin-adjusted calcium in hyper- or hypocalcemia, using lipase as a first marker and amylase-selected scenario, and measuring magnesium in hypocalcemia, hypokalemia, or high lipase values.

Results: Only 9.9% of total bilirubin that was requested was measured, which resulted in savings of $22,492.83. There were 30,036 albumin tests measured, and $15,625.18 was saved replacing total protein. There was $41,374.38 spent to measure lipase and amylase; the difference in costs from the lipase establishment was $16,929.62. Finally, $382.30 was spent for magnesium: 717 magnesium levels were measured given hypocalcemia or hypokalemia (42.8% hypomagnesemia), and 123 tests were added because of high lipase (35% hypomagnesemia). Overall, $53,374.15 was saved.

Conclusion: Progressive changes in stat laboratory procedures resulted in more efficient resources expenditures.

One of the main concerns for most health care organizations is to improve patient care efficiency in the emergency department (ED).[1] The overall ED patient care process is a complex, multiphasic procedure, with many contributing different stakeholders, including the clinical laboratory.

Two of the main features of a stat laboratory request are (1) the relevance for testing, because results may change patient treatment, and (2) the need for a short turnaround time (TAT).[2]

Technology advances and management tools[3] and the focus on improving stat laboratory procedures[4] have considerably and significantly reduced TAT, which needs continuous monitoring over time[5] to reach ED clinicians' needs.[6]

However, laboratory testing is significantly increasing worldwide, and so is demand inadequacy. This phenomenon could result in significant testing delays, which could in turn have dramatic consequences for critically ill patients in the ED, negatively impacting the global outcome efficiency of patients in the ED.

Testing in the ED laboratory is highly variable, with rates of stat test ordering significantly different among providers.[2,7] This variability and lack of homogeneity in test ordering could result in prolonged TAT and consequently a potential overall failure to review stat clinical laboratory reports on time and appropriately.[8]

Research conducted by the College of American Pathologists showed that laboratories offer an average of 206 tests.[9] The fraction of the test menu offered stat varied from 29% at the 10th percentile to 97.8% at the 90th percentile, with a median of 73.3%. This variation could be improved with standardization and optimization, in an effort to utilize stat testing based on a balance between safe and efficient patient management and resource expenditure.[9]

We hypothesized that with consensus from ED physicians, the laboratory could progressively improve utilization of stat laboratory tests without increasing costs. The purpose of this investigation was to illustrate the changes and improvements in the menu and utilization of stat laboratory tests during a 10 year period and the consequent benefits in patient management and expenditure.

Materials and Methods

Study Design

This was a retrospective longitudinal study to evaluate the impact of changes in the stat laboratory test menu on test utilization and impact on patient care from January 2010 to December 2019.

Setting

The stat laboratory is an independent laboratory located in the main laboratory in a university hospital in a health district of Alicante, Spain. The stat laboratory serves a population of 234,403 inhabitants, processes requests for inpatients and patients in the ED, and is staffed by 12 technicians, organized into 2 shifts. They process, verify, and report every hematology, coagulation, blood gas, urinalysis, and chemistry test. Laboratory requests are generated online, and the reports are sent electronically from the laboratory information system to the patient's electronic medical record. The ED care providers can automatically consult the report via the intranet. In 2010, the stat laboratory workload was 620,511 tests, and in 2019, the workload was 749,726 tests.

In 2010, the stat laboratory tests menu included 15 chemistry tests in plasma: alanine aminotransferase, amylase, C-reactive protein, calcium, chloride, creatine kinase, creatine kinase MB, creatinine, glucose, potassium, procalcitonin, sodium, total bilirubin (tBil), total protein (tProt), and troponin. In 2019, the number of tests in the stat laboratory portfolio included 16 chemistry tests in plasma: CK-MB was removed from portfolio, lipase and magnesium were added and tProt were replaced for albumin.

Interventions

Based on bibliography and clinical guidelines,[10-14,15] the laboratory staff detected the inappropriate requests of some stat laboratory markers and in consensus with ED physicians designed and established 5 strategies for corrections. Every intervention was monitored and evaluated.

Intervention 1, established January 2012, consisted of not measuring tBil when the icteric index was below 2 mg/dL (34.2 μmol/L)[10] and reporting through the following comment in the laboratory report: "With a confidence interval of 99%, tBil result is below 1.2 mg/dL (20.5 μmol/L)."

Intervention 2 was established in October 2013. We removed tProt from the stat laboratory tests menu, and we included albumin. This strategy was also agreed upon with the gastroenterologists on staff.

Intervention 3 was established in July 2014. The laboratory would report albumin-adjusted calcium in patients with low and high total calcium values <8.0 mg/dL or >9.5 mg/dL (<2 mmol/L or >2.37 mmol/L). The formula to calculate adjusted calcium is calcium + 0.8 × (4—albumin).

Intervention 4, established in November 2014, enacted sequential testing for pancreatic enzymes: lipase measurement was measured as the first marker, and amylase would be only measured when lipase values were between 393 and 787 IU/L.[11]

Intervention 5 was established in February 2016. Magnesium would be measured when hypocalcemia and hypokalemia were less than 7.5 mg/dL and 2.5 mEq/L, respectively (less than 1.87 mmol/L and 2.5 mmol/L, respectively).[12] Starting in July 2019, magnesium was also measured when lipase was greater than 600 IU/L.

Data Analysis

For Intervention 1, we counted the number of tBil tests that were requested and measured and calculated the savings, accounting for the cost of the reagent per measured tBil (average cost in the 10-year period of 0.24 dollars per test).

For Intervention 2, we evaluated the number of measured albumin levels and tProt levels and calculated the savings through the difference in costs for the reagent for both markers (average cost, 0.32 dollars per test for albumin and 0.84 dollars per test for tProt over the study period). We also evaluated the number of patients with albumin <3.5 g/dL.

For Intervention 3, we counted the number of reported albumin-adjusted calcium tests and calculated the costs for the additional albumin tests that were measured. We also counted the number of patients with corrected hypo- or hypercalcemia.

For Intervention 4, we evaluated the number of measured amylase and lipase tests and calculated the difference in reagent costs (average cost, 1.35 dollars per test for amylase and 0.92 dollars per test for lipase over the study period).

For Intervention 5, we counted the number of patients with hypomagnesemia and calculated the reagent costs to measure magnesium (average cost, 0.45 dollars per measured test over the study period).

The average costs over the years were calculated taking into account the increase in the retail price index. Finally, a global balance of costs was calculated for all the above strategies. The study was approved by the Hospital Research Committee.

Laboratory Methods

In the stat laboratory, tBil, the icteric index, tProt, albumin, calcium, lipase, amylase, and magnesium were measured using a Dimension RxL Max (Siemens Healthcare Diagnostics, Barcelona, Spain).

Statistical Methods

The statistical analyses were conducted with SPSS version 20 for Windows (SPSS Inc., Chicago, IL). The statistical analysis included a descriptive analysis of the variables. Normal quantitative variables were expressed as average and standard deviation. Categorical variables were expressed as percentages.

Results

Intervention 1: Over the 10 year period, 120,723 tBil tests were requested. We found that 108,409 (89.8%) of those were reported by means of the icteric index. **FIGURE 1** shows the total number of tBil tests conducted and reported through the icteric index since January 2012. Thanks to this intervention, $22,492.83 were saved ($2249.28 per year).

Intervention 2: We found that 30,036 albumin tests were conducted instead of tProt tests. The cost of performing albumin tests was $9500.63. The cost of performing the same number of tProt tests would have been $25,125.82 over the 10 year period. Consequently, $15,625.18 dollars was saved ($1562.52 per year). The number of patients with albumin <3.5 g/dL was 14,718 (49%).

Intervention 3: Since July 2014, the average percentage of reported albumin-adjusted calcium levels was 19.7%. **FIGURE 2** shows the monthly reported albumin-adjusted calcium levels. There were 2480 (63.2%) and 3 (1.5%) patients with corrected hypo- or hypercalcemia, respectively. We found that $1299 were spent in the albumin that measured additionally ($236.18 per year).

Intervention 4: **FIGURE 3** shows the number of amylase and lipase tests that were measured during the study period. We found that $45,421 was spent to measure amylase until November 2014 and since then, $41,374.38 ($8007.95 per year) were spent to measure lipase

FIGURE 1. Number of tBil tests conducted and tBil levels requested and reported through the icteric index for 8 years (2012–2019).

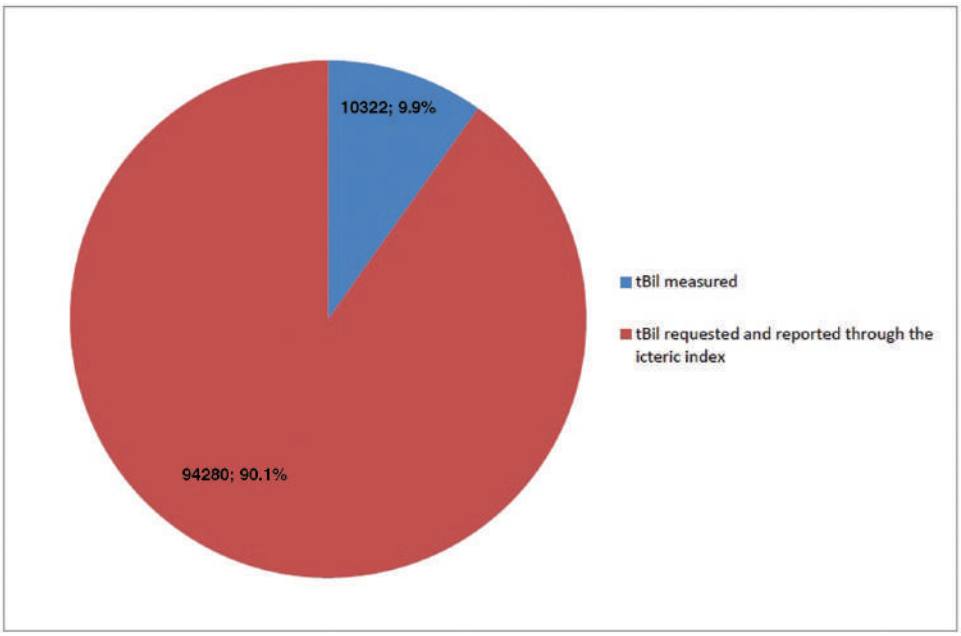

FIGURE 2. Number of reported albumin-adjusted calcium tests conducted since the establishment of the intervention.

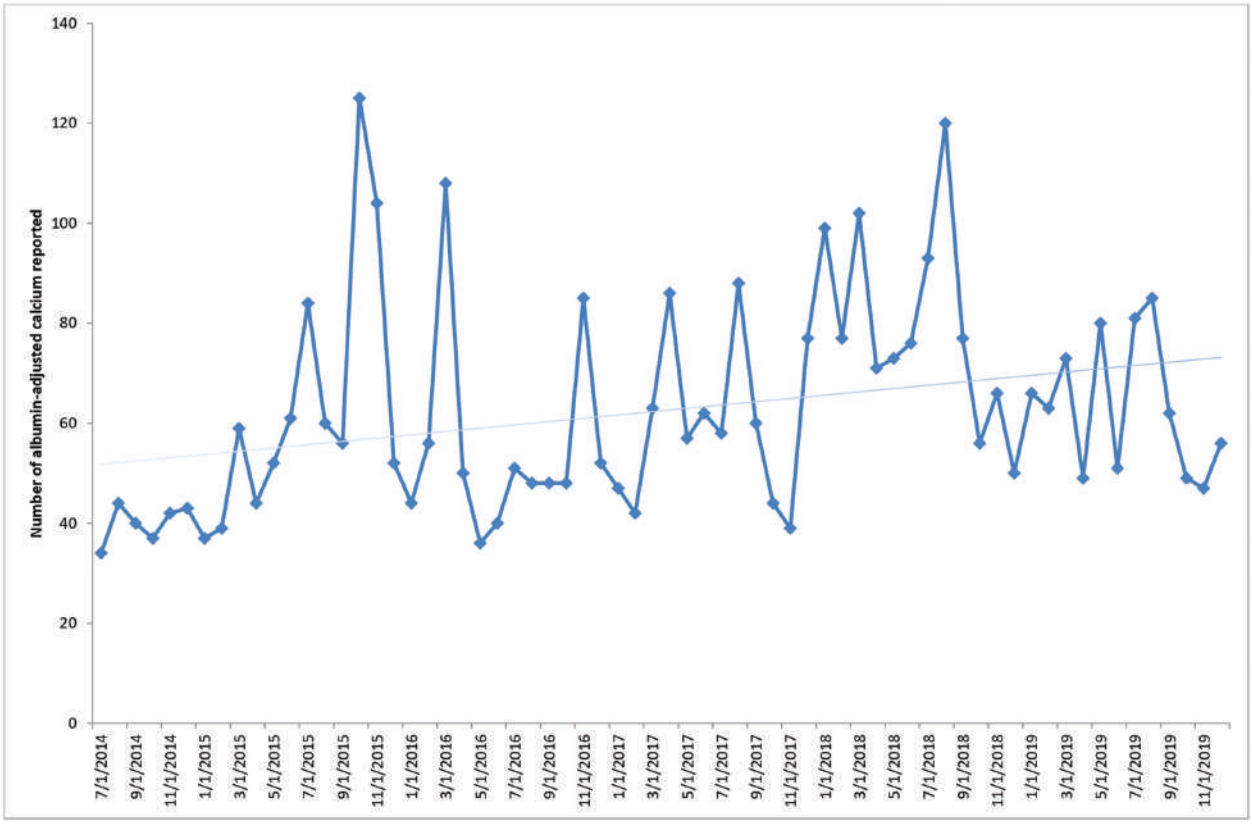

and amylase. The savings from the establishement of lipase testing was $16,929.62 ($3276.70 per year).

Intervention 5: We found that 717 magnesium specimens were measured for hypocalcemia or hypokalemia. The strategy identified 307 patients (42.8%) with hypomagnesemia. In the last 6 months of 2019, 123 magnesium tests were added in patients who presented with lipase >600 IU/L. Of these 123 patients, 43 (35%) showed magnesium deficiency, which was severe in 2 patients. In all, $374.15 was spent on magnesium reagent ($748.30 if extrapolated to 1 year).

FIGURE 3. Number of measured amylase and lipase tests conducted since January 2010.

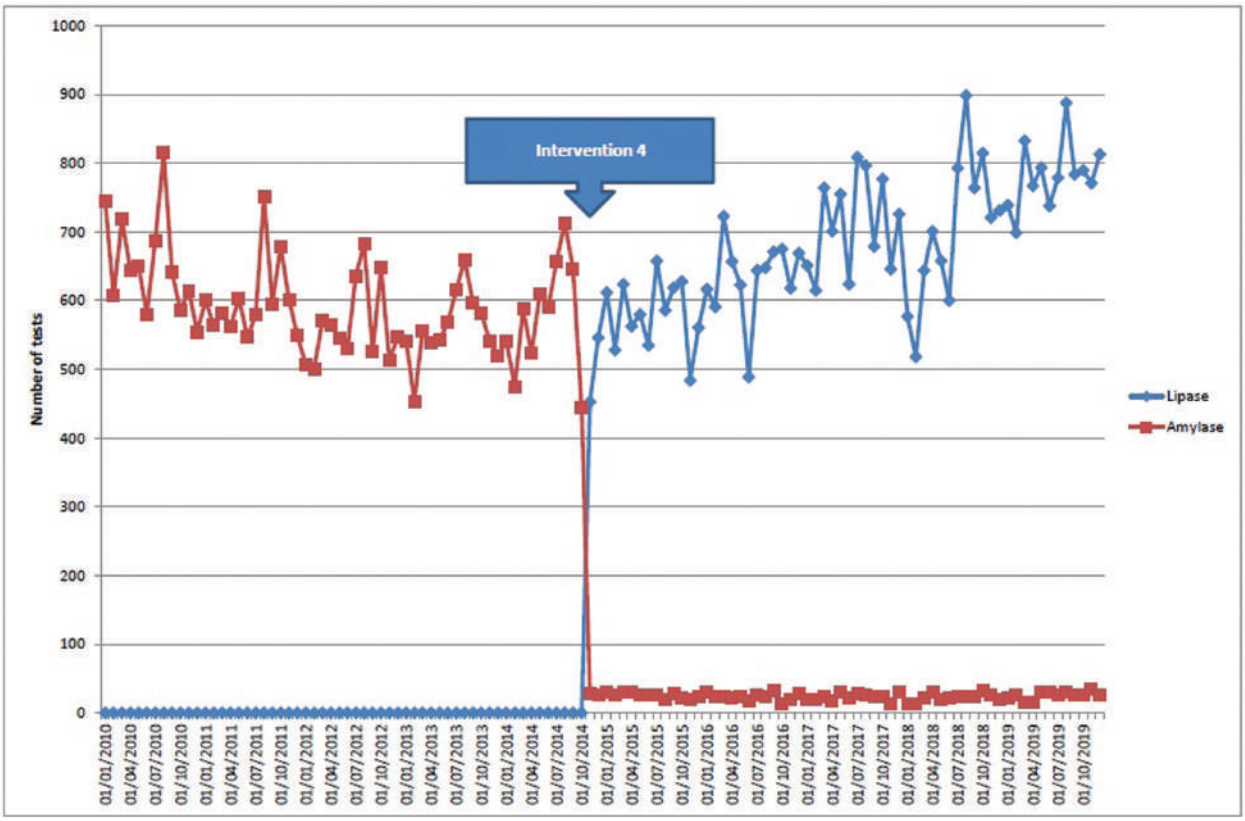

TABLE 1. Summary of Strategies Implemented and Economic and Activity Results

Intervention	Date	Summary	Workload Results	Economic Results ($)	Other Results
1	January 2012	Not measuring tBil when the icteric index is <2 mg/dL (34.2 µmol/L) and reporting through a comment	104,602 tBil tests requested; 10,322 tBil tests conducted; 94,280 tBil tests not conducted and reported through a comment	+22,492.83	…
2	October 2013	Remove tProt from the stat tests menu and include albumin	30,036 albumin tests conducted as a substitute for the tProt measurement	+15,625.18	14,718 patients (49%) showed albumin <3.5 g/dL
3	July 2014	Reporting albumin-adjusted calcium when there are low and high total calcium values	20,905 calcium tests conducted; 4124 calcium tests corrected per albumin	–1299.33	2480 patients corrected for hypocalcemia, 3 patients corrected for hypercalcemia
4	November 2014	Lipase measurement as a first marker and amylase just when lipase reaches certain values	Until November 2014, 34,341 amylase tests conducted; since November 2014, 41,962 lipase tests and 1497 amylase tests conducted	+16,929.62	…
5	(1) February 2016, (2) July 2019	Measuring plasma magnesium test: (1) when hypocalcemia and hypokalemia are present; and (2) when lipase is >600 IU/L	717 magnesium levels measured for hypocalcemia or hypokalemia; 123 magnesium levels measured for lipase values >600 IU/L	–374.15	350 patients diagnosed with hypomagnesemia

tBil, total bilirubin; tProt, total protein.
Total economic balance: $53,374.15.

TABLE 1 shows a summary of the strategies implemented and the economic and activity results. Regarding the overall aggregated financial implications, $53,374.15 was saved because of all the above interventions, when compared to the initial pattern.

Discussion

This study shows the consecutive interventions that involved laboratory tests in patients in the ED over a 10 year period. These changes involved test replacement such as plasma albumin for tProt and lipase

as the first marker for a pancreatitis diagnosis instead of amylase; newly offered tests, namely albumin-adjusted calcium and magnesium; sequential test measurement such as for amylase and albumin-adjusted calcium after lipase and calcium certain values were calculated; and finally test measurement at zero cost when reporting tBil through the icteric index. All these interventions resulted not only in the detection of relevant disorders that would otherwise have remained hidden, such as hypomagnesaemia and hypoalbuminemia, but also in economic savings. Stat testing needs to be adapted to advances in knowledge and technology, and hence changes in the stat laboratory test menu over the years are mandatory. The icteric index, a quantification of bilirubin or "icterus" interference, is currently measured in most of the chemistry analyzers at zero reagent cost. It identifies patients with abnormal tBil values, and only in these patients will the test will be conducted; it has a high efficiency in our stat laboratory, as were just measured 15% of the requested tests.

tProt replacement for albumin was agreed upon not just ED physicians, who pointed out its importance regarding patient prognosis when admitted to the hospital,[13] but also with gastroenterologists, who suggested it would help with better management of patients in the ED with ascites. Moreover, albumin can be utilized as part of a prediction model for 30-day mortality in older patients in the ED.[14] This intervention resulted in 3 important achievements: savings in reagent use; identification of a significant number of patients with low albumin values, suggesting potential malnutrition; and finally, although the best marker for hypocalcemia is ionized calcium, reporting albumin-adjusted calcium in patients with hypo- or hypercalcemia could avoid a second phlebotomy for ionized calcium measurement.

Amylase has been traditionally used in Spain as the stat laboratory marker for abdominal pain.[2,11] This trend is likely because lipase was introduced later than amylase in automatic chemistry analyzers.[16] Currently, however, it is not only included in the analyzers menu but is also considered a more economic test, with additional sensitivity and specificity[15] in the detection of pancreatitis. The proposed algorithm, with lipase as a first marker and amylase when lipase is abnormal, improves the diagnosis of acute pancreatitis[11] at a lower cost than when using amylase alone.

The last intervention involved magnesium, a very important cation that intervenes in more than 600 body reactions.[17] However, magnesium is still the forgotten test in medicine.[12] The high detection rate of hypomagnesemia indicates that it is mandatory to include magnesium in the stat laboratory menu or at least to conduct testing in patients with hypocalcemia, hypokalemia, and pancreatitis.[12]

These interventions have been published individually by the authors[2-6,10-12]; however, this article aims to show how, all together and over time, they contribute to improving patient management and reducing laboratory costs.

This study had certain limitations. Recently, there has been a trend for core laboratories to centralize rather than maintain dedicated stat laboratories focused on the ED; this trend may partially invalidate the generalization of our results. However, management experiences and interventions for a more efficient use of laboratory tests in the ED, especially when improving patient outcomes and use of resources, need to be shared.

Another limitation is that although there is still debate about whether it is better to measure albumin-adjusted calcium or ionized calcium, ionized calcium should become the reference method for measuring actual calcium status.[18] Nevertheless, measuring ionized calcium was a challenge because no specimens were available.

Finally, there are some other plasma stat tests, such as for cardiac markers, that were not considered in this study. And for the economic study, we only counted the cost of the reagent, but additional expenditures in personnel, specimen transport, and so on were not considered.

Conclusion

By using current laboratory knowledge and technologies, and in agreement with ED providers, changes and adaptations of the stat laboratory test menu in the complex and evolving ED setting resulted in the detection of new disorders and also economic savings.

REFERENCES

1. Kyriacou DN, Ricketts V, Dyne PL, McCollough MD, Talan DA. A 5-year time study analysis of emergency department patient care efficiency. *Ann Emerg Med.* 1999;34(3):326–335.
2. Salinas M, López-Garrigós M, Uris J; Pilot Group of the Appropriate Utilization of Laboratory Tests (REDCONLAB) Working Group. Differences in laboratory requesting patterns in the emergency department in Spain. *Ann Clin Biochem.* 2013;50(Pt 4):353–359.
3. Dolci A, Giavarina D, Pasqualetti S, Szőke D, Panteghini M. Total laboratory automation: do stat tests still matter? *Clin Biochem.* 2017;50(10–11):605–611.
4. Salinas M, López-Garrigós M, Flores E, Leiva-Salinas M, Lillo R, Leiva-Salinas C. Additional technician tasks and turnaround time in the clinical stat laboratory. *Biochem Med (Zagreb).* 2016;26(2):243–247.
5. Salinas M, López-Garrigós M, Santo-Quiles A, et al. Customising turnaround time indicators to requesting clinician: a 10-year study through balanced scorecard indicators. *J Clin Pathol.* 2014;67(9):797–801.
6. Salinas M, López-Garrigós M, Gutiérrez M, Lugo J, Llorca F, Uris J. Stat laboratory timeliness management according to clinician needs. *Clin Chem Lab Med.* 2011;49(2):331–333.
7. Sorita A, Steinberg DI, Leitman M, Burger A, Husk G, Sivaprasad L. The assessment of stat laboratory test ordering practice and impact of targeted individual feedback in an urban teaching hospital. *J Hosp Med.* 2014;9(1):13–18.
8. Rodriguez-Borja E, Villalba-Martinez C, Barba-Serrano E, Carratala-Calvo A. Failure to review STAT clinical laboratory requests and its economical impact. *Biochem Med (Zagreb).* 2016;26(1):61–67.
9. Volmar KE, Wilkinson DS, Wagar EA, Lehman CM. Utilization of stat test priority in the clinical laboratory: a College of American Pathologists q-probes study of 52 institutions. *Arch Pathol Lab Med.* 2013;137(2):220–227.
10. Salinas M, López-Garrigós M, Lugo J, Gutiérrez M, Flors L, Leiva-Salinas C. Diagnostic accuracy of icteric index to detect abnormal total bilirubin values. *J Clin Pathol.* 2012;65(10):928–933.
11. Salinas M, Flores E, López-Garrigós M, Díaz E, Esteban P, Leiva-Salinas C. Application of a continual improvement approach to selecting diagnostic markers for acute pancreatitis in an emergency department. *Emergencias.* 2017;29(2):113–116.
12. Salinas M, Flores E, López-Garrigós M, Puche C, Leiva-Salinas C. Automatic laboratory interventions to unmask and treat hypomagnesemia in the emergency department. *Clin Biochem.* 2020;75:48–52.
13. Valmorbida E, Trevisan C, Imoscopi A, Mazzochin M, Manzato E, Sergi G. Malnutrition is associated with increased risk of hospital

admission and death in the first 18 months of institutionalization. *Clin Nutr.* 2020;39(12):3687–3694.

14. Zelis N, Buijs J, de Leeuw PW, van Kuijk SMJ, Stassen PM. A new simplified model for predicting 30-day mortality in older medical emergency department patients: the rise up score. *Eur J Intern Med*. 2020;77:36–43.
15. Yadav D, Agarwal N, Pitchumoni CS. A critical evaluation of laboratory tests in acute pancreatitis. *Am J Gastroenterol.* 2002;97(6):1309–1318.
16. Fossati P, Ponti M, Paris P, Berti G, Tarenghi G. Kinetic colorimetric assay of lipase in serum. *Clin Chem.* 1992;38(2):211–215.
17. de Baaij JHF, Hoenderop JGJ, Bindels RJM. Magnesium in man: implications for health and disease. *Physiol Rev*. 2015;95(1):1–46.
18. Slomp J, van der Voort PH, Gerritsen RT, Berk JA, Bakker AJ. Albumin-adjusted calcium is not suitable for diagnosis of hyper- and hypocalcemia in the critically ill. *Crit Care Med.* 2003;31(5):1389–1393.

CASE STUDY

Identifying Glucocorticoid Insufficiency in Silent Corticotroph Adenoma with Elevated Adrenocorticotropic Hormone

Amnon Schlegel, MD, PhD[1,2,*]

[1]Endocrine Section, Medicine Service, Salt Lake City Veterans Affairs Medical Center, Salt Lake City, UT, US and; [2]Department of Internal Medicine, Division of Endocrinology, Metabolism and Diabetes, University of Utah School of Medicine, Salt Lake City, Utah, US; *To whom correspondence should be addressed. amnons@u2m2.utah.edu

Keywords: endocrine, clinical chemistry, pituitary, metyrapone, cortisol, adrenal

Abbreviations: SCA, silent corticotroph adenoma; ACTH, adrenocorticotropic hormone; OMST, overnight metyrapone stimulation test.

Laboratory Medicine 2022;53:91–94; DOI: 10.1093/labmed/lmab053

ABSTRACT

Silent corticotroph adenoma (SCA) is as an aggressive pituitary tumor. A 48 year old man developed hypogonadotrophic hypogonadism. The basal morning adrenocorticotropic hormone (ACTH) was elevated, but the basal morning and peak after ACTH (1–24) stimulation cortisol were normal. A 3.7 cm sellar mass with evidence of internal hemorrhage, encasement of the right internal carotid artery, and invasion of the right cavernous sinus were identified, resected, and stained positive for ACTH. Over the next 5 years, the basal morning ACTH and cortisol were normal, and imaging revealed the presence of a small residual tumor. One year later, the patient became fatigued and nauseated, with elevated ACTH. An overnight metyrapone stimulation test (OMST) revealed glucocorticoid insufficiency, without further increase in ACTH. Symptoms resolved with hydrocortisone treatment. This case study suggests that SCA can secrete an ACTH precursor that is detected by clinical assays but is not active biologically. Postoperative OMST reveals glucocorticoid insufficiency in this context.

Silent corticotroph adenoma (SCA) is an adenohypophyseal tumor that expresses pro-opiomelanocortin (encoding the POMC peptide) and produces adrenocorticotropic hormone (ACTH) but is not marked by clinical evidence of excess ACTH and cortisol action (ie, Cushing disease is absent). Because there is no accompanying clinical syndrome of cortisol excess, the immunohistochemical detection of ACTH may be inadvertently skipped on pathological examination of the resected tumor. Nevertheless, when identified, SCA is found to have a consistently aggressive natural history, with high rates of recurrence and a need for repeat surgery and radiotherapy.[1,2] This state makes recommendations for adjuvant therapies imprecise and counseling for long-term outcomes incomplete. Because SCA often recurs, firm diagnosis can improve therapeutic decisions. Indeed, in a large cohort of SCA, higher preoperative ACTH levels predict a higher recurrence rate.[3] The molecular basis for this more aggressive natural history is not known but may related to the gene regulatory network active in the tumor. Indeed, to improve diagnostic and therapeutic outcomes, the 2017 World Health Organization *Classification of Tumours of Endocrine Organs* emphasized the hormonal lineage of adenohypophyseal tumors.[4] Central to this classification guideline is a call for consistent staining of tumor specimens with hormonal and transcriptional regulator antibodies (the latter, once fully standardized and available commercially) for better diagnostic and prognostic yield.

Herein is a case study of SCA that was anticipated by comprehensive presurgical biochemical analyses undertaken for an initial presentation of hypogonadotrophic hypogonadism. The preoperative investigation revealed a repeatedly elevated basal, morning plasma ACTH with normal serum cortisol and a normal response to ACTH (1–24) stimulation testing. Appropriate immunohistochemical staining of the tumor specimen detected ACTH production. Repeated evaluation of basal and metyrapone-stimulated ACTH, cortisol, and (in the latter case) 11-deoxycortisol established the presence of glucocorticoid insufficiency 5 years after surgery.

Case Report

A previously eugonadal 48 year old man was referred for evaluation of weakness, fatigue, and hypogonadotrophic hypogonadism identified with 2 sets of morning gonadotrophins and total testosterone: Inappropriately low-normal follicle stimulating hormone (1.7 and 1.9 mIU/mL or 1.7 and 1.9 IU/L; normal range, 0.7–11.1 mIU/mL or 0.7–11.1 IU/L) and luteinizing hormone (1.3 and 1.0 mIU/mL or 1.3 and 1.0 IU/L; normal range, 0.8–7.6 mIU/mL or 0.8–7.6 IU/L), in light of very low total testosterone (57 and 42 ng/dL or 1.98 nmol/L and 1.46 nmol/L; normal range, 241–827 ng/dL or 8.4–28.7 nmol/L) were found. The patient was euthyroid (thyrotropin, 1.06 μIU/mL or 1.06 IU/L; normal range, 0.358–3.74 μ IU/mL or 0.358–3.75 mIU/L). His prolactin was slightly elevated (20.9 ng/

mL, or 20.9 μg/L; normal range, 2.93–21.9 ng/mL or 2.93–21.9 μg/L) and his IGF-1 was normal for age and sex (106 ng/mL or 13.9 nmol/L; normal range, 61–200 ng/mL or 8–26.2 nmol/L), respectively.

The basal morning ACTH and cortisol were measured 3 times. The ACTH was increased, and because the patient did not seem to have cortisol excess on clinical examination, this isolated increase in ACTH raised the possibility of imminent adrenocortical failure (**TABLE 1**). To evaluate the zona fasciculata's function, 250 μg of ACTH (1–24) was administered intramuscularly (ACTH stimulation test), and the rise in cortisol from a baseline measurement was assessed 30 and 60 minutes later. The peak cortisol in response to this injection was normal, 26.8 μg/dL (739 nmol/L), exceeding the minimum value (≥18 mcg/dL; 497 nmol/L) expected in a state of glucocorticoid sufficiency.

A 3.1 cm (craniocaudal) × 3.7 cm (anteroposterior) × 3.2 (mediolateral) sellar mass with evidence of internal hemorrhage encasing the right internal carotid artery, invading the right cavernous sinus, and causing leftward stalk deviation was identified on magnetic resonance imaging (**FIGURE 1**). The optic chiasm had antero-superior displacement; visual field testing did not reveal deficits and there was no evidence of increased intracranial pressure on dilated eye exam. The sellar mass was resected by a trans-sphenoidal approach. Stain for ACTH (1–39) was positive but negative for prolactin, human growth hormone, or thyrotropin beta subunit. The day after surgery (February 2, 2013), the patient's ACTH and cortisol were elevated. He was treated with testosterone cypionate 150 mg intramuscularly weekly.

Over the next 5 years, the basal morning ACTH ranged from 27.5 to 79.0 pg/mL (6.05 L–7.4 pmol/L; normal range, 7.2–63.3 pg/mL or 1.58–13.9 pmol/L), and the cortisol ranged from 7.19 to 12.2 μg/dL (198–337 nmol/L; normal range, 6.2–19.4 μg/dL or 171–535 nmol/L); the thyrotropin ranged from 0.69 to 2.88 IU/L, and the free thyroxine ranged from 0.66 to 0.88 ng/dL (8.5–11 pmol/L; normal range, 0.76–1.46 ng/dL or 9.8–18.8 pmol/L). In the sixth year after surgery, the patient became fatigued and nauseated; the 7 AM ACTH was elevated, but the cortisol was low (**TABLE 1**; May 21, 2018). His thyrotropin was normal twice (2.89 IU/L and 0.958 IU/L), but his free thyroxine was low (0.69 and 0.66 ng/mL, respectively; 8.9 and 8.5 pmol/L). Serum sodium, potassium, and glucose were normal. The urine free cortisol excretion was at the lower end of the normal range: 6 μg/24 hours (165 nmol/24 hours; normal range, 5–64 μg/24 hours or 138–1,770 nmol/24 hours) in a valid specimen containing 2.65 g (23.4 mmol) creatinine. A 4 g (exceeding the usual 3 g limit because the patient's mass was 153 kg, bringing the dose to 26 mg/kg, close to the usual 30 mg/kg dose) overnight metyrapone stimulation test (OMST) showed an insufficient rise in 11-deoxycortisol and low concurrent cortisol. The elevated ACTH did not increase in comparison to a value obtained 3 weeks earlier (**TABLE 1**).

Hydrocortisone was initiated at 20 mg at 8 AM and 10 mg at 5 PM for 6 months and then decreased to 20 mg at 8 AM and 5 mg at 5 PM. The final daily hydrocortisone dose was 10 times the body surface area (in mg), a standard replacement amount. Subsequently, the patient began levothyroxine (1.5 μg/kg/day). All symptoms resolved. Eight years after the resection, the residual tumor did not show evidence of growth.

Discussion

Since its first description in autopsy specimens,[5] SCA has been found repeatedly to represent approximately 10% of seemingly nonfunctioning pituitary tumors.[1,3,6] Careful radioimmunometric studies with assorted antibodies detecting POMC fragments have convincingly revealed that these tumors can produce precursors of ACTH (1–39) that fail to cause Cushing disease (ie, they fail to activate the melanocortin 4 receptor and cause a clinical syndrome of cortisol excess).[7] Unfortunately, these immunometric reagents for detecting POMC fragments are not available commercially. Conversely, commercial ACTH-detecting immune reagents cross-react variably with POMC fragments.[8] Thus, at present, SCA remains a diagnostic challenge and may even be missed if systematic staining of the tumor is not performed postoperatively. Fortunately, direct measurement of ACTH is in development,[9] and this liquid chromatograph-tandem mass spectrometry (LC-MS/MS) quantification of ACTH(1–39), ACTH(1–24), pro-ACTH, or POMC fragments will be useful in SCA. As discussed below, metyrapone stimulation is the best option for evaluating the development of central glucocorticoid deficiency after resection of an SCA.

TABLE 1. Select Basal, ACTH-Stimulated, and Metyrapone-Stimulated Laboratory Tests.

Date	Time	ACTH (7.2–63.3 pg/mL; 1.58–13.9 pmol/L)[a]	Cortisol (6.2–19.4 μg/dL; 171–535 nmol/L)[b]	Cortisol 0 Min (μg/dL; nmol/L)[b]	Cortisol 30 Min (μg/dL; nmol/L)[b]	Cortisol 60 Min (μg/dL; nmol/L)[b]	11-Deoxycortisol (μg/dL, >7; 203 nmol/L)[c]
July 16, 2012	08:30	117.8 (25.92)	7.66 (211)	…	…	…	…
August 13, 2012	08:40	95.0 (20.9)	7.18 (198)	…	…	…	…
November 2, 2012	10:12			8.01 (221)	24.32 (671)	26.8 (739)	…
November 23, 2012	08:13	100.7 (22.15)	9.55 (263)	…	…	…	…
February 2, 2013	12:20	290.0 (63.8)	33.6 (927)	…	…	…	…
May 21, 2018	08:01	159.1 (35.0)	2.9 (80)	…	…	…	…
June 11, 2018	08:01	154.3 (33.95)	2.2 (61)	…	…	…	6.36 (184)

ACTH, adrenocorticotropic hormone; OMST, overnight metyrapone stimulation test.
A 250 μg ACTH (1–39) stimulation test was performed on November 2, 2012. The patient ingested metyrapone 4 g at 11 PM on June 10, 2018, with laboratory collection the next morning. Normal value ranges for ACTH and cortisol are for morning, unstimulated specimens; for 11-deoxycortisol, the normal response from a 30 mg/kg OMST test is shown.
[a]ACTH was measured by electrochemiluminescence immunoassay, LabCorp, Phoenix, AZ.
[b]Cortisol was measured by electrochemiluminescence immunoassay, an in-house assay.
[c]11-deoxycortisol was measured by high-pressure liquid chromatograph-tandem mass spectrometry (Esoterix, Calabasas Hills, CA).

FIGURE 1. **Coronal (upper) and sagittal (lower) T1-weighed presurgical (left) and 6 years postsurgical (right) magnetic resonance imaging. Note that the presurgical sagittal image was obtained after an injection of gadolinium.**

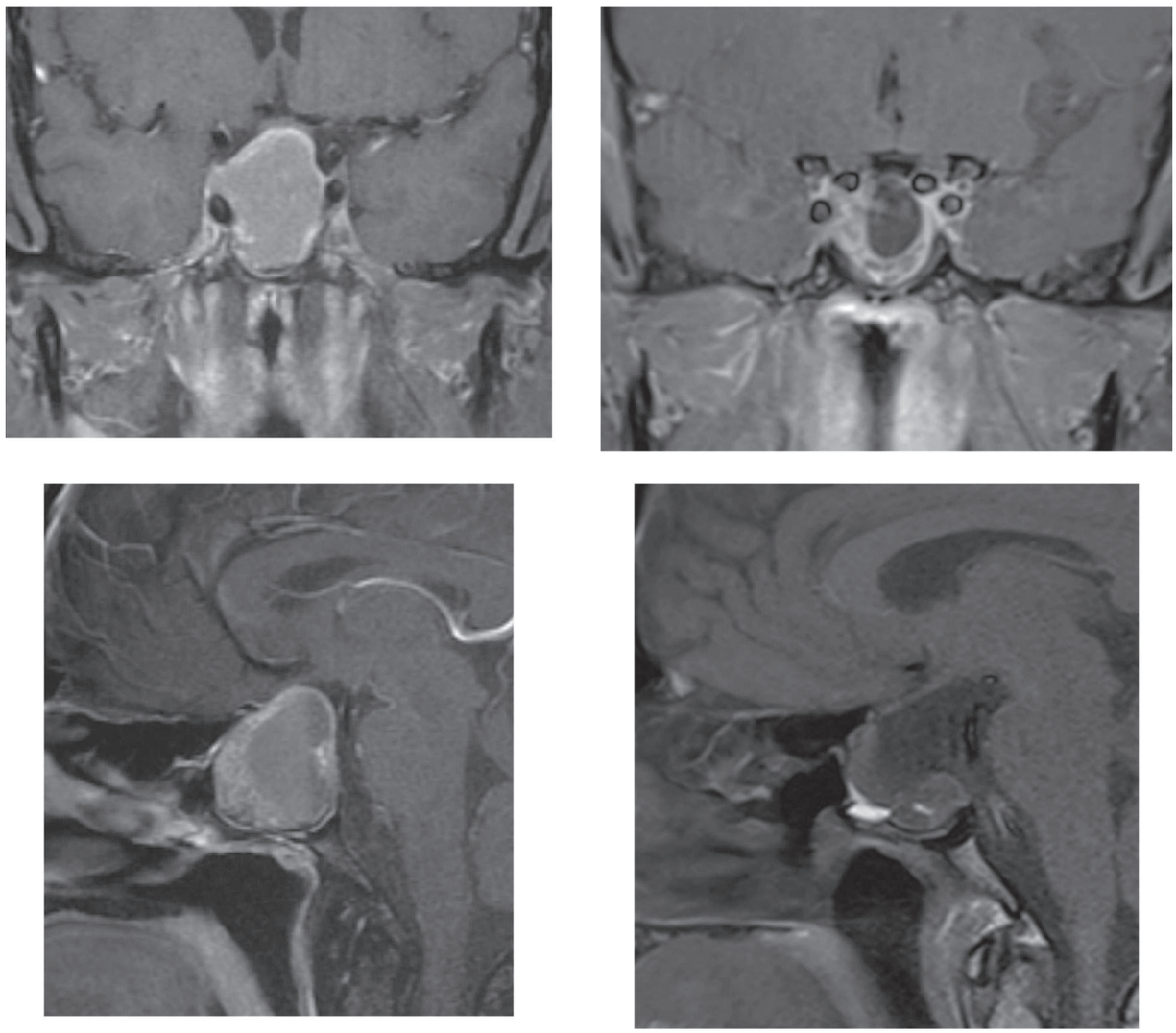

The patient had high preoperative ACTH that prompted the performance of an ACTH(1–24) stimulation test to exclude glucocorticoid deficiency before surgery. He tolerated trans-sphenoidal resection without administration of preoperative glucocorticoid therapy and had clearly and appropriately elevated cortisol immediately after surgery.

This patient was unusual for several reasons. First, there was no recurrence of the SCA despite several predictors of recurrence. Specifically, the initial presentation of a macroadenoma that had undergone internal hemorrhage and had invaded several structures and the elevated preoperative ACTH were not accompanied by recurrence after a single resection.[3] Second, there was sufficient normal ACTH production to cause elevated cortisol immediately postoperatively, indicating that there was biologically active ACTH (1–39) production immediately preoperatively. Third, there was a 5-year delay between surgical resection and the development of glucocorticoid (and thyroid) deficiency.

Identifying persons with post–pituitary surgery central glucocorticoid deficiency is a challenge in that measurements of early-morning cortisol and ACTH are inadequate predictors of the ability to mount a response to stress in this axis. As advocated in earlier research based on an analysis of cohorts subjected to various dynamic endocrine tests, compared to ACTH (1–24) stimulation testing, OMST is a superior test for establishing postpituitary surgical glucocorticoid insufficiency, exceeding the utility of repeat ACTH (1–24) stimulation testing in both positive and negative predictive value.[10-12] The best receiver operating characteristic is achieved when the sum of cortisol and 11-deoxycortisol exceeds 15 μg/dL (approximately 400 nmol/L), excluding the glucocorticoid deficiency with the greatest confidence.[11] The diagnostic value of this sum of clinically measured hormones after OMST recapitulates the observations made by the initial developers of the single-dose OMST, who also observed a high ratio of reduced (active) to administered metyrapone in normal responders.[13] With concurrent measurement of ACTH (outside the rare patient with SCA with incompletely processed ACTH), the OMST allows one to define a partial central glucocorticoid state that might require stress dose therapy during intercurrent illness or surgery but no treatment otherwise.[11] One important caveat to interpreting OMST results is the 15 μg/dL cutoff: This cutoff was devel-

oped using immune assays for 11-deoxycortisol and cortisol that had known high cross-reactivity.[7] Because the patient's 11-deoxycortisol was measured in a commercial laboratory using an industry-standardized LC-MS/MS platform, additional studies are needed to refine and perhaps redefine the results of OMST.

More broadly, repeated testing, especially in asymptomatic patients post-pituitary surgery seems warranted. In a series of 32 patients who had undergone resection of adenohypophyseal masses (excluding corticotroph adenomas), OMST or a 9 AM intravenous insulin tolerance test (as adjudicated by cortisol) seemed to identify more patients who had central glucocorticoid deficiency.[14] This finding may reflect how the OMST was scored: 11-deoxycortisol >7.25 μg/dL (210 nmol/L) was deemed normal, and all patients achieved a cortisol suppression to <7.25 μg/dL (210 nmol/L), but the sum of 11-deoxycortisol and cortisol was not reported or analyzed. Nevertheless, long-term follow-up showed no difference in the ability to remain off hydrocortisone treatment in those patients (7 of 26) who failed the OMST but had normal responses to insulin-induced hypoglycemia. In a previous head-to-head comparison of OMST (using the same cutoff of 11-deoxycortisol >7.25 μg/dL, or 210 nmol/L) and insulin-induced hypoglycemia, 1 of 17 patients with a normal OMST had a subnormal response to insulin-induced hypoglycemia, and no patients who failed the OMST but had normal responses to insulin-induced hypoglycemia were reported (total cohort excluding primary adrenal insufficiency was 380 patients).[15]

More recently, a 4-hour, 40 mg/kg metyrapone stimulation test (MST) was reported. Patients (11 of 25 with pituitary adenomas) ingested 40 mg/kg metyrapone at 8 AM, and their ACTH and cortisol levels were measured at 0, 60, 120, and 240 minutes. From a receiver operating characteristic analysis, plasma ACTH concentration exceeding 87.1 pg/mL (19.2 pmol/L) at 120 minutes was predictive of the lack of need for exogenous glucocorticoid therapy.[16] Critically, cortisol was suppressed maximally between 60 and 240 minutes in this 4-hour, 40 mg/kg MST, suggesting that 0- and 120-minute measurements of ACTH and cortisol might suffice in using this MST. This 4-hour, 40 mg/kg MST may prove particularly helpful in evaluating the much larger population of patients experiencing iatrogenic central glucocorticoid deficiency and seeking a firmer prognosis on if or when they can taper exogenous glucocorticoids. This study did not include measurement of 11-deoxycortisol and thus would not help in the evaluation of patients with SCA and elevated ACTH precursors.

Conclusion

This case study shows that SCA poses diagnostic challenges in that preoperative ACTH may be clearly elevated, yet there are no features of glucocorticoid excess. Conversely, the biological activity of the measured ACTH may be diminished because of incomplete processing to the mature hormone. Because this tumor has an aggressive natural history, firm biochemical and histopathological diagnoses are required. If the elevation of ACTH persists after surgical treatment, then an MST will be superior for establishing postsurgical central glucocorticoid deficiency because it safely interrogates all 3 levels of the corticotropin-releasing hormone neuronal-corticotroph cellular-adrenal zona fasciculata axis.

REFERENCES

1. Fountas A, Lavrentaki A, Subramanian A, Toulis KA, Nirantharakumar K, Karavitaki N. Recurrence of silent corticotroph adenomas after primary treatment: a systematic review and meta-analysis. *J Clin Endocrinol Metab.* 2018;104(4):1039–1048.
2. Jahangiri A, Wagner JR, Pekmezci M, et al. A comprehensive long-term retrospective analysis of silent corticotrophic adenomas vs hormone-negative adenomas. *Neurosurgery.* 2013;73(1):8–17.
3. Langlois F, Lim DST, Yedinak CG, et al. Predictors of silent corticotroph adenoma recurrence; a large retrospective single center study and systematic literature review. *Pituitary.* 2018;21(1):32–40.
4. Mete O, Lopes MB. Overview of the 2017 WHO classification of pituitary tumors. *Endocr Pathol.* 2017;28(3):228–243.
5. Mosca L, Buffa R, Castello A, Gaspa L. Recherche d'une sécrétion dan les microadénomes hypophysaires humains. *Rev Fr Endocr Clin Nutr Metab.* 1975;16(5):433–443.
6. Horvath E, Kovacs K, Killinger DW, Smyth HS, Platts ME, Singer W. Silent corticotropic adenomas of the human pituitary gland: a histologic, immunocytologic, and ultrastructural study. *Am J Pathol.* 1980;98(3):617–638.
7. Braithwaite SS, Clasen RA, D'Angelo CM. Silent corticotroph adenoma: case report and literature review. *Endocr Pract.* 1997;3(5):297–301.
8. Monaghan PJ, Kyriacou A, Sturgeon C, et al. Pro-opiomelanocortin interference in the measurement of adrenocorticotrophic hormone: a United Kingdom National External Quality Assessment Service study. *Clin Endocrinol (Oxf).* 2016;85(4):569–574.
9. Shi J, Dhaliwal P, Zi Zheng Y, et al. An intact ACTH LC-MS/MS assay as an arbiter of clinically discordant immunoassay results. *Clin Chem.* 2019;65(11):1397–1404.
10. Agha A, Tomlinson JW, Clark PM, Holder G, Stewart PM. The long-term predictive accuracy of the short synacthen (corticotropin) stimulation test for assessment of the hypothalamic-pituitary-adrenal axis. *J Clin Endocrinol Metab.* 2006;91(1):43–47.
11. Berneis K, Staub JJ, Gessler A, Meier C, Girard J, Müller B. Combined stimulation of adrenocorticotropin and compound-S by single dose metyrapone test as an outpatient procedure to assess hypothalamic-pituitary-adrenal function. *J Clin Endocrinol Metab.* 2002;87(12):5470–5475.
12. Giordano R, Picu A, Bonelli L, et al. Hypothalamus–pituitary–adrenal axis evaluation in patients with hypothalamo–pituitary disorders: comparison of different provocative tests. *Clin Endocrinol.* 2008;68(6):935–941.
13. Spiger M, Jubiz W, Meikle AW, West CD, Tylor FH. Single-dose metyrapone test: review of a four-year experience. *Arch Intern Med.* 1975;135(5):698–700.
14. Courtney CH, McAllister AS, McCance DR, et al. The insulin hypoglycaemia and overnight metyrapone tests in the assessment of the hypothalamic–pituitary–adrenal axis following pituitary surgery. *Clinical Endocrinology.* 2000;53(3):309–312.
15. Fiad TM, Kirby JM, Cunningham SK, McKenna TJ. The overnight single-dose metyrapone test is a simple and reliable index of the hypothalamic-pituitary-adrenal axis. *Clin Endocrinol (Oxf).* 1994;40(5):603–609.
16. Noe S, von Werder A, Iakoubov R, et al. Dynamics of adrenocorticotropin after application of metyrapone. *Exp Clin Endocrinol Diabetes.* 2017;125(1):53–56.

Variant Acute Promyelocytic Leukemia Presenting Without Auer Rods Highlights the Need for Correlation with Cytogenetic Data in Leukemia Diagnosis

Elizabeth L. Courville, MD,[1,] Lindsey Shantzer, MD,[2] Hans Christoph Vitzthum von Eckstaedt V, BS,[2] Holly Mellot, BSN,[2] Michael Keng, MD,[2] Jeremy Sen, PharmD,[2] Amy Morris, PharmD,[2] Eli Williams, PhD,[1] Firas El Chaer, MD[2]*

[1]Department of Pathology and; [2]Department of Medicine, Division of Hematology and Oncology, University of Virginia School of Medicine, Charlottesville, Virginia, US; *To whom correspondence should be addressed. courville@virginia.edu

Keywords: acute promyelocytic leukemia, venetoclax, bcl2 inhibitor, t(11;17), variant acute promyelocytic leukemia, *ZBTB16*

Abbreviations: vAPL, variant acute promyelocytic leukemia; CBC, complete blood cell; CMML, chronic myelomonocytic leukemia; FISH, fluorescence in situ hybridization; AML, acute myeloid leukemia; G-CSF, granulocyte-colony stimulating factor; CR, complete remission; APL, acute promyelocytic leukemia; ATRA, all-trans retinoic acid.

Laboratory Medicine 2022;53:95–99; DOI: 10.1093/labmed/lmab051

ABSTRACT

Variant acute promyelocytic leukemia (vAPL) is a rare leukemia characterized by rearrangement between *RARα* and a non-*PML* partner gene. This type of leukemia can be difficult to recognize by histomorphologic evaluation, particularly in patients with few or no Auer rods, and by flow cytometry, but it can be identified by distinct cytogenetic features. Herein, we report on a patient with vAPL with t(11;17)(q23;q21) who presented an initial diagnostic challenge. Detailed flow cytometry findings are presented for this rare entity. Our case study also presents novel treatment (chemotherapy in combination with venetoclax) chosen based on mechanistic data from preclinical studies.

Clinical History

A 44 year old male patient presented with a flu-like illness. Leukocytosis and thrombocytopenia were identified on complete blood cell (CBC) count. Based on a bone marrow biopsy performed and interpreted at an outside facility, he was diagnosed with chronic myelomonocytic leukemia (CMML) with increased blasts. After 5 cycles of decitabine over 5 months, he was admitted to our institution with hip pain.

We reviewed the original bone marrow biopsy in conjunction with a repeat bone marrow biopsy performed at our institution to assess the status of disease. Review of the original bone marrow biopsy slides revealed a hypercellular marrow with numerous (67%) atypical promyelocytes and immature cells at the promyelocyte-myelocyte stage (**FIGURE 1A**). Auer rods were not identified on careful review. Megakaryocytes were decreased, and there were scant erythroid precursors. Flow cytometry reportedly showed an abnormal granulocytic maturation pattern with decreased CD16 and CD10 expression and partial CD56 expression (plots not received for review). The peripheral blood was notable for leukocytosis, anemia, and mild thrombocytopenia (CBC data presented in **TABLE 1**). Numerous atypical leukocytes consistent with promyelocytes and myelocytes and hypogranular mature segmented neutrophils were seen on review of the peripheral smear. By report, fluorescence in situ hybridization (FISH) analysis of the peripheral blood was negative for t(15;17) fusion but revealed 3 copies of chromosome 17, and karyotype analysis showed 45,X,-Y,t(11;17)(q23;q21)[20]. A karyotype on the bone marrow was attempted but had an insufficient number of cells for culture.

The bone marrow biopsy performed at our institution after 5 cycles of decitabine was processed for morphologic evaluation using standard methods. Bone marrow aspirate slides were Wright-Giemsa stained using an automated slide stainer (ELITechGroup/Wescor Model 7152; Puteaux, France). The findings were similar to the original biopsy with 80% atypical promyelocytes and cells at the promyelocyte-myelocyte stage. However, in contrast, there were occasional easily identifiable Auer rods within atypical mononuclear cells in the repeat bone marrow (**FIGURE 1B**). Flow cytometric analysis of the patient's bone marrow was performed using a 6-color FACSCanto II (Becton Dickinson Biosciences, BD, San Jose, CA) analyzer using our standard 4-tube myeloid panel, listed in **TABLE 2**. The flow cytometry was interpreted as "no increase in myeloid blasts" based on the evaluation of a CD45dim by low side-scatter gate and CD34 expression. Although not evaluated at the time, the high side-scatter "granulocyte-gate" was evaluated retrospectively and shown to have the following immunophenotype: positive for CD4 (dim), CD9, CD13 (bright homogeneous), CD15 (partial), CD33 (bright homogeneous), CD56, CD64, CD117 (partial), and CD123 (partial), and negative for CD11b, CD11c, CD34, CD14, and HLA-DR. Flow cytometry plots are shown in **FIGURE 2**.

Cytogenetic and molecular analysis was performed on the bone marrow aspirate using standard methods. A comprehensive FISH analysis for CMML-associated abnormalities was performed, and all probe sets showed normal signal patterns. Furthermore, FISH using a standard dual-color dual-fusion t(15;17) probe set indicated an additional *RARα* signal (**FIGURE 1C**). Given bone marrow morphology, this finding

FIGURE 1. **Bone marrow morphologic findings and results of FISH/karyotype analysis. (A) Aspirate smears from original bone marrow biopsy showed numerous atypical mononuclear cells with round nuclear contours, fine to moderately condensed nuclear chromatin, and abundant cytoplasm with secondary granules. (B) Aspirate smears from the repeat bone marrow biopsy performed after 5 cycles of decitabine showed similar findings; however, there were darker and more abundant cytoplasmic granules and occasional cells with multiple Auer rods (inset). (A and B, 100× objective, Wright-Giemsa stain). (C) FISH analysis on interphase nuclei using a standard dual-color, dual-fusion probe set for t(15;17) revealed the presence of 2 red signals (*PML*) and 3 green signals (*RARA*), consistent with an atypical *RARA* translocation. (D) G-banded karyotype analysis revealed the presence of a t(11;17)(q23;q21) (arrowed) and a loss of the Y chromosome. FISH, fluorescence in situ hybridization.**

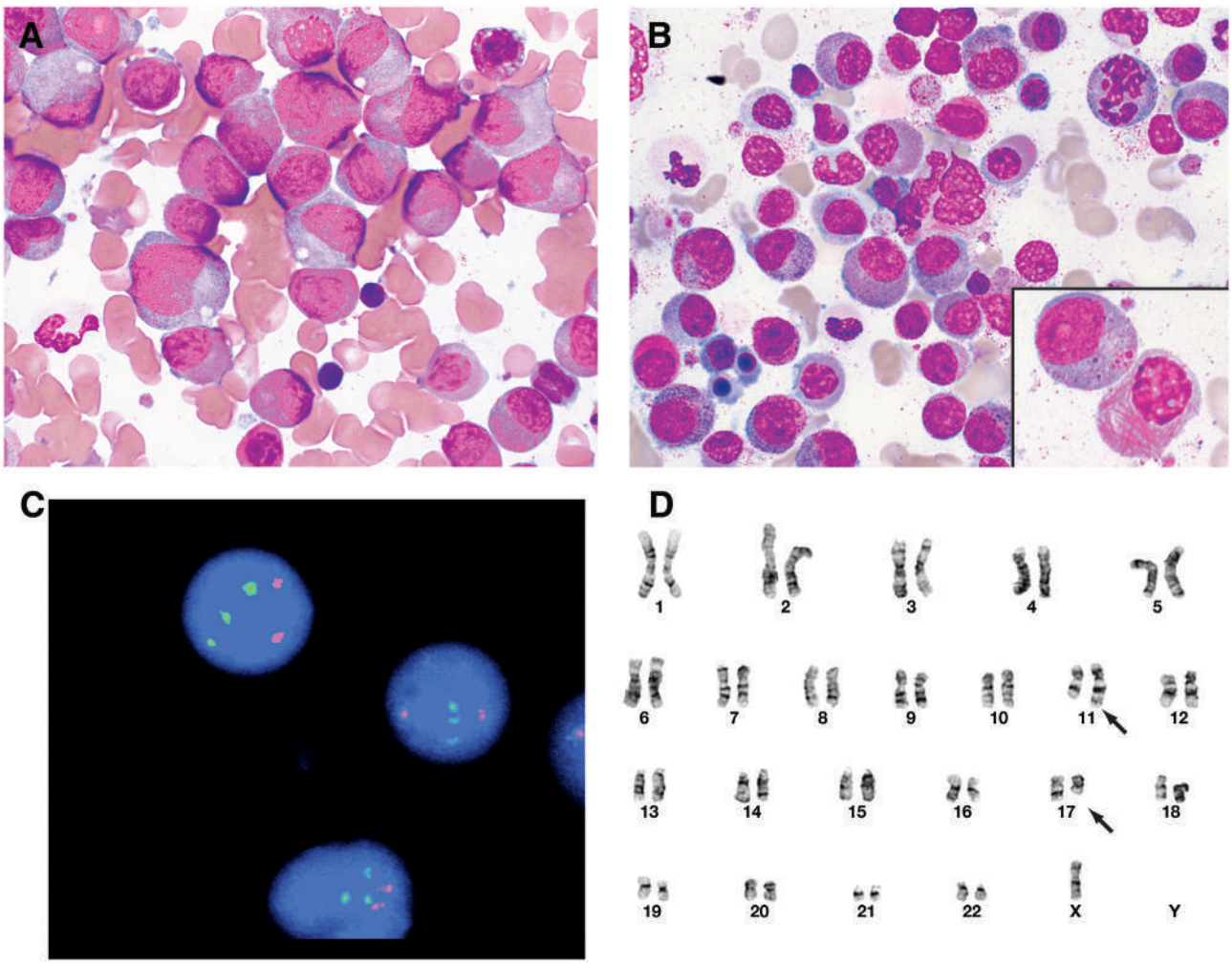

TABLE 1. **CBC Values**

	WBC (K/uL)	RBC (M/uL)	Hb (g/dL)	Hct (%)	MCV (fL)	Platelets (K/uL)
Initial presentation	58	2.6	8.7	25.9	99.6	142
Presentation at our institution (after 5 cycles of decitabine)	35.2	2.3	8.4	25.3	109.1	136
Reference range	4–11	4.6–6.2	14–18	40–52	83–95	150–450

CBC, complete blood cells; Hb, hemoglobin; Hct, hematocrit; MCV, mean corpuscular volume; RBC, red blood cells; WBC, white blood cells.

TABLE 2. **Flow Cytometry Myeloid Panel**

FITC	PE	PerCP-Cy5.5	PE-Cy7	APC	APCH7
CD13	CD33	CD34	CD56	CD117	CD45
CD64	CD11c	CD4	CD56	CD14	CD45
CD15	CD123	CD34	CD4	CD11b	CD45
HLA-DR	CD9	CD19	CD5	CD2	CD45

APC, allophycocyanin; APC-H7, APC-cyanine conjugate; FITC, fluorescein isothiocyanate; PE, phycoerythrin; PerCP-Cy 5.5, peridinin chlorophyll protein complex-cyanine conjugate; PE-Cy7, PE-cyanine conjugate.
All antibodies are from BD Biosciences.

FIGURE 2. Flow cytometry findings. Flow cytometry scatterplots from the repeat bone marrow biopsy. Lymphocytes are blue, monocytes are green, and the population of interest with high-side scatter is purple. The canonical blast gate (CD45 dim and low side-scatter) showed only few cells with a heterogeneous staining pattern. CD34 and CD19 staining in the PerCP-Cy5.5 channel was interpreted as high background; unfortunately, neither an isotype control nor a fluorescence minus one tube could be performed because of the retrospective nature of the evaluation.

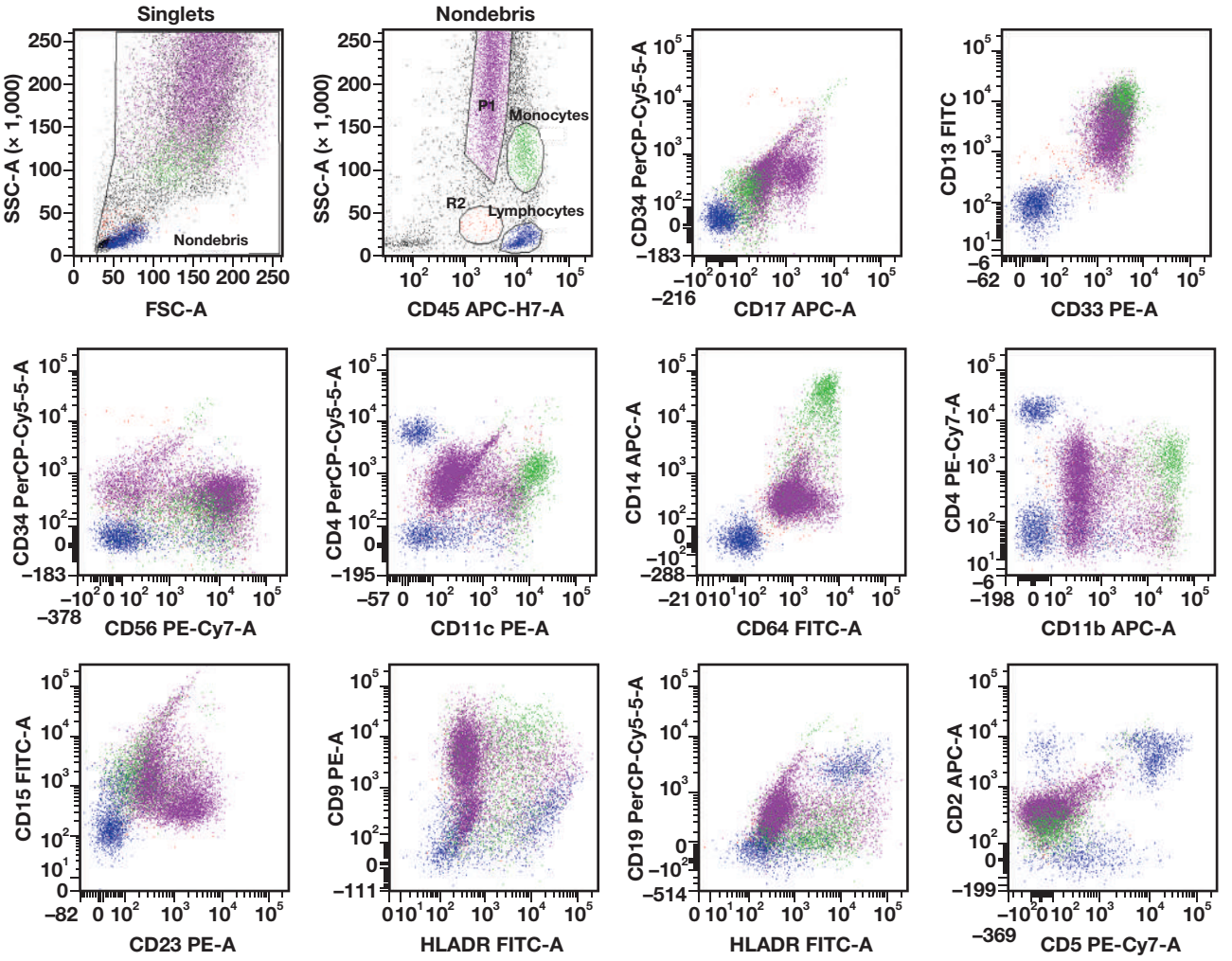

suggested a disruption of *RARα* because of a translocation with a non-*PML* partner rather than an additional copy of the *RARα* locus. Subsequent karyotype analysis identified a t(11;17)(q23;q21), confirming vAPL, and loss of the Y chromosome in 18 of the 20 cells examined (**FIGURE 1D**). We did not perform additional testing to confirm the *ZBTB16/RARα* gene fusion. Next-generation sequencing of the bone marrow aspirate using a 54-gene panel revealed an NRAS p.G12D variant (NM_002524.4; variant allele fraction [VAF] = 24%) and a CDKN2A splice-site variant (NM_058197.4; c.193 + 1G > A; VAF = 54%).

The patient was started on a novel acute myeloid leukemia (AML) regimen using fludarabine, cytarabine, granulocyte-colony stimulating factor (G-CSF), idarubicin and venetoclax.[1] On day 2, the patient developed disseminated intravascular coagulopathy as a complication of G-CSF. He received blood products per standard thresholds with no evidence of bleeding or thrombosis. He tolerated the remainder of chemotherapy well, but subsequent G-CSF was held. Day 21 (D + 21) bone marrow biopsy showed necrosis without leukemia. Upon count recovery (D + 34), the bone marrow was 70% cellular with normal trilineage hematopoiesis and no increase in blasts or blast equivalents, consistent with complete remission (CR). The FISH to evaluate for an extra *RARα* signal was negative, and measurable residual disease testing by flow cytometry from the aspirate was negative. After 3 cycles of consolidation with fludarabine, cytarabine, and venetoclax and 6 months of follow-up, his disease remains in CR with continued measurable residual disease negativity.

Discussion

Research has shown that vAPL is a rare leukemia characterized by rearrangement between *RARα* and a non-*PML* partner gene. Less than 5% of APLs lack the classic translocation t(15;17) and are instead characterized by non-*PML* translocations involving the *RARα* gene. Described variant fusion partners include *ZBTB16* (previously termed *PLZF*), *NPM1, NUMA1,* and *STAT5b,* among others, with *ZBTB16/RARα* being the most common. Leukemia morphology and response to all-trans retinoic acid (ATRA) depend on the variant partner.[2] Studies have shown

that *ZBTB16/RARα* APL blasts are distinct from classic APL, with more regular nuclei with condensed chromatin and abundant cytoplasm with coarse granules and fewer Auer rods.[3] If a pathologist is not attuned to the possibility of this morphology, then the blasts could be interpreted as atypical monocytes or dysplastic granulocytes. Patients with few or no Auer rods can be particularly challenging. The identification of Auer rods on standardized College of American Pathologists proficiency testing surveys shows high proficiency among participants; however, variation in staining methods used among special hematology laboratories may introduce variability in Auer rod visualization. Stains other than Wright-Giemsa have been proposed in the past to aid in the detection of Auer rods[4,5]; however, these are not in routine clinical use.

Compounding the difficulty in recognizing this entity are the flow cytometry features. Flow cytometry features in APL with t(15;17) have been well described.[6-8] In classic APL with t(15;17), there is typically a predominant population of atypical promyelocytes with markedly increased side-scatter, sometimes mistaken for normal maturing granulocytes. The classic APL blast population is predominantly positive for CD13, CD33, CD64, and CD117 and negative for HLA-DR, CD10, CD11b, CD11c, and CD14. Small subsets of patients are positive for CD2, CD4, CD34, and CD56. In hypogranular APL or in patients with the bcr3 transcript of the *PML-RARA* fusion gene, the blasts are frequently positive for CD2 and CD34. Sainty et al[3] assessed the immunophenotypic features of 7 patients with vAPL with *ZBTB16/RARα* fusion. The patients were universally negative for HLA-DR and CD34 and positive for CD13, with 6/7 positive for CD33 and 4/6 positive for CD56; the results of CD117 and CD15 staining were not provided. Other reports have documented CD117 staining in *ZBTB16/RARA* vAPL.[9] Immunophenotypic profiling of granulocytes was not a standard part of our flow cytometry evaluation, delaying the identification of the population of interest and somewhat limiting the interpretation (isotype controls and additional immunophenotypic markers could not be added). Our patient showed bright and homogeneous CD13 and CD33 expression and partial CD117 but lacked CD11b, compatible with a cell at the promyelocyte-myelocyte stage. There was aberrant expression of CD4, CD56, and partial CD123 and partial CD15 expression.

This case study emphasizes the vital importance of correlation with cytogenetic analysis in the diagnosis of a new leukemia. Most AML FISH analyses employ standard t(15;17) probe sets, which reveal an additional signal for *RARα* in variant APLs, as in our patient. Correct interpretation of this additional *RARα* signal as a disruption of *RARα,* rather than an additional copy of the *RARα* locus, is key to the timely and accurate diagnosis of variant APL. Karyotype analysis aids this interpretation by indicating a translocation involving the *RARα* locus (17q21). Karyotype analysis also indicates the putative translocation partner by ascertaining the t(11;17) (q23;q21). Direct confirmation of the *ZBTB16/RARα* fusion requires custom FISH probes or polymerase chain reaction primers, which are unavailable in most clinical laboratories because of the rarity of this entity.

Research has shown that vAPL with *ZBTB16/RARA* shows poor response to ATRA and arsenic-based APL treatments and traditional AML regimens.[10] Preclinical work suggests key functional differences between *PML/RARα* and *ZBTB16/RARα* fusion proteins underlying the refractoriness of *ZBTB16/RARα* vAPL. Both *RARα* portions are identical; they recruit nuclear corepressors that complex with histone deacetylases and form corepressors that downregulate targets of retinoic acid, preventing transcription and eventual cellular differentiation.[11] In vAPL, *ZBTB16* recruits additional corepressors via its *POZ/BTB* binding domain. This binding cannot be reversed by ATRA, leading to ATRA insensitivity.[12] The *ZBTB16/RARα* fusion protein has also been shown in vitro to have anti-apoptotic activity, supporting the survival of quiescent immature cells. This activity has been proposed as a contributing mechanism to myeloid differentiation resistance.[13]

Although strong treatment guidelines for vAPL are lacking, the current recommendation is management with AML-like approaches in ATRA-resistant variants.[10,14] Interestingly, our patient was first treated for 5 months with decitabine, a hypomethylating agent, with minimal clinical improvement and without any evidence of disease remission. Decitabine has been used in the treatment of vAPL as part of combination chemotherapy and has been reported to successfully treat a patient with vAPL using a *STAT5B/RARA* fusion transcript, with achievement of molecular remission.[14,15] After the vAPL diagnosis at our institution, the patient was treated with fludarabine, cytarabine, G-CSF, idarubicin and venetoclax, a regimen recently shown to result in high rates of CR in the setting of relapsed/refractory AML.[1] Based on preclinical studies, we hypothesized that the G-CSF component of this regimen could overcome the differentiation block in vAPL, as was shown in in vitro murine 32Dc13 cells expressing the *ZBTB16* gene.[13] In retrospect, G-CSF should have been avoided during induction, given the risk of disseminated intravascular coagulopathy that our patient experienced.[16] In addition, we hypothesized that venetoclax, a *BCL-2* inhibitor and promoter of apoptosis, may be effective in combating apoptosis dysregulation inherent to these variant cancers.[13]

This case report presents a challenging morphologic and flow cytometric presentation of vAPL, emphasizing the vital importance of both awareness of this entity and correlation with cytogenetic findings. Detailed flow immunophenotypic data are presented for this rare entity. In addition, our case study presents the novel treatment of this entity with chemotherapy in combination with venetoclax, based on mechanistic data from preclinical studies.

Acknowledgments

All authors drafted the manuscript, provided critical revisions, gave final approval, and agreed to be accountable for the work. The authors have no relevant conflicts of interest to report.

REFERENCES

1. Aboudalle I, Konopleva MY, Kadia TM, et al. A phase Ib/II study of the BCL-2 inhibitor venetoclax in combination with standard intensive AML induction/consolidation therapy with FLAG-IDA in patients with newly diagnosed or relapsed/refractory AML. *Blood*. 2019;134(Supplement_1):176.
2. Adams J, Nassiri M. Acute promyelocytic leukemia: a review and discussion of variant translocations. *Arch Pathol Lab Med.* 2015;139(10):1308–1313.
3. Sainty D, Liso V, Cantù-Rajnoldi A, et al. A new morphologic classification system for acute promyelocytic leukemia distinguishes cases with underlying PLZF/RARA gene rearrangements. *Blood.* 2000;96(4):1287–1296.
4. Hanker JS, Ambrose WW, James CJ, et al. Facilitated light microscopic cytochemical diagnosis of acute myelogenous leukemia. *Cancer Res.* 1979;39(5):1635–1639.

5. Yue QF, Xiong B, Chen WX, Liu XY. Comparative study of the efficacy of Wright-Giemsa stain and Liu's stain in the detection of Auer rods in acute promyelocytic leukemia. *Acta Histochem.* 2014;116(6):1113–1116.
6. Foley R, Soamboonsrup P, Carter RF, et al. CD34-positive acute promyelocytic leukemia is associated with leukocytosis, microgranular/hypogranular morphology, expression of CD2 and bcr3 isoform. *Am J Hematol.* 2001;67(1):34–41.
7. Gorczyca W. Acute promyelocytic leukemia: four distinct patterns by flow cytometry immunophenotyping. *Pol J Pathol.* 2012;63(1):8–17.
8. Lin P, Hao S, Medeiros LJ, et al. Expression of CD2 in acute promyelocytic leukemia correlates with short form of PML-RARalpha transcripts and poorer prognosis. *Am J Clin Pathol.* 2004;121(3):402–407.
9. Dowse RT, Ireland RM. Variant ZBTB16-RARA translocation: morphological changes predict cytogenetic variants of APL. *Blood.* 2017;129(14):2038.
10. Sanz MA, Fenaux P, Tallman MS, et al. Management of acute promyelocytic leukemia: updated recommendations from an expert panel of the European LeukemiaNet. *Blood.* 2019;133(15):1630–1643.
11. Grignani F, De Matteis S, Nervi C, et al. Fusion proteins of the retinoic acid receptor-alpha recruit histone deacetylase in promyelocytic leukaemia. *Nature.* 1998;391(6669):815–818.
12. Guidez F, Ivins S, Zhu J, Söderström M, Waxman S, Zelent A. Reduced retinoic acid-sensitivities of nuclear receptor corepressor binding to PML- and PLZF-RARalpha underlie molecular pathogenesis and treatment of acute promyelocytic leukemia. *Blood.* 1998;91(8):2634–2642.
13. Shaknovich R, Yeyati PL, Ivins S, et al. The promyelocytic leukemia zinc finger protein affects myeloid cell growth, differentiation, and apoptosis. *Mol Cell Biol.* 1998;18(9):5533–5545.
14. Sobas M, Talarn-Forcadell MC, Martinez-Cuadron D, et al. PLZF-RARalpha, NPM1-RARalpha, and other acute promyelocytic leukemia variants: the PETHEMA Registry experience and systematic literature review. *Cancers (Basel)*. 2020;12(5):1313.
15. Wang A, Cai X, Qiang P, Duan Q. Successful treatment of a patient with acute promyelocytic leukemia with a STAT5B/RARA fusion gene using decitabine. *Leuk Lymphoma.* 2018;59(3):763–765.
16. Miyauchi J. All-trans retinoic acid and hematopoietic growth factors regulating the growth and differentiation of blast progenitors in acute promyelocytic leukemia. *Leuk Lymphoma.* 1999;33(3-4):267–280.

Myeloid Sarcoma Expressing Keratins and Mimicking Carcinoma—Case Report and Literature Review

Vanessa J. Dayton, MD,[1] *Amy Beckman, MD,*[1] *Michael Linden, MD, PhD*[1]

[1]Department of Laboratory Medicine and Pathology, University of Minnesota Medical Center-Fairview, Minneapolis, Minnesota, USA; *To whom correspondence should be addressed. dayt0002@umn.edu

Keywords: myeloid sarcoma, immunohistochemistry, CD33, AE1/AE3, poorly differentiated carcinoma, melanoma, histiocytic sarcoma, flow Cytometry, anchoring bias

Abbreviations: IHC, immunohistochemistry; H&E, hematoxylin and eosin; AML, acute myeloid leukemia.

Laboratory Medicine 2022;53:100–106; DOI: 10.1093/labmed/lmab025

ABSTRACT

Unusual presentations of otherwise common hematopoietic neoplasms are a well-recognized diagnostic challenge. Herein, we present a case study of a previously healthy 64 year old woman with myeloid sarcoma whose diagnosis was delayed by an unusual immunohistochemical staining pattern, including cytokeratin expression, by the neoplastic cells and by possible anchoring bias introduced by radiographic and flow cytometric immunophenotyping reports. This case study emphasizes the need to integrate clinical, radiographic, histologic, and immunophenotyping data for rapid and accurate tissue diagnoses while being wary of the lack of specificity for many common immunophenotypic markers.

Unusual presentations of otherwise common hematopoietic neoplasms are a well-recognized diagnostic challenge.[1] The challenge is compounded when there is overlap between the immunohistochemical staining patterns of hematopoietic and nonhematopoietic neoplasms. Anchoring bias, the tendency to rely too heavily on an initial piece of information, and overreliance on radiographic or other laboratory findings to guide the microscopic pathology workup can introduce diagnostic errors and delays.[2] Herein, we present a patient whose ultimate diagnosis of myeloid sarcoma was delayed by both an unusual pattern of immunohistochemical staining and bias introduced by suspicion for lymphoma described in radiologic and flow cytometric immunophenotyping reports.

Clinical History

A previously healthy 64 year old female patient presented to her primary care physician with a painful right inguinal lump associated with swelling in her right leg that had appeared over the previous week. Review of systems was essentially negative. On physical exam, the woman was described as appearing well, with normal vital signs including normal oxygen saturation levels. Notable findings included a palpable inguinal mass and leg swelling. Laboratory studies including an automated complete blood count with leukocyte differential, routine chemistries, liver function tests, and urinalysis were all within normal limits. A computed tomography scan of the abdomen and pelvis performed with contrast showed right-sided inguinal (up to 10 cm), pelvic, retroperitoneal, and axillary lymphadenopathy. The radiologist interpreted the findings as concerning for lymphoma.

Right inguinal lymph node biopsy was performed immediately after the radiographic studies. The local pathologist examined a frozen tissue section, requested additional tissue, and forwarded fresh tissue to a reference laboratory with instructions that paraffin blocks were to be sent to the same reference laboratory the following day. Fresh tissue analyzed by flow cytometry at the reference laboratory identified a population of cells that was suspicious for, but not diagnostic of, a clonal B-cell population. The report noted the possibility of B-cell lymphoma, with the caveat that interpretation was limited by poor cell viability.

A final tissue diagnosis was delayed for some weeks. Although the patient was initially managed symptomatically as an outpatient, development of symptomatic anemia, thrombocytopenia, coagulopathy, and elevated serum lactate dehydrogenase (LDH) prompted transfer to our institution.

At the patient's admission to our hospital, we did not have access to the original diagnostic material but were able to see the outside pathology report, which described a metastatic high-grade malignant neoplasm expressing multiple cytokeratins and S-100 by immunohistochemistry (IHC) and offered a differential that included melanoma and poorly differentiated carcinoma. In addition, our own clinical team noted the possibility of B-cell lymphoma, primarily based on a review of outside electronic medical records.

Because the original tissue biopsy was not readily available for our review, needle core biopsy of an enlarged right inguinal lymph node was repeated, with specimens sent for permanent sections and flow cytometry. On review of our flow cytometry and IHC,

we verbally communicated our findings to the clinical team and recommended evaluation of the patient's bone marrow. On the seventh hospital day, bone marrow biopsy confirmed the diagnosis of myeloid sarcoma with bone marrow involvement by myeloid leukemia. However, by this time, the patient had developed severe lactic acidosis. At the request of her family, life support was removed and the patient died.

Laboratory Evaluation

Lymph Node Needle Core Biopsy

Hematoxylin and eosin (H&E) stained sections of the lymph node core biopsy showed complete effacement by large atypical cells with morphologic characteristics suggestive of blasts, and focal necrosis (**IMAGE 1**, **A**). Immunohistochemical stains were positive for the

IMAGE 1. Stained sections from needle core biopsy of lymph node. A, H&E; B, CD45; C, AE1/AE3; D, BCL6; E, S100; F, CD30; G, CK8/18; H, CD43; I, CD4; J, lysozyme. H&E, hematoxylin and eosin.

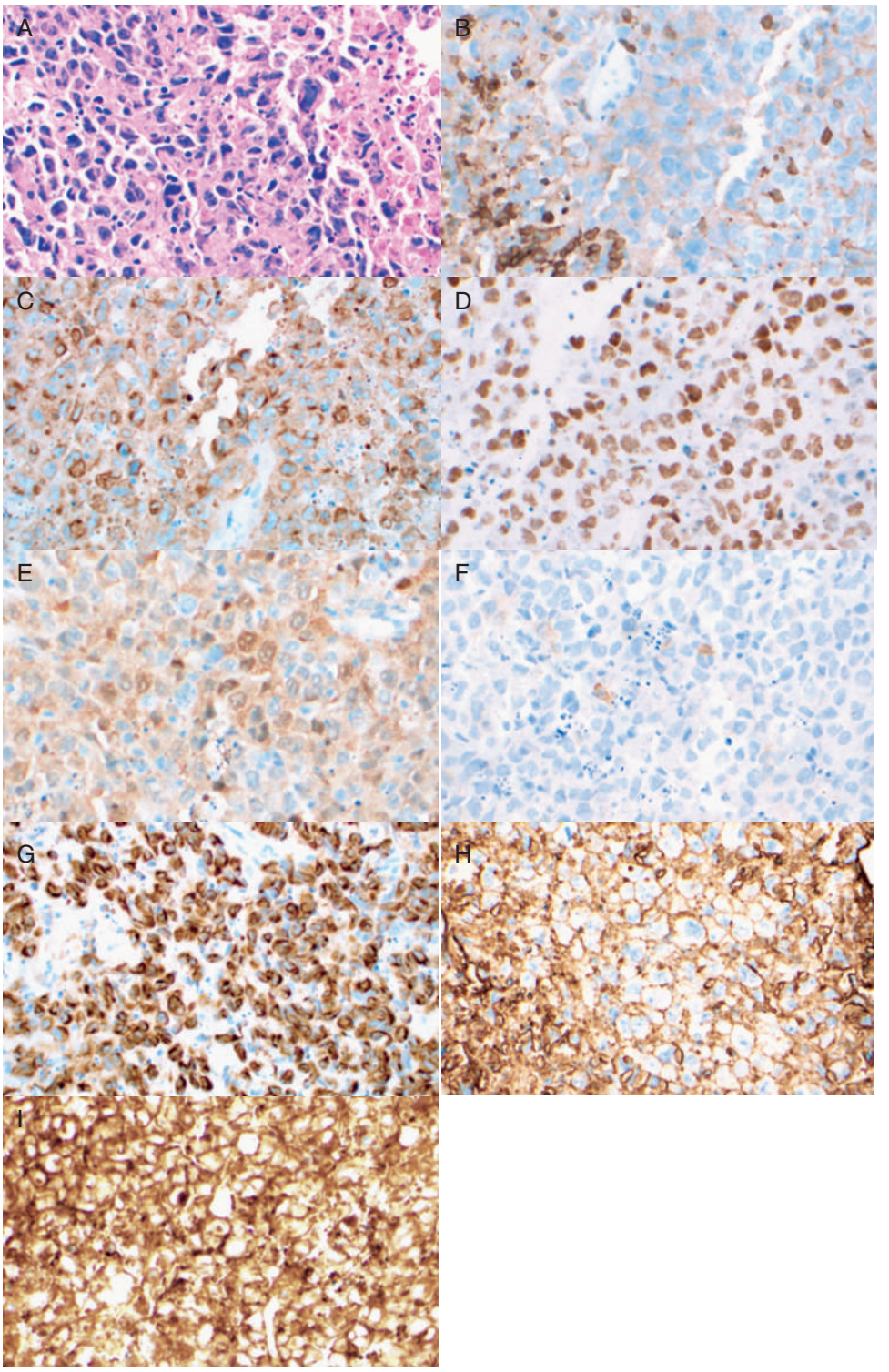

cytokeratin markers AE1/AE3 and CK8/18; positive for BCL-6, CD43, CD4, and lysozyme; and equivocal for S-100 (very weak staining of cytoplasm only with this antibody). Staining was negative for CD45 and CD30 (**IMAGE 1, B–J**) and for CD3, other T-cell markers (CD2, CD5, CD7, and CD8), CD20, CD34, CD68 KP-1, CD117, CD123, CD138, PAX5, and MPO (not illustrated). Flow cytometric immunophenotyping performed on tissue from the needle core biopsy using B- and T-cell tubes was noncontributory because of poor cell preservation.

Peripheral Blood and Bone Marrow Aspirate

Rare neoplastic cells were identified on a blood smear (**IMAGE 2**). However, flow cytometric immunophenotyping performed on blood using B-cell, T-cell, and myeloid tubes was again noncontributory, likely a result of the small number of circulating neoplastic cells present.

A Wright-Giemsa stained bone marrow aspirate smear showed trilineage hematopoiesis with dysgranulopoiesis and a high proportion of atypical blasts (**IMAGE 3**). The bone marrow had abundant viable neoplastic cells, so a sufficient number of cells survived processing to form a discrete population for analysis by flow cytometric immunophenotyping. Overall, flow cytometry showed an abnormal cell population with high forward-scatter expressing bright CD4 and CD45 but lacking CD56 (**FIGURE 1**). However, the size/complexity of the cells combined with some degree of autofluorescence made it difficult to reliably interpret antigen expression/intensity for all antigens tested. Therefore, for the purposes of this report, only select antigens from the T-cell tube are presented because we could confidently distinguish the expression of these antigens from nonspecific staining of nonviable events.

The H&E and immunoperoxidase stains for the bone marrow clot section showed focal and interstitial marrow infiltration by atypical blasts. In addition to immunohistochemical stains performed on the lymph node needle core biopsy, CD33 immunoperoxidase stain was performed on the bone marrow clot section (Allina Laboratories, Minneapolis, MN). Blasts in bone marrow clot sections showed the expression of CD43, lysozyme, and CD33 (**IMAGE 4**). Neoplastic cells in bone marrow trephine biopsy sections also showed the expression of BCL-6, CD4, and weak CD45 (not illustrated). The discrepancy between bright CD45 expression as detected by flow cytometry and weak expression as interpreted by IHC was attributed to the use of different monoclonal antibodies (RPD/18 for IHC and HI30 for flow cytometry). Slides for this patient's original lymph node biopsy were not available for review.

Discussion

Herein, we describe a patient with acute myeloid leukemia (AML) presenting as myeloid sarcoma in a lymph node where the ultimate diagnosis was delayed and the outcome was poor. The consulting pathologists' comments in the initial lymph node biopsy report raise the possibility that diagnostic delays and interpretations of possible carcinoma, melanoma, and lymphoma may have resulted from a combination of the unusual immunoperoxidase staining pattern with keratin and S100 expression by the tumor cells as interpreted by their laboratory, along with anchoring bias based on the reported flow cytometric immunophenotyping.

This case study highlights common diagnostic challenges for pathologists that all practicing physicians need to be aware of. Unusual presentations of otherwise well-recognized and treatable malignancies can lead to delayed and/or inaccurate diagnoses, particularly when:

- There is an unusual pattern of immunoperoxidase staining, as was seen in this patient.
- There is anchoring bias based on suspicions described in radiology or other laboratory reports.

Myeloid sarcoma (de novo presentation of AML outside of the bone marrow) presenting in a lymph node is a well-recognized diagnostic challenge.[1] Expedient and accurate diagnosis is critical; large series and case reports have established that myeloid sarcoma can be highly treatable and even curable.[3,4] Rapid and accurate diagnosis of any malignancy

IMAGE 2. Circulating myeloid blast on blood smear.

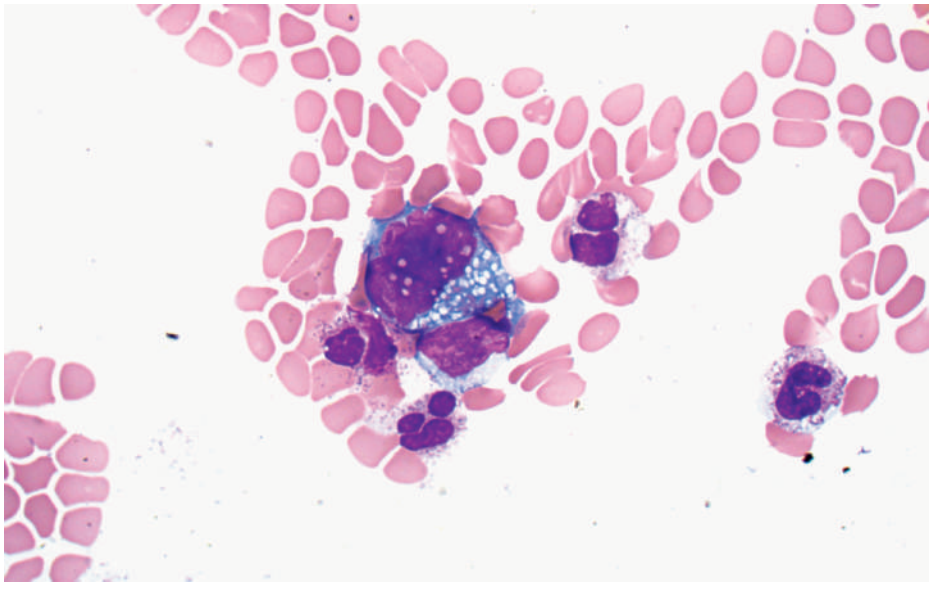

2022;53;100–106 | DOI: 10.1093/labmed/lmab025

IMAGE 3. Bone marrow aspirate smear. A, Bone marrow aspirate smear showing dysgranulopoiesis; B, Bone marrow aspirate smear showing high proportion of large and atypical blasts.

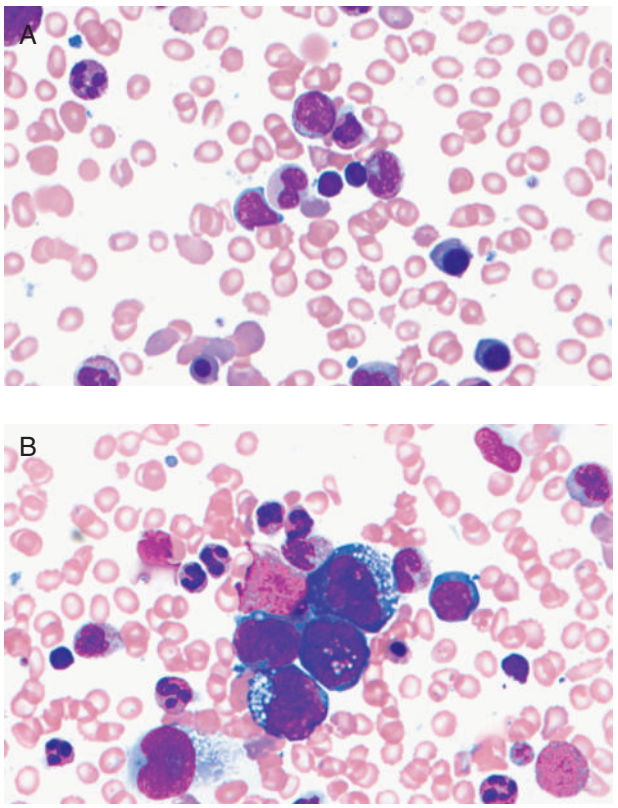

in the current era requires clinicopathologic correlation and the ability to discern useful from nonuseful data.

A careful review of the medical literature reveals a substantial overlap in immunostaining patterns between hematopoietic and nonhematopoietic neoplasms (**IMAGE 5**). Nonspecific/aberrant staining of myeloid neoplasms in addition to T-cell lymphomas with cytokeratin markers in paraffin tissue sections has been described in the medical literature.[5-8] However, there are only a handful of case reports describing myeloid sarcomas that express cytokeratins.[9,10] In addition, recently published algorithms for the use of immunoperoxidase stains to accurately diagnose poorly differentiated large-cell neoplasms may not fully address CD45-negative hematopoietic neoplasms that express cytokeratins.[11]

In this case study, we were guided to a diagnosis of myeloid sarcoma/AML upon detecting a strong surface expression of both CD4 and CD43 in the absence of other T-lineage markers. Uniform surface staining of neoplastic cells by CD43 has been shown to be specific and sensitive for the detection of hematopoietic neoplasms. However, focal weak nuclear staining has been described for some carcinomas,[12] and CD43 has not been described as being expressed in all reported patients with myeloid sarcoma.[13] The CD4 expression appears specific for neoplasms of hematolymphoid origin and has not been described as being expressed for any cell types other than those of T-cell, histiocytic, or myeloid lineage. Histiocytic sarcoma should also be considered in the differential diagnosis of undifferentiated large-cell neoplasms that express S-100 protein along with lysozyme and cytoplasmic CD4. Our patient's condition can be distinguished from having histiocytic sarcoma by the expression of the myeloid marker CD33 and the absence of staining for CD68, as described in the current World Health Organization classification.[14]

FIGURE 1. Representative histograms from flow cytometric immunophenotyping of bone marrow aspirate. NK cells, natural killer cells.

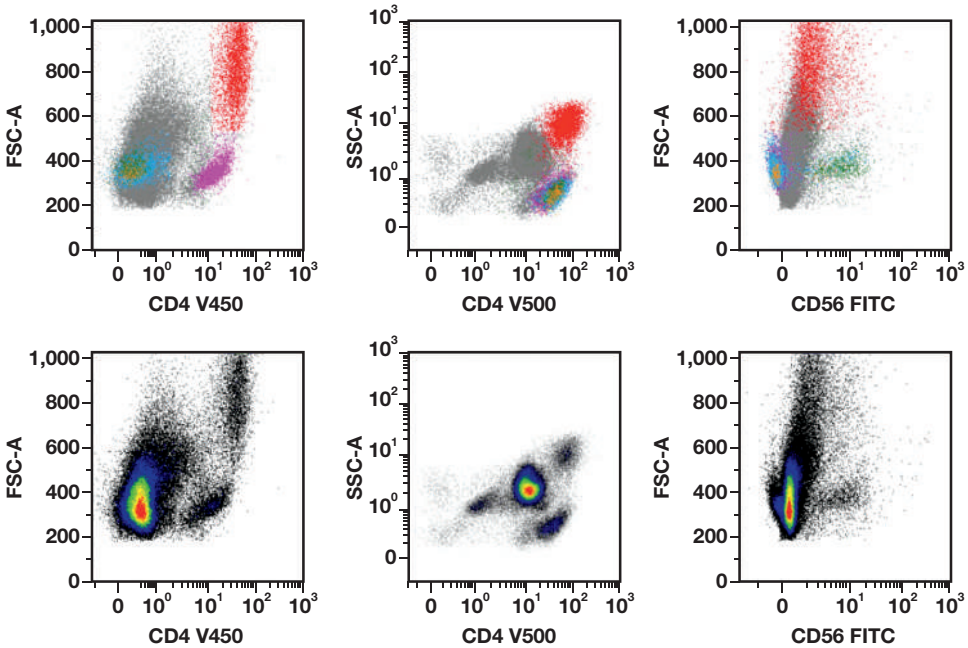

IMAGE 4. **Bone marrow aspirate clot section. A, H&E stain of bone marrow with subtle interstitial infiltration by blasts; B, H&E stain of bone marrow with focal effacement by blasts; C, CD45 immunostained section of bone marrow; D, CD43 immunostained section marrow; E, Lysozyme immunostained section of marrow; F, CD33 immunostained section of marrow. H&E, hematoxylin and eosin.**

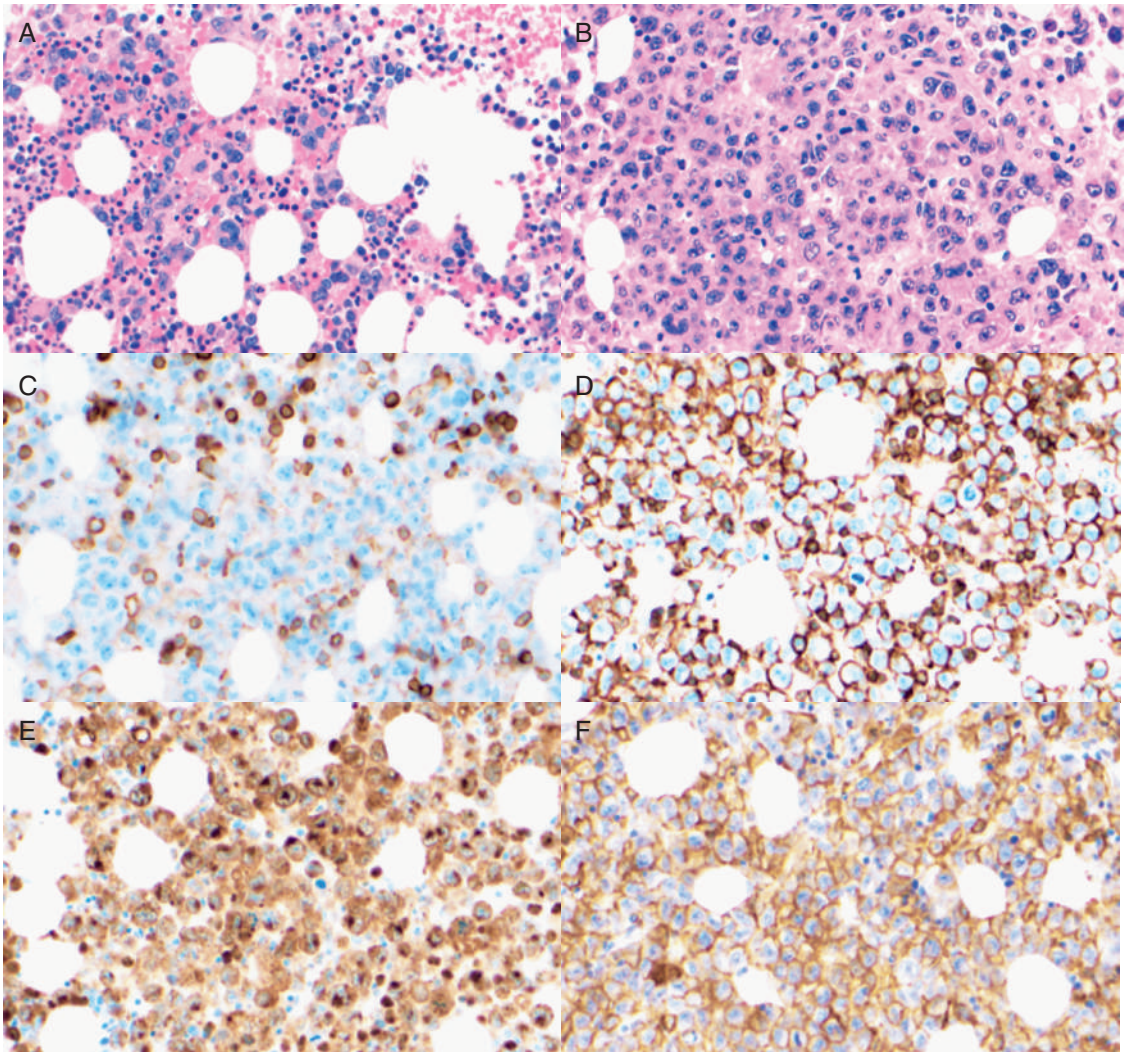

Flow cytometric immunophenotyping represents a powerful diagnostic tool that has become standard for evaluating specimens from lymph nodes, blood, bone marrow, and/or any tissue specimen suspected of harboring a hematopoietic neoplasm. Nonetheless, published series of flow cytometric analyses presented by respected reference laboratories have identified patients suspected of having a diagnosis or classification of a lymphoid neoplasm that was subsequently excluded by microscopy and IHC.[15,16] Notably, pathologists or other practitioners not specifically trained or experienced in the interpretation of flow cytometric immunophenotyping may be unaware of the limitations of this modality.

Anchoring bias, defined as an overreliance on the initial information offered, may have played a role in the delay of a specific diagnosis for the patient described in this report.[2] Although the authors did not have the opportunity to review this patient's original excisional lymph node biopsy, both clinical physicians and pathologists at our institution were expecting to confirm the outside diagnosis based on the original radiographic, flow cytometry, and surgical pathology reports that were available in the electronic record. It was only when flow cytometric immunophenotyping performed on a repeat lymph node needle core biopsy showed low viability and autofluorescence that we paused to consider unusual presentations of neoplasms in lymph nodes and gathered additional information before making a specific diagnosis.

Conclusion

A previously healthy woman presented to her primary care practitioner with concerning findings on physical exam. A rapid clinical laboratory and radiographic workup with diagnostic lymph node biopsy were performed by her community health system. Unfortunately, deadly

2022;53;100–106 | DOI: 10.1093/labmed/lmab025

IMAGE 5. Immunohistochemical Staining in Select Neoplasms.[1,5-14,17-34] ***The purpose of this table is to provide current available data on published findings for immunohistochemistry and does not necessarily reflect published immunophenotyping by flow cytometry methods.**

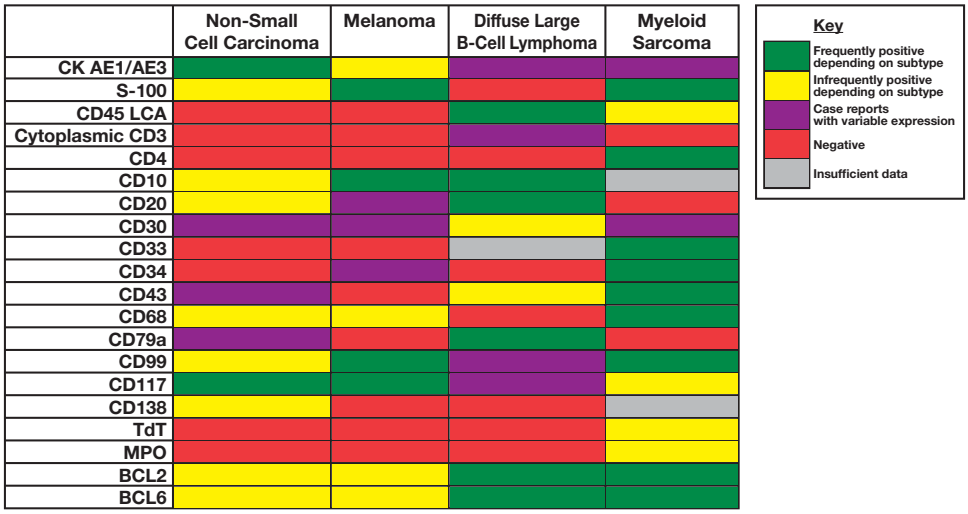

complications occurred while the diagnosis of her potentially treatable neoplasm was delayed, with an unusual immunohistochemical staining pattern and anchoring bias as likely contributors. We emphasize the importance of the integration of clinical, radiographic, histologic, and immunophenotypic data to arrive at a comprehensive diagnosis for the patient.

REFERENCES

1. Dayton V, Linden M, Anderson S, et al. Unusual presentation of extramedullary hematopoietic neoplasms in lymph nodes. *Human Pathol.* 2017;62:13–22.
2. Volmar KE. Personality and cognitive considerations. In: Nakleh R, Volmar KE, eds. *Error Reduction and Prevention in Surgical Pathology.* 2nd ed. Cham, Switzerland: Springer Nature; 2019: 116–118.
3. Zhang L, Reilly N, Wahed A, et al. Aleukemic myeloid sarcoma in female reproductive system: report of two rare cases. *Am J Clin Path.* 2018;150:S102.
4. Breccia M, Mandelli F, Petti MC, et al. Clinico-pathological characteristics of myeloid sarcoma at diagnosis and during follow-up: report of 12 cases from a single institution. *Leuk Res.* 2004;28(11):1165–1169.
5. Pileri SA, Weisenburger DD, Sing I, et al. Peripheral T-cell lymphoma, NOS. In: Swerdlow SH, Campo E, Harris NL, et al., eds. *WHO Classification of Tumours of Haematopoietic and Lymphoid Tissues*. Revised 4th ed. Lyon, France: IARC; 2017: 403–407.
6. Pletneva MA, Smith LB. Anaplastic large cell lymphoma, features presenting diagnostic challenges. *Arch Path Lab Med.* 2014;138:1290–1294.
7. Pileri SA, Orazi A, Falini B. *Myeloid sarcoma*. In: Swerdlow SH, Campo E, Harris NL, et al., eds. *WHO Classification of Tumours of Haematopoietic and Lymphoid Tissues*. Revised 4th ed. Lyon, France: IARC; 2017: 167–168.
8. Pileri SA, Ascani S, Cox MC, et al. Myeloid sarcoma: clinico-pathologic, phenotypic and cytogenetic analysis of 92 adult patients. *Leukemia.* 2007;21(2):340–350.
9. Schmitt-Graeff A, Marks R. Cytokeratin-type intermediate filaments in a gastric myeloid sarcoma: a diagnostic pitfall. *Blood.* 2016;128(3):460.
10. Comerford C, Mhaolcatha SN, Hayes B, Mykytiv V. The first case of myeloid leukemia/myeloid sarcoma with cytokeratin expression on blasts diagnosed on urine specimen. *Hematol Oncol Stem Cell Ther.* Published online March 18, 2020. doi: 10.1016/j.hemonc.2020.02.007
11. Fan L, Haiyan L. Immunohistochemistry in undifferentiated neoplasm/tumor of uncertain origin. *Arch Pathol Lab Med*. 2014;138:1583–1610.
12. Batdorf BH, Kroft SH, Hosking PR, Harrington AM, Mackinnon AC, Olteanu H. Evaluation of CD43 expression in non-hematopoietic malignancies. *Ann Diagn Pathol.* 2017;29:23–27.
13. Quintanilla-Martinez L, Zukerberg LR, Ferry JA, et al. Extramedullary tumors of lymphoid or myeloid blasts: the role of immunohistology in diagnosis and classification. *Am J Clin Path.* 1995;104:431–443.
14. Weis LM, Pileri SA, Chan JKC, et al. Histiocytic sarcoma. In: Swerdlow SH, Campo E, Harris NL, et al., eds. *WHO lassification of Tumours of Haematopoietic and Lymphoid Tissues. Revised 4th ed*. Lyon, France: IARC; 2017: 468–470.
15. Savage EC, Vanderheyden AD, Bell AM, et al. Independent diagnostic accuracy of flow cytometry obtained from fine-needle aspirates. *Am J Clin Path.* 2011;135:304–309.
16. Cheng J, Klairmont MM, Choi JK. Peripheral blood flow cytometry for the diagnosis of pediatric acute leukemia: highly reliable with rare exceptions. *Pediatr Blood Cancer.* 2019;66(1):e27453.
17. Stelow EB, Yaziji H. Immunohistochemistry, carcinomas of unknown primary, and incidence rates. *Semin Diagn Pathol.* 2018;35(2):143–152.
18. Krishna M. Diagnosis of metastatic neoplasms: an immunohistochemical approach. *Arch Path Lab Med*. 2010;134:207–215.
19. Kuberappa PS, Bagalad BS, Ananthaneni A. Certainty of S-100 from physiology to pathology. *J Clin Diagnost Res.* 2016;10:10–15.
20. Zaccarini DJ, Deng X, Tull J, Maciak C, Valente AL, Zhang S. Expression of TLE-1 and CD99 in carcinoma: pitfalls in diagnosis of synovial sarcoma. *Appl Immunohistochem Mol Morphol.* 2018;26(6):368–373.
21. Wong HH, Wang J. Merkel cell carcinoma. *Arch Pathol Lab Med.* 2010;134(11):1711–1716.
22. Alonso SR, Ortiz P, Pollan M, et al. Progression in cutaneous malignant melanoma is associated with distinct expression profiles. *Am J Path*. 2004;164:193–203.
23. Fang D, Nguyen TK, Leishear K, et al. A tumorigenic subpopulation with stem cell properties in melanomas. *Cancer Res.* 2005;65(20):9328–9337.
24. Weissinger SE, Keil P, Silvers DN, et al. A diagnostic algorithm to distinguish desmoplastic from spindle cell melanoma. *Mod Pathol.*

2014;27(4):524–534.

25. Carter RC, Romano JM, Folpe AL. Aberrant intermediate filament and synaptophysin expression is a frequent event in malignant melanoma: an immunohistochemical study of 73 cases. *Mod Path*. 2015;28:1033–1042.
26. Wilkerson AE, Glasgow MA, Hiatt KM. Immunoreactivity of CD99 in invasive malignant melanoma. *J Cutan Pathol*. 2006;33(10):663–666.
27. Gascoyne RD, Campo E, Jaffe ES, et al. Diffuse large B-cell lymphoma, NOS. In: Swerdlow SH, Campo E, Harris NL, et al., eds. *WHO Classification of Tumours of Haematopoietic and Lymphoid Tissues*. Revised 4th ed. Lyon, France: IARC; 2017: 291–297.
28. Singh N, Ketkar A, Gujral S. Poly immunophenotypic expression in a case of diffuse large B-cell lymphoma. *Indian J Pathol Microbiol.* 2017;60(2):304–306.
29. Kandukuri SR, Lin F, Gui L, et al. Application of immunohistochemistry in undifferentiated neoplasms: a practical approach. *Arch Pathol Lab Med.* 2017;141(8):1014–1032.
30. Vakiani E, Cattoretti G, Calovai E. CD117 expression in diffuse large B-cell lymphoma: fact or fiction? *Pathol Int*. 2005;55(11):716–723.
31. Turner JJ, Milliken S. A case of keratin-positive acute myeloid leukemia: a possible role for cytokeratin 19 as a specific epithelial marker. *Pathology.* 2000;32(2):98–101.
32. Wang HQ, Li J. Clinicopathological features of myeloid sarcoma: report of 39 cases and literature review. *Pathol Res Pract.* 2016;212(9):817–824.
33. Kang LC, Dunphy CH. Immunoreactivity of MIC2 (CD99) and terminal deoxynucleotidyl tranferase in bone marrow clot and core specimens of acute myeloid leukemias and myelodysplastic syndromes. *Am J Clin Path.* 2006; 130:153–157.
34. Brenner AK, Bruserud Ø. S100 proteins in acute myeloid leukemia. *Neoplasia.* 2018;20(12):1175–1186.
35. Sangle NA, Schmidt RL, Patel JL, et al. Optimized immunohistochemical panel to differentiate myeloid sarcoma from blastic plasmacytoid dendritic cell neoplasm. *Mod Pathol.* 2014;27(8):1137–1143.

CASE STUDY

A Persistent Positive Antibody Test in a Patient with No History of COVID-19 Infection

Jordan McMurry[1,*] *and Ezekiel Fink, MD*[1]

[1]Cedar Health Research, LLC, Dallas, Texas, USA; *To whom correspondence should be addressed. jordan.mcmurry@aspeninsights.com

Keywords: COVID-19, SARS-CoV-2, antibody, testing, diagnostics, false positive

Abbreviations: RT-PCR, reverse-transcription polymerase chain reaction; Ab, antibody; COI, cutoff index.

Laboratory Medicine 2022;53:e1–e3; DOI: 10.1093/labmed/lmab038

ABSTRACT

Antibody testing for SARS-CoV-2 has been established as a tool with broad utility in the surveillance and control of the COVID-19 pandemic. However, because of limited knowledge about the duration of humoral immunity to COVID-19 and the existence of unique individual immune responses, the potential role of antibody testing in the diagnosis of current and past infections of COVID-19 remains ambiguous. Herein, we describe a unique case of an asymptomatic patient showing a persistent positive total antibody test for SARS-CoV-2 while testing negative for SARS-CoV-2 RNA and IgG-specific antibodies. This case study shows how a combination of tests can be employed to identify a false positive and draw conclusions about a patient's COVID-19 status. It also highlights the complexity of using antibody testing for the diagnosis of COVID-19.

The infectious disease COVID-19, caused by SARS-CoV-2, has spread rapidly around the world, causing a pandemic. Many recent studies have focused on the utility of SARS-CoV-2 antibody testing for identifying current and past infections.[1,2] In addition, antibody testing has been explored as a tool for obtaining information on the stage of disease progression,[2-4] for identifying undiagnosed infections past the point of viral shedding,[5,6] and as a promising option for monitoring the portion of a population previously infected.[7,8] However, despite the development of tests offering high levels of sensitivity and specificity for SARS-CoV-2 antibodies,[9] many limitations exist for these potential uses. These include a lack of knowledge of the duration of SARS-CoV-2 antibodies after infection[10] and the impact of low population seroprevalence on the ability to make accurate predictions using antibody testing.[9] In addition to these limitations, multiple unique cases have been reported that illustrate the complexity and lack of clarity of the role that antibody tests should play in diagnosing COVID-19 infection.[6,11] Additional research is needed to explore the factors that influence antibody test accuracy and to clarify how to manage patients in whom the test results do not give a straightforward answer. Here, we report a unique case of a patient with no evidence of current or past infection with COVID-19 who persistently tested positive for SARS-CoV-2 antibodies on 1 test while testing negative on another.

Case Report

On June 10, 2020, a 45 year old woman and her husband and daughter presented to a testing clinic in Dallas, Texas to undergo testing for COVID-19. She reported a potential exposure to COVID-19 approximately 10 days prior through a close interaction with a family member who had direct exposure to someone diagnosed with COVID-19. The patient received a SARS-CoV-2 reverse transcription-polymerase chain reaction (RT-PCR) test using a self-administered throat swab that returned negative. She was also evaluated using a plasma total antibody (Ab) Elecsys Anti-SARS-CoV-2 serology test supplied by Roche Diagnostics (Rotkreuz, Switzerland), completed according to the manufacturer's instructions. The total Ab test results came back positive with a cutoff index (COI) of 3.51. The patient's husband and daughter received negative results on both the SARS-CoV-2 RNA and total Ab tests. On June 12, 2020, the patient's 3 other children received the SARS-CoV-2 RNA and Roche total Ab tests, and all results came back negative.

Because the patient and her family showed no evidence of SARS-CoV-2 infection, the patient's immune response was re-evaluated on June 15, 2020 with a fresh serum specimen using the Abbott ARCHITECT i2000sr platform from Abbott Laboratories (Chicago, IL) to test for plasma IgG Abs. This test was performed according to the manufacturer's instructions and returned negative. The specificities of the total Ab assay and IgG assay to specimens with SARS-CoV-2 were determined as 99.7% (1151/1154) and 99.2% (1145/1154), respectively, by testing SARS-CoV-2–negative serum specimens collected before the outbreak.[9]

To minimize the probability of laboratory error for the Roche total Ab test, the serum from the June 10 blood draw was retested on June 17 and returned positive with a COI of 3.54, confirming the result of the previous test. Because a false positive was suspected for the Roche test, a third serum specimen was collected on June 19. Portions of this specimen were sent to 2 laboratories: One conducted a Roche total Ab test and the other conducted a Roche test and an Abbott IgG test. The Roche

total Ab test returned positive for both laboratories, with COI values of 3.36 and 3.6. The repeated Roche tests with similar COI values confirmed that laboratory error was likely not the cause of the positive result. The Abbott IgG test returned negative with a COI of 0.1, confirming the original Abbott results. The median COI value for each type of antibody test was compared to characteristic COI values for different specimen types, as shown in **TABLE 1**. As of late August 2020, neither the patient nor her family had exhibited any symptoms of COVID-19.

Retrospectively, the patient disclosed experiencing flu-like symptoms in early February 2020 that included 3 to 5 days of fatigue, weakness, runny nose, and chills. Two of the patient's children experienced similar symptoms approximately 1 week later and tested positive for the flu by point-of-care testing of viral RNA. The patient reported a quick recovery with no enduring symptoms. The patient reported no history of chronic medical conditions or serious illness, does not regularly take any medications other than melatonin, has no known allergies, and does not believe she was exposed to previous outbreaks of SARS-CoV-1 or MERS-CoV. The patient also reports no other potential exposures to COVID-19.

Discussion

We report a case of a patient who persistently tested positive for SARS-CoV-2 total Abs despite no evidence of previous COVID-19 infection, a negative SARS-CoV-2 RNA test, and a negative IgG Ab test. The combination of the repeated test results and the clinical presentation suggest that the patient did not have COVID-19 and that the Roche total Ab test returned a replicable false positive. Although it is currently unclear how many patients develop antibodies to SARS-CoV-2 after infection, some literature suggests it is possible for 100% of patients with COVID-19 to produce detectable antibodies.[3,4] However, there is also evidence that some patients may not develop antibodies[9,11] or may show a delayed antibody response.[6] Although the immune response to SARS-CoV-2 infection is not uniform, it is unlikely that none of the patient's family would have tested positive for total Abs if some or all had contracted COVID-19 in February or June 2020. It is possible that the patient could have contracted COVID-19 independently of her family if she was able to successfully isolate herself from them during her symptomatic period in February 2020 or postexposure in June 2020. However, given that the patient had no symptoms of infection in June 2020 and was negative for viral RNA and IgG-specific Abs, the positive result on the total Ab test alone is not consistent with the unique patients in whom antibody response is delayed or undetectable.[6,9,11] Furthermore, the lack of detectable IgG Abs for this patient indicates that infection in February 2020, when she experienced flu-like symptoms, was also reasonably unlikely. IgG Abs are indicative of the long-term immune response to an infection,[2] and recent data have shown that up to 90% of patients with a positive SARS-CoV-2 PCR test continue to exhibit detectable levels of anti-SARS-CoV-2 IgG Abs between 40 and 199 days after testing positive.[12]

In a typical patient with COVID-19, testing positive for total Abs—antibodies of any kind—but not IgG alone may indicate that the infection is active and recent.[2] However, median seroconversion times for total Abs and IgG Abs to SARS-CoV-2 have been reported at 11 and 14 days after symptom onset, respectively,[3] making it unlikely that this patient would continue to test negative for IgG 9 days after the first positive total Ab test and 20 days after potential exposure. In addition, data reported by Roche Diagnostics shows that the COI (a ratio of a specimen readout to the cutoff value for a positive result) for the total antibody test, although not directly indicative of antibody concentration, continues to increase for up to at least 35 to 40 days after diagnosis.[13] However, the patient's repeated Roche total Ab tests showed negligible change in COI value over time, and her result more closely matched the median COI for a false positive test than for a true positive, according to research conducted by Perkmann et al[9] that compares the Roche and Abbott antibody tests (**TABLE 1**).

Notably, Perkmann et al[9] also reported that of 12 specimens in their data set that returned a false positive on either the Abbott test or Roche test, none returned a false positive on both. Given that both antibody tests have comparable sensitivities and use the same viral protein,[9] the discrepancy is not likely caused by differing abilities to detect low concentrations of antibodies. One possibility is that the replicable false positive is caused by some aspect of the composition of the Roche test, or the particular recombinant SARS-CoV-2 protein it employs, that is significant to the patient's serum and that the Abbott test does not share. For example, antibodies to a similar virus or nonspecific heterophile antibodies in the patient's serum could bind to the recombinant protein, leading to an apparent positive result despite SARS-CoV-2–specific antibodies being absent. Alternatively, anti-antibodies in the patient's serum could interfere by binding to any antibodies utilized in the immunoassay, although this mechanism of interference is only minimally likely for antibody tests; most use indirect detection methods, where serum is washed away before the addition of any secondary antibodies. The details of antibody test composition are not publicly available and thus cannot be analytically compared, precluding our ability to make a definitive conclusion on what could have caused the false positive result. However, this hypothesis would explain the discrepancy between manufacturers for the patient and the lack of other evidence of COVID-19 infection.

In summary, we report a unique case in which a patient had a persistent test-specific false positive result for SARS-CoV-2 antibodies. This

TABLE 1. SARS-CoV-2 Antibody Test COI Values for Positive and Negative Serum Specimens

Serology Specimen	Median COI Value	
	Roche T-Ab (cutoff, 1.0)[a]	Abbott IgG (cutoff, 1.4)[a]
Patient	3.54	0.1
Confirmed positive[b]	24.2 (7.22–52.90)	4.87 (2.77–6.78)
False positive[b]	1.65 (1.47–1.72)	2.21 (2.14–2.67)
Confirmed negative[b]	0.08	0.03

COI, cutoff index; T-Ab, total antibody.
[a]Cutoff represents the smallest COI value at which the specimen is considered positive for SARS-CoV-2 antibodies.
[b]Median COI data taken from Perkmann et al.[9] Values in parentheses indicate the interquartile range for the COI values of the specimens in this category.

case study addresses the complexity of interpreting antibody test results and suggests that additional testing with another brand or manufacturer of antibody test would be a useful strategy for confirming a suspected false positive. It is important to consider several factors, including RT-PCR, clinical presentation, antibody test results, exposure timeline, population seroprevalence, and the progression of SARS-CoV-2 antibody seroconversion when attempting to make a diagnosis and issue guidance to a patient. False positive results on an antibody test can give patients a false sense of security that they are protected from future COVID-19 infection and thus can encourage behaviors that carry a higher chance of infection.[8] Further research and surveillance are needed to address the causes of test-specific false positive results and to clarify the use of antibody tests for the diagnosis of COVID-19 in patients with ambiguous combinations of test results.

REFERENCES

1. Deeks JJ, Dinnes J, Takwoingi Y, et al.; Cochrane COVID-19 Diagnostic Test Accuracy Group. Antibody tests for identification of current and past infection with SARS-CoV-2. *Cochrane Database Syst Rev.* 2020;6:CD013652.
2. Jacofsky D, Jacofsky EM, Jacofsky M. Understanding antibody testing for COVID-19. *J Arthroplasty.* 2020;35(7S):S74–S81.
3. Zhao J, Yuan Q, Wang H, et al. Antibody responses to SARS-CoV-2 in patients with novel coronavirus disease 2019. *Clin Infect Dis.* 2020;71(16):2027–2034.
4. Long QX, Liu BZ, Deng HJ, et al. Antibody responses to SARS-CoV-2 in patients with COVID-19. *Nat Med.* 2020;26(6):845–848.
5. Suhandynata RT, Hoffman MA, Kelner MJ, McLawhon RW, Reed SL, Fitzgerald RL. Longitudinal monitoring of SARS-CoV-2 IgM and IgG seropositivity to detect COVID-19. *J Appl Lab Med.* 2020;5(5):908–920.
6. Zhao J, Liao X, Wang H, et al. Early virus clearance and delayed antibody response in a case of coronavirus disease 2019 (COVID-19) with a history of coinfection with human immunodeficiency virus type 1 and hepatitis C virus. *Clin Infect Dis.* 2020;71(16):2233–2235.
7. Atchison C, Pristerà P, Cooper E, et al. Usability and acceptability of home-based self-testing for SARS-CoV-2 antibodies for population surveillance. *Clin Infect Dis.* 2021;72(9):e384–e393.
8. Peeling RW, Wedderburn CJ, Garcia PJ, et al. Serology testing in the COVID-19 pandemic response. *Lancet Infect Dis.* 2020;20(9):e245–e249.
9. Perkmann T, Perkmann-Nagele N, Breyer MK, et al. Side-by-side comparison of three fully automated SARS-CoV-2 antibody assays with a focus on specificity. *Clin Chem.* 2020;66(11):1405–1413.
10. Long QX, Tang XJ, Shi QL, et al. Clinical and immunological assessment of asymptomatic SARS-CoV-2 infections. *Nat Med.* 2020;26(8):1200–1204.
11. Zhang X, Li M, Chen T, Lv D, Xia P, Qian W. Persistent negative antibody test in COVID-19 patient: a case report. *Clin Infect Dis.* 2021;72(5):901–903.
12. Figueiredo-Campos P, Blankenhaus B, Mota C, et al. Seroprevalence of anti-SARS-CoV-2 antibodies in COVID-19 patients and healthy volunteers up to 6 months post disease onset. *Eur J Immunol.* 2020;50(12):2025–2040.
13. Elecsys Anti-SARS-CoV-2. Package insert. Roche Diagnostics. https://www.fda.gov/media/137605/download. Accessed May 5, 2021.

CASE STUDY

Mycobacterium mucogenicum Infection in a Patient with an Open Fracture: A Case Report

Wanxiang Li, MM,[1] *Min Li, MM,*[1] *Mi Liu, MM,*[1] *Jie Ma, MM*[1,*]

[1]Department of Clinical Laboratory, Weifang People's Hospital, Weifang, Shandong, China; *To whom correspondence should be addressed. longjie623@163.com

Keywords: open fracture, *Mycobacterium mucogenicum*, nontuberculous mycobacteria

Abbreviations: NTM, nontuberculous mycobacteria; MS, mass spectrometry

Laboratory Medicine 2022;53:e4–e7; DOI: 10.1093/labmed/lmab031

ABSTRACT

Mycobacterium mucogenicum is a nontuberculous mycobacterium that is ubiquitous in nature. However, *M. mucogenicum* infection in patients with orthopedic trauma is rarely reported in the literature. Herein, we describe a 48 year old male Han Chinese patient whose right leg was squeezed by agricultural machinery, resulting in open tibial fractures. Postoperative antimicrobial treatment was administered because the wound had been contaminated by soil. However, no long-term wound closure occurred, and a culture of the wound exudation tested positive for *M. mucogenicum*. We established the clinical treatment plan according to the characteristics and drug sensitivity test results of *M. mucogenicum*, and the patient was discharged uneventfully. Increasingly, more reports of infection caused by nontuberculous mycobacteria are being published; however, to our knowledge, this is the first report of an orthopedic infection caused by *M. mucogenicum*. Because the treatment process of *M. mucogenicum* infection is long and complex, isolation and identification of *M. mucogenicum* are of great significance to effective clinical treatment.

Nontuberculous mycobacteria (NTM) are mostly conditional pathogenic bacteria that are routinely found in water, air, soil, and other features of the natural environment. In recent years, the incidence of NTM-related diseases has substantially increased.[1,2] More than 30 species of NTM have been found to cause infections. Most of these NTM are conditional pathogenic bacteria; only a few are pathogenic bacteria. NTM are divided into slowly growing mycobacteria and rapidly growing mycobacteria, all of which are closely related to nosocomial infections.

Clinical infections are commonly caused by rapidly growing mycobacteria. The symptoms of NTM infections and the laboratory identification of NTM are similar to those of *Mycobacterium tuberculosis*; therefore, NTM is easily misdiagnosed. Routine culture may fail to identify NTM, resulting in an infection that is difficult to control. Thus, isolation and identification of NTM are of great significance to achieving a correct clinical diagnosis.

Mycobacterium mucogenicum was first reported in 1995. This species is a rapidly growing type of mycobacterium that shows mucoid colonies on agar.[3] Although uncommon, infections by *M. mucogenicum* most commonly occur in immunocompromised individuals and frequently involve the skin and soft tissue. Few reports have described orthopedic infections caused by *M. mucogenicum*.

Herein, we present the first case in the literature, to our knowledge, of an *M. mucogenicum*–associated soft-tissue infection in a patient with an open fracture. Our purpose in reporting this case is to provide a reference for laboratory identification and clinical treatment. We have received and archived written patient consent forms in this study, along with approval by the ethics committee of Weifang People's Hospital, Weifang, Shandong, China, for the use of specimens from human patients.

Case Report

Case Description

A 48 year old Han Chinese man was injured when his right leg was squeezed by agricultural machinery, resulting in skin defects of approximately 20 cm in size, soft-tissue defect, and pollution of the wound by a large amount of silt. He was admitted to the hospital for an emergency operation.

On presentation, the patient had no fever (his temperature was 36.8°C) and had a pulse of 62 beats per minute, respiratory rate of 18 breaths per minute, and blood pressure of 162/104 mmHg. Physical examination results were unremarkable. The patient had no consciousness disorder, dizziness, headache, chest tightness, or suffocating discomfort. He underwent open reduction with plate fixation for treatment of the tibial fractures, along with surgical debridement.

Approximately 2 weeks after the first-stage surgery, the infection remained uncontrolled, and the patient presented with wound nonclosure but no obvious wound exudate. Routine antibiotic treatment had no obvious effect, and the fractured end of the bone was unstable.

The patient underwent a second-stage surgery involving debridement, external fixation of the tibial fractures, and application of antibiotic bone cement. Approximately 2 weeks after the second-stage

surgery, poor wound healing and soft-tissue infection were observed. Antiinflammatory and other conservative treatments did not result in significant improvement.

The patient underwent a third-stage surgery involving soft-tissue debridement and negative-pressure vacuum-sealing drainage. Thorough debridement was performed to remove contaminants, foreign matter, and dead tissues. The patient received systemic antibiotic therapy throughout this treatment.

Laboratory Examinations

Laboratory-study findings showed leukocytosis (10.78×10^9/L) with 78% neutrophils, a procalcitonin concentration of 42.5 μg/L, and an erythrocyte sedimentation rate of 80 mm per hour. X-ray examination showed fractures of the right tibial plateau.

A swab specimen was collected for culture of the wound. Eleven days after the first-stage surgery, the bacterial culture of the wound exudate tested positive for *Pseudomonas putida*. The wound remained unhealed after antibiotic treatment. However, 9 days after the third-stage surgery, another wound swab specimen was inoculated on Columbia blood agar, and slender mucoid colonies were observed after 48 hours (**FIGURE 1A**). After 72 hours, the colonies appeared waxy and grayish white, and exhibited a round protuberance, uneven edges, and rough surface (**FIGURE 1B**). Gram staining showed weakly colored gram positive bacilli (**FIGURE 2A**), and Ziehl staining revealed positivity for acid-fast bacilli (**FIGURE 2B**).

Examination of the bacteria under a microscope revealed slender, straight, or slightly curved microorganisms with different thicknesses and occasional branching. MALDI-TOF mass spectrometry (MS) showed that the bacterial strain was *M. mucogenicum* (**FIGURE 3**). The strain showed 100% similarity to *M. mucogenicum*, as determined from a phylogenetic tree of *rpoB* genes linked in a series (**FIGURE 4**). The in vitro susceptibility to antibiotics was measured by the disk diffusion method on Mueller Hinton II agar. The results are shown in **TABLE 1**. The bacterium showed susceptibility to kanamycin and high concentrations of ethambutol and ofloxacin; however, it was resistant to first-line antituberculosis drugs.

Clinical Treatment

The antibiotic treatment was adjusted according to the literature and drug sensitivity test results. The patient was treated with 2 months of intravenous amikacin, clarithromycin, cefoxitin, and moxifloxacin, after which the treatment was changed to oral clarithromycin and oral moxifloxacin for 18 months. Complete wound healing was achieved, and the infection did not recur during the 1-month follow-up.

Discussion

As illustrated in the present case (long-term nonhealing wound after treatment of open tibial fractures), the clinician must maintain a high index of suspicion for NTM whenever considering an infection as the cause of a nonhealing open wound. Because NTM infections are similar to tuberculosis in terms of clinical symptoms, imaging findings, smear results, pathological-examination findings, and other characteristics, isolation and identification of NTM are necessary for a diagnosis. The treatment should then be selected according to the species of NTM with which the patient is infected.

The current NTM practice guidelines do not explicitly describe a specific treatment protocol for *M. mucogenicum* but they do state that most isolates are susceptible to multiple antimicrobial agents, including macrolides, quinolones, linezolid, amikacin, cefoxitin, imipenem, doxycycline, compound sulfamethoxazole, and some other drugs.[4] Drug-sensitivity results have been reported to varying degrees, and a high rate of drug resistance has been noted.[5] Also, the use of combination antimicrobial regimens is reportedly superior to monotherapy and tends to be associated with a lower relapse rate.

Although the incidence of NTM infections is increasing, the lack of awareness of these pathogens and the difficulty of isolating NTM by culture may lead to diagnostic delay, threatening successful treatment. In a retrospective review of 31 cases of atypical mycobacterial infections of the upper extremity (mean diagnostic delay, 10 months), delays and inappropriate management resulted in a higher risk of treatment failure (as high as 68%).[6] The authors considered that a lack of clinical suspicion of NTM infection until the primary infection, which did not resolve with administration of the initial antimicrobial treatment regimen, may have led to a much higher diagnostic delay and treatment-failure rate than the actual values typically observed in such cases.

NTM species are ubiquitous environmental organisms found in soil, water, and dust. Out-of-hospital infections are usually associated

FIGURE 1. Bacterial cultures of wound exudate (Columbia blood agar). A, 48-hour culture colony. B, 72-hour culture colony.

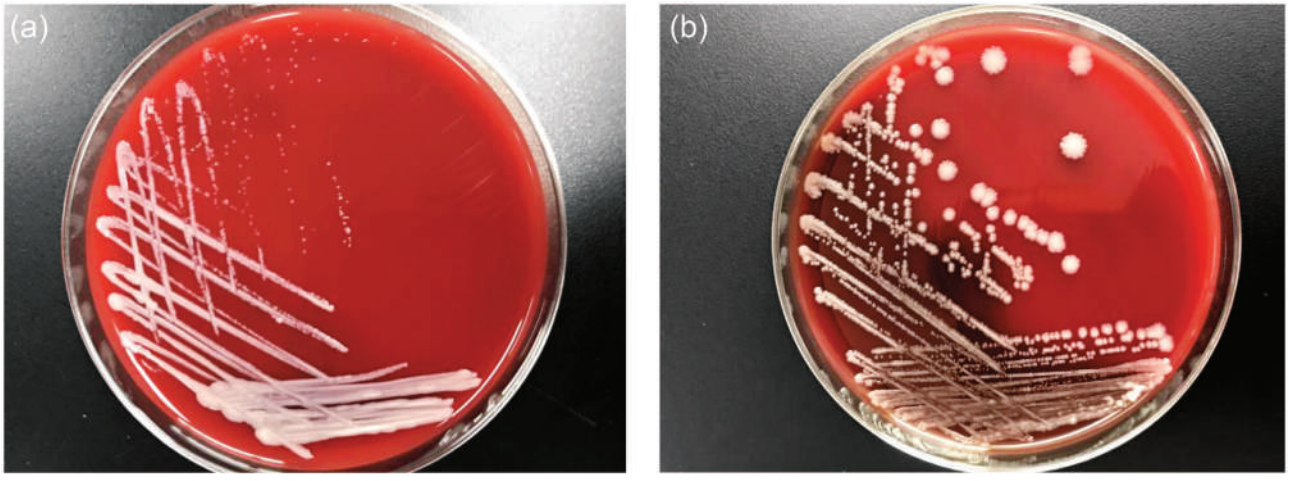

FIGURE 2. Staining images (original magnification, ×1000). A, Gram stain. B, Acid-fast bacilli.

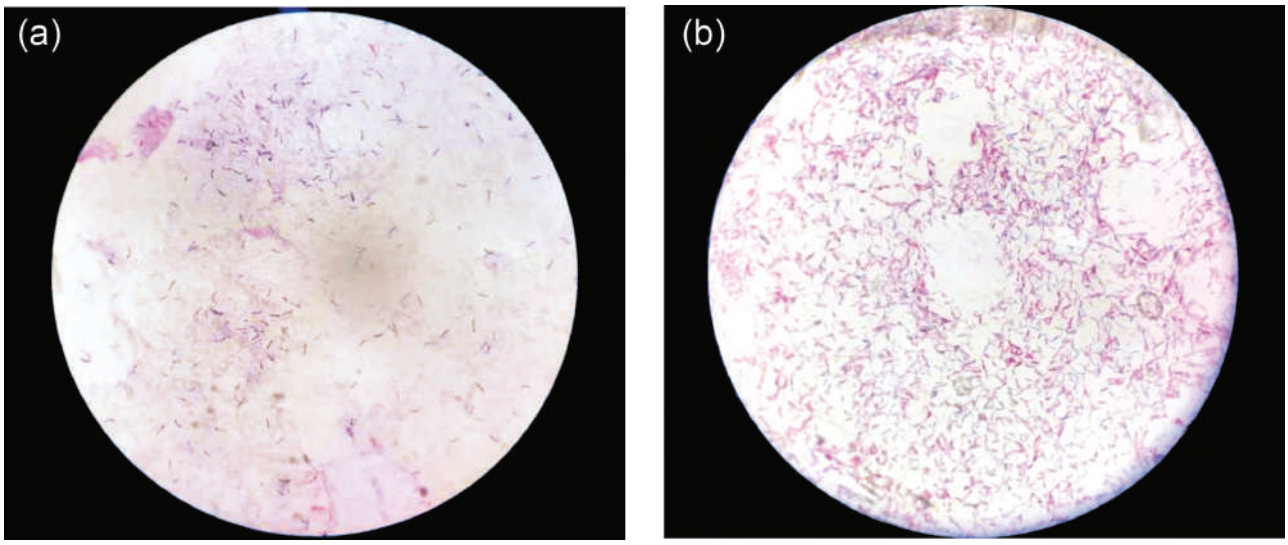

FIGURE 3. The result of MALDI-TOF mass spectrometry (MS) analysis.

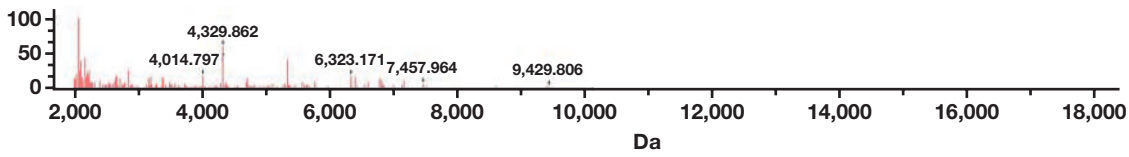

FIGURE 4. A phylogenetic tree of *rpoB* genes linked in a series.

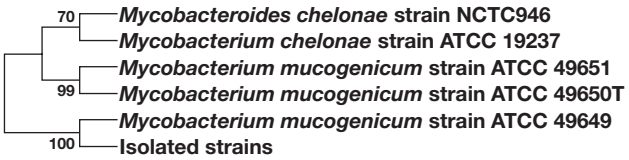

TABLE 1. Results of Drug Sensitivity Testing for *Mycobacterium mucilage* (Absolute Concentration Method)

Antimicrobial Agent	Concentration (μg)	Results
Streptomycin	10	R
	100	R
Ioniazid	1	R
	10	R
Rifampin	50	R
	250	R
Ethylaminobutyl alcohol	5	R
	50	S
Ofloxacin	2	R
	20	S
Canamycin	10	S
	100	S
P-nitrobenzoic acid		+
Thiophene-2-carboxylate hydrazine		+

with skin trauma or injuries, and nosocomial infections are related to contaminated hospital equipment and water supplies. The hospital water supply can contaminate medical devices, such as endovascular mcatheters, peritoneal dialysis equipment, central venous catheters, and hemodialysis equipment. The water supply may be the main source of nosocomial NTM infections.[7,8]

Most investigations have involved NTM contamination of water, which was found to be closely related to clinical infection. Hospitalized patients with NTM infections were studied together with drinking-water specimens from their respective areas of residence. Dovriki et al[9] indicated that drinking water may be linked to NTM cases in humans. Thorough disinfection of hospital water and medical devices is necessary to prevent nosocomial infection caused by NTM. Disinfectants must be strictly prepared according to the requirements and standardized operations. After medical devices are disinfected, they should be washed with sterilized water to prevent secondary contamination.

M. mucogenicum rarely produces clinical disease; however, it has been shown to cause a wide spectrum of infections in immunocompromised hosts.[10] Because of the slow growth of mycobacteria, the diagnosis is often difficult and delayed. Appropriate wound cultures are critical, and verification with repeat cultures may be required.

A significant number of NTM infections are misdiagnosed as tuberculosis; however, *M. mucogenicum* is resistant to antituberculosis drugs.[11] Therefore, antituberculosis therapy is not effective against NTM. These patients are then misclassified as having chronic or multidrug-resistant tuberculosis, which adversely impacts not only their health status but also the associated health care costs.[12] It is therefore important to correlate *M. mucogenicum* isolates with the patient to ensure clinical significance of the isolates.

Conclusions

Application of MALDI-TOF MS and sequencing technology for the identification of microbial strains in recent years has greatly improved the speed and accuracy of laboratory NTM identification, which has played an important role in the formulation of reasonable clinical treatment plans. Awareness should be raised among clinicians and microbiologists to avoid considering *M. mucogenicum* as a contaminant and to choose the appropriate antibiotic treatment. Improvement of the detection rate of NTM is crucial for effective clinical treatment.

Acknowledgments

We thank Angela Morben, DVM, ELS, from Liwen Bianji, Edanz Editing China (www.liwenbianji.cn/ac), for editing the English text of a draft of this manuscript. The present study was supported by the fund from the Health and Family Planning Commission of Weifang (wfwsjs_2020_035), and research grants from the Health Commission of Shandong Province (2020W11466), the Health and Family Planning Commission of Weifang (wfwsjs_2018_110), and the Health Commission of Shandong Province (2018WS078).

Personal and Professional Conflicts of Interest

None declared.

REFERENCES

1. Brode SK, Daley CL, Marras TK. The epidemiologic relationship between tuberculosis and non-tuberculous mycobacterial disease: a systematic review. *Int J Tuberc Lung Dis.* 2014;18(11):1370–1377.
2. Lai C-C, Tan C-K, Chou C-H, et al. Increasing incidence of nontuberculous mycobacteria, Taiwan, 2000-2008. *Emerg Infect Dis.* 2010;16(2):294–296.
3. Adékambi T, Drancourt M. Dissection of phylogenetic relationships among 19 rapidly growing *Mycobacterium* species by 16S rRNA, *hsp65*, *sodA*, *recA* and *rpoB* gene sequencing. *Int J Syst Evol Microbiol.* 2004;54(Pt 6):2095–2105.
4. Misch EA, Saddler C, Davis JM. Skin and soft tissue infections due to nontuberculous mycobacteria. *Curr Infect Dis Rep.* 2018;20(4):6.
5. Griffith DE, Aksamit T, Brown-Elliott BA, et al; ATS Mycobacterial Diseases Subcommittee; American Thoracic Society; Infectious Disease Society of America. An official ATS/IDSA statement: diagnosis, treatment, and prevention of nontuberculous mycobacterial diseases. *Am J Respir Crit Care Med.* 2007;175(4):367–416.
6. Smidt KP, Stern PJ, Kiefhaber TR. Atypical mycobacterial infections of the upper extremity. *Orthopedics.* 2018;41(3):e383–e388.
7. Thomson RM, Tolson CE, Carter R, Huygens F, Hargreaves M. Heterogeneity of clinical and environmental isolates of *Mycobacterium fortuitum* using repetitive element sequence-based PCR: municipal water an unlikely source of community-acquired infections. *Epidemiol Infect.* 2014;142(10):2057–2064.
8. Bringhurst J, Weber DJ, Miller MB, et al. A bronchoscopy-associated pseudo-outbreak of *Mycobacterium mucogenicum* traced to use of contaminated ice used for bronchoalveolar lavage. *Infect Control Hosp Epidemiol.* 2020;41(1):124–126.
9. Dovriki E, Gerogianni I, Petinaki E, Hadjichristodoulou C, Papaioannou A, Gourgoulianis K. Isolation and identification of nontuberculous mycobacteria from hospitalized patients and drinking water samples–examination of their correlation by chemometrics. *Environ Monit Assess.* 2016;188(4):247.
10. Dhruve MJ, Bunce PE, D'Gama C, Chan CT. Case of *Mycobacterium mucogenicum* in a home hemodialysis patient. *Hemodial Int.* 2017;21(4):E79–E81.
11. Behra PRK, Pettersson BMF, Das S, Dasgupta S, Kirsebom LA. Comparative genomics of *Mycobacterium mucogenicum* and *Mycobacterium neoaurum* clade members emphasizing tRNA and non-coding RNA. *BMC Evol Biol.* 2019;19(1):124.
12. Nishiuchi Y, Iwamoto T, Maruyama F. Infection sources of a common non-tuberculous mycobacterial pathogen, *Mycobacterium avium* complex. *Front Med (Lausanne).* 2017;4:27.

LABORATORY QA

Lean Principles to Improve Quality in High-Throughput COVID-19 Testing Using SwabSeq: A Barcoded Sequencing-Based Testing Platform

Janae Jones, BS, MS,[1,2,a] Rosita Saul, BS,[1,2,a] Laila Sathe, BS,[2,3] Joanna Xie, MD,[2] Dawn Marquette, BS, MLS(ASCP)[CM],[1,2] Valerie A. Arboleda, MD, PhD[1,2,3,4,]*

[1]Department of Computational Medicine, David Geffen School of Medicine, University of California Los Angeles, Los Angeles, California, US; [2]UCLA SwabSeq COVID19 Laboratory, David Geffen School of Medicine, University of California Los Angeles, Los Angeles, California, US; [3]Department of Pathology and Lab Medicine, David Geffen School of Medicine, University of California Los Angeles, Los Angeles, California, US; [4]Department of Human Genetics, David Geffen School of Medicine, University of California Los Angeles, Los Angeles, California, US; *To whom correspondence should be addressed. VArboleda@mednet.ucla.edu [a]These authors contributed equally.

Keywords: next-generation sequencing, quality control, quality assurance, Lean Six Sigma, SARS-CoV-2, COVID-19 screening.

Abbreviations: QC, quality control; RT-qPCR, reverse-transcription quantitative polymerase chain reaction; UCLA, University of California Los Angeles; IQCP, individualized quality control plan; NNVA, necessary but non-value-adding operation; NVA, non-value-adding operation; VA, value-adding operation; TAT, turnaround time; CLS, clinical laboratory scientist.

Laboratory Medicine 2022;53:e8–e13; https://doi.org/10.1093/labmed/lmab069

ABSTRACT

Objective: To describe and quantify the effect of quality control (QC) metrics to increase testing efficiency in a high-complexity, Clinical Laboratory Improvement Amendments–certified laboratory that uses amplicon-based, next generation sequencing for the clinical detection of SARS-CoV-2. To enable rapid scalability to several thousands of specimens per day without fully automated platforms, we developed internal QC methods to ensure high-accuracy testing.

Methods: We implemented procedures to increase efficiency by applying the Lean Six Sigma model into our sequencing-based COVID-19 detection.

Results: The application of the Lean Six Sigma model increased laboratory efficiency by reducing errors, allowing for a higher testing volume to be met with minimal staffing. Furthermore, these improvements resulted in an improved turnaround time.

Conclusion: Lean Six Sigma model execution has increased laboratory efficiency by decreasing critical testing errors and has prepared the laboratory for future scaling up to 50,000 tests per day.

Demand for robust screening for the SARS-CoV-2 virus has increased during the COVID-19 pandemic and with the lockdown measures; such screening will be needed to enable the reopening of society and provide surveillance for outbreaks and for future pandemics. The need for a highly scalable and high-throughput screening test led to the development of SwabSeq.[1] Unlike reverse-transcription quantitative polymerase chain reaction (RT-qPCR) methods, SwabSeq uses barcoded primers to amplify viral RNA and then pools the barcoded amplicons for detection of the virus using next-generation sequencing. This quantitative readout allows for improved accuracy and sensitivity, even with unpurified specimens, without sacrificing the limit-of-detection of the assay.[1] One key aspect of SwabSeq is that it is flexible and rapidly expandable to take advantage of an existing genomic core facility infrastructure that was underutilized at many universities at the start of the pandemic. Therefore, maintaining the flexibility of such core facilities can allow for the rapid deployment of massive testing protocols in the early phases of a pandemic without overwhelming clinical and health care settings.

To meet the demands of COVID-19 population screening, we implemented operational efficiency methods in a newly deployed Clinical Laboratory Improvement Amendments laboratory, the University of California Los Angeles (UCLA) SwabSeq COVID-19 Testing Laboratory, using the Lean Six Sigma model. The testing process was and continues to be optimized through the application of the model's 5 phases: define, measure, analyze, improve, and control.[2] At the deployment of testing in November 2020, we made plans to scale up our capacity to >10,000 tests per day.

In this article, we outline our individualized quality control plan (IQCP)[3] and our use of Lean principles to improve our workflow as we scaled up to >4,500 tests per day over a 3-month period by optimizing critical steps in our process (Lean principles represent a 5-step thought process to improve operational processes, and include identifying value, mapping the value stream, creating a flow, establishing pull and seeing

perfection: https://www.lean.org/WhatsLean/Principles.cfm). In addition, we suggest fixed times for processes that are value-adding and non-value-adding. In this way, the steps necessary to scale up, such as hiring and training more staff, in addition to increasing consumable inventory, can be anticipated.[4] Although few laboratory tests leveraging next generation sequencing are performed at significant scale, we have developed flexible, non-automation-dependent processes that can be rapidly deployed for future surveillance needs.

Methods

To further the efficiency of our testing system, we built upon the existing quality control (QC) measures by using the Lean Six Sigma model[2] and its tools. Three sets of variables were defined for the entirety of our process: necessary but non-value-adding operations (NNVAs), non-value-adding operations (NVAs), and value-adding operations (VAs). The NNVAs include heat inactivation, making swabseq reaction master mix, the time on the thermal cycler, and the time needed for sequencing. The NVAs include inventory, kit assembly, collections, and accessioning. The VAs include pipetting and library preparation. We used these variables to execute Lean Six Sigma's analysis phase by calculating our turnaround time (TAT) and determining how to produce more test results simply by hiring more staff. The QC was validated using tools such as weekly huddles and QC forms.

Results

A value stream map was created to identify key people, resources, activities, and information flows required to deliver test results (**FIGURE 1**).[2] The SwabSeq test begins with materials that are received from the supply chain being added to the running inventory with anywhere from a 2- to 6-week lag time. Critical supplies are warehoused on site, maintaining a capacity for scale. The SwabSeq customer service team is responsible for managing kit assembly and works with staff from our testing clients to coordinate delivery of test collection materials for their sites. Each organization can use nasal swabs or neat saliva specimens that are collected into the same receptacle: a double-barcoded, internally threaded collection tube. Using PreciseQ Technologies, Inc., an electronic health care operations system, our clients can directly place order information for patient tests and we can auto-upload results. Specimens arrive racked in 96-well format on ice at the UCLA SwabSeq COVID-19 Testing Laboratory by shipment services or by client-supplied couriers. Each rack of specimens is accessioned on a 96-specimen scanner into the SwabSeq laboratory-developed database.

SwabSeq Testing Platform

After accessioning, specimens are heat-inactivated in a circulating water bath at 85°C to 95°C for 30 minutes. Simultaneously, another staff member will make swabseq reaction mastermix consisting of TaqPath 1-Step RT-qPCR swabseq reaction mastermix CG (Thermo Fisher), a synthetic RNA S2 standard developed and manufactured by Octant Bio, and Ambion Nuclease Free Water. After heat inactivation, the pipetting event can take place. After all specimens have been pipetted, each Applied Biosystems MicroAmp EnduraPlate 384-well plate is placed on a Thermo Fisher Veriti 384-well thermal cycler for an endpoint PCR with 50 cycles for 1 hour and 20 minutes.

SwabSeq currently uses 1536 unique dual indices (UDI), separated into four 384-well plates.[1] The primer sets were designed by Octant Inc. and manufactured by Integrated DNA Technologies. The 384-well plate is divided into 4 quadrants of 96 specimens. The 96-well racks received by the laboratory are designated as either A, B, C, or D. The letter determines which quadrant the rack is pipetted into and can be identified by specific water tube placement and our workbook file (**FIGURE 2**). Two specimen tubes containing nuclease-free water are placed into each of these 96-well racks in a location based on the assigned primer set, quadrant, and time of testing (Supplemental Figure 1).

Finally, to clearly distinguish each 384-well PCR plate, we designate a specific color to ensure that no duplicates of the same molecular indexes are sequenced simultaneously. The water tube barcodes and

FIGURE 1. SwabSeq value stream map showing the process of testing from supply chain to specimen collection, testing, and reporting results. Each heart represents the number of staff members required for that step. We also describe the timing for each run to indicate the feasibility of running 3 runs per day with minimal staff.

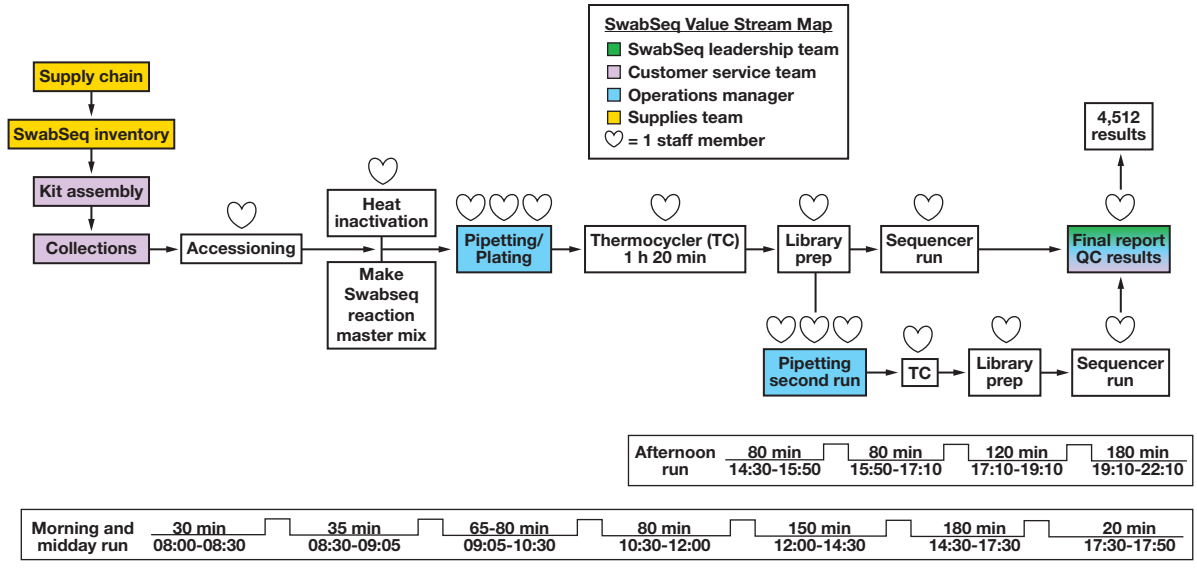

FIGURE 2. The 384-well plate organizational setup using four 96-well racks. Each 384-well plate is made up of 4 racks of specimens, each with 96 tubes. Each rack must be oriented properly at the pipetting stage and at the scanning stage to ensure that the correct specimen tube is associated with the correct plate and location.

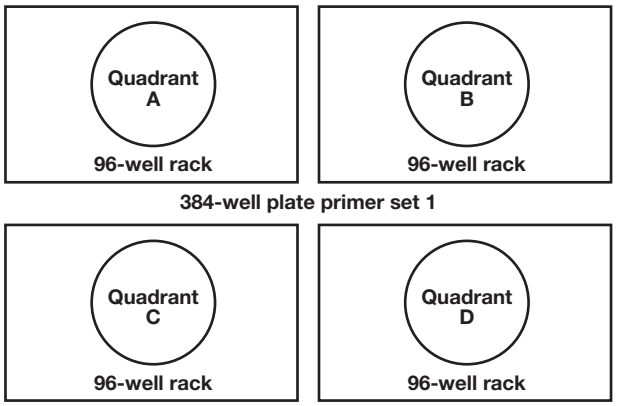

location are recorded during the scanning step. Therefore, during data analysis we can confirm that the expected locations of the water tube barcodes match their locations on the PCR plate. If the location of the water tubes (aka, negative control specimens) does not match the water tubes' expected location on the plate, we can definitively see that there has been an error in either pipetting of the plate or the scanning of the plate. This simple and low-tech visualization method allows us to identify potential plate misorientation errors before reporting results.

Library preparation for the Illumina sequencers can begin as soon as the thermocycler program is completed. The Illumina NextSeq or MiniSeq can then be run, with results de-multiplexed using a continuously running informatics pipeline, developed in-house.[1] The informatics pipeline creates a series of plate visualization heatmaps for the interpretation of results and quality control. After reviewing the results, staff manually upload them into an internal network drive where an internally developed script automatically uploads results into PreciseQ every 5 minutes. Upon this upload, results are sent to the patient's preferred method of contact and the California Department of Public Health.

To interpret results, the SwabSeq automated analysis pipeline outputs a heatmap with the read counts for each of the amplicons that are sequenced associated with their plate and well position.[1] The 3 possible amplicons we detect correspond to PCR products that represent the S2 (virus), S2-standard (internal control), and RPP30 (human input control). Therefore, for a positive virus specimen, we would expect to see a high read count of the S2, and RPP30 amplicons. The absence of reads in the RPP30 (**FIGURE 3**, dark purple-grey) indicates that no human specimen is present in that well. The absence of reads in S2-standard suggests that the well did not have sufficient S2 primer or swabseq reaction or that there was a significant PCR inhibitory effect on amplification. Finally, the presence of reads for the S2 amplicon of the SARS-CoV-2 virus suggests that there is virus present; however, a final determination of a positive or negative result is based on the ratio of the number of S2/S2-standard reads that must be above our designated threshold from internal validation.

Quality Improvement Using Lean Six Sigma

Improvements to our testing process were implemented after the identification of errors that occurred during testing. Before the first scale-up in the laboratory, our minimal QC resulted in errors such as plate flips and the incorrect placement of water tubes. One such error was identified in our early testing (**FIGURE 3**). Here, we observed that for a plate that was run in duplicate, one plate was misoriented during the pipetting event but not during scanning. Therefore, we observed that the location of the id_tubes (**FIGURE 3A**) did not match the locations with no RPP30 reads (**FIGURE 3B**, red circles). Therefore, the Plate 1B rack was oriented incorrectly, causing a 180° flip of each specimen and thus a misidentification of specimens with their corresponding results. In addition, the location of high viral reads (yellow/orange) seems to be flipped between plates 1 and 4 (**FIGURE 3B**). The proper placement of water tubes provides valuable information that links the pipetted specimens to the plate to the specimen identifier and allows us to detect errors at the scanning and pipetting stage (**FIGURE 3**).

To alleviate these errors, the improve phase of the Lean Six Sigma model[2] was applied. We assigned specific roles to staff to ensure that quality system cross-checks were completed during each stage of the testing process. The staff member assigned the role of "support" is responsible for accessioning, heat inactivation, and setting up the pipetting event. This includes the placement of water tubes. The support role also ensures that plate flips, specimen mis-scans, and incorrect water tube placement are minimized by visually checking each orientation. The second role is that of the "pipettor." This staff member is expected to make swabseq reaction master mix for the runs, pipette during the pipetting event, and place the 384-well plate onto the thermal cycler. After the run is set up, the pipettor verifies that each of the tasks performed by the support role is correct before progressing with the pipetting process.

To further minimize plate flips and specimen mis-scan occurrences, rack orientation checks and A1 specimen position tracking are implemented. The proper rack orientation is confirmed by the support role employee, who checks that the A1 position on the 96-well rack and the A1 position on the plate holder of the pipetting instrument match. In addition, this staffer ensures that the quadrant being plated corresponds to the correct position of the 384-well plate primer set to prevent manual plate flips. The A1 specimen position tracking form confirms that the physical tube in the A1 position and the barcode scanned into the workbook for the A1 position match, verifying that an informatic plate flip has not occurred (Supplemental Figure 2). These elements are all checked both at the time of pipetting and after all pipetting is completed, allowing 2 independent checks of the plate orientation.

Finally, because of the high volume of plates per run, we developed a visual management system through a custom-designed 3-dimensional rack template to ensure that water tube placement was in the correct row and column[5] and thereby reduce errors in the location of water tube placement. To further verify the correct water tube placement, water tube QC forms were also added (Supplemental Figure 2).

Control Phase of Lean Six Sigma

The control phase of Lean Six Sigma[2] was accomplished through the creation of QC variances, clinical laboratory scientist (CLS) review of QC testing forms (Supplemental Figure S2), development of a validated

FIGURE 3. **(A) Each run has a designated control water tube placement with prevalidated water tubes (id_tubes). The location is indicated by the green color (true), which confirms that these tubes were present at the expected orientation (see Supplemental Figure 1). In this example, we have two 96-well racks that were mirrored, meaning that they should have the same water tube placement (A) and location with low RPP30 reads on heat map (B). The location of the negative control water tubes within the 96-well plate do not match between plate 1B but do match between plate 4B. Plate 1 had a misorientation, resulting in a 180° plate flip identified by the rotated location of the water tubes. Comparing the S2 virus read heatmap of both plates, the plate flip is further realized because the locations of positive specimens are altered. The colors expressed in the log10 count correspond to the high presence of amplicons, purple equating to a low read count and yellow equating to a high read count. The S2 amplicon is the viral SARS-CoV-2 gene present in the specimen. The S2-standard amplicon is SwabSeq's in vitro RNA standard to normalize viral read counts within each well. The RPP30 amplicon serves as a human-input control to determine whether a patient specimen is present in each well.**

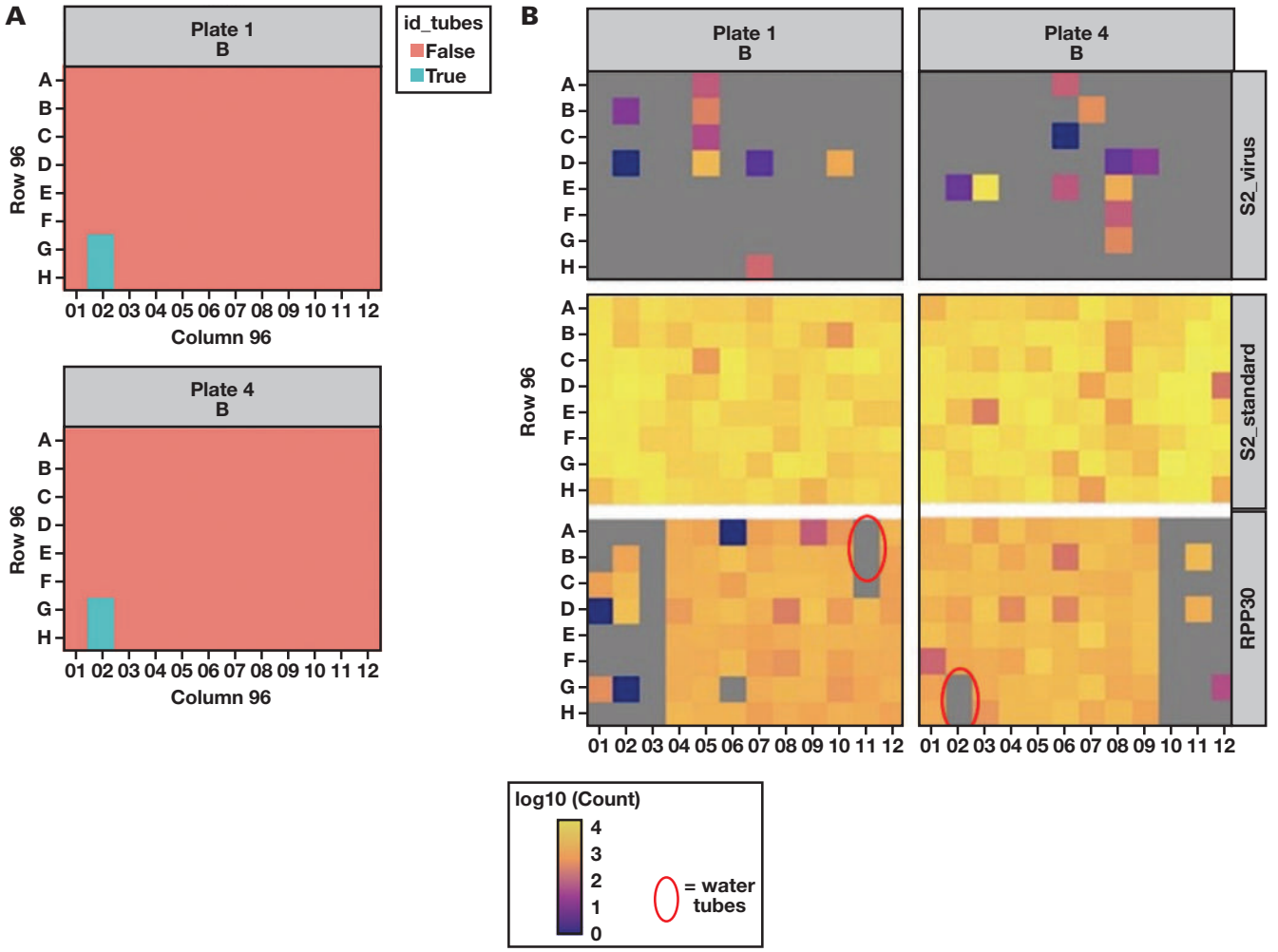

TABLE 1. **Performance Metrics After the Implementation of the Lean Six Sigma Model**

Month	Pipetting Time	Total TAT from Accession to Result	Water Tube Placement, %	Orientation Checks Signed, %
December 2020	1.1	17	95 (10.45/11)	88
January 2021	1.2	18	95.4 (41/43)	100
February 2021	1.1	18	97.7 (43/44)	96
March 2021	0.8	16	95.7 (45/47)	99

Times listed are averages in hours.

training program, and weekly staff huddles. The QC variances are given after the review of QC testing forms by CLS or CLS trainees if errors are identified. The use of QC variances allows staff to identify errors and ensure that recurrence of that error is minimized. New training protocols ensure that newly hired staff are fully trained in all roles and are aware of the QC systems implemented and their importance. Weekly huddles allow for the discussion of roadblocks faced in the laboratory and how to overcome them. During these huddles, metrics are discussed to col-

FIGURE 4. TAT improves after implementation of improved QC metrics. Our goal TAT is 24 hours from when specimens are accessioned to when they indicate results, which is represented by the blue line. Comparing the January 2021 TAT (A) to the March 2021 TAT (B), an increase in efficiency is observed after an increase in specimens and implementation of Lean Six Sigma. QC, quality control; TAT, turnaround time.

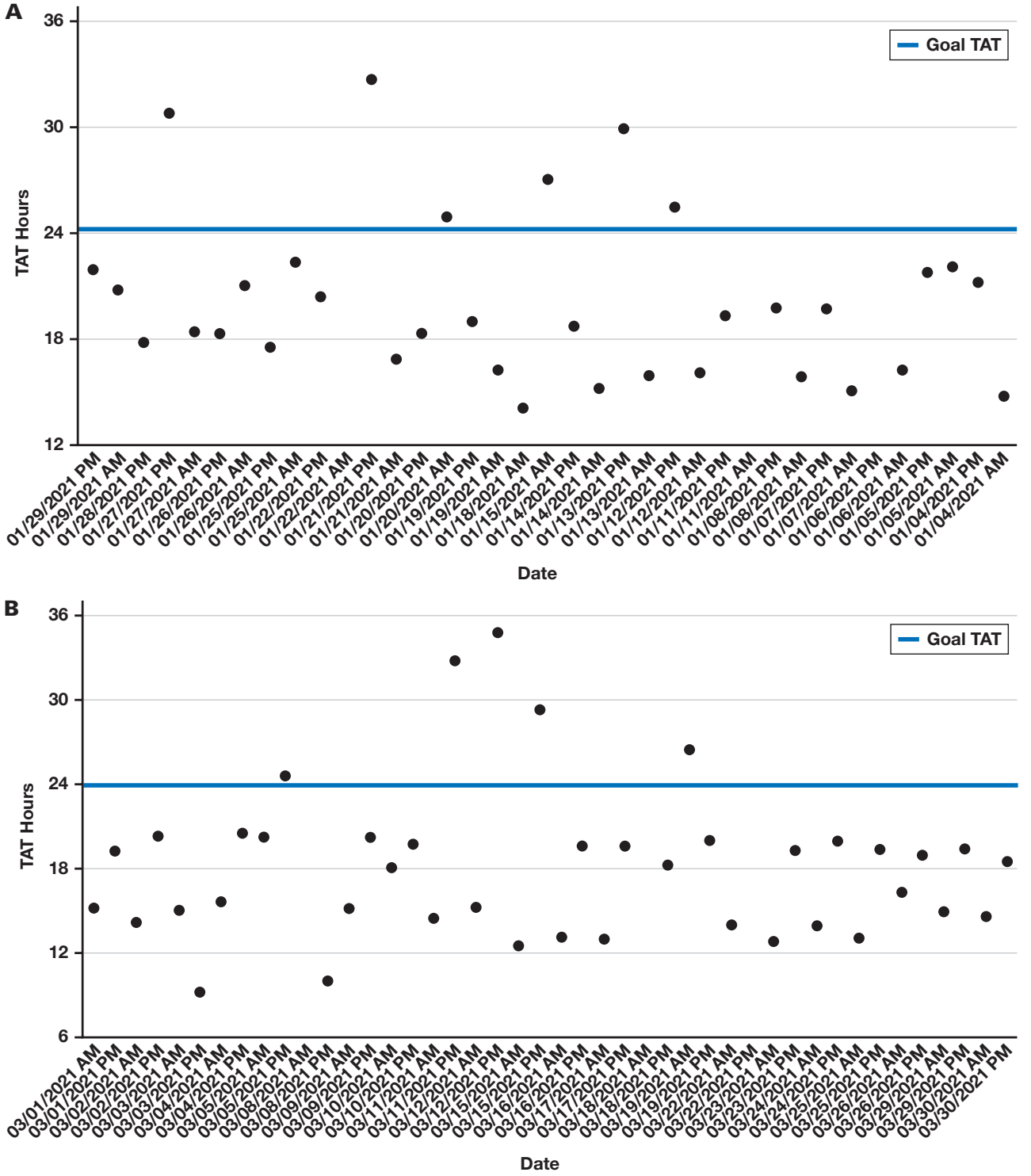

laboratively identify sources of testing error and to implement fixes to increase the efficiency of the laboratory.

After the execution of the identification and control phases of Lean Six Sigma, we moved on to the measurement phase to determine how the implemented solutions impacted the efficiency of the testing process. The following variables were measured: average times of pipetting, total TAT from accessioning to result, the percentage of correct water tube placement, and the percentage of signed orientation checks. Average pipetting time continually decreased from 1.1 hours in December 2020 to 0.8 hours in March 2021 (**TABLE 1**).

TAT also decreased from 17 hours in December 2020 to 16 hours in March 2021. In January 2021, we had an increase in specimen volume during a scale-up, altering our pipetting time and TAT. The percentage of water tube placement increased overall, but in March 2021 new staff training accounted for the small decrease. Improvements in orientation checks were also seen as the months progressed.

The acceptable TAT from accessioning to result is 48 hours, and the goal TAT is 24 hours. Comparison of the January 2021 TAT (**FIGURE 4A**) and March 2021 TAT (**FIGURE 4B**) indicated that most runs resulted within our goal TAT of 24 hours. March 2021 had an influx of specimens, further indicating that Lean Six Sigma optimization[2] improved efficiency.

Discussion

Our Lean Six Sigma[2] approach identified common points of error within our testing processes. We developed quality control metrics in our process and analytics with the placement of water tubes (Supplemental Figure S1), several layers of independent checks in our testing processes (Supplemental Figure S2), and the development of a 3-dimensional printed model to ensure the correct placement of these tubes. Our approaches have improved efficiency and TAT within our laboratory.

To continue scaling up, it was important to identify variables in accordance with Lean Six Sigma Optimization guidelines.[2] In our lab, we perform up to 3 runs per day during operational hours of 7:00am to 8:30pm. Some of the times in our assay are fixed, such as those for heat inactivation, the thermal cycler, and the sequencer run, adding up to 295 minutes. Accounting for an additional 50 minutes for accessioning and resulting, the fixed time is 345 minutes. The value added events during pipetting takes approximately 65 minutes per run, and library preparation takes 60 minutes per run. Therefore, a total of 470 minutes are thus allocated for total production, encompassing pipetting and library preparation. At this rate, with 1 staff member in the support role and 2 in the pipettor roles, we can perform 3 runs, each of which can test up to 1,504 specimens. Therefore, 4,512 tests can be conducted across 3 runs. By creating 2 teams, each team having 1 staff member in the support role and 2 staff members in the pipettor roles, laboratory staff can conduct a total of 9,024 tests per day.

Each team will follow the same processes, but by increasing staffing, the results will be doubled. At the writing of this article in June of 2021, the UCLA SwabSeq COVID-19 Testing Laboratory has conducted over 140,000 tests, with 6 full-time and 6 part-time testing staff, operating Monday through Friday from 7:00am to 8:30pm.

One key aspect to the SwabSeq approach is that deployment did not require full-scale automation to achieve 10,000 specimens per day. Our testing protocols require sequencing and liquid handlers as part of the critical infrastructure. However, our process is distinct enough from traditional RT-qPCR approaches that our supply chain has remained robust throughout the pandemic. Our assay uses 1 pipette tip per specimen when running extraction-free protocols, which decreases our reliance on these critical consumables that continue to be limited across clinical and research laboratories.[6,7]

Conclusion

Herein, we have discussed the rapid deployment and scaling of our high-throughput COVID-19 testing program. Lean Six Sigma approaches[2] were key to developing a robust IQCP program to improve the efficiency of our testing processes and decrease critical laboratory errors. Although we have found solutions to the issues encountered in our first scale-up to a capacity of up to 3,000 specimens per day, we are continually adding fail-safes to this procedure.

Acknowledgments

V.A.A. supported by NIH (DP5OD024579).

Supplementary Data

Supplemental figures can be found in the online version of this article at www.labmedicine.com.

REFERENCES

1. Bloom JS, Sathe L, Munugala C, et al. Massively scaled-up testing for SARS-CoV-2 RNA via next-generation sequencing of pooled and barcoded nasal and saliva samples. *Nat Biomed Eng.* 2021;5(7):657–665. doi:10.1038/s41551-021-00754-5. Epub 2021 Jul 1. PMID: 34211145.
2. Koning H, de Koning H, Verver JPS, van den Heuvel J, Bisgaard S, Does RJM. Lean Six Sigma in healthcare. *J Healthc Qual*. 2006;28(2):4–11.
3. Centers for Disease Control and Prevention. Individualized Quality Control Plan (IQCP). https://www.cdc.gov/labquality/iqcp.html. Accessed August 4, 2021.
4. Schweikhart SA, Dembe AE. The applicability of Lean and Six Sigma techniques to clinical and translational research. *J Investig Med.* 2009;57(7):748–755.
5. Coakley M, Hurt DE. 3D printing in the laboratory: maximize time and funds with customized and open-source labware. *J Lab Automat.* 2016;21(4):489–495.
6. Maggiore JA, Bakst J, Managing supply chain disruptions during the COVID-19 pandemic. https://www.aacc.org/cln/articles/2021/march/managing-supply-chain-disruptions-during-the-covid-19-pandemic. Accessed May 20, 2021.
7. American Society for Microbiology. Supply shortages impacting COVID-19 and non-COVID testing. https://asm.org/Articles/2020/September/Clinical-Microbiology-Supply-Shortage-Collecti-1. Accessed August 4, 2021.

AQ18
AQ20
AQ22

On LabMedicine.com

Several articles featuring practical information are now available on Labmedicine.com.

This month, the website features papers on COVID-19 relevant to today's laboratory professionals and pathologists. First, McMurry et al present the case of a patient with a presumptive false-positive anti-SARS-CoV-2 test in "A Persistent Positive Antibody Test in a Patient with No History of COVID-19 Infection." In "Lean Principles to Improve Quality in High-Throughput COVID-19 Testing Using SwabSeq: A Barcoded Sequencing-Based Testing Platform," Jones et al use the Lean Six Sigma model to prepare their laboratory for increased SARS-CoV-2 testing. And finally, Li et al present the case of a patient with *Mycobacterium mucogenicum* infection.

Check out these articles, podcasts, and more on Labmedicine.com.

Lablogatory

Recent contributions to the blog for medical laboratory professionals include discussions microaggressions in medical school and pathology training, microbiology case studies, and laboratory safety. To see why over 350,000 readers visited Lablogatory in 2020, visit labmedicineblog.com.